https://doi.org/10.15388/vu.thesis.339
http://orcid.org/0000-0001-5415-2796

VILNIUS UNIVERSITY
CENTER FOR PHYSICAL SCIENCES AND TECHNOLOGY

Carlos Viscasillas Vázquez

Chemical abundances of neutron capture elements in the Milky Way

DOCTORAL DISSERTATION
Natural sciences,
Physics (N 002)

VILNIUS 2022

This dissertation was written between 2017 and 2021 at Vilnius University (VU), Institute of Theoretical Physics and Astronomy (ITPA). The research was supported by the Research Council of Lithuania.

Academic supervisor:

Habil. Dr. Gražina Tautvaišienė (Vilnius University, Natural sciences, Physics, N 002).

Chairman – Habil. Dr. Gediminas Gaigalas (Vilnius University, Natural sciences, Physics, N 002).

Members:

Habil. Dr. Tamara Mishenina (I. I. Mechnikov Odessa National University, Natural sciences, Physics, N 002),

Prof. Dr. Paulius Miškinis (Vilnius Gediminas Technical University, Natural sciences, Physics, N 002)

Dr. Andres Moya Bedón (University of Valencia, Natural sciences, Physics, N 002),

Habil. Dr. Leonid Piliugin (Main Astronomical Observatory, National Academy of Sciences of Ukraine, Natural sciences, Physics, N 002).

The dissertation shall be defended at a public meeting of the Dissertation Defence Panel at 14 h on 14 of September, 2022, in National Center for Physical Sciences and Technology, A101 room. Address: Saulėtekio av. 3, LT–10257, Vilnius, Lithuania, tel. +370 5 2234637; email tfai@tfai.vu.lt

The text of this dissertation can be accessed at the libraries of Vilnius University and Center for Physical Sciences and Technology, as well as on the website of Vilnius University: www.vu.lt/lt/naujienos/ivykiu-kalendorius

https://doi.org/10.15388/vu.thesis.339

http://orcid.org/0000-0001-5415-2796

VILNIAUS UNIVERSITETAS

FIZINIŲ IR TECHNOLOGIJOS MOKSLŲ CENTRAS (FTMC)

Carlos Viscasillas Vázquez

Neutronų pagavimo cheminių elementų gausėjimo Paukščių Tako galaktikoje raida

DAKTARO DISERTACIJA

Gamtos mokslai,

fizika (N 002)

VILNIUS 2022

Disertacija rengta 2017– 2021 metais Vilniaus universiteto Teorinės fizikos ir astronomijos institute (TFAI). Mokslinius tyrimus rėmė Lietuvos mokslo taryba.

Mokslinė vadovė:

habil. dr. Gražina Tautvaišienė (Vilniaus universitetas, gamtos mokslai, fizika, N 002).

Gynimo taryba:

Pirmininkas – habil. dr. Gediminas Gaigalas (Vilniaus universitetas, gamtos mokslai, fizika, N 002).

Nariai:

habil. dr. Tamara Mishenina (I. I. Mechnikov Odessa National University, gamtos mokslai, fizika, N 002),

prof. dr. Paulius Miškinis (Vilniaus Gedimino technikos universitetas, gamtos mokslai, fizika, N 002),

dr. Andres Moya Bedón (University of Valencia, gamtos mokslai, fizika, N 002),

habil. dr. Leonid Piliugin (Main Astronomical Observatory, National Academy of Sciences of Ukraine, gamtos mokslai, fizika, N 002).

Disertacija ginama viešame Gynimo tarybos posėdyje 2022 m. rugsėjo mėn. 14 d. 14 val. Nacionalinio fizinių ir technologijos mokslų centro posėdžių salėje A101. Adresas: Saulėtekio al. 3, LT–10257, Vilnius, Lietuva, tel. +370 5 2234637; el. paštas tfai@tfai.vu.lt

Disertaciją galima peržiūrėti Vilniaus universiteto ir Fizinių ir technologijos mokslų centro bibliotekose ir Vilniaus universiteto interneto svetainėje adresu: https://www.vu.lt/naujienos/ivykiu-kalendorius

TABLE OF CONTENTS

List of Acronyms and Abbreviations

Term	Abbreviation
Asymptotic Giant Branch	AGB
Continuous Viewing Zone	CVZ
Equivalent width	EW
Gaia-ESO Survey	GES
Galactic Chemical Evolution	GCE
Hertzsprung–Russell diagram	HRD
Hyperfine structure	HFS
Initial Mass Function	IMF
Interstellar medium	ISM
Kernel density estimation	KDE
Lighter element primary process	LEPP
Low and intermediate-mass stars	LIMS
Main sequence	MS
Neutron star merger	NSM
Non-local thermodynamic equilibrium	NLTE
North Celestial Pole	NCP
North Ecliptic Pole	NEP
North Galactic Pole	NGP
Open cluster	OC
Ordinary Least Squares	OLS
Orthogonal distance regression	ODR
Pearson correlation coefficient	PCC
Planetary nebula	PN
PLAnetary Transits and Oscillations of stars	PLATO
Red giant branch	RGB
Ritchey–Chrétien telescope	RCT
Signal-to-noise ratio	SNR
Spectral type	SpT
Spectroscopic and Photometric Survey of the Northern Sky	SPFOT
Supernova	SN
Star formation history	SFH
Star Formation Rate	SFR
Transiting Exoplanet Survey Satellite	TESS
Turn off	TO
Vienna Atomic Line Data Base	VALD
Vilnius University Echelle Spectrograph	VUES
Weighted Least Squares	WLS
White dwarf	WD

Problem statement and relevance of the research topic

The understanding of the formation, structure and evolution of the Galaxy is one of the main open questions in astronomy. For a full comprehension, it is necessary to know precisely the chemical and kinematic properties of the different stellar populations, contrast them with Galactic models and simulations, and interrelate them to fit all the pieces of the galaxy puzzle. In this framework, the neutron-capture elements are a key tool. On the one hand, they have a different nucleosynthesis origin with respect to the lighter elements, up to Ni, which are formed by exothermic nuclear reactions during the stellar lifetimes. On the other hand, there are produced in multiple astrophysical sites, involving phenomena of different origin and nature and different timescales. These special features make the neutron-capture elements among the most interesting ones, with a very high potential to unveil different aspects of the Milky Way.

For instance, the variation with time of their abundance ratios allows us to infer the timescales of the evolution of the different Galactic components. On the one hand, we have elements produced by the rapid (*r*)-process, of a primary nature, whose origin is associated with massive stars (M $\geq$ 10 $M_{\odot}$) and SN type II; and on the other hand, we have elements of the slow (*s*)-process, of a secondary nature (products of the pre-existing iron "seeds"), associated both with helium burning cores in intermediate stars and with the thermal pulse (TP) helium shells in low and intermediate mass stars during their asymptotic giant branch (AGB) phase (Busso et al., 2001; Truran et al., 2002). The *r*-process nuclei are formed on time scales shorter than 100 Myr while most of the *s*-process nuclei are poured to the interstellar medium (ISM) on time scales larger than 1 Gyr. Such different timescales allow us to use the former as tracers of the evolution of the oldest component, i.e. the Galactic halo, and the latter as tracers of the evolution of the Galactic discs.

The problems that still persist with neutron-capture elements are varied, and at different levels. For example, the large scatter in the abundances of *r*-process elements in old metal-poor stars, which is not observed in other elements such as the α ones (François et al., 2007; Cowan et al., 2011; Matteucci, 2021), suggests that there may have been large inhomogeneities in the halo over very short time scales (see, e.g. Cescutti and Chiappini, 2014). The very recent announcement that the Milky Way's environment is not homogeneously mixed (De Cia et al., 2021) seems to sustain this hypothesis. On the other hand, the early appearance of Ba as well as fractions of [Eu/Fe] < 0 at the time of their appearance (e.g. Travaglio et al., 1999; Spite et al., 2018) represents another problem that still awaits for a good explanation (Matteucci, 2003).

In this context, the role of the dwarf galaxies in the formation of the Milky Way,

confirmed by the existence of stellar streams, have been shown to be an important factor to consider (Helmi et al., 2018). It still needs to be clarified with precision, and in this the neutron-capture elements play a key role once again. This problem is related to the metal-poor stars in the halo, some of which are *r*-rich and others are *r*-poor for the same metallicity. A clear example is found in the discovery of metal-poor stars in the halo of our Galaxy with an extremely high *r*-process enhancement and α-element deficiency (e.g. Xing et al., 2019). This type of stars has been found in present-day dwarf galaxies.

There are also many open questions about the contribution of various processes to the formation of these elements, and although many advances have been made in recent years, some of them are still unresolved (e.g. for the case of molybdenum). Moreover, there is still a lack of consensus on the astrophysical sites of the *r*-process and their yields, which are still under discussion. The traditional places for the ejection of the elements of the *r*-process, were revisited due the spectroscopic identification of *r*-process nucleosynthesis in a double neutron-star merger. That phenomenon, associated with the gravitational-wave source GW170817 confirmed a new scenario (Pian et al., 2017), which had already been proposed in the past by the group of F. Matteucci (Matteucci et al., 2014). The recent identification of a new type of supernovae through the event called VTJ121001+495647 (Dong et al., 2021), as well as the possibility that some massive stars collapse into a black hole directly without becoming a supernova (Mao et al., 2021) show us that there are still things to know about how exactly the chemical enrichment of the Galaxy occurs.

Neutron-capture elements can also help define the abundance gradients, whose existence is well agreed based on different data from various Galactic objects (e.g. HII regions, PNs, B stars, OCs), and as predicted by the models. Assuming an inside-out disc formation, the gradients would be induced by the variations of the gas fraction, the star formation rate (SFR), initial mass function (IMF), and the stellar yields along the Galactic disc. The abundance gradients for elements up to Fe are well established for a few decades (e.g. Maciel and Koppen, 1994; Gummersbach et al., 1998; Friel, 1999), although a broader consensus is still necessary for the neutron-capture elements. In this thesis, special attention is paid to this, analysing in detail the abundance gradients of neutron-capture elements as a function of age, the mean galactocentric distance and the maximum vertical height above the Galactic midplane, for the thin-thick discs.

Moreover, only recently that the great contribution that *s*-elements can make as tracers of stellar ages has been realised. In the era of Gaia and the large spectroscopic surveys, where astrometrics and chemistry of considerable amounts of stars are combined, the missing variable is time. The age of the stars is then one

of the most coveted parameters in astronomy. Its knowledge involves placing the stars and astronomical events at specific times. Some attempts for its determination based on different techniques has proliferated in the last decades (Soderblom, 2010; Howes et al., 2019). An example is the isochrone fitting method, whose use is more widespread, where observed and derived parameters are compared with theoretical values. However, that method gives unsatisfactory results for stars on the main sequence and the giant branch in the Hertzsprung-Russel (HR) diagram, where the isochrones are particularly congested. In the search for new and more reliable techniques, the abundances of neutron-capture elements have been revealed in recent years also as excellent age indicators in stellar clusters and solar twins, but usually in a limited volume close to the Sun. Their use as cosmic clocks is currently a hot topic in astronomy, in refinement and discussion (e.g. Morel et al., 2021) and their ranges of applicability have to be extended and further specified. This thesis also makes a contribution to its knowledge.

Finally, and related to the above is the problem of the complex behavior of the elements of the *s*-process at young ages (D'Orazi et al., 2022). Unusual enhancements of [Ba/Fe] in the young open clusters populations have been observed in recent years (D'Orazi et al., 2009; Baratella et al., 2021). There is a disagreement in the literature regarding its behavior compared to that of other *s*-process elements. It has not yet been possible to explain these enhancements, so the so-called Ba puzzle is another issue related to neutron-capture elements that remains unsolved.

All of the above are some of the main problems involving the neutron-capture elements, some of them addressed in this thesis to a greater or lesser extent.

Aims and tasks

Neutron-capture elements, due to the specificity of their nucleosynthesis processes, as well as their astrophysical sites of origin, provide privileged information on the formation and evolution of the Galaxy. The main objective of this thesis is to review the state-of-the-art in this field, show its high potential, and contribute to its better knowledge by identifying its role in the solar neighbourhood first, and hence, in the Galactic disc.

To achieve this goal, the abundance trends of 10 elements of the *s*- and *r*-processes in various ranges of metallicity, age, mean galactocentric distance, and maximum height from the Galactic mid-plane are analysed in detail, all of which are interrelated. For this, the spectra of more than half a thousand FGK bright stars ($V < 8$ mag) were analysed. These stars are placed in the Kiel Diagram as main sequence (dwarfs) and evolved stars (subgiants and giants). The sample is divided into the thin and thick components of the Galactic disc, which make possible to identify their different evolutionary histories.

Since neutron-capture elements, depending on their production sites, belong to different classification groups and subgroups, among our tasks is also to identify their differentiated behaviour, to determine their spatial and temporal gradients with precision, as well as evaluate their use as cosmic clocks and their ranges of applicability in the components of the Galactic disc. For this task, we also rely on a sample of open clusters observed in the Gaia ESO Survey (GES, Gilmore et al. 2012 and Randich et al. 2013), the largest used so far for this purpose, with the aim of extending the analysis to a larger galactocentric distance.

Our goals include the interpretation, comparison and a critical analysis of the results in the Galactic context, and the discussion in light of the state-of-the-art in the field, as well as the comparison with some of the most recent theoretical models.

Scientific novelty and statements for defence

The first part of this thesis analyses bright stars in the solar neighbourhood with high resolution spectroscopy, which together with the methodology used based on synthetic spectra, guarantees accurate and high-quality results. For most of the stars studied in this thesis, it is the first time that their abundances of neutron-capture elements are provided, so their future usefulness may be of high value. In addition, the fact that these stars are targets of the TESS and PLATO space missions also increases their future potential. The number of stars studied, which exceed half a thousand, as well as the large number of neutron-capture elements analysed, includes less studied elements such as Sr, Pr and Sm, as well as the most representative of each process. The high number of elements also allows a comparison between the ones of the *s*-process, *r*-process and mixed. Likewise, the separation of the stars into the thin and thick discs allows a differentiated study of neutron capture processes in those Galactic components. On the other hand, another part of the thesis uses a sample of open clusters from the sixth internal data release of the Gaia-ESO survey (GES) to calibrate stellar ages and abundance ratios, comparing *s*-process elements to alpha-elements [s/α]. The powerful results of the Gaia mission are amplified here by combining them with ground-based large spectroscopic surveys such as GES. Open clusters offer the unique advantage of allowing a more precise measurement of their ages and distances than isolated stars, as well as more reliable measurements of their chemical composition, placing them among the best tracers of the chemical evolution of our Galaxy. Thanks to the wide Galactocentric coverage of our clusters sample, the largest one so far used at this stage (62 clusters), we investigated the radial variations of the shape of the relations. Given the above, the following is stated:

An evaluation of the **[El/Fe I] ratios as a function of metallicity** is provided first, comparing the results with the GCE models. We found a particular trend for each element according to its origin and in general in good agreement with the literature. On the other hand, the observations suggest that for the elements of the second *s*-process peak, modifications should be made to the inputs in the models used. **Specifically, the models of Prantzos et al. (2018) could reach a better agreement with the observations if the LIMS input at higher metallicities (about −0.7 dex) were taken into account, which would shift the maximum to approximately [Fe/H] = −0.2 dex.** Regarding the behavior of the **thin and thick disc populations** in our sample, for some elements **a clear distinction is observed between both components of the Galactic disc, especially for Ba and Eu**, representative elements of the pure *s*-process and *r*-process, respectively; while **for other elements both populations seem to intermingle**. We also tested the

[hs/ls] ratio to monitor the *s*-process efficiency and the reliability of the GCE models, finding a clearly **differentiated behavior for the thin and thick Galactic discs**. It is also made a comparison of the *r*-process and α-elements, through the Eu and Mg. We found **for thick-disc stars an evident decrease in [Eu/Mg] with increasing metallicity compared to the thin-disc stars**, which proves a different chemical evolution of the Galactic thin and thick discs. Regarding the variation of [El/Fe] as a function of [Fe/H] in our sample of open clusters, **the clusters in the outer disc are generally more metal poor than the clusters in the inner and in the solar region**, while the differences in [El/Fe] are less pronounced.

Abundance gradients are also provided with precision. Thus, with regard to **age gradients**, we found abundance correlations consistent with the nature of each group of elements, in the GCE context and with the available literature. Therefore, **in the thin disc we find the elements of the first *s*-process peak Y, Sr and the element of the second *s*-process peak Ba showing a clear anti-correlation with age; and on the other hand the mixed element Pr, and the *r*-process dominated elements Sm and Eu showing a positive gradient**. Concerning the **age gradients on the thick disc**, they have a **similar behavior, but with a tendency to soften or disappear**. Also for the youngest stars of our thin-disc sample, **we did not find evidence of the barium abundance anomaly (also known as "barium puzzle").**

Regarding the **age gradients in our open clusters sample**, we find that the **[El/Fe] are underabundant for a given age in the inner disc (R_{gc} < 7 kpc) with respect to those of the outermost regions**. We also found a **decreasing gradient with stellar age**, being the **[Ba/Fe] the one with the strongest trend**. For all *s*-process dominated elements, **the slope of the regression is steeper in the inner disc than in the other regions**.

The spatial gradients of neutron-capture elements, which we were able to obtain thanks to access to the Gaia data, are also provided and discussed. Specifically, we calculate them for the mean galactocentric distances and maximum vertical distance. These gradients are very scarce in the literature, so their value is remarkable.

The radial abundance-to-iron gradients in the thin disc are negligible for the *s*-process dominated elements and become positive for the *r*-process dominated elements. The vertical gradients are negative for the light *s*-process dominated elements and become positive for the *r*-process dominated elements. In the thick disc, the radial abundance-to-iron slopes are negligible, and the vertical slopes are predominantly negative.

Regarding our findings on cosmic clocks, we sampled the most sensitive and reliable *s*-process and α-elements in Galactic disc stars and open clusters. In the **thin disc** of Solar vicinity we obtained the relation **[Y/Mg]$_{thin}$=0.022(±0.015)−0.027 (±0.003)·age [Gyr]** based on 371 stars which is similar to the relation found in the

AMBRE project based on 325 stars. This shows that for the Solar vicinity stars the [Y/Mg]-age relation is rather robust. **[Y/Al], [Sr/Al], and [Sr/Mg] also can be used as age indicators**. For this relation we also found that **differences in mean galactocentric distances for different samples can lead to variations in the coefficients of the stellar dating relations**. Regarding the **thick disc**, we expanded the sample taking data from other works and in a broader age and metallicity range, finding that the slope is negligible, which shows its different evolutionary history and its **disability as an age indicator**. Regarding the **open clusters**, we provide ten different relationships: five based on Y and five based on Ba. We confirm that **there is no single age-chemical clock relationship valid for the whole disc, but that there is a dependence on the Galactocentric position**, related to the radial variation of the star formation history (SFH), combined with the non-monotonic dependence on metallicity of the yields of the *s*-process elements from low- and intermediate-mass stars. We also found that **the abundance ratios [Ba/α] are more sensitive to age than those with [Y/α] for young disc stars, and their slopes vary less with Galactocentric distance**.The thesis also provides observational evidence **for the non-universality applicability of the [Y/Mg] ratio as cosmic-clock due to the different efficiency of the *s*-process at high metallicity**.

As a corollary we can state that all these results seen as a whole are consistent with each other, and in agreement with the origin of the *s*-process and *r*-process dominated elements, their production sites, their solar contributions, and in the framework of the time-delay model and the Galactic formation.

Personal contribution

The main part of this thesis, based on data obtained at the Molėtai Astronomical Observatory, was carried out entirely in Lithuania, through collaborative work done by the Astro-spectroscopy and Exoplanets Team, and with own infrastructures of Vilnius University. The data collection and reduction was carried out by the aforementioned team. The personal contribution of the author include preparation of the atomic data, pre-selection of spectral lines, analysis of the hyperfine structure (HFS); and partially the abundances determination and calculations of parameters such as ages, orbits and kinematics; as well as the complete processing of data, statistical treatment, investigation, conceptualization, and its critical and scientific analysis, original draft preparation, visualization, review and editing, all under the supervision of the thesis director.

Part of the thesis uses data from UVES, the high-resolution optical spectrograph of the Very Large Telescope (VLT), operated by the European Southern Observatory (ESO) on Cerro Paranal (Chile). The work was carried out within the framework of the consortium of the Gaia-ESO survey (GES), involving an international team of astronomers and institutes. This includes data analysis tasks such as abundances normalization, stellar membership to open clusters, derivation of ages and orbits, statistical treatment, as well as conceptualization and final scientific analysis. Part of that work was carried out by the author *in situ* at the INAF-Arcetri Astronomical Observatory in Italy during a granted COST scientific mission.

Structure of the dissertation

The core of this thesis consists of 6 chapters, preceded by the preliminary pages and ending with the bibliography, also including an appendix with auxiliary figures and tables. The chapters are distributed as follows:

- The *first chapter* is introductory and is devoted to the definition and classification of the neutron-capture elements, its role in the chemical evolution of the Galaxy, their astrophysical sites, and to contextualize the problem.
- The *second chapter* makes a detailed description of the sample and the methods used to achieve the objectives of the thesis, including an explanation of the abundance determination and their uncertainties, as well as the calculation of ages and orbits, separation of components and membership selection to the clusters.
- The *third chapter* deals with the abundance ratios of neutron-capture elements in metallicity, dividing the elements into groups and comparing them with each other and for the two components of the galactic disc.
- The *fourth chapter* analyzes the abundance gradients of neutron-capture elements in age and in the radial and vertical directions.
- The *fifth chapter* is dedicated to the use and application of abundances of neutron-capture elements to derive ages (the so-called cosmic clocks), both for the stars of the solar neighborhood and for the open clusters sample.
- In the *sixth chapter* a short review of the contents is made, the conclusions are presented, and the future prospects are glimpsed.

1. INTRODUCTION

1.1. Preamble and framework

The progress in astronomy has always gone hand in hand to the development of new technologies. Astronomers have sought the applications of new advances in physics and engineering through astronomical instrumentation. Two key moments were the appearance of the telescope and the spectroscope, which produced a huge leap in this branch of knowledge. The spectroscopes point out the birth of astrophysics, and thanks to which the composition and other fundamental properties of stars could be known. Newton's findings first, and Fraunhofer's improvements later, were followed by Kirchhoff and Bunsen's explanations based on laboratory results, laying the foundation for modern spectroscopy. After this, a new task of comparing the laboratory and observatory results begins. The pioneers in this were Rutherfurd (1863), Donati (1863), and Huggins and Miller (1864) who identified the spectral lines of some already known elements in some of the brightest stars. Contemporaneously with these, Secchi was developing a system of stellar classification based on spectra for thousands of stars. At that time some elements such as He, a fundamental component of the stars, had not yet been discovered. The move from spectroscopes to spectrographs occurred with the first photograph of a stellar spectrum (Vega) in 1872, thanks to Draper Jr., who developed a technique based on calotypes. From then on, the spectra could be properly recorded for later analysis.

The development of astro-spectroscopy gave way to the study of stellar atmospheres through the so-called chemical abundances. Chemical analyses were then inaugurated, a discipline already centuries old. At this point, the doctoral thesis of Payne (1925) was a revolution. Until then it was thought that the chemical composition of stellar atmospheres was similar to that of the Earth's crust. She determined the relative abundances of 18 elements in different types of stars, finding that their chemical composition was almost the same for all of them, and H and He were the most abundant elements. This was in accordance with the suggestions of Eddington (1919), who a few years earlier had proposed hydrogen as the possible source of stellar energy. At this point, the discovery of the curve of growth by Minnaert and Slob (1931) marked the beginning of a new stage for the analysis of stellar spectra, establishing the relationship between the width of a spectral line and the number of the effective absorbing atoms. Another milestone

was the appearance of the first photospheric model of the solar atmosphere by Strömgren (1940). Afterwards, studies have been carried out trying to determine the chemical composition of stellar atmospheres with precision, but at that time the origin of the elements in the stars was still unknown. This was possible thanks to the progress of nuclear physics, and its application to nuclear astrophysics. The discovery of the neutron and artificial radioactivity gave way to the discovery of neutron-induced radioactivity by Fermi (1934). Thereby the advances in nuclear physics led to the advent of stellar nucleosynthesis studies, with pioneering works such as Bethe (1939) deriving the CNO cycle, and culminating with the complete explanation given by Burbidge et al. (1957), laying the foundations to know how elements are formed in stars. Initially it had been thought that all the elements had been synthesized during the Big Bang (Alpher, 1948), but later work established that this only happened for the lightest elements (mainly H and He). As explained in the aforementioned Burbidge et al. (1957), the elements up to Fe are formed inside stars by nuclear fusion, and only the heaviest elements are formed by neutron capture reactions, which are the object of this thesis. With the advent of modern spectrographs, it was possible to determine the chemical compositions of stellar atmospheres with high precision, fostering synergy between theoretical nucleosynthesis and astronomical observations.

In addition to the stellar mechanisms by which stars synthesize new elements in their interior, another crucial factor is to know how they return them to the environment. This is determined mainly by its initial mass, and also by its metallicity, defining how the star will die and how will return mass to the medium. Thus, stars can return nuclides to the medium during their lifetime (through stellar winds), or at the end of this (through a supernova). In this sense, the stars are the chemical engine of the Galaxy, constantly enriching the interstellar medium (ISM) with baryonic matter. In the same way as the "water cycle" on Earth, in which water moves from one reservoir to another by physical processes, we can speak of the cycle of interstellar matter or the star-gas-star cycle. The ways in which the stars of different classes renew the Galactic environment with fresh elements are very diverse and at different rates, but almost always related to the end of their lives. This phenomenon is ubiquitous in several phases of stellar evolution. For example, de Jager et al. (1988) made a general study of the mass loss rates in the Hertzsprung-Russell diagram including population I stars from O to M SpTs. Thus, the return of mass to the medium occurs in different phases of stellar evolution, some of which are shown below: mass loss during the asymptotic giant branch

(AGB) phase (e.g. Bloecker, 1995), which removes most of the envelope from a star to form a planetary nebula (PN); less studied is the mass loss during the red giant branch (RGB) phase (e.g. Deutsch, 1959); during the mass transfer due to the gravitational attraction of a binary companion (e.g. Huang, 1956); flares, also known as coronal mass ejections (CMEs) and thermal winds in dwarf stars (e.g. Coleman and Worden, 1976); mass loss due to stellar winds in massive stars such as Wolf Rayet (WR) (e.g. Nugis and Lamers, 2000) or during the red supergiant (RSG) phase (e.g. Mauron and Josselin, 2011); and even mass loss due to pulsating neutron stars (NS) (Stothers, 1969) and neutron stars binaries (Meszaros and Rees, 1992); and finally, the supernovae (SNs), which are the great actors and major contributors to Galactic enrichment, where the massive stellar progenitor spreads most of its mass to the ISM. Its quantity is determined by the so-called Supernova Rate (SNr) (e.g. Tammann et al., 1994), which together with the yields are crucial factors to understand the chemical evolution of the Galaxy. Given that the initial mass of the stars is a determining factor of the end of their lives and how they will enrich the environment, the rate at which this occurs depends on the probability that a star is born with a certain mass. But not all the matter of the stars is recycled and returns to the ISM, part of it remains blocked by the so-called stellar remnants (or compact stars), such as white dwarfs, neutron stars and black holes, which suggests that more and more matter remains fixed. Other objects like brown dwarfs or planets also retain matter. All of the above indicates that the mixture is not homogeneous, occurs at different speeds and varies over time. A quantity of the matter returned by the stars to the ISM was synthesized inside of them during its lifetime, however, another amount was already pre-existing when it was formed. Thus, we can define the concept of stellar yield, differentiating the elements restored to the medium between the newly synthesized ones and those that were already present at the time of their formation, and only then know how the medium is chemically enriched.

All the mass returned to the medium by the stars comes to mix with the already existing ISM matter, formed by the hydrogen and helium of the primordial nucleosynthesis and with the heavier elements returned by previous generations of stars, together with the dust particles and cosmic rays. In this way, the ISM of the Galaxy is undergoing a progressive enrichment. It is in the resulting enriched ISM, in its densest regions, where the new generations of stars are formed. This will depend, among other factors, on the way the matter is found (ionic, atomic, or molecular) and its physical properties (temperature and density). And this is where another crucial factor in the chemical evolution of the galaxy comes into play,

which is a consequence of the previous one: the birthrate function. This involves the concepts of star formation rate SFR, the rate at which new stars are formed from the gas, and the initial mass function (IMF), which describes the initial mass distribution for a stellar population. The SFR thus defines the total mass of stars formed per year (usually given as solar masses per year) and its variation over time and space defines the so-called star formation history (SFH). The first idea of a link between interstellar gas density and SFR was given by Schmidt (1959), the so-called Schmidt law, where ν describes the star formation efficiency. Other expressions for the SFR based on the previous one were given by successive authors (e.g. Talbot and Arnett, 1975; Dopita and Ryder, 1994; Boissier and Prantzos, 1999). It should also be noted that since all the deuterium (D) in the universe is thought to be of primordial origin (Epstein et al., 1976), and the stars deplete it during the PMS (Bodenheimer, 1966), there is a proportional relationship between the D abundance decrease in interstellar gas and the SFR. The most recent observations point out that the star formation is triggered by cloud–cloud collisions, rather than single gas clouds collapsing (Fukui et al., 2021).

On the other hand, the IMF describes the mass distribution of stars when at the moment of their formation, that is, when they enter the MS and the hydrogen fusion reactions begin. The relationship between the IMF and the SFR is thus evident. It was first proposed by Salpeter (1955) and later improved by other authors (e.g. Miller and Scalo, 1979; Scalo, 1986; Kroupa et al., 1993; Kroupa, 2001; Chabrier, 2003; Weidner and Kroupa, 2005).

Another factor that must be taken into account is the gas flows that occur in the Galaxy, both in and out. On a Galactic scale, the combined effect of multiple supernovae can heat up and expel gas from the ISM to the IGM. That same gas could return to the ISM due to the effect of gravity and continue to favor star formation. It is known that the Galactic halo is populated by high-velocity clouds (HVCs), from which baryonic matter falls to the Galactic disc, favoring the SFR. On the other hand, there are some traces that there is a circulating gas between the disc and the Galactic halo caused by supernovae. These heat and drive the ISM of the disc outwards, forming a halo of hot gas, also observed in other spiral galaxies, and that when it cools returns to the disc in the form of condensed clouds. They are the so-called Galactic fountains (Shapiro and Field, 1976; Bregman, 1980).

Other material entering the galaxy may be due to accretion and interactions from satellite galaxies, and that also influences the properties of ISM, and consequently, the SFR and the IMF. Indeed, the role of the dwarf galaxies that collided and

merged with the Milky Way is increasingly being shown as an important factor in their chemical evolution. So far several of the most massive have already been identified, such as Gaia-Enceladus (Helmi et al., 2018), the Helmi streams (Helmi et al., 1999), Sequoia (Myeong et al., 2019) and Sagittarius (Ibata et al., 1994; Lynden-Bell and Lynden-Bell, 1995), and others have been proposed, such as the Kraken galaxy (Kruijssen et al., 2020). Spectroscopic analysis also revealed *r*-process-rich stellar streams in the Milky Way (e.g. Helmi stream), suggesting that the progenitors of these stellar associations were prolific in *r*-process events (Gull et al., 2021). Evidence of these events they are not far from us, and has also been found in the vicinity of the Sun passing by our solar neighbourhood in the opposite direction to the other stars born in the disc. However, we can also find debris in prograde motion such as Nyx, a vast stellar stream which is interpreted as the remnant of a disrupted dwarf galaxy (Necib et al., 2020). On the contrary, new studies of the MW analog galaxy UGC 10738, which is seen from "edge on" suggest that galaxies like ours are common and that the thin and the thick disc is not the product of a violent merger but of their natural evolution (Scott et al., 2021). Therefore, the issue is still under debate, and the role of chemical abundances is remarkably important. All those events that happened in the history of our galaxy left their chemical trail in the stars, allowing us to go back in time and rebuild the past.

Everything mentioned above must fit with the observational constraints, that is, the solar abundance pattern, the G-dwarf distribution, the evolution of abundance ratios, the PDSFR and SN rates, age-metallicity relation, gas and abundance gradients, and isotopic abundances.

Another important aspect worth mentioning is the time lag in the production of the α-elements and iron. The α-elements, say O, Ne, Mg, Si, S, Ca and Ti, all of them of even atomic number, have their origin in massive stars (M > $10M_{\odot}$) that explode in SN type II and with a life range between 1-10 Myrs; while iron is supposed to have an origin mainly in SN type Ia, which involve WD in binary systems, of much longer life, which implies time ranges between 10 Myr and 10 Gyr. This delay in the production of the bulk of the Fe can be used to infer time scales in the formation of the Galaxy. That is why the [O/Fe] versus [Fe/H] observed shows a strong descent or "knee" at [Fe/H] = -1 in the solar neighbourhood, making the [O/Fe] ratio an excellent Galactic clock (Matteucci and Francois, 1992). On the other hand, it should be noted that the [O/Fe] ratio has great sensitivity to SFH, where the traces of the different evolution of the Galactic components are

reflected. Thus, in the context of the time delay model, the enrichment of Galactic components (e.g. halo, thick disc, thin disc, bulge) occurred at different speeds and efficiencies. For example, the models show a faster SFH in the bulge, where the gas would be more abundant and dense and the enrichment faster; an intermediate SFH in the solar neighbourhood, and slower in the outer Galactic regions or in outer galaxies such as the Small Magellanic Cloud (SMC) or the Large Magellanic Cloud (LMC), producing the decline or "knee" from higher to lower metallicity respectively (see, e.g. Matteucci, 2003).

All of the above and draw the different scenarios and gave rise to different models of the chemical enrichment of the Galaxy, many of them based on the so-called "inside-out" scenario of Larson (1976) and the "time delay" model of Pagel (1989). On a similar basis, the model of Chiappini et al. (1997) assumes that the Galaxy formed during two infall episodes, the first one giving rise to the halo, the bulge and most of the thick disc, and the second one to the thin disc. That model proposes that during the second infall the gas accumulated preferentially in the inner disc, which gave rise to a faster chemical enrichment of these region, which would explain a natural gradient in the disc. Indeed, different models of Galactic formation have been proposed in the past decades. Those that suggest the formation from a protogalactic single cloud, two clouds, or by the aggregation of fragments of multiple clouds. Examples of the first are found in the "ELS" model (Eggen et al., 1962); the "serial" model (Chiosi, 1980); and the "parallel" model (Pardi et al., 1995). On the other hand the aforementioned "two infall" model (Chiappini et al., 1997) and the models based on multiple clouds fragments aggregations and the hierarchical merging hypothesis (e.g. Searle and Zinn, 1978; White and Rees, 1978). The models can also be seen from the perspective of the input and output Galactic flows, from their absence ("closed box") formulated in the "simple model" (Tinsley, 1980) to the "extreme infall model" (Larson, 1976), "biased galactic wind model" (Recchi et al., 2008), "radial flows model" (Portinari and Chiosi, 2000), or a combination of them. That the Galaxy has increased in mass throughout its history due to the infall of gas seems evidenced by the relatively low amount of metal deficient G-dwarf stars with respect to what one might expect from the Simple model. It is the so-called "G-dwarf problem" (e.g. Pagel and Patchett, 1975), also observed in K and M dwarfs (Woolf and West, 2012) and in other galaxies (Worthey et al., 1996). Another clue is given by Gratton et al. (2000) investigations, who found a "gap" during the transition from the thick to thin disc phases in the solar neighbourhood in which α-elements were not produced. Thus, they observed

increases in [Fe/O] and [Fe/Mg] of approximately 0.2 dex while the [O/H] and [Mg/H] ratios remained constant, indicating a sudden decrease in the SFR. Recent studies based on spectral energy distribution suggest that the bulges in galaxies like ours were formed in two waves, those of the first with a very fast formation rate, and those of the second with slower formation (Costantin et al., 2021). Due to the complexity of the issue, current models of the Milky Way also involve N-body and hydrodynamic simulations (e.g. smoothed particle hydrodynamics method) and cosmological simulations.

In the exposed context, the role of the neutron-capture elements is crucial, since they leave their traces in the processes described above, being essential pieces to unravel the puzzle. Thus, in addition to its different synthesis mechanism, the neutron-capture elements production is site-specific and involve long and short-lived stars. Because of that, by studying their chemical abundances it is also possible to unravel some of the keys to the formation, structure and evolution of the Milky Way. The synergy between observations and theory gave rise to the first models of neutron-capture elements. In that purpose also noteworthy are the efforts of Clayton et al. (1961) by calculating the first time-dependent models of neutron-capture elements of both processes, and the semi-empirical models by Pagel and Tautvaisiene (1997), the first attempt to model evolution of the neutron-capture elements elements in the Galaxy.

At the observational level, once the chemical composition of the individual stars was known, and the mechanisms by which the stars accrete, synthesize and spread the elements, the next step was their study at a global level for the different stellar populations in the Galactic context. I end this section with the words of Chiappini (2001) defining our Galaxy as *a highly evolved entity (...) not merely a random assortment of stars, like so many grains of sand on a beach, it is an elegant structure that shows both order and complexity*.

1.2. neutron-capture elements. Classification and nucleosynthesis

The elements of the periodic table can be classified in various ways, according to the purpose or field of interest. One of them is due to its nucleosynthesis of origin (primordial, stellar, supernova and interstellar), which is of interest in astrophysics. In addition, and to associate them with its production processes, the chemical elements can be divided between elements lighter and heavier than iron (trans-Fe

elements). This is so because the binding energy of nucleus particles around iron is the maximum (*vide* Figure 1-1).

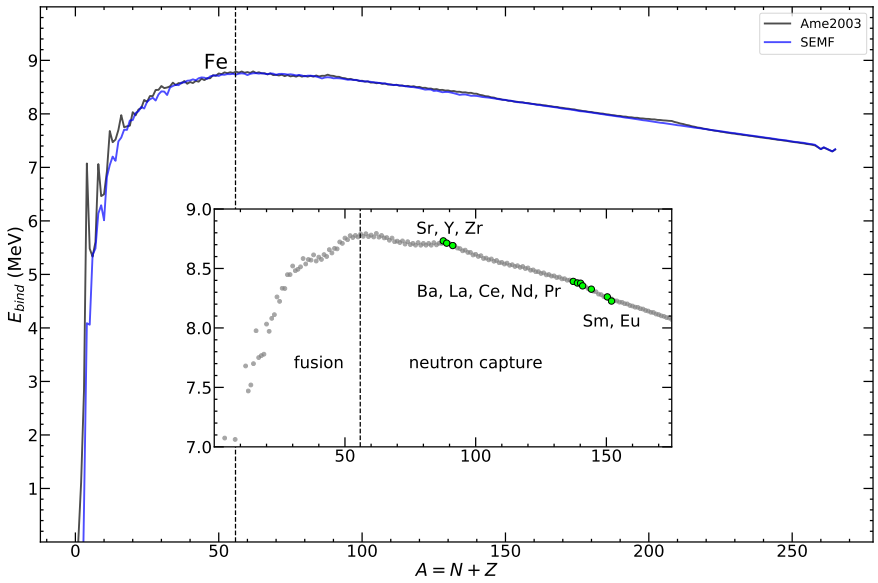

Figure 1-1: Recommended by NEA and SEMF approximation Binding energy per nucleon (MeV) against atomic mass (A). The inner panel shows in more detail the position of the neutron-capture elements related to this thesis.

The above implies that the nucleosynthesis reactions of the elements up to iron are fusion and exothermic; and the heaviest elements up to uranium are endothermic and by neutron capture. This, as we will see in the next section 1.4, is related to their astrophysical sites of origin. Beyond iron, due to the increasing number of protons, electrostatic forces tend to dominate over strong nuclear forces, which are short range and between neighbours, and the atomic nucleus tends to break (e.g. nuclear fission reactions). This effect is more significant from the heaviest elements, such as $^{210}_{84}$Po, in which the nuclei cannot bear so much positive charge, and they emit their excess protons in the form of alpha particles through a spontaneous nuclear fission process. Neutrons can penetrate the atomic nucleus without having to overcome the Coulomb electrostatic barrier, and this is the basis of neutron capture reactions, which play an important role in cosmic nucleosynthesis. In the Figure 1-2 we show a periodic table of the elements highlighting the neutron-capture elements from krypton ($Z > 35$), for which their nucleosynthesis and formation environments are best known, and up to polonium ($Z < 84$).

In neutron capture reactions, when a neutron penetrates the initial seed nucleus,

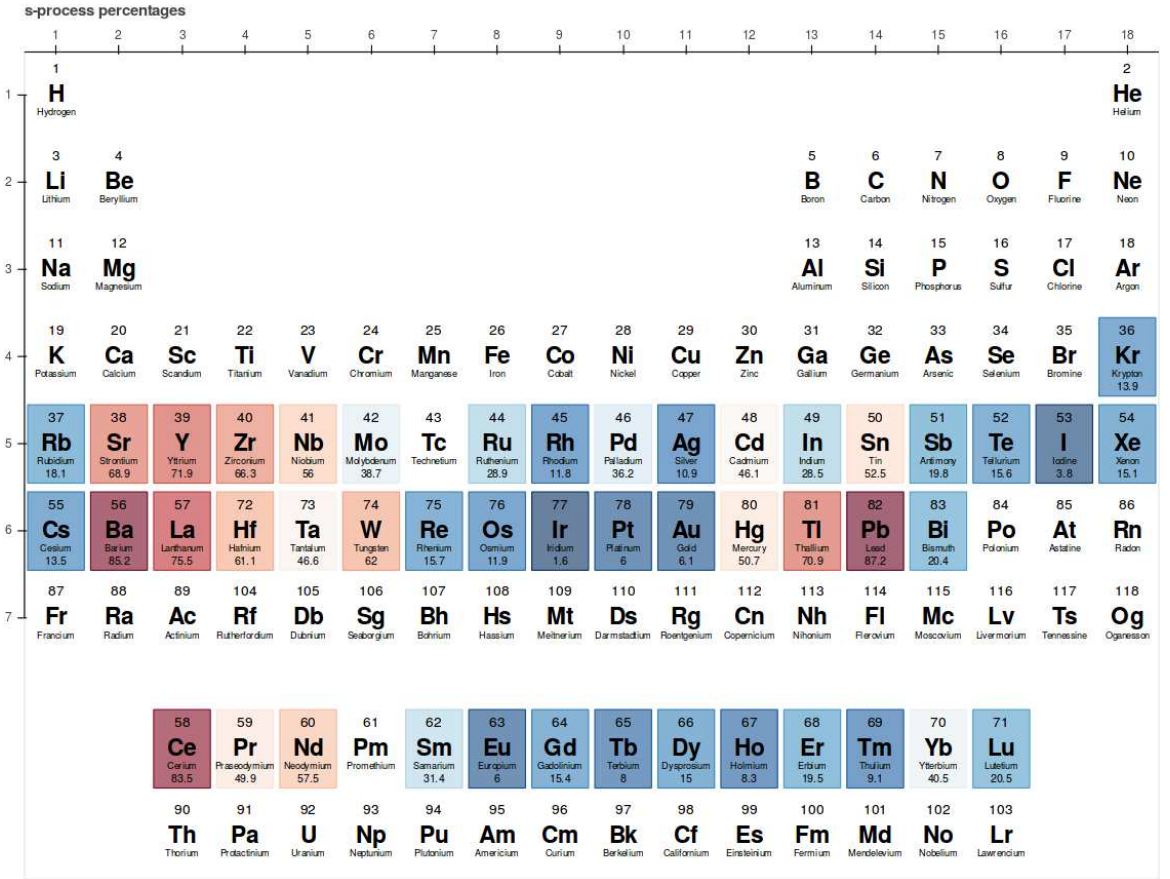

Figure 1-2: Periodic table of elements with colour code according to the solar *s*-process contributions (in %) for the neutron-capture elements [generated by the author using Mentel (2014–) and adapting the values obtained by Bisterzo et al. (2014)]

an isotope with a higher atomic mass ($A + 1$) is formed and a gamma particle is released. If the newly formed isotope is stable, successive increases in atomic mass can occur, but if the isotope is unstable, then it is beta emitter, and is transmuted into an element of a higher atomic number ($Z + 1$).

A key parameter that defines the different neutron capture processes and the relative abundances of elements and isotopes produced is the neutron flux. The neutron source and its gradient in time is given by the number of neutrons and their velocity, and its units are cm^2s^{-1}. Together with the neutron cross section, both allow to estimate the reaction rates, and are key to the different processes inside the stars. If the time between a neutron penetrating the atomic nucleus and the next neutron is long enough for beta decay to occur before another neutron is captured ($\tau_\beta \ll \tau_n$), then we speak of an *s*-process (slow, time up to thousands of years); and if the neutron bombardment occurs rapidly, without sufficient time for radioactive decay to occur before capturing another neutron ($\tau_\beta \gg \tau_n$), then it is *r*-process (fast, fractions of second). The flows necessary for the *s*-process are in the order of $10^7 - 10^{11}$ cm^2s^{-1}, and 10^{20} cm^2s^{-1} for the *r*-process, which can reach into the exotic neutron-rich region and synthesise the heaviest isotopes near the Neutron drip line.

It is also important to point out that the *s*-process is secondary in nature, in the sense that it needs the pre-existence of isotopes of heavy elements to generate new ones; while the *r*-process is primary in nature, generating the seed nuclei by itself. This has important implications for the astrophysical sites that generate them, as we will see in the section 1.4.

There are thus several classifications for neutron-capture elements. The first according to the dominant process, as we will see in the next section; the second, according to its atomic weight, thus, for the *s*-process we can divide them into light and heavy (hereafter ls and hs respectively), depending on whether they are in the first or second peak; and the third according to their origin, we find the "main", "weak" and "strong" *s*-process, as we will see in the section 1.4. In the diagram of the Figure 1-3 we show this classification.

1.3. Abundances in the Sun and Solar System

In the chemical composition of the different celestial objects are the traces of the formation and evolution of the universe. Once the chemical composition of the

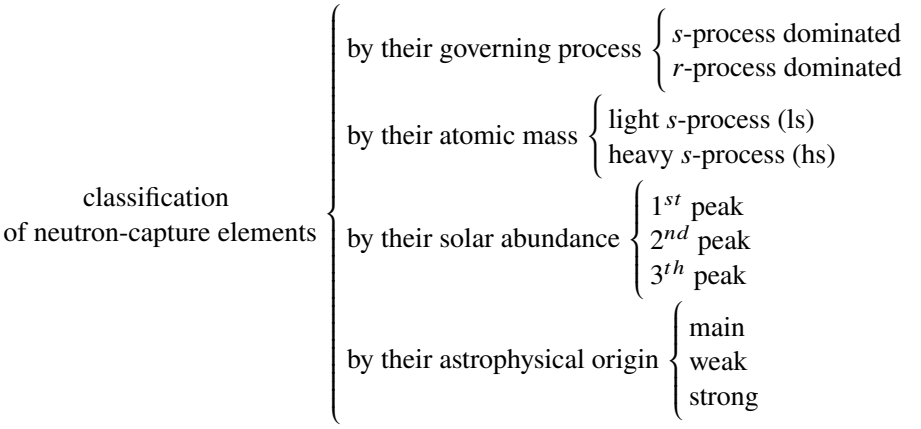

Figure 1-3: Classification of neutron-capture elements by their different nature

Earth's crust and the atmosphere was known in detail, the next step was to study the composition of our Sun, the closest star. The space missions also gave the possibility of taking samples from the Moon (e.g. Apollo), the planets, asteroids and comets of our Solar System (e.g. Hayabusa, Rosetta), and even travel outside of it. Studies can also be done with observations from the ground, analysing the reflected spectrum, when transits occur, or studying meteorites that fall to Earth naturally. The main neutron-capture elements found in stellar atmospheres and which are the object of this study, are relatively abundant in the Earth's crust. Some are part of the so-called rare-earth (lanthanides) and alkaline Earth metals, which are so named in the context of their physical and chemical properties. The former include Y, La, Ce, Pr, Nd, Sm, and Eu, and the latter include Sr and Ba. The Sun is therefore the star that we can best know, our standard star. It soon became known that the composition of the stars was very different from that of the Earth's crust.

Knowing the properties of the Sun, and specifically its chemical composition, is key in many fields of astronomy, since most cosmic objects are referenced to it. The study of the solar spectrum was inaugurated with Wollaston (1802), and his discovery of the absorption lines. More than a century later the relative abundance of the elements in the Sun began to be quantitatively studied. In those first steps, the work of Payne (1925) already included the abundances of several neutron-capture elements (Sr, Y and Ba). Three years later St. John and Moore (1928) identified the presence of La, Ce, Pr, Nd, and Eu, among other elements, in the Sun's atmosphere. Later, in Russell's pioneering work (Russell, 1929), the abundances of almost all

the elements in the Sun appear, including the ten neutron-capture elements studied in this thesis. Thanks to Stromgen's atmospheric models, Unsöld (1948) was able to determine the detailed composition of the solar atmosphere by calculating the abundances of the elements. From there, the studies continued improving the techniques of analysis and refining the results.

Since the Sun contains almost the entire mass of the Solar System, the Sun's composition should be representative of the composition of the entire Solar System, except for the deuterium consumed by the early Sun during the T-Tauri phase in the pre-main-sequence (PMS). Indeed, this is the reason for the absence of deuterium in the solar photosphere (Lodders, 2019). Furthermore, the Sun is in the main sequence (MS) and the transformations due to nuclear fusion remain in the core. However, a portion of the helium and heavy elements have settled from the photosphere towards the center by gravity. That is why meteorites are important to know the composition of the protostellar Sun, taking into account that they have not reached melting temperatures, in addition to the possibility of analysing them in the laboratory. Thus, this was visible in the good agreement between the abundances presented by Suess and Urey (1956) for the Sun, and those of Goldberg et al. (1960) for the meteorites, although with differences between the most abundant elements. An incipient study with *s*- and *r*-process contributions to the abundances of the Solar System material is found in Seeger et al. (1965). Since then the progress in the measurements of the abundances of the elements and their isotopes in the Solar System has been considerable, improving with technology. For a review of the history of Solar System elemental abundances we recommend the detailed work of Lodders (2019) and the last work of Asplund et al. (2021) to have a vision from the 21st century perspective.

In the Figure 1-4 we show the abundances of almost all the elements in the solar photosphere as a function of their atomic number (Z). The compilation of abundances was measured by Asplund et al. (2009) using a realistic new 3-dimensional and time-dependent hydrodynamical model of the solar atmosphere.

As we can see in the Figure 1-4, H and He are the most abundant, they are the elements of the Big-Bang; Li, Be, and B (LiBeB) differ from the others, as they were poorly synthesized in the Big-Bang and later in the stars and to which an interstellar origin is attributed; from here (starting in C) there are two general trends: for elements produced inside stars (Z > 5), given an element with even Z, its abundance is bigger than that of the two adjacent elements (with $Z \pm 1$) (Oddo – Harkins rule); likewise, a general tendency to decrease abundance with increasing

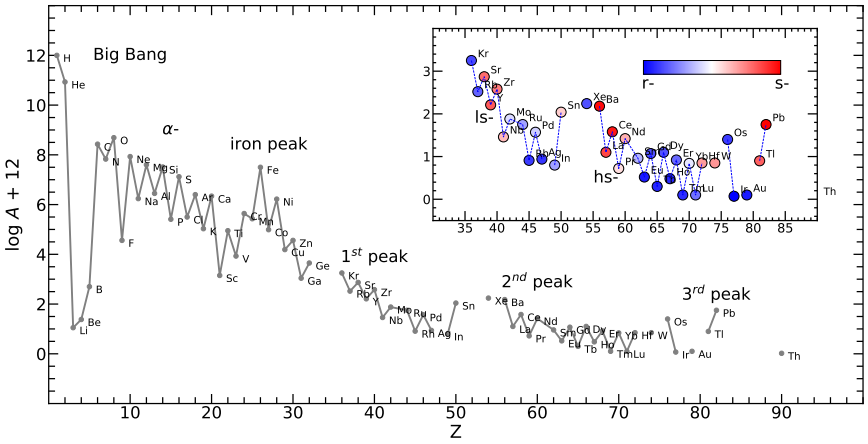

Figure 1-4: Abundances of the elements in the solar photosphere as a function of their atomic number. The abundances are taken from Asplund et al. (2009). In the inner box, the neutron-capture elements are shown in detail according to the colour code as a function of the percentage of *s*-process given by Bisterzo et al. (2014).

Z is observed. Applying this to our case, we see in the aforementioned Figure 1-4 that for the even elements (e.g. Sr, Zr, Ba, Ce, Nd and Sm) the abundance is larger than for the odd ones (e.g. Y, La, Pr and Eu). This is because they are more stable and their nuclides are more bound, and therefore less susceptible to capturing neutrons during the *s*- and *r*- processes.

Another important point is that in the aforementioned Figure 1-4 we see how there are peaks where the abundance is higher. These peaks often correspond to the magic numbers of nucleons (protons or neutrons), that is, they give it more stability against nuclear decay by having a higher binding energy per nucleon. Currently the elements around these three *s*-process peaks are identified in optical spectra obtained with spectrographs and ground-based observations. Thus, the first peak is found at N = 50 (Sr, Y and Zr), the second at N = 82 (Ba, La, Ce, Pr, and Nd), and a third at N = 126 (Pb). If the nucleus of an element has a magic number of protons and a magic number of neutrons, as in Pb, it is said to be a "double magic". In the Figure 1-5 we show the elements of the first and second peak, and also the isotopes of Sm and Eu (*r*-process dominated) in a nuclides chart; in the black boxes the extraordinarily stable isotopes and with the longest half lives, which also correspond to the peak in solar abundance. They are located in the so-called valley of stability. In this chart it is also possible to follow the path of the isotopes, which when they have a short half-life, will have time to decay before capturing another

neutron: isotopes with excessive protons or neutrons are unstable and suffer a β+ (pink) or β- (light blue) decay. In yellow α emissions, which are much more common at high atomic numbers (especially beyond Po), along with spontaneous fission (beyond Cm); horizontally we have the isotopes and vertically the isotones. On the other hand, the *r*-process peaks correspond to the elements around Ge, Xe and Pt, whose isotopes with magic numbers are unstable.

Taking into account the contribution of each process to the abundances in the Sun, we can make another classification of the neutron-capture elements, such as that introduced by Overbeek et al. (2016). Thus, we can consider that for an element to be dominated by a process if it is at least responsible for 70 % of its abundance in the Sun. Considering these, there seems to be a consensus in considering as dominated *s*-processes elements to Sr, Y, Zr, Ba, La, Ce. If we assume that the remaining contribution is mainly due to the *r*-process, we can consider Eu and Sm as *r*-dominated. The highest purity can be given to the Ba (*s*-process) and Eu (*r*-process). In the Table 1.1 we see these percentages given by different authors for comparison, which we also provide in the appendix as Figure A1 for a better visualization. As we can see, these authors coincide quite well for the heaviest elements, although for ls elements such as Zr, Y and Sr there are considerable differences for some of them. The Figures 1-2 and 1-4 (inner box) are colour-coded based on the contributions of the *s*-process in the Sun to given by Bisterzo et al. (2014), which we also compare in the Figure 1-6 ordered from bottom to top in increasing contribution to the *s*-process. As we can see in the aforementioned figure, the hs elements (except Nd and Pr) are the ones that contribute the most to the *s*-process, followed by the ls that reach an almost mixed behavior in the case of Zr, and which are followed by the hs elements Pr and Nd, which already have a mixed behavior. From there the elements become increasingly *r*-process dominated culminating in the Eu, which is representative of the pure *r*-process. In the Figure 1-7 we break down these total percentages into the partial contributions of each stable isotope of the referred elements, which we can find in the nuclide chart of the Figure 1-5 (stable isotopes boxed in black).

Another useful aspect is the comparison of abundances of elements with each other, and for this the purity of each n-capture process. In this sense, the comparison of the different elements with Ba and Eu, representative elements of the *s*- and *r*-process respectively, is very useful. In the Figure 1-8 we show the pure *r*-contribution of [El/Ba] and [El/Eu] for the 10 neutron-capture elements discussed in this thesis, calculated from the percentages of process contributions in the Sun

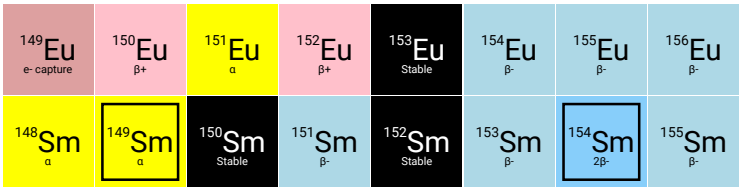

(a) *r*-process

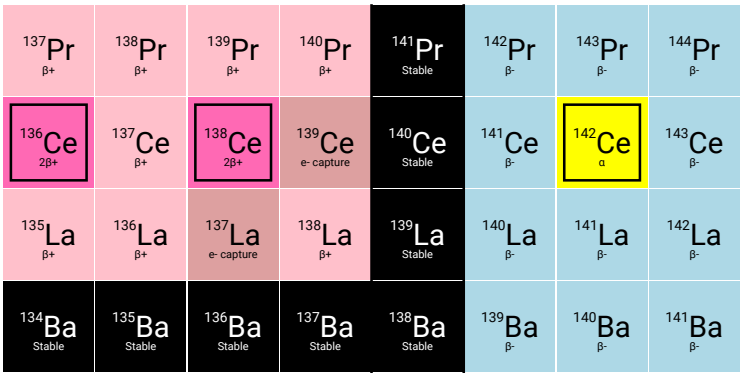

(b) *s*-process (second peak)

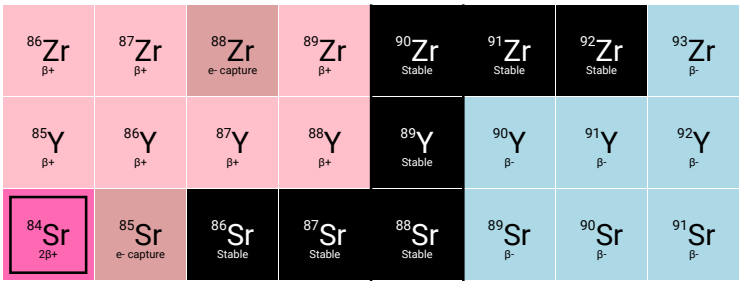

(c) *s*-process (first peak)

Figure 1-5: Extract from the chart of nuclides by type of decay for the isotopes of the *s*- and *r*- process elements studied in this thesis, ordered by the number of neutrons (N) and the number of protons (Z) in the atomic nucleus and coloured by their primary decay mode. Framed in black, the particularly stable ones, which correspond to the first and second peaks by their abundances (generated using the Edward Simpson's tool "The colourful Nuclide Chart").

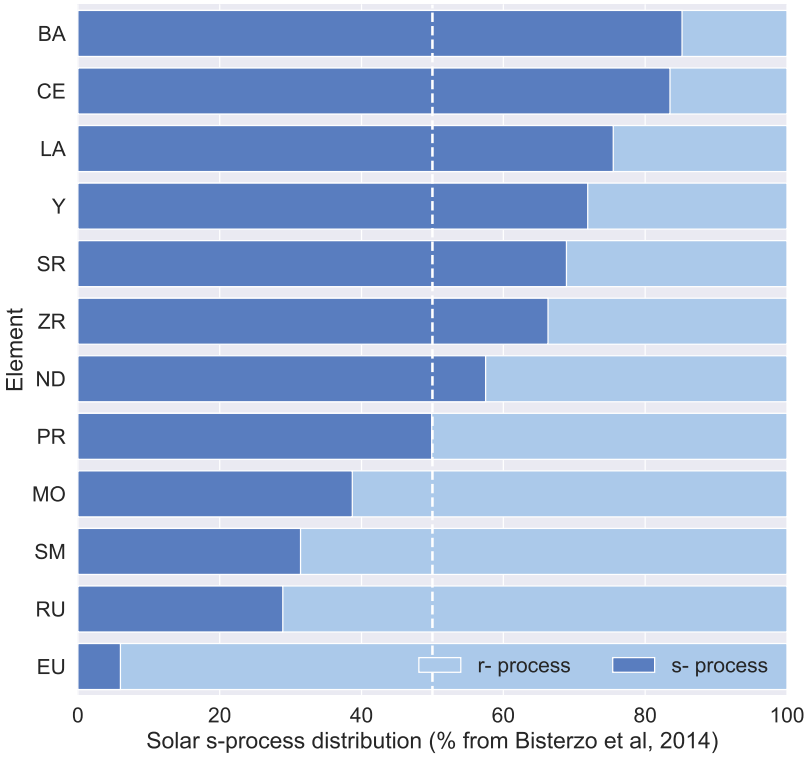

Figure 1-6: Stacked bar chart for the solar *s*-process distribution ordered in decreasing percentage from top to bottom. Percentages taken from Bisterzo et al. (2014).

(Bisterzo et al., 2014) and the solar abundances of Grevesse et al. (2007). We will see this in detail in the subsection 3.3.

In addition to its importance for the understanding of our Solar System, the solar composition is an essential reference standard to compare with the compositions of other stars. As we will see in the next chapter (section 2.1.4.2), the Sun is therefore our reference star and scale.

1.4. Astrophysical sites and evolution

One of the great challenges of modern astrophysics is to associate each of the chemical elements with the cosmic event from which they come. The astonishing

Table 1.1: Solar percentage of *s*-process input for the n-capture elements related to this thesis work.

El.	Arlandini et al. (1999)	Simmerer et al. (2004)	Bisterzo et al. (2014)	Prantzos et al. (2020)
Sr	85	89	69	91
Y	92	72	72	78
Zr	83	81	66	82
Ba	81	85	85	89
La	62	75	76	80
Ce	77	81	84	85
Pr	49	49	50	54
Nd	56	58	58	62
Sm	29	33	31	33
Eu	6	2	6	5

discovery of Tc (Z = 43) in the spectrum of cool giants S-type stars by Merrill (1952) was the first evidence of the nucleosynthesis of neutron-capture elements in AGB stars, currently related to the "third dredge-up" (Lebzelter and Hron, 2003). This was due to the long life of those stars (of the order of 10^9), in comparison with the half-live of technetium (of the order of 10^6 years). As we have seen in the previous section, for neutron capture reactions to occur, it is necessary to have neutron sources with the appropriate density and duration. During the fusion phases of H and He, no neutron source is efficient enough. However, during the AGB phase we find an important source of neutrons in the reaction ^{13}C(α,n)^{16}O, making them one of the most important polluters of the interstellar medium (Cristallo et al., 2018). For this reason, the *s*-process is related to stars in the asymptotic giant branch (AGB) phase (Gallino et al., 1998), which are cool and luminous evolved low-intermediate mass stars. The pre-existing iron in the star, coming from the gas left behind by supernovae from previous generations of stars, is the seed and the target nucleus of the neutrons of the AGB phase that triggers the *s*-process. The ^{22}Ne(α,n)^{25}Mg reaction during the Neon-burning process in massive stars is also an important source of neutrons (Longland et al., 2012). In these hot stars *s*-process occurs during core He burning and in the convective C-burning shell, before it explodes into a supernova (The et al., 2000). However, due to the high temperatures necessary for it to be effective, this reaction can also be efficient in AGB stars with initial masses $\geq 4M_{\odot}$ during convective thermal pulses (Karakas and Lattanzio, 2014). In fact, that reaction had already been identified as a source of neutrons in the AGB stars by Cameron (1960). It should be noted that recent studies

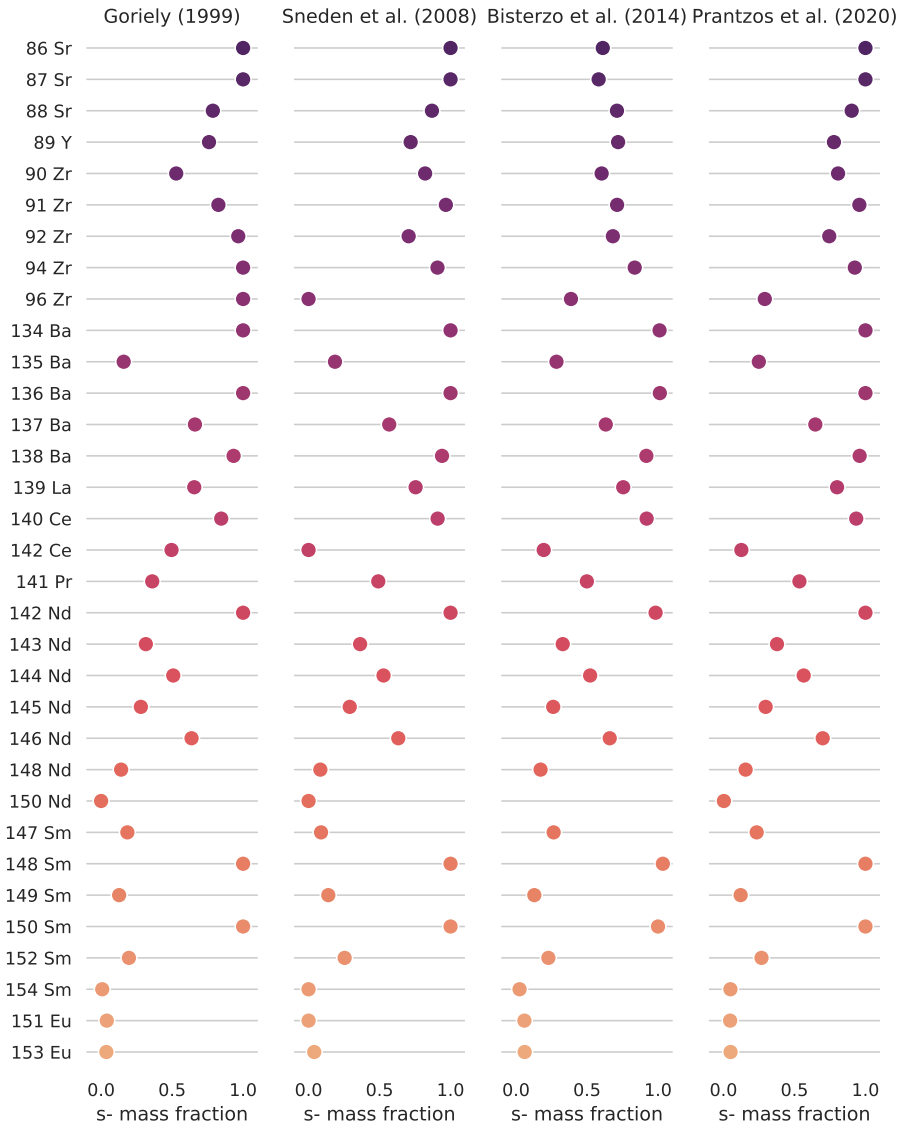

Figure 1-7: Contributions to the Solar System in mass fractions for 33 stable isotopes of neutron-capture elements related to this thesis. Figure based on the values obtained by Goriely (1999), Sneden et al. (2008), Bisterzo et al. (2014), and Prantzos et al. (2020), and adapted from Table 3 of the last.

indicate that the probability of occurring the ^{22}Ne(α,n)^{25}Mg reaction is lower than what was assumed, which would imply changes in the final *s*-process abundances of elements such as strontium and zirconium (Jayatissa et al., 2020). For low-mass AGB stars, the neutron source is then ^{13}C(α,n)^{16}O. Other reactions proposed as an astrophysical source of neutrons for the production of weak *s*-process elements are

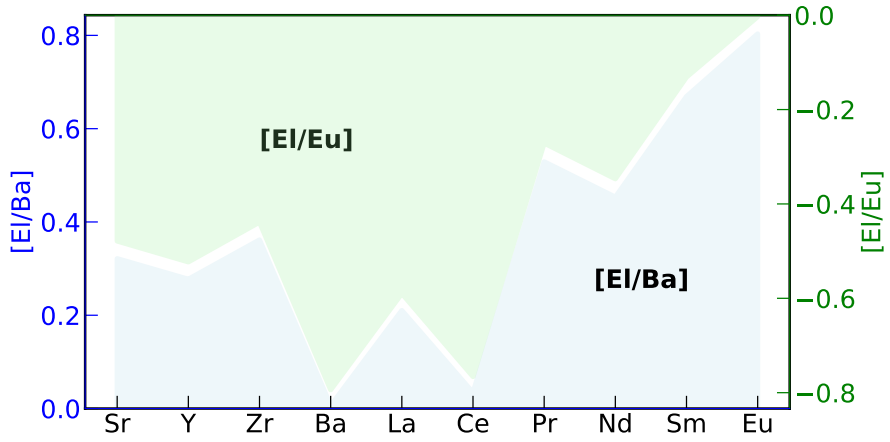

Figure 1-8: Pure *r*-process [El/Ba] (blue) and [El/Eu] (green) ratio derived using the percentages of Bisterzo et al. (2014) and the solar abundances of Grevesse et al. (2007).

the fusion of carbon ^{12}C(^{12}C,n)^{23}Mg (Bucher et al., 2015).

According to this, and as we mentioned in the section 1.2, the *s*-process can be subdivided into "weak", "main", and "strong" (e.g. Kappeler et al., 1989). The "weak" component, which is less understood, would be associated with the aforementioned massive stars (> $10M_{\odot}$) and would be partly responsible for the production of the isotopes of the elements between $56 \leq A \leq 90$ (e.g. Peters, 1968; Lamb et al., 1977; Raiteri et al., 1993; Heil et al., 2007; Pignatari et al., 2010). This would include isotopes from the iron peak to the limit with the first peak elements strontium and yttrium. Low-mass asymptotic giant branch (AGB) stars are mostly responsible for the "main" *s*-process component, contributing mostly to production of isotopes of elements between $90 \leq A \leq 209$ (e.g. Busso and Gallino, 1997; Busso et al., 1999, 2001; Käppeler et al., 2011; Bisterzo et al., 2015; Karakas and Lugaro, 2016; Cristallo et al., 2018; Busso et al., 2021). This would cover elements from the first peak around zirconium to the third peak around bismuth. The Figure 1-9 shows this classification of elements according to whether their component s-process is "main" or "weak". Lastly, it should be mentioned that there was a "strong" *s*-process component which was associated with the production of ^{208}Pb and ^{209}Bi (e.g. Clayton and Rassbach, 1967; Gallino et al., 1998; Travaglio et al., 2001), but later the missing fractions of those elements were attributed to the main *s*-process in low-metallicity stars (Käppeler, 2012).

Conversely, the astrophysical site for the *r*-process is controversial, and is still

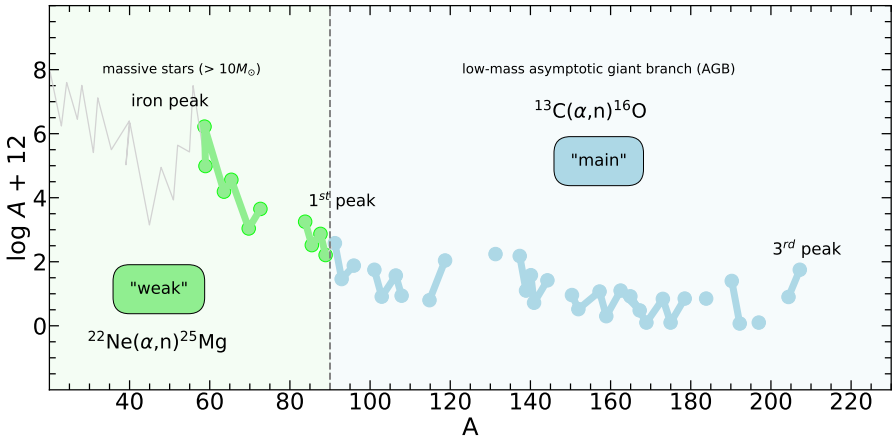

Figure 1-9: Abundances of the elements in the solar photosphere from Asplund et al. (2009) as a function of their atomic mass (A) and classified by their origin into "weak" (light green color) and "main" (light blue color).

in dispute. There is a long list of potential production sites, extremely varied and complex (*vide* Table 1.2 for a summary). However, there is consensus that its production must take place in a violent environment, where neutron fluxes and temperatures are high. Several possible sites of *r*-process have been proposed, being initially attributed to supernovae (*vide* Kajino et al., 2019, for a complete review of progress in the last decades and the current status of *r*-process nucleosynthesis). Thus, neutrino-induced winds from core-collapse supernovae (Woosley et al., 1994), polar jets from rotating core-collapse supernova (Nishimura et al., 2006), collapsars (failed supernovae) (Siegel et al., 2019), ejecta from neutron star (NS) mergers (Freiburghaus et al., 1999) or from neutron star and black hole mergers (Surman et al., 2008) are some of the proposed sources. The NS–NS merging events revealed in the LIGO/Virgo experiment by detecting gravitational waves (e.g. Abbott et al., 2017) hosted in the galaxy NGC4993 showed that binary neutron stars (BNS) create heavy elements more efficiently than supernovae, definitely changing the picture. Finally, the most recent study (Chen et al., 2021) points to the binary neutron star mergers and collisions between neutron stars as the most probable source of heavy elements, to the detriment of mergers between a neutron star and a black hole. Indeed, the NS–NS mergers could be a dominant source of *r*-process dominated elements such as cesium and tellurium (Smartt et al., 2017; Côté et al., 2018), moreover *s*-process dominated elements also can be produced in such a kind of events, as evidenced by the recent identification of strontium in

the merger of two neutron stars by Watson et al. (2019). Indeed, the latter appears as a common product of these events (Perego et al., 2022). Even so, some parameters controlling the production of *r*-process by NSMs (e.g. yields, time-delay, frequency and merging rate) still need to be clarified (see, e.g Vangioni et al., 2016; Ojima et al., 2018, for a discussion on the coalescence time). However, although GW170817 is the first direct observation of the *r*-process elements, the question of its origin remains unresolved. Thus, new works from a post GW170817 perspective continue to point to two distinct *r*-process sites. Thereby, Skúladóttir and Salvadori (2020) proposes a quick source with timescales $\lesssim 10^8$ yr and a delayed source with timescales $\gtrsim 4$ Gyr, which corresponds to the NSMs, as the only way to explain the data. Indeed, Blanchard et al. (2017) calculated the binary merger timescale probability distribution finding a median merger timescale of 11.2 Gyr, with a 90% confidence range of 6.8-13.6 Gyr. In order to explain the decreasing trend of [Eu/Fe] at low metallicities in the Galactic disc, a new work by Côté et al. (2019) propose an additional production site of Eu only active in the early universe, which would disappear with increasing metallicity. This hypothetical source would be responsible for approximately half of the Eu production before the beginning of the SNe Ia. On the other hand, Simonetti et al. (2019) have shown that a change in the fraction of NSM/Massive stars (higher at low metallicity, lower at high metallicity) would allow to reproduce observational constraints, although it remains an *ad hoc* assumption. The debate is therefore still open.

Table 1.2: Summary of some proposed astrophysical sites and physical mechanisms of production of *r*-process with its references.

Source	Reference
Neutrino-driven wind	Woosley et al. (1994)
Magnetic neutrino-driven wind	Thompson and ud-Doula (2018)
Shock-induced ejection	Hillebrandt et al. (1984)
Compact-object binary mergers	Lattimer and Schramm (1974)
Magneto-hydrodynamic jet	Nishimura et al. (2006)
Collapsar	Fujimoto et al. (2006)
Fall-back supernovae	Bramante and Linden (2016)
Dark matter induced black hole collapse	Famiano et al. (2008)

Because the production of most n-capture elements in the early stage of formation of the Galaxy is dominated by the *r*-process, they are often used to trace the *r*-process nucleosynthesis (see, e.g. Frebel, 2018; Horowitz et al., 2019). Besides, the large scatter of neutron-capture elements and highly *r*-process enhancement in

metal-poor stars has been known for decades (Goriely, 1999; Sneden et al., 1994), and knowledge of these stars has increased in recent years (e.g. Hansen et al., 2018). Their orbital properties were studied by Roederer et al. (2018), suggesting that these stars were accreted from satellite galaxies, in environments with low SFR and Fe production. In consequence, recent works (e.g. Skúladóttir et al., 2020) have addressed the abundances of neutron-capture elements in stars of dwarf galaxies such as Sculptor. This offers a unique opportunity to track the contributions of the metal-poor AGB stars, due to the slow chemical enrichment of those satellite dwarf galaxies. Another recent example of *r*-process enhancements is found in Gaia-Enceladus, a dwarf galaxy that merged with the Milky Way about 8–11 Gyr ago (Matsuno et al., 2021). Finally, from higher metallicities ([Fe/H] > -1.5) the *s*-process become more efficient (Gallino et al., 1998), and elements such as Eu (still with a tiny *s*-component) are essential to investigate the evolution of the *r*-process in the Milky-Way discs.

2. RESEARCH METHODOLOGY

2.1. The solar neighborhood stellar sample from SPFOT survey

2.1.1. Instrumentation, observations and stellar sample

This study is based on the observations of 506 stars made between 2016 and 2019 from the Molėtai Astronomical Observatory (MAO) in Lithuania, and using the Vilnius University Echelle Spectrograph (VUES). VUES is a multimode high resolution spectrograph that was designed and constructed at the Exoplanet Laboratory of the Yale University (Jurgenson et al., 2014, 2016) and was installed on the $f/12$ Ritchey-Chretien telescope (RCT), M_1 = 1.65 m, at MAO in 2016. The instrument covers a spectral wavelength range between 4000 to 8800 Å and can operate in three spectral resolution modes (R = 30,000, 45,000, and 60,000). The stars studied are part of the so-called Spectroscopic and Photometric Survey of the Northern Sky (SPFOT), which aims to provide a detailed chemical composition from high-resolution spectra and photometric variability data for bright stars in the northern sky. The sample includes bright stars ($V < 8$ mag) of spectral type F, G, and K in the Morgan-Keenan (MK) system. The sample corresponds mainly to dwarf and giant stars, almost equally distributed, and they are located in the solar neighbourhood. The Figure A3 in the appendix shows the distribution of stars by spectral type and log$g$.

The stars are divided into three fields in the sky, as they were studied by Mikolaitis et al. (2018, 2019), and Tautvaišienė et al. (2020) (Ref. I). The first two fields, of approximately 20° radii centered at $\alpha(2000) = 161°.03552$, $\delta(2000) = 86°.60225$ and at $\alpha(2000) = 265°.08003$, $\delta(2000) = 39°.58370$, respectively, correspond to Mikolaitis et al. (2018) and Mikolaitis et al. (2019); and a third field of approximately 12° radii centered at $\alpha(2000) = 270°$, $\delta(2000) = 66°$, which corresponds to Ref. I. These first two fields are of the same size, and target of the ESA's PLATO mission (Rauer et al., 2014; Miglio et al., 2017), the first being the preliminary PLATO STEP02 field, located very close to the North Celestial Pole (NCP), and the second is the preliminary PLATO NPF field. The third field corresponds to the Continuous Viewing Zone (CVZ) field of the NASA's TESS mission (Ricker et al., 2015), and is centered in the North Ecliptic Pole (NEP). The first aforementioned two fields overlap on their edges with the third. In this thesis,

our final list includes 506 stars, of which 247 are from the PLATO fields (138 in the first and 109 in the second preliminary field), and 275 from the TESS field, having 16 stars in common in both fields. The Figure 2-1 shows the equatorial positions of the 506 stars plotted on a celestial sphere and divided into the three sky fields: in blue those corresponding to PLATO and in magenta those corresponding to TESS, with 16 stars overlapping. The NCP, NEP and NGP and the circles that define their fundamental planes are also shown for reference.

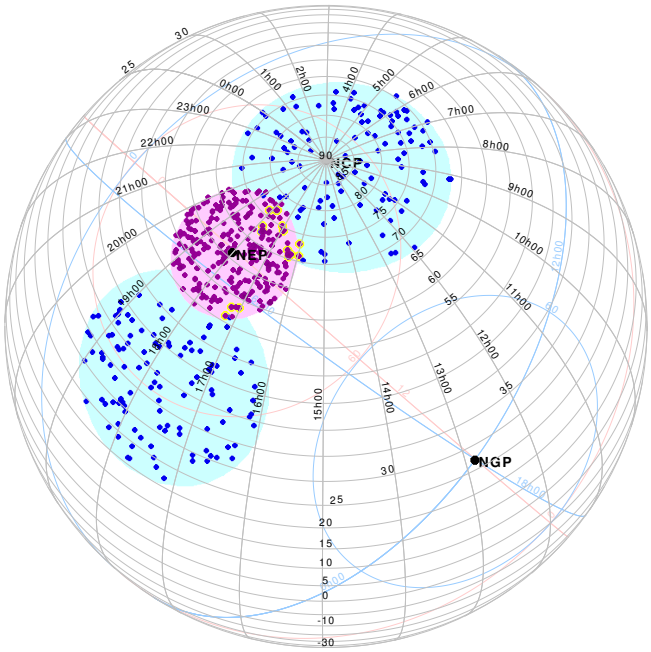

Figure 2-1: Positions of our sample of 506 stars plotted on a celestial sphere. In blue colour the PLATO fields and in magenta the TESS field. The NCP, NEP and NGP and the circles that define their fundamental planes are also shown for reference.

The two PLATO fields contain MS dwarf stars of spectral type FGK, and the TESS field contains both dwarf and giant stars cooler than F5 spectral type ($T_{\rm eff}$ < 6700 K). Our final list of 506 stars excluded double-line spectroscopic binaries and stars with rotational velocity > 25 km s^{-1}. For more details on the target selection we refer to Mikolaitis et al. (2018) and Ref. I.

Table 2.1: Data collection used in this thesis.

Publication	Observation campaign	Number of objects
Mikolaitis et al. (2018)	2016-2017	213
Mikolaitis et al. (2019)	2017-2018	192
Tautvaišienė et al. (2020)	2018-2019	302

2.1.2. Data acquisition and reduction

Nowadays, the Echelle spectrographs are the most common instruments used in astronomical spectroscopy, providing precise and detailed spectra. From the moment in which the data is collected by the telescope and instrument until it reaches the scientific analysis and its interpretation, a chain of treatment and reduction processes follow one another, which implies the use of different techniques and procedures. Some of those steps are the same as in CCD imagin, for example bias and/or dark frame subtraction and flat fielding, but others are specific to spectroscopy. The data collection referred to in the previous section 2.1.1 is summarized in the Table 2.1.

Some stars were observed several times, which allowed combining their spectra to increase the Signal-to-noise ratio (SNR). Taking advantage of the fact that VUES is a multimode spectrograph, $R \sim 68{,}000$ was used for M stars and $R \sim 36{,}000$ for the other objects. Regarding the time that the detector was exposed to light to obtain the spectra (exposure time), this was in an interval between 900 and 2,400 s., with SNRs between 75 and 200, depending on stellar magnitudes. Prior to the collection of spectra by the instrument and telescope, bias, flat field, and calibration lamp measurements were acquired. The VUES calibration unit is equipped with ThAr and quartz calibration lamps, with a computer controlled flip mirror that allows to select between both sources. The quartz lamp, which is a bright enough source, is used for the flat fielding, and the ThAr lamp for the wavelength calibration. Thorium lamps are the most used today because of its spectral features as well as its mono-isotopic nature and the absence of hyperfine structure (HFS), and they are usually filled with Argon or Neon. VUES is equipped with a full data reduction pipeline, which after calibrations provides as final product the extracted spectrum in a three dimensional FITS file, including the wavelength of each pixel, the flux for each pixel, and the echelle order. The details of the primary data reduction and calibration procedures for VUES data are described in Jurgenson et al. (2016).

2.1.3. Atmospheric parameters

As a prerequisite to a detailed abundance analysis, it is necessary to have the stellar atmospheric parameters. In addition to their value in classifying stars, the individual element abundances depend on them, so their accuracy is important for abundance determination. In addition, these parameters are related to the fundamental properties of a star, that is, mass, radius and luminosity. The main of these (effective temperature $T_{\rm eff}$, surface gravity $\log g$, metallicity [Fe/H], and microturbulence velocity $v_{\rm t}$) for the 506 stars were adopted from the aforementioned Mikolaitis et al. (2018), Mikolaitis et al. (2019) and Ref. I.

Stellar atmospheric parameters in these papers were determined based on equivalent widths (EW) of neutral Fe I and ionized Fe II lines using standard spectroscopic techniques. Effective temperatures were derived by minimizing a slope of abundances determined from Fe I lines with different excitation potentials. Surface gravities were found by requiring Fe I and Fe II lines to give the same iron abundances. The microturbulent velocity values were attributed by requiring Fe I lines to give the same iron abundances regardless their equivalent widths. In total, 299 Fe I and Fe II lines were used in computing the stellar atmospheric parameters with the 10th version of the MOOG code (Sneden, 1973) and the MARCS grid of stellar atmosphere models of spectral types F, G and K (Gustafsson et al., 2008), based on the Vienna Atomic Line Data Base VALD (Piskunov et al., 1995).

In the Figure 2-2 we can see a $T_{\rm eff}$ - $\log g$ diagram (Kiel diagram), colour coded by metallicity, and showing a density estimation with bivariate distribution and a metallicity histogram. If we do a $\log g$-based dwarf-giant separation, our sample contains 227 stars with $\log g \leq 3.5$ that correspond to the giants, and 279 with $\log g > 3.5$ which correspond to the sub-giants and dwarfs. For the latter, we have 125 stars with $T_{\rm eff} < 6000$ K ("cool dwarfs") and 154 stars with $T_{\rm eff} \geq 6000$ K ("hot dwarfs"). In the Table 2.2 we show a basic stellar parameters statistics for the 506 stars according to their $\log g$. In the Figure A4 in the Appendix we show pairwise relationships of these parameters with a grid of axes. In that plot each stellar parameter is shared between the y-axes in a single row and the x-axes in a single column; where diagonal plots represent the univariate distribution to show the marginal distribution of the stellar parameters in each column, and with the stars divided into thin and thick discs, with kernel density estimate (KDE) on the diagonal.

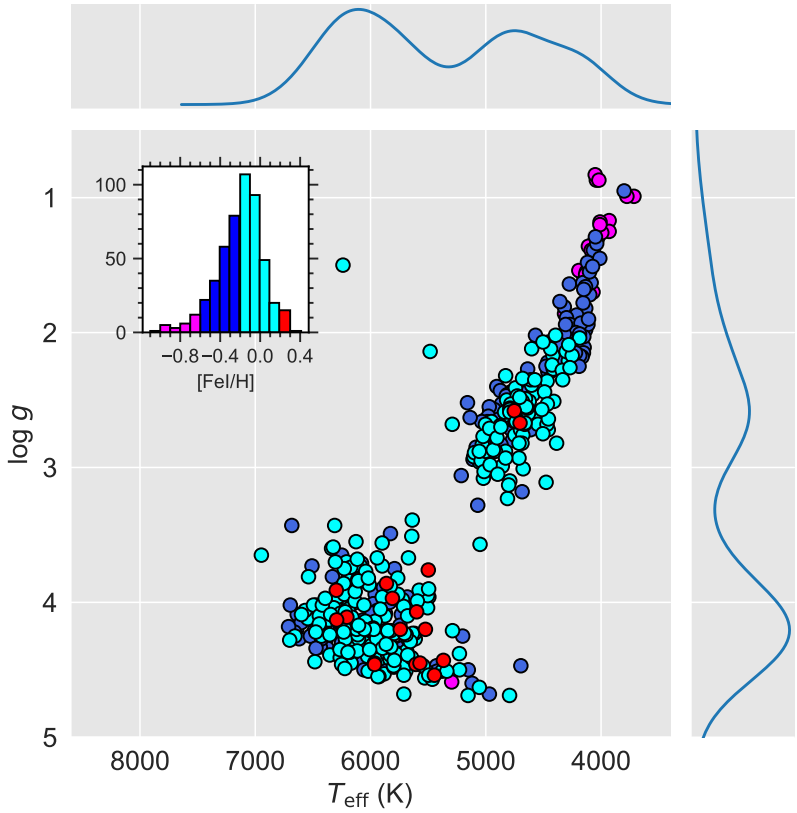

Figure 2-2: Kiel diagram colour coded by metallicity, and showing a density estimation with bivariate distribution and a metallicity histogram for our 506 stars.

2.1.4. Abundance determination

2.1.4.1. Spectral lines

We made an exhaustive line list selection based on line quality in terms of its purity and depth, considering only those relatively unblended. It is worth noting that there are many lines of neutron-capture elements in the blue / UV spectra (<4000 Å) which cannot be reached due to technological limitations (e.g. large blending and lower sensitivity of CCD detectors). However, promising projects are already underway to improve the sensitivity at near-UV wavelengths (e.g. CUBES), so there are still many expectations placed on neutron-capture elements in the near future.

Our line list begins with Sr I (4607.33Å) and ends with Eu II (6645.13Å), covering a spectral range of about 2000Å. Our final list comprises 35 spectral lines

Table 2.2: Statistics of the stellar parameters for the stars according to their $\log g$.

Name	Mean	SD	Minimum	Maximum	N
		$\log g > 3.5$			
$T_{\rm eff}$ (K)	6012.65	368.31	4696	6947	279
$\log g$	4.18	0.24	3.51	4.69	279
[Fe I/H]	-0.15	0.20	-0.80	0.33	279
vt (km/s)	1.21	0.29	0.24	2.10	279
		$\log g \leq 3.5$			
$T_{\rm eff}$ (K)	4602.52	416.30	3715	6683	227
$\log g$	2.35	0.54	0.83	3.49	227
[Fe I/H]	-0.26	0.25	-1.05	0.26	227
vt (km/s)	1.59	0.35	0.78	2.83	227

of neutron-capture elements, which are shown in the Table 2.3, together with the solar abundances in two modes of resolution and those obtained by Asplund et al. (2009).

We used the latest version of the Gaia-ESO Survey (GES) line-list (Heiter et al., 2021), intended for the abundance analysis of FGK-type stars carried out during the years 2012 to 2019. The Gaia-ESO Survey (Gilmore et al., 2012; Randich et al., 2013) is one of the most important stellar spectroscopic surveys generating abundances on a large scale.

In the Table 2.4 below we give a summary of references for transition probabilities (oscillator strengths, $\log gf$); and in Table 2.5 the information for the hyperfine structure and isotopic splitting (hereafter HFS and IS) when applicable. The HFS effects were taken into account for the investigated lines of Ba, La, Nd, Pr, Sm, and Eu. For the remaining lines we assume that the HFS influence is small.

2.1.4.2. Differential abundance analysis

We made an abundance analysis differentially with respect to the Sun, our reference star. To do this, we first need to level the abundances on the solar scale, using as reference abundances those obtained with VUES, and which are presented in the Table 2.3, taken from Ref. II. As our target stars were observed using two different spectral resolutions (36,000 and 68,000), their spectra were investigated differentially to the solar spectra observed in the corresponding resolution mode. In order to increase precision in determining the solar elemental abundances, we averaged the abundances derived from several observations. In the table we can see the solar abundance values for each investigated line and the corresponding values

Table 2.3: Spectral lines used in this work and their solar abundance

.

El.	λ (Å)	VUES (R = 68 000)	VUES (R = 36 000)	Asplund et al. (2009)
Sr I	4607.33	2.86	2.85	2.87 ± 0.07
Y II	4883.69	1.98	2.05	
Y II	4900.12	2.18	2.22	
Y II	4982.13	1.96	2.05	
Y II	5087.42	1.98	2.00	
Y II	5200.42	2.28	2.34	
Y II	5289.81	2.22	2.26	
Y II	5402.78	2.27	2.31	
Y II	5728.87	2.28	2.25	
Y*		2.18 ± 0.13	2.19 ± 0.12	2.21 ± 0.05
Zr I	5384.96	2.52	2.50	
Zr I	6127.44	2.60	2.62	
Zr I	6134.20	2.75	2.81	
Zr I	6143.18	2.62	2.63	
Zr*		2.62 ± 0.08	2.63 ± 0.10	2.58 ± 0.04
Zr II	5350.09	2.50	2.53	2.58 ± 0.04
Ba II	5853.67	2.12	2.19	
Ba II	6141.71	2.21	2.26	
Ba II	6496.91	2.33	2.37	
Ba*		2.22 ± 0.09	2.27 ± 0.07	2.18 ± 0.09
La II	4748.72	1.00	1.04	
La II	5123.01	1.16	1.18	
La II	5303.53	0.99	1.02	
La II	6320.41	1.03	1.06	
La II	6390.48	1.15	1.15	
La*		1.07 ± 0.07	1.09 ± 0.06	1.10 ± 0.04
Ce II	5274.22	1.50	1.53	
Ce II	5512.06	1.76	1.77	
Ce II	5975.82	1.32	1.31	
Ce II	6043.38	1.62	1.63	
Ce*		1.55 ± 0.16	1.56 ± 0.17	1.58 ± 0.04
Pr II	5219.02	0.82	0.86	
Pr II	5259.72	0.63	0.60	
Pr II	5322.77	0.88	0.89	
Pr*		0.78 ± 0.13	0.78 ± 0.16	0.72 ± 0.04
Nd II	5092.80	1.29	1.27	
Nd II	5276.86	1.25	1.26	
Nd II	5356.97	1.61	1.58	
Nd II	5740.86	1.45	1.50	
Nd*		1.40 ± 0.14	1.40 ± 0.14	1.42 ± 0.04
Sm II	4854.37	0.87	0.90	0.96 ± 0.04
Eu II	6645.13	0.49	0.49	0.52 ± 0.04

Table 2.4: References for oscillator strength (log gf) values

Element	Reference
Sr I	Parkinson et al. (1976)
Y II	Biémont et al. (2011)
Zr I	Biemont et al. (1981)
Zr II	Cowley and Corliss (1983)
Ba II	Davidson et al. (1992); Miles and Wiese (1969)
La II (6320.4 Å)	Corliss and Bozman (1962)
La II	Lawler, Bonvallet and Sneden (2001)
Ce II	Lawler et al. (2009)
Pr II	Ivarsson et al. (2001)
Nd II	Den Hartog et al. (2003)
Sm II	Lawler et al. (2006)
Eu II	Lawler, Wickliffe, den Hartog and Sneden (2001)

Table 2.5: References for HFS values

Element and lines	Reference
Ba II	Davidson et al. (1992)
La II (5123, 5303, 6390 Å)	Lawler, Bonvallet and Sneden (2001)
Pr II	Ivarsson et al. (2001)
Nd II (5092, 5740 Å)	Den Hartog et al. (2003)
Nd II (5276 Å)	Meggers et al. (1975)
Sm II	Lawler et al. (2006)
Eu II	Lawler, Wickliffe, den Hartog and Sneden (2001)

by Asplund et al. (2009) for comparison. This is graphically exposed in the Figure 2-3 for the averaged values of each element in the 12+log(X/H) form, where can be seen that the agreement is very good.

The method of analysis is thus the same for spectra of different resolution, with the only difference being the use of different instrumental profiles (IP), which are necessary to convolve the synthetic spectra. Differential analysis is based on determining the abundances in the same way for two stars, the target star and a well-known reference star. The more similar the reference star is to the target star, the greater the precision. This allows uncertainties due to blends, incomplete atomic data, non-local thermodynamic equilibrium (hereafter NLTE) effects, etc. to be canceled to some degree (Jofré et al., 2019).

Due to the shallow depth of some lines, for some stars it was not possible to determine the abundances, more frequent in lines of elements such as Zr I and Sm II.

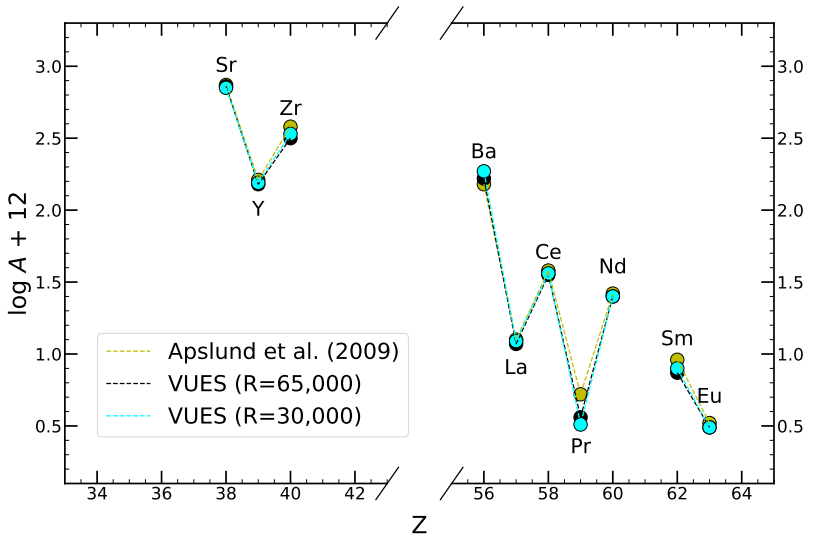

Figure 2-3: Comparison of averaged solar abundances as a function of its atomic number (Z) for each of our 10 elements measured with VUES in two different resolutions, as well as by Asplund et al. (2009) for comparison.

2.1.4.3. Abundance determination

Each energy transition of an ion, atom or molecule in the atmosphere of a star corresponds to a specific spectral line, which allows us to determine the composition of a star. The abundance of the elements is understood as the measure of the relative quantity of these with respect to another element given in the same environment. In general, that reference element is hydrogen, since it is the most abundant element in the Sun. For other applications in the Solar System, silicon (Si), the second most abundant element in the earth's crust, can be used (e.g. Goldschmidt, 1937). In astrophysics the abundance is usually measured in mass-fraction or in atomic-fraction. The latter is the most used in spectroscopy, which it is usual to be measured on a decimal logarithm scale. It is then necessary to introduce the so-called "decadic logarithmic units" or "dex", a contraction of "decimal exponent" widely used in astronomy, where 1 dex represents a factor 10^1. To avoid the negative values of log (A), a log (A) + 12 scale is used (*vide* Figure 2-4), normalization introduced for the first time by Claas (1951) [Payne (1925) had already defined log A (H) = 11 in her doctoral thesis]. After scaling to the Sun, these abundances can be converted into [El/Fe] ratios, following the formulas shown in the eq. 2.1, where N is the number

of atoms per unit of volume.

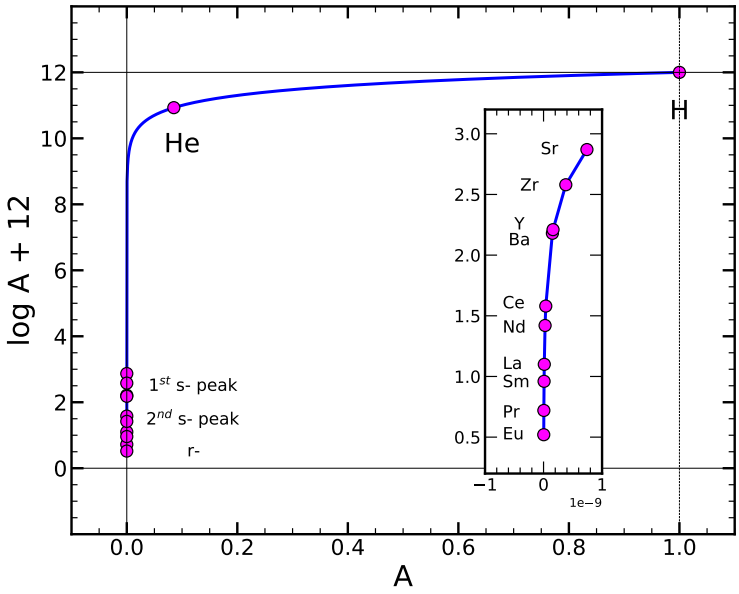

Figure 2-4: Solar abundances on the log (A) + 12 scale. The values of hydrogen, helium, as well as those of the neutron-capture elements analyzed in this thesis are shown. The inner box show a zoom of the neutron-capture elements (values from Asplund et al. (2009)).

$$\begin{cases} A = \frac{N_{El}}{N_H} \\ [El/H] = \log_{10}\left(\frac{N_{El}}{N_H}\right)_* - \log_{10}\left(\frac{N_{El}}{N_H}\right)_\odot \\ [El/Fe] = \log_{10}\left(\frac{N_{El}}{N_{Fe}}\right)_* - \log_{10}\left(\frac{N_{El}}{N_{Fe}}\right)_\odot \end{cases} \tag{2.1}$$

Metallicity [Fe/H] is the stellar parameter determined from equivalent widths, whereas [Fe I/H] is the abundance of neutral iron calculated from synthetic spectra. Therefore, we calculate the [El/Fe I] ratio using the iron abundance derived from neutral iron lines instead of global metallicity. The preference between Fe I and Fe II is based on the fact that the Fe I has many more lines than Fe II, and therefore a better accuracy can be achieved.

For the quantitative determination of photospheric abundances, the calculation of the emitted spectrum based on a model atmosphere and its comparison with the observed spectrum is necessary. A detailed explanation about current techniques, as well as a review of the analysis steps and the available tools are given in Allende Prieto (2016).

Abundances of all investigated chemical elements in this thesis were determined using spectral synthesis. For modelling of synthetic spectra, we used the 1D LTE spectrum synthesis code Turbospectrum v12.1.1 (Plez, 2012), an enhanced version of the Spectrum package developed at Uppsala Observatory which uses the treatment of line broadening described by Barklem et al. (1998).

In order to model stellar atmospheres, several assumptions are traditionally introduced: a) plane-parallel geometry: all physical variables a function of only one space coordinate (1D); b) homogeneity: no fine structures and no granularity; c) stationarity: time-independence of stellar spectra on human timescales; d) equilibrium: hydrostatic (no large scale accelerations in photosphere and no significant mass loss), radiative (flux constancy), and local thermodynamic equilibrium (LTE); e) no winds, magnetic fields, chromopsheres; f) simple convection and standard mixing length theory (MLT).

Thereby, to compute synthetic spectra of our stars, we used a set of plane-parallel, one-dimensional, hydrostatic, and constant-flux local thermodynamic equilibrium (LTE) atmospheric models of spectral types F, G and K taken from the MARCS 1 stellar model atmosphere and flux library described by Gustafsson et al. (2008). Therefore, we assume that the atmosphere is in statistical equilibrium, homogeneous in abundances, constant in time, $R_{\rm atm} \ll R_{\rm star}$, and that the energy transport takes place only by radiation and convection.

Because the strongest Ba II lines are affected by deviations from LTE, for the barium abundances we applied the non-local thermodynamic equilibrium (NLTE) corrections taken from Korotin et al. (2015), which are available for our three lines 5853, 6141, and 6496 Å. In our sample, for stars with [Fe/H] > 0, the corrections are about -0.027 ± 0.01 dex, in the interval $-0.5 <$ [Fe/H] < 0 the corrections are about -0.033 ± 0.016 dex, and for [Fe/H] < -0.5 the corrections are about -0.06 ± 0.02 dex. In the J/A+A/649/A126 table available online we provide both the LTE and NLTE barium abundances.

2.1.4.4. Abundance uncertainties

Systematic and random uncertainties should be taken into consideration when determining the abundances. Systematic uncertainties are those that always produce the same measurement error (e.g. due to the instrument), while random uncertainties are due to unpredictable causes and lead to different results when measurements are repeated (e.g. due to the observer). When chemical abundances are calculated, the systematic uncertainties may occur due to uncertainties in atomic data, but

they are mostly eliminated because of the differential analysis relative to the Sun. The random uncertainties can be attributed to the local continuum placement and a specific line fitting. A suitable way to represent random uncertainty is by the scatter when averaging abundances from multiple lines of the same element. For elements with a single line (Sr I , Zr II , Sm II and Eu II), we assign a standard deviation value of 0.07 dex, which is the average of all standard deviations from all the stars and all elements with more than one measured line. Uncertainties in atmospheric parameters also give rise to uncertainties in abundances. These are quantified by calculating the changes in the abundances caused by the error of each atmospheric parameter taken individually, while keeping the others fixed. The uncertainties in atmospheric parameters were given in Mikolaitis et al. (2018), Mikolaitis et al. (2019), and Ref. I; and the uncertainties in the abundances of the neutron-capture elements are presented in the J/A+A/649/A126 table available online.

The medians of atmospheric parameter uncertainties for the subsamples are as follows: a) dwarfs ($\log g > 3.5$): $\sigma T_{\rm eff} = 48$ K, $\sigma \log g = 0.30$, σ[Fe/H] = 0.11, and $\sigma v_{\rm t} = 0.28$ km s^{-1}; b) giants ($\log g \leq 3.5$): $\sigma T_{\rm eff} = 57$ K, $\sigma \log g = 0.21$, σ[Fe/H] = 0.11, and $\sigma v_{\rm t} = 0.22$ km s^{-1}. The median dwarf star ($\log g > 3.5$) in our sample has $T_{\rm eff} = 6057$ K, log$g$ = 4.20, [Fe/H] = −0.10, and $v_{\rm t} = 1.21$ km s^{-1} and the median giant has ($\log g \leq 3.5$) $T_{\rm eff} = 4646$ K, log$g$ = 2.50, [Fe/H] = −0.14, and $v_{\rm t} = 1.49$ km s^{-1}.

The sensitivity of the abundances to the uncertainties in atmospheric parameters for the three subsamples, namely stars with log g above or below than 3.5 as well as for solar twins are presented in Table 2.6. Because most of the investigated chemical elements are ionised, the sensitivity to the uncertainties in log g is highest. The Ba lines, which are relatively strong, are also quite sensitive to $v_{\rm t}$.

The total uncertainty $\sigma_{\rm El}$ was estimated for every individual abundance by taking into account both uncertainties, the random ones and those due to the atmospheric parameters by their quadrature sum, which is shown in the eq. 2.2:

$$\sigma_{\rm El} = \sqrt{\sigma_{\rm atm}^2 + \left(\frac{\sigma_{\rm rand}}{\sqrt{N}}\right)^2} \tag{2.2}$$

where $\sigma_{\rm rand}$ is the line-to-line scatter and N is the number of analysed atomic lines. When the number of lines is $N = 1$, we adopted 0.07 dex for a given element as $\sigma_{\rm rand}$. The uncertainties from four stellar parameters were quadratically summed for every star and gave us $\sigma_{\rm atm}$, as in equation 2.3:

$$\sigma A_{atm} = \sqrt{|\sigma A_{T_{eff}}|^2 + |\sigma A_{logg}|^2 + |\sigma A_{[FeI/H]}|^2 + |\sigma A_{v_t}|^2} \qquad (2.3)$$

The Figure 2-5 show the individual uncertainties $\sigma_{\rm El}$ as a function of $T_{\rm eff}$, log g, and [Fe I/H].

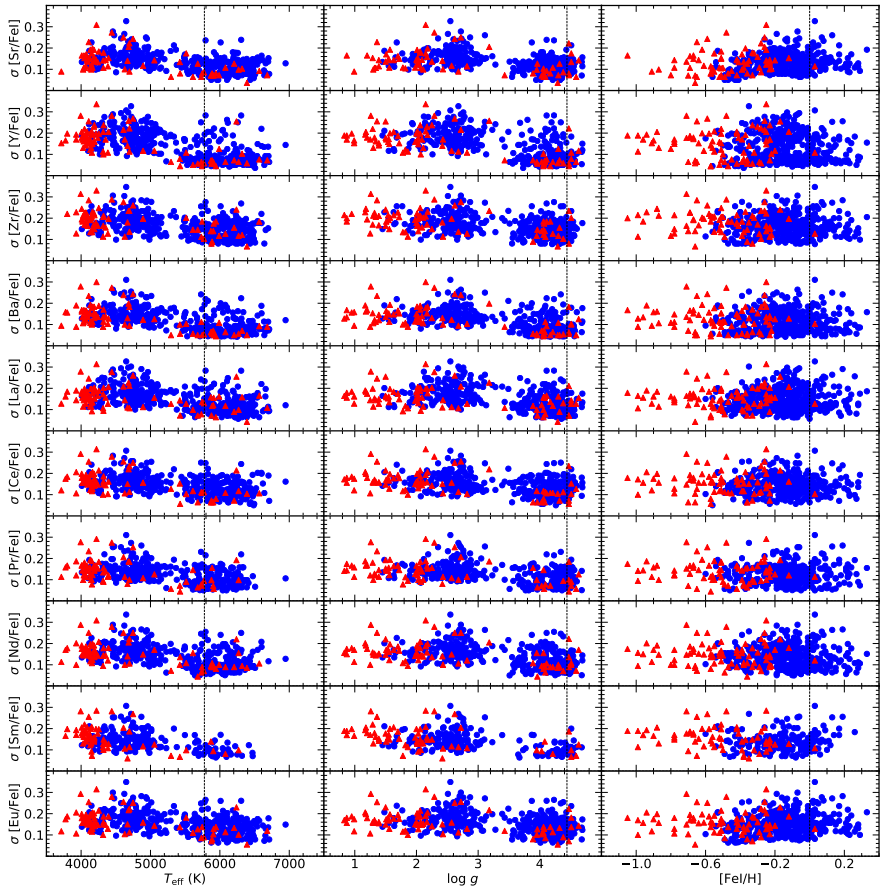

Figure 2-5: Uncertainties on the abundance ratios as a function of $T_{\rm eff}$, log g, and [Fe/H]. The blue dots represent the thin-disc and the red triangles are the thick-disc stars.

2.1.5. Ages and orbits

The age of the stars is an important physical parameter that measures the period of time that elapses from their birth to the point of reference. Its knowledge allows ordering Galactic events in sequences, establishing a past and its evolution. The fact that the stars spend most of their life in the MS, together with the issue that it is

Table 2.6: Sensitivity of abundances to the median values of uncertainties in atmospheric parameters and random uncertainties.

El.	$\Delta T_{\rm eff}$	$\Delta \log g$	Δ[Fe/H]	$\Delta v_{\rm t}$	Random
			$\log g > 3.5$		
Sr I	±0.05	±0.01	±0.01	±0.07	±0.07
Y II	±0.01	±0.10	±0.02	±0.07	±0.06
Zr I	±0.06	±0.05	±0.01	±0.01	±0.10
Zr II	±0.01	±0.11	±0.02	±0.01	±0.07
Ba II	±0.03	±0.04	±0.01	±0.18	±0.06
La II	±0.02	±0.12	±0.02	±0.01	±0.10
Ce II	±0.02	±0.11	±0.02	±0.01	±0.11
Pr II	±0.02	±0.09	±0.02	±0.01	±0.08
Nd II	±0.01	±0.13	±0.03	±0.01	±0.08
Sm II	±0.03	±0.11	±0.03	±0.01	±0.07
Eu II	±0.01	±0.12	±0.02	±0.01	±0.07
			$\log g \leq 3.5$		
Sr I	±0.05	∓0.01	∓0.01	∓0.08	±0.08
Y II	±0.01	±0.11	∓0.06	∓0.07	±0.08
Zr I	±0.08	∓0.06	∓0.01	∓0.01	±0.11
Zr II	±0.01	±0.12	∓0.04	∓0.01	±0.08
Ba II	±0.04	±0.05	∓0.01	∓0.17	±0.07
La II	±0.03	±0.13	∓0.02	∓0.01	±0.11
Ce II	±0.02	±0.12	∓0.04	∓0.01	±0.12
Pr II	±0.03	±0.09	∓0.03	∓0.02	±0.08
Nd II	±0.02	±0.11	∓0.04	∓0.01	±0.10
Sm II	±0.03	±0.11	∓0.04	∓0.01	±0.08
Eu II	±0.01	±0.13	∓0.03	∓0.01	±0.09
			Solar twins		
Sr I	±0.04	∓0.01	∓0.01	∓0.07	±0.08
Y II	±0.01	±0.02	∓0.02	∓0.04	±0.04
Zr I	±0.07	∓0.06	∓0.01	∓0.01	±0.11
Zr II	±0.01	±0.10	∓0.04	∓0.01	±0.07
Ba II	±0.01	±0.05	∓0.01	∓0.04	±0.04
La II	±0.03	±0.09	∓0.02	∓0.01	±0.09
Ce II	±0.02	±0.09	∓0.04	∓0.01	±0.12
Pr II	±0.02	±0.07	∓0.03	∓0.02	±0.07
Nd II	±0.01	±0.08	∓0.04	∓0.01	±0.07
Sm II	±0.01	±0.04	∓0.01	∓0.01	±0.05
Eu II	±0.01	±0.09	∓0.03	∓0.01	±0.06

the phase in which most of the stars are found, is a problem for their determination. Various properties and techniques can be used to infer the age of the stars, often associated with an individual characteristic or with the end of their lives, where the stars show some distinguishing feature. Some of them include isochrone placement, nucleocosmochronometry and asteroseismology. A good summary of the available techniques for age-dating stars can be found at Soderblom (2010), and in the chapter 5 we will discuss this topic in more detail.

An estimate of ages for the investigated stars in this thesis were taken from the aforementioned Mikolaitis et al. (2018), Mikolaitis et al. (2019), and Ref. I. The ages in the referred papers were estimated with a Unified tool to estimate Distances, Ages and Masses (UniDAM) (Mints and Hekker, 2017). This code combines spectroscopic data with infrared photometry from 2MASS (Skrutskie et al., 2006) and AllWISE (Cutri et al., 2021) and compares them with PAdova and TRieste Stellar Evolution Code (PARSEC) isochrones (Bressan et al., 2012) to derive probability density functions (PDFs) for ages. We imposed on our stars the condition eAge < 3 Gyr. The mean uncertainty of the age determination calculated from uncertainties of individual stars is 2 Gyr.

Regarding the mean galactocentric distances and maximum vertical distance, they are necessary to know the radial and vertical distribution of the abundances in the Galaxy, and specifically they are associated with the stellar's birthplace and to the apogalacticon respectively. Its interest will be discussed in more depth in the chapter 4.

The mean galactocentric distances $R_{\rm mean}$ and maximum heights from the Galactic plane $|z_{\rm max}|$ were taken in this thesis from Mikolaitis et al. (2019) and Ref. I, where they were computed using input data (parallaxes, proper motions and coordinates) from the Gaia DR2 catalogue (Luri et al., 2018; Katz et al., 2019; Gaia Collaboration et al., 2016, 2018) and *galpy*, a python based and *astropy* affiliated package for galactic-dynamics calculations (Bovy, 2015).

There are 101 stars in our sample which are kinematically visitors from the inner disc ($R_{\rm mean} < 7$ kpc, 68 stars) and outer ($R_{\rm mean} > 9$ kpc, 33 stars) Galactic regions that are passing through the solar neighbourhood ($7 < R_{\rm gc} < 9$ kpc, Carigi et al. 2015; Rojas-Arriagada et al. (2016)), on highly eccentric orbits.

2.1.6. The thin and thick disc separation

For reasons of perspective, observing the structure of other galaxies similar to ours gives us valuable clues about what the structure of our own would be like. The discovery of the existence of thick discs in outer galaxies by Tsikoudi (1979) and Burstein (1979), led to its search also on the Milky Way. Its identification and subsequent confirmation of its existence in our Galaxy too came with the works of Yoshii (1982) and Gilmore and Reid (1983). While thick discs are detected in most edge-on disc galaxies, where thick discs have larger scale heights (h_Z) and longer scale lengths (h_R) than the thin discs (e.g. Yoachim and Dalcanton, 2006), their formation scenarios are still the subject of debate (Kasparova et al., 2016). An important distinguishing feature between the two discs is that they have different chemistry and spatial distributions. Thus, when we compare both components of the Galactic disc, we see that the thick disc stars are enhanced in [α/Fe] with the overall metallicity lower than that of the thin disc. On the other hand, the thick disc has a larger scale height (around $\sim$ 900 pc), compared to that of the thin disc ($\sim$ 300 pc) (Jurić et al., 2008). Furthermore, the stars in the thin disc (among which our Sun is found), have a tendency to remain in the Galactic plane due to their low vertical component (W) of space velocity; while thick disc stars have higher vertical speeds. In addition, the vertical motions of Galactic disc stars are known to increase with stellar age (e.g. Ting and Rix, 2019, and references therein). Taking advantage of this, different authors have proposed several methods to separate the thick disc from the thin disc in the Milky Way, based on kinematics, chemistry or age (e.g. Prochaska et al., 2000; Fuhrmann, 1998; Haywood et al., 2013; Adibekyan et al., 2012; Recio-Blanco et al., 2014). According to Kordopatis et al. (2011), who analyzed thick disc stars outside the solar neighbourhood, the properties of the distant thick disc seem to differ only slightly from the thick disc in the solar vicinity. However, it should be noted that the separation between the thin and the thick disc is not always clear, but rather is a smooth transition (Bovy et al., 2012, 2016), so it is required to adopt several criteria and characteristics. Furthermore, Hayden et al. (2017) urge to reserve the term thick disc for the geometric thick disc, which varies with the Galactic radius, being in the inner Galaxy and solar neighbourhood dominated by metal-poor high-[Mg/Fe] populations, differing from the values in the outer disc.

For our sample of half a thousand stars in the solar neighbourhood, the distinction between thin and thick disc stars was taken from Mikolaitis et al. (2018),

Mikolaitis et al. (2019) and Ref. I. We separate the stars of our sample into the substructures of the Galactic disc, attending to two kinematic criteria and a chemical composition criterion. For the first kinematic criterion we follow Bensby et al. (2003), which introduces the probabilities of belonging to the thin, thick disk and halo (TD, D, H respectively) establishing that the potential stars to belong to the thick disc must have twice the probability of belonging to the thin disc (TD/D > 2); and the opposite, candidates to belong to the thin disc they must have half the probability than thick disc (TD/D < 0.5). On the other hand, stars with TD/H <1 are potentially Galactic halo stars, which were excluded from this thesis. This procedure is exposed in the Appendix A of Bensby et al. (2014), and shown in Eq (2.4), where X are the observed fractions of stars for the populations in the solar neighbourhood in the Galactic plane, and f is defined by Eq (2.5), where in turn k is defined by Eq (2.6), the σ are the respective velocity dispersions, and LRS and asym refers to the local standard of rest and the asymetric drift respectively:

$$TD/D = \frac{X_{TD}}{X_D} \cdot \frac{f_{TD}}{f_D} \tag{2.4}$$

$$f(U,V,W) = k \cdot exp\left[-\frac{U_{LRS}^2}{2\sigma_U^2} - \frac{(V_{LRS} - V_{asym})^2}{2\sigma_V^2} - \frac{W_{LRS}^2}{2\sigma_W^2}\right] \tag{2.5}$$

$$k = \frac{1}{(2\pi)^{3/2}\sigma_u\sigma_v\sigma_w} \tag{2.6}$$

In Figure 2-6 we show the probability as a function of metallicity. Accordingly, of our 506 stars, we have 489 that meet TD/D < 0.5 (more than twice as likely to belong to the thin disc than to the thick disc); 5 stars "in between" (0.5 ≤ TD/D ≤ 2); 12 with TD/D > 2 (double probability of belonging to the thick disc than to the thin disc).

The second kinematic criterion is based on the total Galactic space velocity Eq. (2.7), where U is the radial velocity (km/s) toward the Galactic center, V the tangential velocity (km/s) in the direction of Galactic rotation, and W the vertical velocity (km/s) toward the North Galactic Pole. This is illustrated by the so-called Toomre diagram (Figure 2-7). Different authors found different ranges to attribute the stars to the different Galactic components combining different selection criteria. These intervals vary slightly from author to author, thus Feltzing et al. (2003) in their Figure 1 shows that $V_{\rm tot} < 60$ km s^{-1} belong mostly to the thin disc and stars with $V_{\rm tot}$ between 80 and 180 km s^{-1} belong to the thick disc; in Bensby et al.

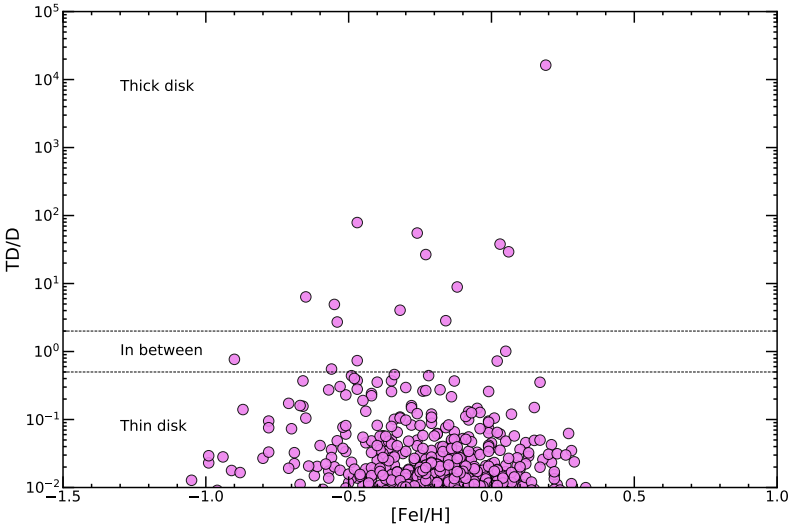

Figure 2-6: TD/D probability ratio versus metallicity for the sample of 506 stars

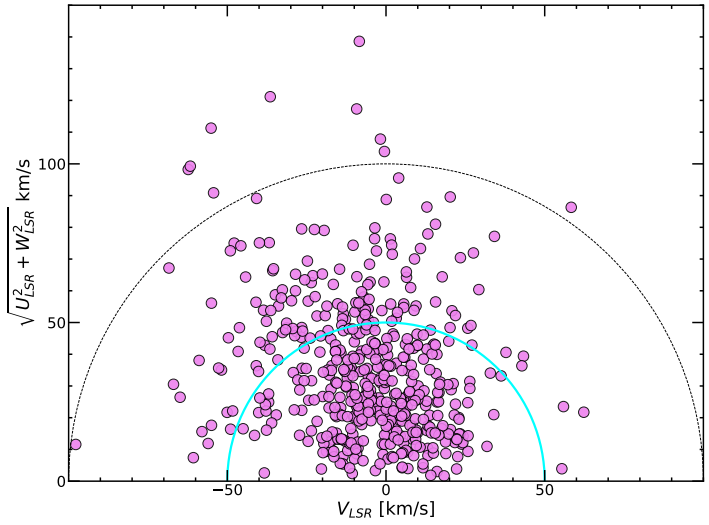

Figure 2-7: Toomre diagram in steps of 50 km s^{-1} for the sample of 506 stars

(2014) we see that stars with $V_{\rm tot}$ below 50 km s^{-1} belong mostly to the thin disc, stars between 70 and 180 km s^{-1} belong to the thick disc; and stars with $V_{\rm tot} > 200$ km s^{-1} are attributed to the Galactic halo; Fuhrmann (2000) reduces the range of the thick disc to velocities between 85 and 180 km s^{-1}.

$$V_{tot} = \sqrt{U_{LSR}^2 + V_{LSR}^2 + W_{LSR}^2} \tag{2.7}$$

The definitive criterion used for the separation of the components in the aforementioned papers is the chemical criterion. This separation based on the α-elements is most prominent in the case of magnesium, as shown in the Figure 2-8 for the 506 stars. The α-elements averages used were Mg I, Si I, Si II , Ca I, Ca II , Ti I, and Ti II.

The following Figure 2-9 shows the same 506 stars but using a quantile-based discretization function, dividing the underlying data into equal sized bins (each marker represents the same number of stars). In the aforementioned figure, the separation of both components is very clear, where the cyan squares represent the stars of the thin disc and the yellow triangles those of the thick disc. The data for each population is divided into 10 bins each (q = 10), and the Figure 2-9 also shows the standard deviation of each bin.

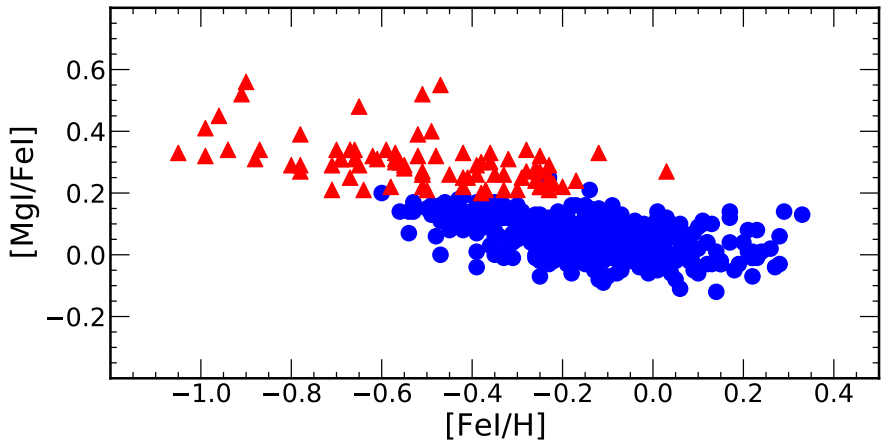

Figure 2-8: [Mg I/Fe I] ratio as a function of metallicity for the 506 stars sample. This relationship is usually used as a chemical separator of components.

In the following Figure 2-10 we see how the thick disc population is usually older than that of the thin disc, as well as an increasing trend of the maximum height above the galactic midplane ($|z_{\rm max}|$) with age, while for the mean galactocentric

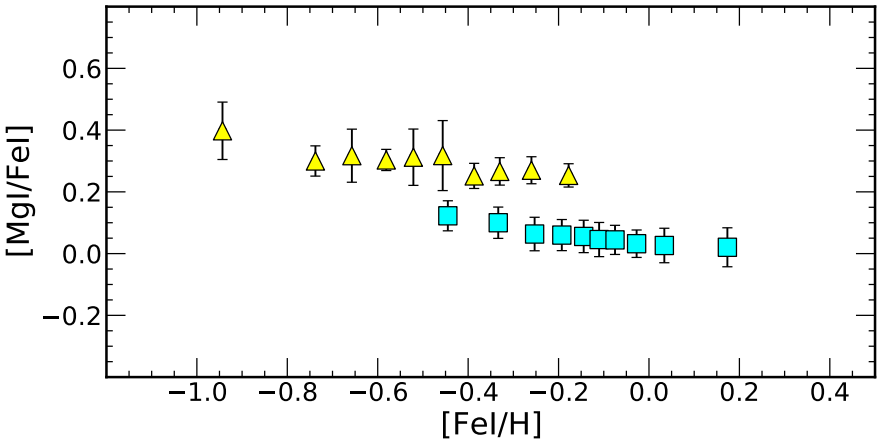

Figure 2-9: The same as in Figure 2-8, the [Mg I/Fe I] ratio as a function of metallicity for the 506 stars sample, but with the results equally binned (q=10).

distance (R_{mean}) no significant trends are seen. The last panel shows a kernel density estimate (KDE) distribution for both populations, represented using a continuous probability density curve.

The Figure 2-11 shows the main stellar parameters histograms for the two populations of the Galactic disc.

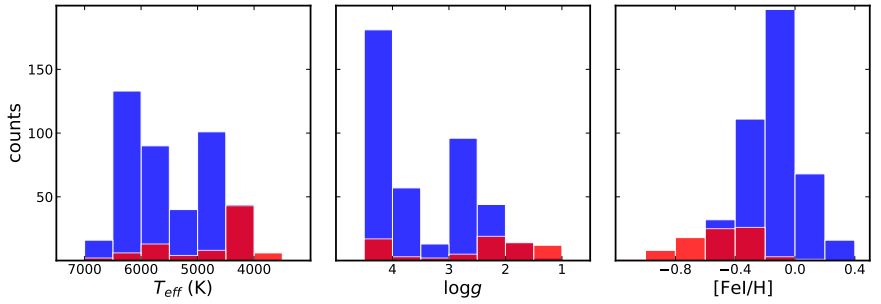

Figure 2-11: Main stellar parameters histograms for the two populations of the Galactic disc. Blue colour for thin disc and red colour for the thick disc

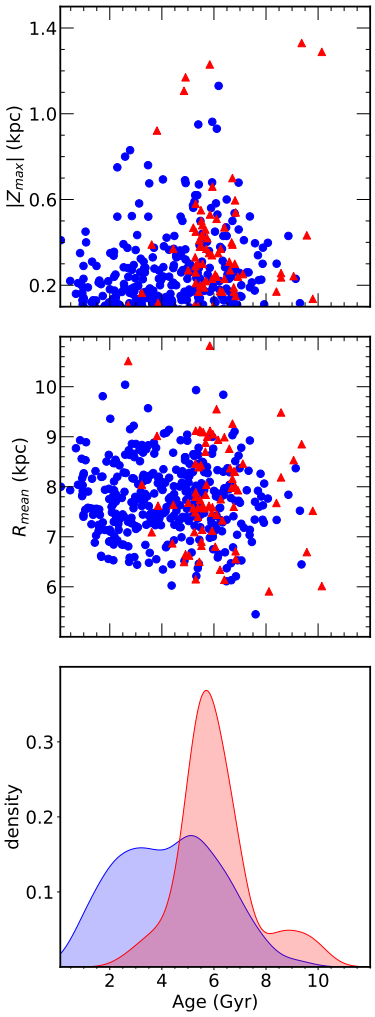

Figure 2-10: R_{mean} and $|z_{\mathrm{max}}|$ as a function of Age for the two populations of the disc, and a KDE distribution showing a continuous density estimate of the two populations

2.2. The open clusters sample from Gaia-ESO survey (GES)

2.2.1. Data reduction and analysis

2.2.1.1. Tha Gaia-ESO IDR6

For the analysis of open clusters, this thesis is based on data from IDR6 of the Gaia-ESO Survey obtained from the spectral analysis from the UVES spectra (resolving power R=47,000 and spectral range 480.0−680.0 nm). The spectra were reduced

and analysed by the Gaia-ESO consortium and the data analysis is organised in different working groups (WGs). The spectra are analysed with several pipelines, internally combined by each WG, and then the results from the different WGs are homogenised using a database of calibrators, such as benchmark stars and open or globular clusters selected following the calibration strategy by Pancino et al. (2017) and adopted for the homogenisation by WG15 (Hourihane et al. in preparation). The analysis process for the UVES spectra have been described in Smiljanic et al. (2014); the main steps are here listed. The data reduction, radial and rotational velocity determinations are undertaken in INAF-Arcetri (Sacco et al., 2014) using the FLAMES-UVES ESO public pipeline. The analysis process for the UVES spectra of F, G, and K stars in the field of the Milky Way (MW), in open clusters, and in calibration targets, including globular clusters, was described in Smiljanic et al. (2014).

The recommended parameters and abundances are distributed in the IDR6 catalogue, which includes atmospheric stellar parameters, such as effective temperature, $T_{\rm eff}$, surface gravity, $\log g$, and metallicity, [Fe/H], and abundances of 32 elements, several of them in their neutral and ionised forms. Here we will discuss the abundances of five *s*-processes, four α elements, and an odd-Z element. All the abundances (by number) are expressed in their usual logarithmic form: A(El)=12+log(n(El)/n(H)), while the abundances normalised to the solar scale are indicated with [El/H]= log(n(El)/n(H))-log(n(El)/n(H))$_\odot$).

2.2.1.2. Solar abundance scale

In Table 2.7, we show, for the elements used throughout this thesis, both the solar abundances derived for the Sun in *Gaia*-ESO IDR6 and those from Grevesse et al. (2007), which are used in *Gaia*-ESO to build up both the model atmospheres and the synthetic spectra used by the consortium. We also include the average abundances of M67, which has a chemical composition very similar to the solar one (see, e.g. Önehag et al., 2011; Liu et al., 2016), and the abundances of their giant and dwarf member stars observed in *Gaia*-ESO IDR6. We separate dwarf and giant stars in M 67 on the basis of their surface gravity: we define a giant star if $\log g < 3.5$, and a dwarf star if $\log g \geq 3.5$. In the first part of Table 2.7, we present the adopted α and odd-Z elements, namely Mg, Al, Si, Ca, and Ti. In the second part, we show the slow neutron-capture elements (Y, Zr, Ba, La, Ce). The agreement between the solar and the average M67 *Gaia*-ESO abundances, and those of Grevesse et al. (2007), is very good, within 1-σ. In the last two columns, we show the abundances

Table 2.7: iDR6 solar and M67 abundances for neutron-capture elements and α-elements.

A(El)	Sun (iDR6)	Sun Grevesse et al. (2007)	M67 (iDR6)	M67 (iDR6) (giants)	M67 (iDR6) (dwarfs)
Mg I	7.51 ±0.02	7.53 ±0.09	7.50 ±0.04	7.53 ± 0.04	7.49 ± 0.04
Al I	6.40 ±0.02	6.37 ±0.06	6.42 ±0.03	6.49 ± 0.03	6.39 ± 0.03
Si I	7.44 ±0.02	7.51 ±0.04	7.44 ±0.03	7.50 ± 0.02	7.41 ± 0.02
Ca I	6.32 ±0.02	6.31 ±0.04	6.26 ±0.02	6.25 ± 0.02	6.29 ± 0.03
Ti I	4.89 ±0.02	4.90 ±0.06	4.90 ±0.03	4.87 ± 0.03	4.91 ± 0.03
Y II	2.19 ±0.04	2.21 ±0.02	2.17±0.04	2.09 ± 0.02	2.21 ± 0.05
Zr I	2.62 ±0.13	2.58 ±0.02	2.54±0.02	2.51 ± 0.03	2.61 ± 0.02
Ba II	2.20±0.04	2.17 ±0.07	2.17±0.06	2.12 ± 0.07	2.19 ± 0.06
La II	1.13±0.02	1.13 ±0.05	1.17±0.07	1.17 ± 0.02	1.17 ± 0.09
Ce II	1.70±0.02	1.70 ±0.10	1.66±0.07	1.66 ± 0.03	1.67 ± 0.09

of the giant and dwarf members of M67 separately, to estimate the impact of a single set of normalising values to both giant and dwarf stars. Bertelli Motta et al. (2018) investigated variations in the surface chemical composition of member stars of M67 as a possible consequence of atomic diffusion, which takes place during the main-sequence (MS) phase (see, e.g. Bertelli Motta et al., 2017; Souto et al., 2019). They found that the abundances of MS stars differ with respect to those of the giant stars, consistently with the predictions of stellar evolutionary models. In our sample, these differences and other possible effects due to spectral analysis are also noted on the average values of M67 dwarfs and giants, in particular for Al, and for Si among the odd-Z and α-elements and Y among the neutron capture.

Although these variations are not very large, they can affect our comparison between giant stars (essentially cluster members) and dwarf stars (most of them composing the field star sample), modifying their abundance scale. We thus normalised the abundances of dwarf and giant stars using two different values, corresponding to average values of M67 for dwarf and giant stars (fifth and sixth columns of Table 2.7).

2.2.2. Sample and stellar membership

Open clusters are among the best calibrators between the properties of stars and their ages. The member stars of the same cluster show homogeneity in age and chemical composition for most elements (an exception are those processed within the nuclear region of the star and brought to the surface by convection during the evolved phases of giants, such as C, N and Li, see, e.g., Randich and Magrini, 2021) and within the effect related to secondary process as atomic diffusion.

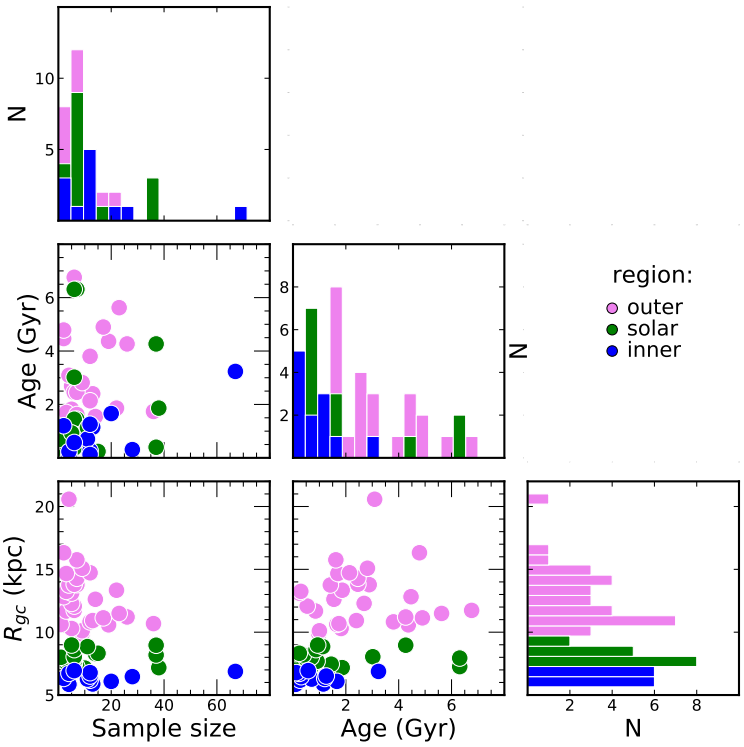

Figure 2-12: Distributions of ages, galactocentric distances and sizes (number of observed members in DR6) for our sample of clusters colour-coded by R_{gc} (inner disc R_{GC} <7 kpc in blue; solar region 7 kpc<R_{GC} <9 kpc in green; outer disc R_{GC} >9 kpc in pink).

In this thesis, we consider 62 OCs with age≥100 Myr, which contain a total number of 788 member stars. Among the cluster members, we only consider those that have at least one abundance value of an *s*-process and of one of the considered α- or odd-Z elements, which reduced our sample to 716 stars. The analysis of younger clusters needs a specific analysis, as detailed in Baratella et al. (2020, 2021), and the determination of their abundances are affected by activity, rotation, and problems in the derivation of the microturbulent velocity, ξ. For this reason, they are not included in this thesis. For our sample clusters, we adopt ages and galactocentric distances from the homogeneous analysis with *Gaia* DR2 data of (Cantat-Gaudin et al., 2020). In Figure 2-12, we show the distributions of their number of member stars (sample size), age, and R_{gc}. Since we are using only the UVES data, for most clusters we have about ten members, but in some cases we can have more. The ages ranges from 100 Myr to about 7 Gyr, while the R_{gc}

from about 6 kpc to 20 kpc. An interesting aspect of the open cluster sample is the absence of clusters older than about 3 Gyr in the inner disc. A comparison with the age distribution in the same three radial intervals used in our work of the whole cluster sample in Cantat-Gaudin et al. (2020) clearly shows the same effect: almost total absence of old clusters in the inner disc, as shown in Figure 2-13.

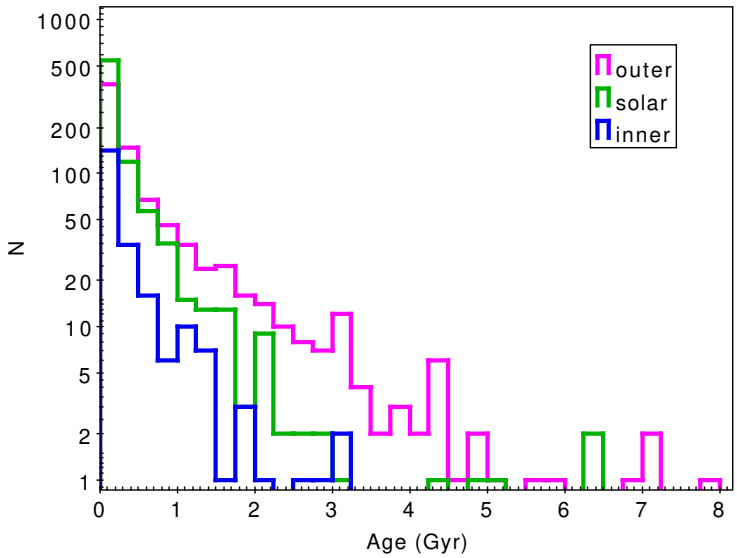

Figure 2-13: Distributions of ages in the three radial bins for the sample of 2017 open star clusters of Cantat-Gaudin et al. (2020). The histograms are colour-coded by R_{gc} (inner disc R_{GC} <7 kpc in blue; solar region 7 kpc<R_{GC} <9 kpc in green; outer disc R_{GC} >9 kpc in pink).

The limitation is likely intrinsic, due to the higher efficiency of destructive processes in higher density areas, as recently observed in M51. Messa et al. (2018) found, indeed, that the age distribution of clusters is dependent on the region considered, and is consistent with rapid disruption only in dense regions, while little disruption is observed at large galactocentric distances and in the inter-arm region.

This lack of inner old clusters has important consequences in our calibration work, because it will not allow us to date the oldest stars in the inner disc unless we accept extrapolations of the relationships.

The membership and the corresponding probability are computed in different ways depending on how many stars are observed in the clusters. For 41 clusters (676 stars) we used the membership analysis described in Jackson et al. (2022), and for the remaining clusters we used the analysis of Magrini et al. (2021b). The former

used a maximum likelihood technique to determine membership probabilities for each star based on their 3D kinematics, combining the parameters of GES with *Gaia* EDR3, 2MASS and VISTA. Using the membership of Jackson et al. (2022), we include only members with probability > 0.9 (MEM3D). For the other clusters, following Magrini et al. (2021b), the selection of members was done in two different ways, according to the number of observed candidate stars. When the cluster had more than 20 potentially member stars, the selection was done by performing a simultaneous fit of the *Gaia*-ESO radial velocities, RVs, and the parallaxes and proper motions from Gaia EDR3 (Gaia Collaboration et al., 2021*a*). When the cluster had fewer than 20 potentially member stars, the authors derived the peak and standard deviation of the RV distribution and selected stars within 2σ of the peak, then computing the average parallax, proper motion, and their standard deviations, and excluding those differing more than 2σ from the average values.

Since the median signal to noise ratio (SNR) of the cluster member stars (<SNR~100) is higher than that of field stars, and since for clusters we do not use individual abundances of member stars, but we adopt average values from all members, we did not apply any selection criteria based on the SNR or errors in parameters. We only discarded some stars with high errors in abundance of neutron-capture elements (error in abundance $\geq$ 0.1 dex).

In addition, for each cluster, we used the interquartile range rule to detect potential outliers that fall outside of the overall abundance pattern. This range is defined by (Q1 - 1.5×IQR, Q3 + 1.5×IQR), where IQR is the difference between the 75th and 25th percentiles of the data, being Q1 the lower quartile, Q2 the median, and Q3 the upper quartile (*vide* Figure A5 in which the outlier stars stand out from the main distribution for each cluster).

We examined the outliers for each cluster individually and in the context of the entire data set, finding some stars with anomalous abundances, in several cases extremely rich in abundance of *s*-process elements (e.g. "07465200-0441557" in Berkeley 39, with differences above 4 σ for Y2 and Ba2, "06025078+1030280" in NGC2141 and "06071407+2406547" in NGC2158, where those IDs are the CNAMEs given in the Gaia-ESO survey). The exclusion of those stars out of range (26 stars that are outlier in more than one *s*-process element) in addition to reducing the scatter improves the correlations. These stars will be analysed in detail in a future work, in which the overabundance of s-elements will be correlated with stellar properties, including binarity and rotation. The Kiel diagram and distribution of stellar parameters of our sample of member stars in open clusters

are shown in Figure 2-14. The sample contains both dwarf and giant members, with a predominance of giants. The 385 non-members are incorporated into the sample of field stars, as described above. In the Appendix of Ref. V we provide the global metallicity of each cluster from Randich et al. (2022)), together with its R_{gc} and age (Cantat-Gaudin et al., 2020), and the abundance ratios used here. We give both [El/H] and [El/Fe] because the transition between the two ratios is not straightforward, as they are calculated star by star and then averaged, while the overall metallicity [Fe/H] is generally calculated with a larger number of members.

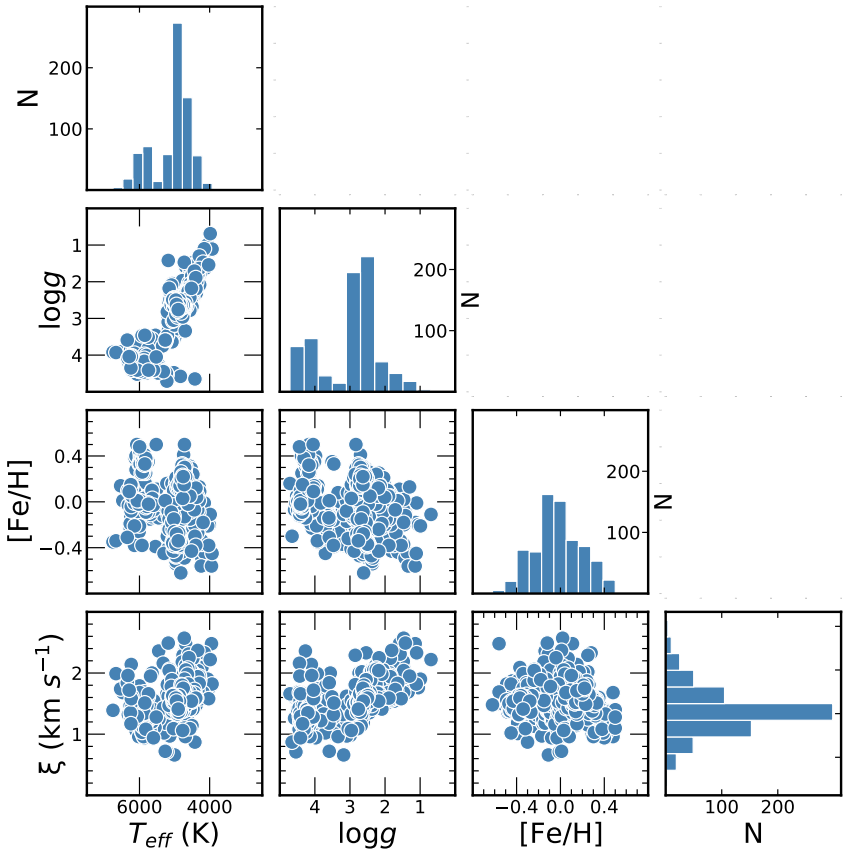

Figure 2-14: Kiel diagram diagram and distributions of stellar parameters (T_{eff}, log g, [Fe/H] and ξ) for our sample of member stars in open clusters.

Finally, in order to verify the applicability of the relations, we also used a sample of field stars with similar characteristics to those of the clusters with which we calibrated the relations. A detailed description of that sample can be found in section 3.2 of the Ref. V.

3. ABUNDANCE RATIOS

Among the multiple ways of studying the chemical evolution of the Galaxy, one of the preferred ones for its advantages is that which relates the abundances of elements to iron (the element to iron ratio) along the metallicity. The study of the [El/Fe] ratios should be interpreted taking into account that iron is produced for about 50% in type Ia supernovae, which are attributed to binary systems with CO white dwarfs, of much longer life than the progenitor stars of supernovae type II, and for the remaining 50% by supernovae type II (Woosley and Weaver, 1995; Nomoto et al., 1997). This means that the time scale in which the Fe is injected into the ISM is larger than that of the elements produced only in short-living sources. The general metallicity of the Galaxy is usually measured in the form of [Fe/H], which increases with time and gives us an idea of the progressive chemical enrichment of the Milky Way. It can be considered, in a first approximation, as the time variable. The variety of chemical abundances and their multiple combinations hide the secrets of the evolution of the Galaxy. Combining elements from different sources we can achieve different applications: abundances of *s*-process elements combined with α-elements are excellent age indicators; α-elements combined with iron are indicators of the components of the disc; heavy *s* combined with light *s* are the *s*-process indicators; etc.

3.1. The [El/Fe I] ratios versus [Fe I/H]

The abundance ratios results for the 10 neutron-capture elements calculated using the methods described in the previous chapter are presented below and are fully reproducible. The table with all the data is published online (J/A+A/649/A126) and available in the VizieR astronomical Catalogue provided by the *Center de données astronomiques de Strasbourg* (CDS), as an annex to Ref. II. In the Table 3.1 we present the basic abundance statistics with the mean, the standard deviation, as well as the maximum and minimum values and the number of stars for each element. Most of the elements studied are in an ionized state, although we also study elements in a neutral state such as Sr I and Zr I. As can be seen in the aforementioned table, in elements such as Y II it was possible to calculate the abundances in all the stars, followed in number by Ba and La. For elements like Sm II and Zr I this number was considerably lower.

In the Figure 3-1 we show the abundance ratios of the 10 neutron-capture

Table 3.1: Basic statistics of abundance ratios for the dwarfs and giants stars.

Name	Mean	SD	Min.	Max.	N (total)	N (thin)	N (thick)
			$\log g > 3.5$				
Sr I/Fe I	-0.02	0.10	-0.29	0.25	254	231	23
Y II/Fe I	-0.03	0.10	-0.38	0.38	279	255	24
Zr I/Fe I	0.01	0.11	-0.25	0.34	89	85	4
Zr II/Fe I	0.02	0.11	-0.18	0.45	252	232	20
Ba II/Fe I	-0.01	0.10	-0.36	0.44	278	254	24
Ba II/Fe I (NLTE)	-0.03	0.10	-0.38	0.42	278	254	24
La II/Fe I	0.01	0.11	-0.34	0.31	277	253	24
Ce II/Fe I	0.02	0.12	-0.34	0.40	241	221	20
Pr II/Fe I	0.14	0.13	-0.13	0.45	177	161	16
Nd II/Fe I	0.04	0.12	-0.24	0.38	240	216	24
Sm II/Fe I	0.08	0.15	-0.21	0.42	61	52	9
Eu II/Fe I	0.07	0.11	-0.22	0.39	263	245	18
			$\log g \leq 3.5$				
Sr I/Fe I	-0.01	0.10	-0.23	0.24	199	151	48
Y II/Fe I	-0.05	0.11	-0.31	0.33	227	169	58
Zr I/Fe I	0.07	0.11	-0.20	0.49	218	167	51
Zr II/Fe I	0.06	0.10	-0.17	0.55	224	169	55
Ba II/Fe I	-0.05	0.13	-0.32	0.29	226	169	57
Ba II/Fe I (NLTE)	-0.09	0.13	-0.38	0.27	226	169	57
La II/Fe I	0.06	0.10	-0.24	0.39	227	169	58
Ce II/Fe I	-0.02	0.11	-0.34	0.30	226	169	57
Pr II/Fe I	0.25	0.13	-0.04	0.62	225	168	57
Nd II/Fe I	0.13	0.10	-0.16	0.61	226	169	57
Sm II/Fe I	0.19	0.12	-0.07	0.51	196	142	54
Eu II/Fe I	0.18	0.17	-0.14	0.94	225	167	58

elements as a function of [Fe I/H], and in the two populations of the Galactic disc as referred above. The Galactic evolution models by Pagel and Tautvaisiene (1997) and Prantzos et al. (2018) for the aforementioned elements are also shown, as an example of pioneering and modern models respectively; and the dashed black lines represent the solar values. In the aforementioned Figure we show the abundance ratios of the ionized Zr, whereas in the online table we also provide the values for neutral Zr. For the case of Ba, we provide results in the Local thermodynamic equilibrium (LTE) and Non-local thermodynamic equilibrium (NLTE), which we also provide in the table published online.

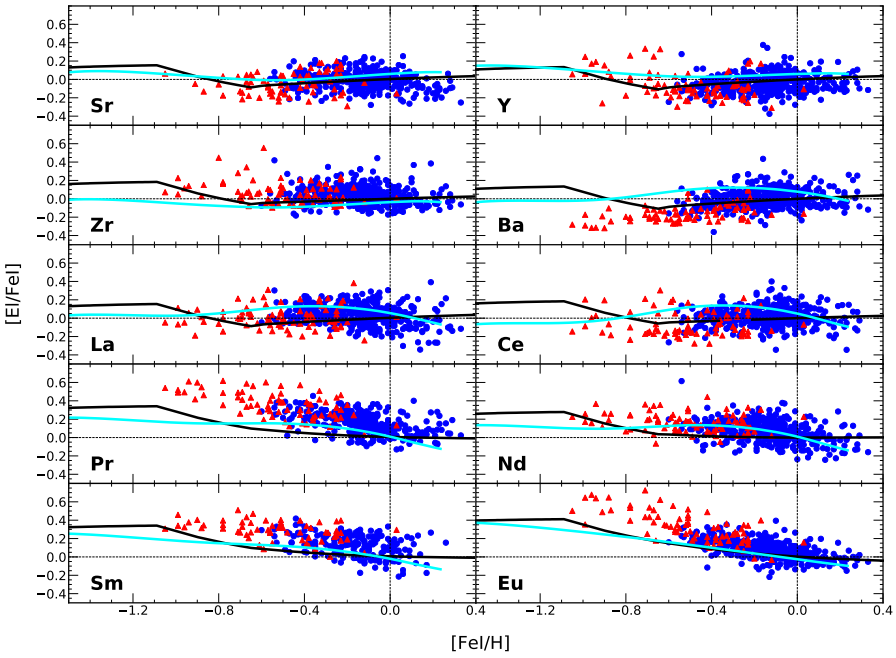

Figure 3-1: Elemental abundance trends relative to [Fe I/H]. As in 2-8 and followings, the blue dots represent the thin-disc stars, and red triangles indicate the thick-disc stars. The continuous cyan lines show the models by Prantzos et al. (2018) and the black ones Pagel and Tautvaisiene (1997).

In the Figure 3-2 we show the same results of the Figure 3-1 but divided into 10 equally distributed bins (each marker represents the same number of stars). As in the Figure 2-9, the cyan coloured squares represent the stars of the thin disc and the yellow triangles those of the thick disc. Each bin also provides vertical bars that represent the standard deviation, and the dashed black lines show the solar values.

In the Figure 3-3 we show the boxplots for the abundance ratios of each el-

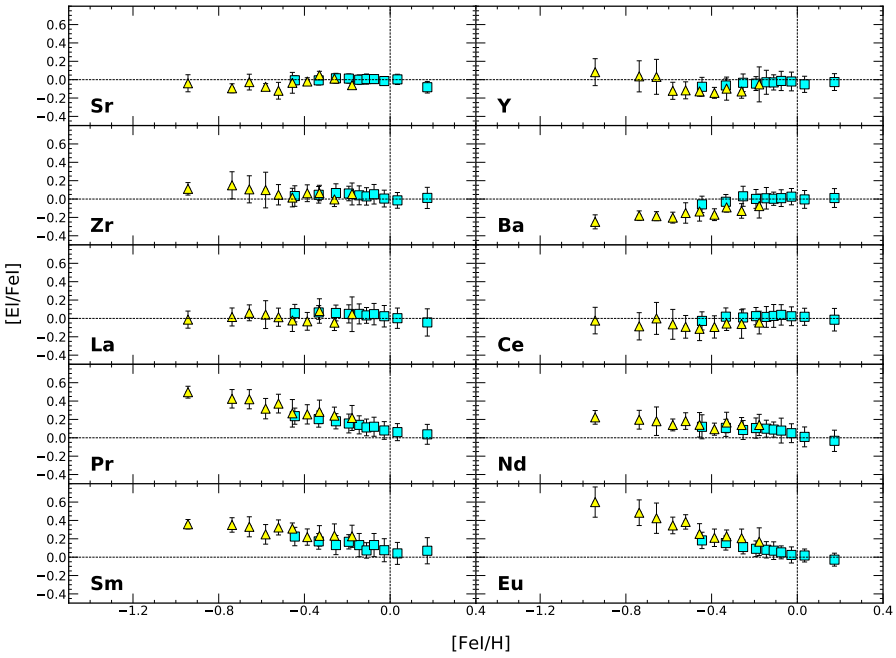

Figure 3-2: Elemental abundance trends relative to [Fe I/H] with the results shown in 10 equally distributed bins (q=10). The dashed black lines show the solar values (colours as in Figure 2-9)

ement for the thin and the thick disc. In the aforementioned figures, the boxes extend from the Q1 to Q3 quartile values, with a line at the median (Q2), and the whiskers extend from the edges of box to show the ranges of the abundance ratios. The dashed line marks the solar values for reference. The dimensions of the boxes as well as the length of the whiskers give us an idea of the degree of dispersion and skewness, which is also reflected in their trends. It also allows us to compare the different groups of elements, and the elements to each other for the components of the Galactic disc in our ranges of metallicity. Thus, as we can see, the difference between components for Ba and Eu (pure *s*- and pure *r*-process elements respectively) is evident, and which we will comment on in the following sections.

The abundance trends themselves provide essential clues for unraveling stellar and Galactic evolution. For these to be held on a solid basis, successive improvements and confirmations are necessary, as well as to extend the study to the different populations and locations in the Galaxy. As we will see in the following sections, neutron-capture elements offer increasing potential in that goal. Aware of this,

different authors have set their sights and directed their efforts in this direction.

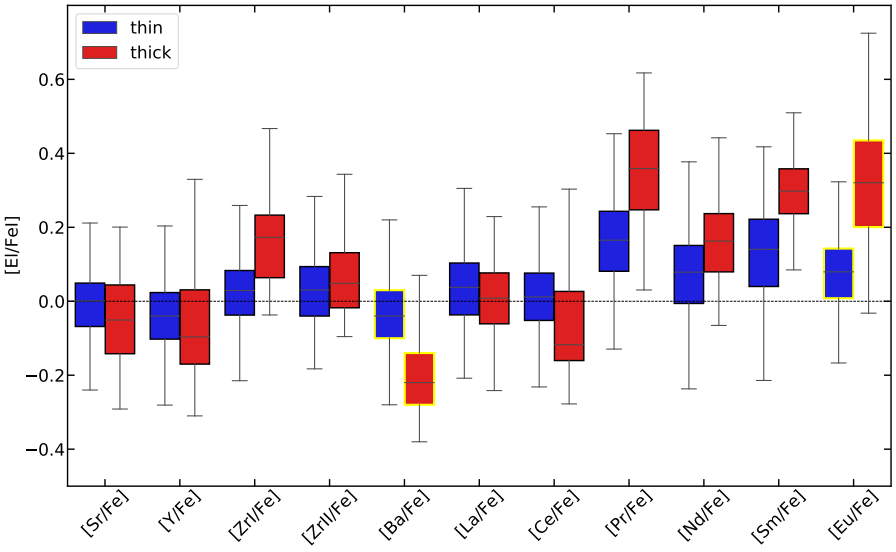

Figure 3-3: [El/Fe I] box plot for the thin and thick disc comparison. The box shows the quartiles of the [El/Fe I] data with a line at the median while the whiskers extend to show the whole distribution.

In general, the trends shown in the Figure 3-1 are in line with those previously obtained by other authors within the uncertainties, which once again confirms its validity. Some of them are reference works and deserve a special attention, laying a solid foundation to build research around neutron-capture elements. Mishenina et al. (2013) made a study of the abundances of 8 neutron-capture element (Y, Zr, Ba, La, Ce, Nd, Sm, and Eu) for 276 FGK dwarfs, located in the Galactic disc, in a metallicity interval between −1 and +0.3 dex and assigning for most of the stars to a Galactic substructure according to their kinematics. That study was followed by Bensby et al. (2014) and Battistini and Bensby (2016), which analysed the abundance of 9 neutron-capture elements using spectral synthesis; in the first study, Y and Ba for 714 FG dwarf and subgiant stars, and in the second Sr, Zr, La, Ce, Nd, Sm, and Eu for 593 FG dwarf stars, all of them in the solar neighbourhood and providing temporal and spatial relations. Afterwards, Delgado Mena et al. (2017) analyzed the abundances of 7 neutron-capture elements (Sr, Y, Zr, Ba, Ce, Nd, and Eu) for 1111 FGK dwarf stars in the different populations of the Galactic disc by the method of equivalent widths (EWs). Then came the study of Magrini et al. (2018), who provided the abundances of 5 neutron-capture elements (Y, Zr, Ba, La, and Ce) homogenised using several different methods for field stars and

open clusters for the Gaia-ESO Survey, deriving statistical ages and distances of field stars, and separating them into thin and thick disc populations. Finally, it is worth mentioning the work of Forsberg et al. (2019), who derived abundances from Zr, La, Ce and Eu in 45 bulge giants and 291 local disk giants separated into thin and thick disk components combining abundances and kinematics. To the list of elements studied previously we add Pr, for which there are fewer studies.

Regarding the abundances of strontium, it is worth noting the [Sr/Fe] ≈ -0.2 for solar metallicity stars in the Battistini and Bensby (2016) sample, which contrasts with our results, taking into account that we use the same single neutral line of strontium (4607.33 Å), also used by Delgado Mena et al. (2017). For a more detailed discussion in this regard, we refer to Mishenina et al (2019).

3.1.1. The first *s*-process peak. The light *s*-process elements Sr, Y, Zr

As we saw in the Figure 1-4 in Chapter 1, Sr, Y and, Zr belong to the first *s*-process peak and are called the light *s*-process (ls) dominated chemical elements. As we also show in the Figure 1-5 c in Chapter 1, that first *s*-process peak is around the magic number N = 50. Although the *s*-process is primarily responsible for the abundances of Sr, Y and Zr, their production in exact quantities is still debated. For instance, the low percentage (66%) of contribution of the *s*-process in the Sun that Bisterzo et al. (2014) gives to Zr contrast with the high values given by other authors, closer to those of the other elements of the first peak, as seen in the Table 1.1. Furthermore, chemical evolution models often underestimate the Galactic production of Sr, Y, and Zr (Cristallo et al., 2015). Thus, its production is due to a combination of the main *s*-process, the weak *s*-process and the *r*-process in less quantity. The estimates of the contributions for the Sun are shown in the Figures 1-2, 1-7 and Table 1.1 in Chapter 1. To solve this question, Travaglio et al. (2004) revised the *r*- and *s*-process contributions to the solar Sr, Y, and Zr abundances and introduced the possibility of a primary process in low-metallicity massive stars different from the classical *s*- and *r*-process, which they tentatively called lighter element primary process (LEPP). This hypothesis was also approached for instance by Cristallo et al. (2015), Trippella et al. (2016), Prantzos et al. (2018), and Kobayashi et al. (2020), some of them investigating possible alternative solutions.

In the Figure 3-1 we compare our observational results with the theoretical models of Prantzos et al. (2018) (cyan colour). In that models, the authors used a new grid of metallicity-dependent isotopic stellar yields of LIMS from the FRUITY

repository and massive stars from Limongi and Chieffi (2018) taking into account the joint effect of metallicity, mass loss, and rotation for a large stellar mass range and for all stages of stellar evolution. The yields of massive stars were weighted *ad hoc* by a metallicity-dependent function of the rotational velocities, constrained to obtain the observed primary behaviour of nitrogen versus [Fe/H] and to avoid overproduction of *s*-elements at around [Fe/H] ~ -1. Besides, and for the purpose of comparing with the first evolutionary model of neutron-capture elements in the Galaxy (already available two decades ago), we show the semi-empirical model of Pagel and Tautvaisiene (1997) (black line), which had been previously applied to oxygen, α- and *r*-process elements (Pagel and Tautvaisiene, 1995). This model considers two separate time delays of about 37 Myr and 2.7 Gyr, corresponding to progenitor masses of about 8 and 1.5 $M_{\odot}$ respectively. Both early and modern models seem to reproduce the observations for the elements in this section quite good. Regarding the thick disc, our results differ slightly from those of Delgado Mena et al. (2017), for which in metal-deficient thick-disc stars the zirconium abundances are much higher than those in the thin-disc stars. Our results for the case of Zr seem to be closer to those of Mishenina et al. (2013). In any case, the discussion remains open.

3.1.2. The second *s*-process peak (I). The heavy *s*-process elements Ba, La, and Ce

As seen in the Figure 1-4 in Chapter 1, Ba, La and Ce belong to the second *s*-process peak and are called the heavy *s*-process (hs) elements. Like the first *s*-process peak, and as seen in the Table 1.1 in Chapter 1, they are *s*-process dominated elements. As we also show in the Figure 1-5 b in the above-mentioned first Chapter, the second *s*-process peak is around the magic number N = 82. As noted in Käppeler et al. (2011), all isotopes beyond between ^{90}Zr and ^{209}Bi are mainly produced by the *s*-process "main" component, leaving the remaining element yields to the *r*-process component. Therefore, we would expect a similar production pattern for these 3 elements and it should be reflected in their abundances. Indeed, we found a similar behavior for these elements, with slight differences for Ba. When looking at the models, in the Prantzos et al. (2018) baseline model, the Low and intermediate-mass stars (LIMS) contribution to Ba, La, and Ce abundances reaches its maximum at around [Fe/H] = -0.4. Observations seem to suggest that this maximum should be around [Fe/H] = -0.2, and the model should start accounting for the LIMS input a

metallicities around ~ -0.7 dex, as was modeled by Pagel and Tautvaisiene (1997). However, the model by Prantzos et al. (2018) reproduces the elemental abundances in the supersolar metallicities stars very precisely. In contrast to the elements of the first *s*-process peak, for the elements of the second peak, it is observed that the [El/Fe I] ratios are slightly lower in the thick disc than in the thin disc. This is clearly seen in the Figure 3-2 with the binned results. It is also seen in the Figure 3-3, where the Ba is well below the solar value in the case of the thick disc. This difference is more visible in the case of Ba, probably due to its *s*-process purity (81-89% in the Sun according to different authors). In any case, they still agree with the thin-disc model by Pagel and Tautvaisiene (1997). This also suggests that the timedelay of the main *s*-process contribution should be longer in the Prantzos et al. (2018) model.

3.1.3. The second *s*-process peak (II). The mixed elements Pr and Nd

Like Ba, La and Ce, and as seen in the Figure 1-4 in Chapter 1, Pr and Nd also belong to the second *s*-process peak. However, and unlike Ba, La and Ce, and as seen in the Table 1.1 in Chapter 1, they are mixed elements, and are not dominated by any process. The estimates of the contributions for the Sun are shown in the Figures 1-2, 1-7 and Table 1.1 in Chapter 1. This circumstance should be reflected in its trends.

When analyzing the Pr, our results agree with the Prantzos et al. (2018) model from slightly sub-solar to super-solar metallicities, with a higher [Pr/Fe] ratio at metallicities below than -0.2 dex. The Pagel and Tautvaisiene (1997) model also underestimates the [Pr/Fe] ratio for low metallicities. The *r*-process compensates the lower LIMS effect on Pr compared to Ba, La, or Ce. According to our observational results for Pr, the *r*-process contribution to the praseodymium production may be higher. This suggests that the *r*-process effect was underestimated both by Prantzos et al. (2018) and Pagel and Tautvaisiene (1997). From Figure 3-1, the Pr behavior seems to be closer to elements such as Sm or Eu, especially in the thick disc (also see Figure 3-3), as we will see in the next section.

On the other hand, Pr is the element of the 10 studied in this thesis with the smallest solar abundance after Eu (*vide* Figure 2-4), as well as the one with a higher average [El/Fe I] ratio, followed by the Sm and Eu (*vide* Figure 3-3). The Pr is a poorly studied element at an observational level, so these findings are very valuable.

Regarding Nd, it seems to have a behavior more halfway from its mixed origin.

Thus, the model by Prantzos et al. (2018) fits to the distribution of [Nd/Fe] perfectly. Unlike [Pr/Fe], at sub-solar metallicities [Nd/Fe] abundances show flatter behavior, due to the higher percentage of *s*-process input in Nd than in Pr.

The thick-disc stars have higher ratios of Pr and Nd to Fe than in the case of *s*-process dominated elements, which qualitatively agree with the GCE predictions for the thin disc. This also can be seen in the Figure 3-3. Furthermore, the abundance difference between the *s*- and *r*-process dominated chemical elements in the metal-deficient thick-disc stars is even larger.

3.1.4. The *r*-process dominated elements Sm and Eu

Sm and Eu are the two *r*-process dominated elements among the 10 neutron-capture elements analyzed in this thesis. An amount close to 70% of Sm and more than 90% of Eu is made by this process. The *s*-process "main" component is only responsible for the remaining abundances. Due to the characteristics and weakness of the lines, samarium abundances were determined for fewer stars than in the case of other chemical elements. Despite this, the abundances form a clear increasing trend towards lower metallicities, as expected for an element with a high *r*-process input. This trend is in general agreement with those obtained, for example, by Battistini and Bensby (2016), among others. However, when comparing our results with Mishenina et al. (2013), we can notice how some stars have higher [Sm/Fe] ratios. Besides, Forsberg et al. (2019) debated that europium abundances might be super-solar at the solar metallicity. In addition to europium, they analyzed abundances of Zr, La, Ce in a sample of 45 bulge giants and 291 giants in the Galactic thin and thick discs. In their Figure 5 can be seen that the abundances of zirconium, which were determined from the neutral lines, are in agreement with the results of other works, while the abundances of La, Ce, and Eu, which were determined from the ionised lines, are systematically higher. One possible cause would be the systematic uncertainties in determining the surface gravity of these stars. The authors used the stellar atmospheric parameters from Jönsson et al. (2017), who reported that the surface gravities are overestimated while comparing the results with the Gaia stellar parameter benchmark values. If this would be the case, the abundances of the ionised elements would be overstimated as well.

If we look at the chemical evolution models used, both by Prantzos et al. (2018) and Pagel and Tautvaisiene (1997), which agree fairly with each other for these two dominated *r*-process elements, they still underestimate the abundance

ratios. Regarding the relative differences between thin and thick disc in our sample, as seen in the Figures 3-1, 3-2 and 3-3, the stars of both components show in general higher abundances, especially for europium, compared with the *s*-process dominated elements, which agrees with the GCE theory. This is more evident in the case of the thick disc, contrasting with the low values of Ba. This fact could be used as an additional method of chemical separation of components *a posteriori*. In fact, for both Eu and Ba, if we consider only the values between the lower and the upper quartile around the median, the component separation is well defined, which makes the Eu a key and promising element in this regard as well.

In the meantime, new developments in modeling the *r*-process yields and time delays in its production are progressing, and new production sites are close to being unveiled (e.g. Côté et al., 2019; Schönrich and Weinberg, 2019). The additional origin in Eu production is associated to neutron star mergers and other sources, as discussed in the Chapter I. Thus, Matteucci et al. (2014) found that the models with only neutron star mergers or together with type II supernovae can reproduce the observed Eu abundances in the Galactic disc. In any case, Côté et al. (2019) emphasized that the neutron star mergers cannot reproduce alone the observational constraints at all metallicities, proposing to consider as inputs magnetorotational or other unusual supernovae active in the early universe and vanished with increasing metallicity.

3.2. The [hs/ls] ratios versus [Fe I/H]

In this section we make then a comparison between the elements of the first and second *s*-process peaks, discussed in the subsections 3.1.1 and 3.1.2. The main interest of the [hs/ls] ratio (also called *s*-process indicator) is that it is a good tracer of the *s*-process efficiency. As the metallicity decreases, the number of atoms of elements other than H and He inside the stars also decreases, and consequently the number of seed nuclei for neutron-capture is lower. This would imply that more neutrons per iron seed nuclei will be available, which should favors the production of heavy *s*-process dominated elements. Indeed, models and observations suggest the dependence on metallicity of the *s*-process nucleosynthesis (e.g. Gallino et al., 2006; Karakas and Lattanzio, 2014; Prantzos et al., 2018).

This comparison between the ls and hs elements, in addition to monitor the *s*-process efficiency due to their low neutron capture cross-sections, allows us to test the reliability of the GCE models. In the Figure 3-4 we compare our observations

of the two populations of the disc with the aforementioned models of Prantzos et al. (2018) and Pagel and Tautvaisiene (1997). We consider as hs (Ba, La, Ce, Nd) and ls (Sr, Y, Zr). It should be noted that to reliably reproduce the *s*-process indicators, it is necessary to take into account only those stars in which there are measurements of all the [hs/Fe] and [ls/Fe] abundances.

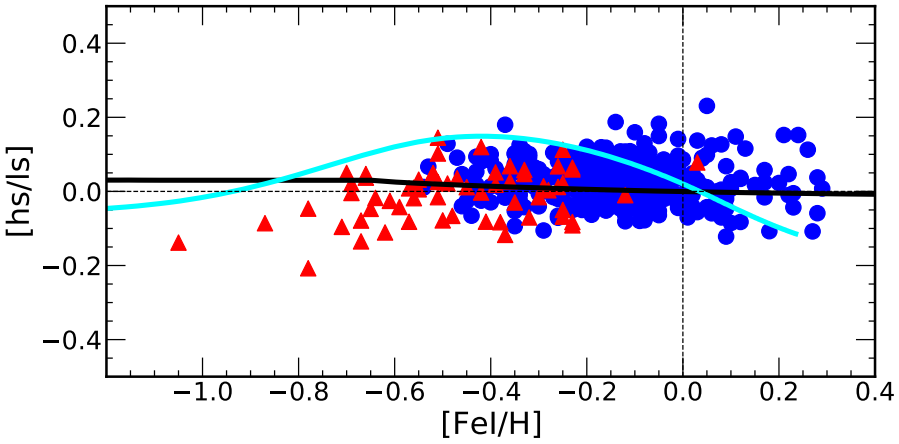

Figure 3-4: Hs (Ba, La, Ce, Nd) and ls (Sr, Y, Zr) abundance ratio with respect to [Fe I/H] compared with the GCE model predictions by Prantzos et al. (2018) and thin disc model by Pagel and Tautvaisiene (1997). colour code and markers as in Figure 3-1.

In Figure 17 of those referred authors Prantzos et al. (2018), they compare their models with the observed heavy-s (Ba, Ce, Nd) to light-s (Sr, Y, Zr) of Delgado Mena et al. (2017), concluding that the yields used in their baseline GCE model are reliable and reproduce the observational trends of unevolved stars. Due to the absence of La as hs in the aforementioned work, we made a comparison of our results considering both possibilities (with and without La), finding a difference in the [hs/ls] ratios of just 0.003 dex. Our observations suggest that the referred model should have its *bump* not at [Fe/H] ~ -0.5 dex, but at about -0.2 dex, and would start accounting for the LIMS input at higher metallicities (about -0.7 dex) as we discussed in the previous subsections. The aforementioned models show that rotating massive stars contribute significantly to the light *s*-process elements at subsolar metallicities, since in the absence of these, the [hs/ls] maximum would be much higher than in the observations; while the non-rotating case where the *r*-component is not considered is more noticeable for [Fe/H] < 1. The stars of the thin disc in our sample seem to follow a smooth, almost flat trend, while those of the

thick disc show a clear downward trend with decreasing metallicity. This behavior of the thick disc is very similar to that found by Delgado Mena et al. (2017). They suggested that low-mass AGB stars are not the only important contribution to *s*-elements of thick disc stars. Another example of models of *s*-process indicators are those of Cristallo et al. (2015b) using the FRUITY repository. These models show a strongly dependency on the initial stellar mass. Thus, a displacement of the peak of the maximum [hs/ls] ratio versus metallicity depending on the initial mass of the star is seen. Stars with the lowest initial mass have a higher [hs/ls] ratio with a peak at lower metallicities, and stars with higher mass produce lower [hs/ls] ratios with a peak at higher metallicities. This also means that low-mass AGB stars produce relatively more hs than ls elements at metallicities lower than the solar one. The lower [hs/ls] ratio values for the thick disc, can be related to both the different SFH and the metallicity dependence of the yields of neutron-capture elements.

3.3. The [*r*/*s*] ratio versus [Fe I/H]

In the previous section we compared the *s*-process dominated elements of the different peaks between themselves (*s*-process indicators). In this section we will compare them with those of the *r*-process. Its trace allows to draw the different star formation histories in the Galactic disc due to its different origin. A good way to do this is by studying the abundance ratio between the highest purity elements in each process, and that would correspond to Ba and Eu for the *s*- and *r*- processes respectively (see, for example Figure 1-6). In the Figure 1-8 of the Chapter 1 we showed the pure *r*-contribution of [El/Ba] and [El/Eu] for the 10 neutron-capture elements discussed in this thesis, calculated using the percentages of Bisterzo et al. (2014) and the solar abundances of Grevesse et al. (2007), and that we will now use to compare with the different element ratios.

The Figure 3-5 show the abundance ratio of the *r*-process dominated element of higher purity europium and *s*-process dominated element of higher purity barium [Eu/Ba] as a function of [Fe I/H]. In the Figure 3-6 and for comparison, we show the same relationship but using Sm as the *r*-process dominated element [Sm/Ba], and in the Figure 3-7 we compare both *r*-process elements [Sm/Eu]. In those figures, we also compare the abundance ratios with the GCE model predictions for the thin disc by Prantzos et al. (2018) and by Pagel and Tautvaisiene (1997) described before, as well as with a pure *r*-process ratio derived as explained above. As can be clearly seen in the figures, the GCE models of the thin disc have to be further

developed in order to account for the higher europium and samarium production.

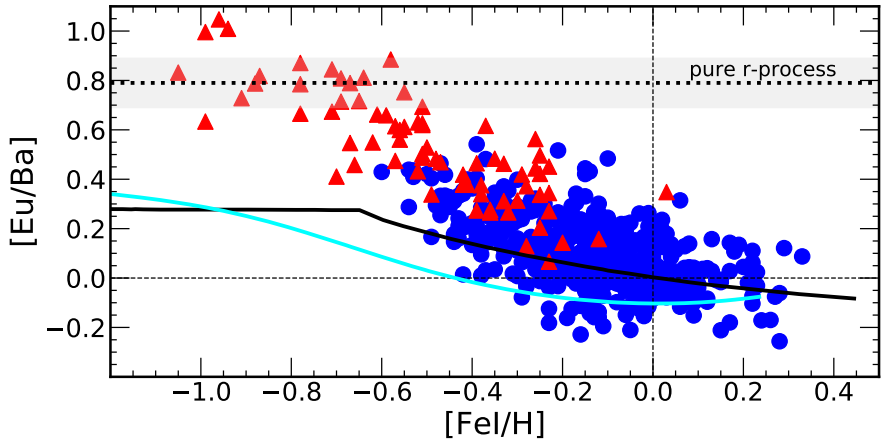

Figure 3-5: [Eu/Ba] ratio as a function of [Fe I/H]. Symbols are the same as in Figure 3-1. The dotted line and the shadowed area of ±0.1 dex uncertainty shows a pure *r*-process ratio derived using the percentages of Bisterzo et al. (2014) and the solar abundances of Grevesse et al. (2007).

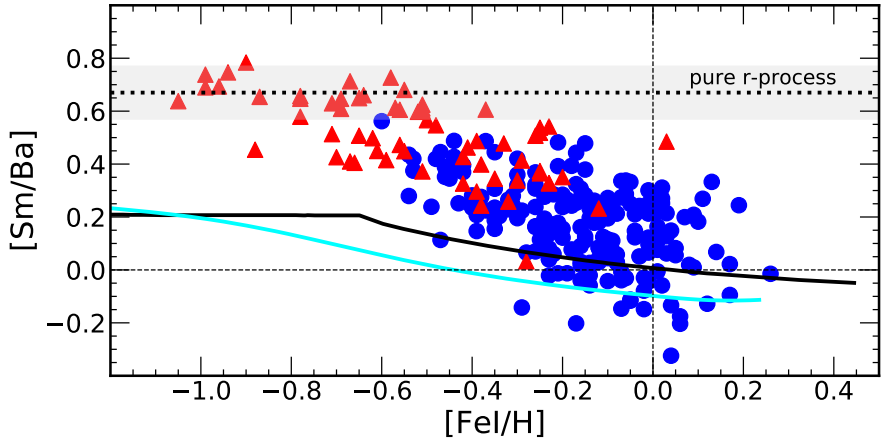

Figure 3-6: [Sm/Ba] ratio as a function of [Fe I/H]. Symbols and references are the same as in Figure 3-5.

Regarding the [Eu/Ba] ratio in the thick disc, Guiglion et al. (2018) pointed out that it should be constant with metallicity. However, for gadolinium and dysprosium (also *r*-process dominated elements) that study showed an [El/Ba] ratios decreasing with increasing metallicity, concluding that there is a different nucleosynthesis history in the thick disc between Eu and Gd-Dy. However, in the Figure 3-5 we can

see the decline of [Eu/Ba] ratio as a function of metallicity also for the thick disc, something also found in other studies (e.g. Battistini and Bensby, 2016; Delgado Mena et al., 2017; Magrini et al., 2018). As seen in the mentioned Figures 3-5 and 3-6, both the [Eu/Ba] and the [Sm/Ba] ratios for metal-poor thick-disc stars reach the pure *r*-process line, which can be interpreted as the *n*-capture process was the predominantly active at the beginning of the formation of the thick disc. Regarding the trend of the [Sm/Ba] ratio in the thin and thick discs, this is steep, although not so prominent as in the case of [Eu/Ba], which fits with the relatively lower production of samarium in the *r*-process sites. This slight difference in purity is well seen in the Figure 3-7.

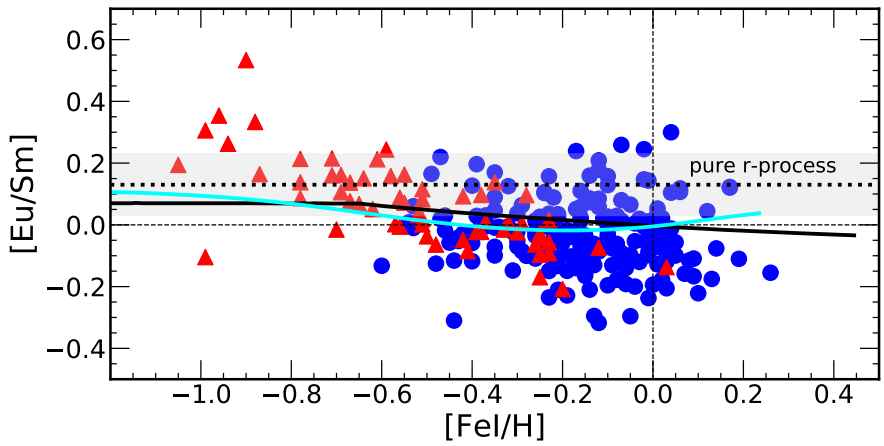

Figure 3-7: [Eu/Sm] ratio as a function of [Fe I/H]. Symbols and references are the same as in previous Figures 3-5 and 3-6.

Regarding the [Eu/Ba] ratio in the super-solar metallicity range, it should be noted that Delgado Mena et al. (2017) found an increase in this when increasing the metallicity for stars of the thin disc. However, from the work of Trevisan and Barbuy (2014) which was focused on the analysis of metal-rich stars, is inferred a slightly decreasing trend of [Eu/Ba] in super solar metallicity ranges, which also coincides with our results and other studies (e.g. Battistini and Bensby, 2016; Magrini et al., 2018).

3.4. The [r/α] ratios versus [Fe I/H]

Due to their origin and nature, the abundances of magnesium and europium are key elements that when associated with the Galactic components give us invalu-

able information on the formation and evolution of the Galaxy. In Chapter 1 we mentioned the possible production sites for europium, the origin of which is still debated. On the other hand, magnesium production is attributed to massive and intermediate-mass (IM) stars with masses between 2 and 8 $M_{\odot}$. The interest of magnesium also lies in the fact that its three isotopes are produced at different astrophysical sites, including AGB and massive stars (Vangioni and Olive, 2019). The study and comparison of Eu with and Mg is then crucial to understand if the r-process and the α-process share the same production sites or are released to the ISM over the same timescales. Such comparisons are specially useful to probe the chemical enrichment of the early Galaxy.

The importance [Eu/Mg] ratio was already pointed out by Mashonkina and Gehren (2001) already two decades ago, who studied it for 63 cool stars with metallicities ranging from −2.20 dex to 0.25 dex. In the referred work they found a [Eu/Mg] ratio tending to decrease with increasing metallicity both for the thin- and thick-disc stars. They also found an overabundance of Eu relative to Mg in three halo stars. However, in Mashonkina et al. (2003) they revisited the sample including 15 additional moderately metal-deficient stars and this overabundance of Eu relative to Mg was only found for two thick-disc and halo stars (*vide* their Figure 5). Later Delgado Mena et al. (2017) also found an almost flat [Eu/Mg] ratio (*vide* their Figure 15), suggesting that these two elements receive an important contribution from SNe progenitors with similar masses but less massive than oxygen progenitors. Finally, Guiglion et al. (2018) took up the topic for the AMBRE project in a large sample of FGK Milky Way stars in a range of metallicities very similar to our sample, reporting a decreasing [r/α] trend for increasing metallicity, suggesting that supernovae of different properties probably contribute differently to the synthesis of the elements of both processes, which was one of the important conclusions from their work.

The [Eu/Mg] ratio results as a function of [Fe I/H] for our thin and thick disc stars are shown in the Figure 3-8. To calculate the [Eu/Mg] ratio, the magnesium abundances were taken from Mikolaitis et al. (2019) and Ref. I. As seen in the above Figure 3-8, the [Eu/Mg] ratio has a decreasing trend with increasing metallicity for the thin disc, which is even more evident for the thick disc sample. This behaviour coincides with the negative trend of [r/α] with increasing metallicity for the thin-disc stars found by Guiglion et al. (2018) for the AMBRE project. However, for the thick disc they used 25 stars, so it was difficult to reach solid conclusions. We also confirm this decreasing trend of [Eu/Mg] with increasing metallicity for our

sample of 76 thick-disc stars, which seems steeper than for the thin disc. As we see in the Figure 3-8, the semi-empirical model of Pagel and Tautvaisiene (1997), which considers the production of Eu by type II supernova alone, underestimates the observations, while the model of Prantzos et al. (2018) overestimates them.

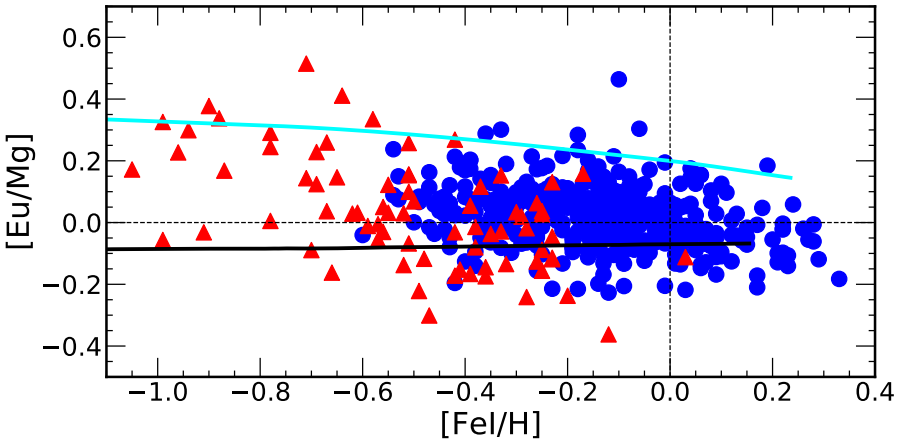

Figure 3-8: [Eu/Mg] ratio as a function of [Fe I/H]. Symbols and references are the same as in previous figures.

4. ABUNDANCE GRADIENTS

The different abundances of the ISM in different radial regions of the Galaxy are an indication of the progressive and varied enrichment that it undergoes throughout the successive generations of stars. Thus, by studying the chemical composition of the current ISM in different regions of the Milky Way we can know their different evolutionary histories. There is clear evidence that gas in the outer regions of the spiral galaxies tends to be more metal-poor than in the inner regions (e.g. Searle, 1971). This would be a consequence of a higher SFR in the Galactic centers, as it happens in our Galaxy at the present day (e.g. Rana, 1991). In fact, we can assume that the abundance gradients arise naturally as a result of the inside-out formation of the disc (e.g. Matteucci and Francois, 1989; Matteucci, 2014), meaning that this progressive enrichment occurs at different rates in different places of the Galaxy. Thus, this scenario gives predictions of abundance gradients in good agreement with observations, for example in the GCE model of Chiappini et al. (2001), which assumes two main accretion episodes for the formation of the Galaxy. The abundance gradients are then shown as an important observational constraint for the GCE models. The gradients along the Galactic disc have been known for decades and are proven by observations through different sources, such as the HII regions (e.g. Peimbert et al., 1978; Shaver et al., 1983; Esteban et al., 2002), PNs (e.g. D'Odorico et al., 1976; Maciel et al., 2006; Stanghellini et al., 2010), early B type stars (e.g. Gehren et al., 1985), Cepheids (e.g. Harris, 1981; Andrievsky et al., 2002; Genovali et al., 2015), and OCs (e.g. Janes, 1979; Hou et al., 2002; Cunha et al., 2016; Magrini et al., 2009). The advantages of using these specific observational tracers are related to their particular features: it is possible to estimate their ages and in some cases also their distances, and, taken all together, they can trace the evolution of the gradient with time, since they belong to different stellar populations.

Examples of the use of these tracers in the study of the radial abundance gradients of neutron-capture elements in the Galaxy are scarce. Some are found in Luck et al. (2011) and Lemasle et al. (2013) for Cepheids, or Overbeek et al. (2016) for OCs. While radial abundance gradients for the light and α-elements are better established, for neutron-capture elements they are still debated. It should be noted that radial gradients can be affected by the migration of stars along the Galactic radius, as well as by changes in their orbits, which can give biased information, so knowing their original position (their birth radii) is very important.

Several phenomena have been proposed as capable of inducing the radial mixing (Schönrich and Binney, 2009), from causes involving resonance mechanisms and spiral waves (Sellwood and Binney, 2002), to radial mixing caused by an orbiting satellite (Quillen et al., 2009).

From a theoretical point of view, one of the first models of radial abundance gradients in a wide galactocentric distance range (4-22 kpc) and for elements of different origin (α, iron peak and neutron capture) were provided by Cescutti et al. (2007). These models, which include Ba, La, and Eu, were compared with observed data Yong et al. (2006), Yong et al. (2005), and Carney et al. (2005) from Cepheids, open clusters and red giants respectively, and resulting in negative [El/H] gradients.

4.1. Age gradients

While the trends of the abundance ratios as a function of metallicity, associated with the progressive enrichment due to the different generations of stars, provide us with fundamental information about the stellar populations of our Galaxy, the study of the age gradients illustrates their evolution from another rewarding perspective. Simply seen, it is possible to find stars of the same type and age, with a different metallicity, which would indicate their birth in a different chemical environment (chemically evolved at different times); or on the contrary, stars with the same metallicity but different age, indicating that even having been born in a similar environment, their evolutionary state is different.

In this context, the origin of the time-evolution of the *s*-process abundances is one of the most attractive open topics in chemical evolution. This is due to the fact that, on the one hand, it involves the largest population of stars (LIMS stars), and on the other hand, it has multidisciplinary a nature, reconciling astronomical observations with models of stellar evolution up to nucleosynthesis. Among its most important applications, we recall its value as direct stellar age estimators, as we will see in the next chapter. D'Orazi et al. (2009)'s work first for Ba and then completed by Maiorca et al. (2011, 2012); Magrini et al. (2018) for the Y, Zr, La and Ce, established an increasing trend of the abundances of the *s*-process towards younger ages in open clusters, later confirmed in field stars by other works (e.g. Reddy and Lambert, 2017; Nissen et al., 2017; Spina et al., 2018; Horta et al., 2021). However, there is still no unanimous consensus on the origin of this growing trend, having been suggested phenomena such as mixing effects, observational effects, chromospheric or magnetic activity (e.g Bisterzo et al., 2014; Magrini et al., 2018;

Busso et al., 2021). The Maiorca et al. (2012) GCE model was able to reproduce this increasing trend towards younger ages, based on the fact that the production of the elements of the *s*-process from low-mass stars occurs later in the lifetime of the Galaxy. Among their arguments, they claimed that to produce the recent increase in the *s*-process abundances, low-mass AGB stars (M < 1.5 $M_{\odot}$) should release more neutrons than more massive AGB stars (M > 1.5 $M_{\odot}$).

4.1.1. The [El/Fe I] versus Age gradients for the thin and thick disc sample

The Figure 4-1 shows the distributions of element-to-iron ratios as a function of stellar ages for the two populations of the Galactic disc, including ordinary least-squares regressions (OLS) and theoretical models by Prantzos et al. (2018) and Maiorca et al. (2012). The Figure 4-2 shows the same results but binned at q = 10, in a uniform distribution.

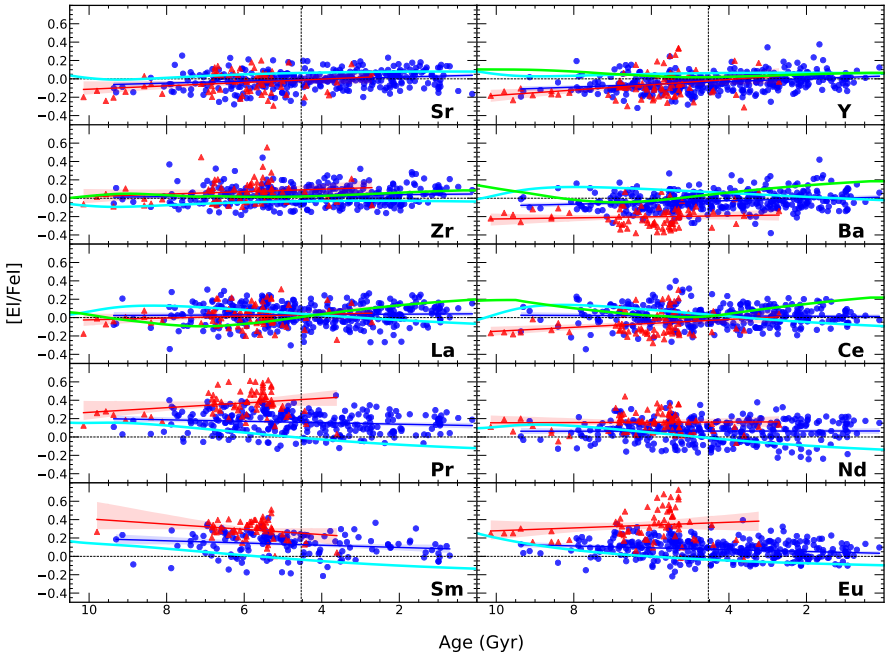

Figure 4-1: Elemental abundance trends relative to Age in Gyr. As in 2-8 and followings, the blue dots represent the thin-disc stars, and red triangles indicate the thick-disc stars. The green lines are the models by Maiorca et al. (2012) and the cyan ones are those of Prantzos et al. (2018). The blue lines are the linear fits for the thin-disc stars and the red ones show the thick-disc stars, with a 95% confidence interval for the ordinary least-squares regressions (OLS). The vertical dashed lines indicate the adopted age of the Sun (4.53 Gyr).

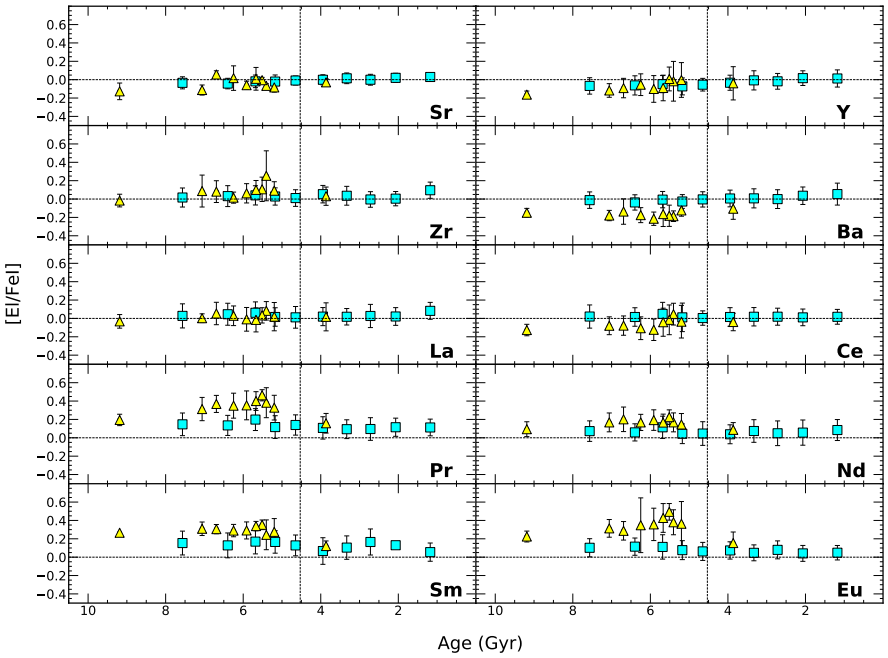

Figure 4-2: Elemental abundance trends relative to Age in Gyr with the results shown in 10 equally distributed bins (q=10). The dashed black lines show the solar values (colours as in Figure 2-9).

The coefficients of the regressions applied to the [El/Fe I] and age relations, are presented in Table 4.1. Specifically, in the referred table we provide the slopes, y-intercepts, Pearson correlation coefficients (PCC), and standard errors of the linear fits. We also computed the regressions for potentially thin disc stars (those with TD/D < 0.5) from Battistini and Bensby (2016) for Sr, Zr, La, Ce, Nd, Sm, and Eu, and data by Bensby et al. (2014) for Y and Ba, and with age determination uncertainties better than 3 Gyr. As seen in the aforementioned table, the slopes from our sample agree quite well with the slopes determined using the Battistini and Bensby (2016) and Bensby et al. (2014) studies. Nevertheless, we find some differences in the Ba abundances, which on average are higher in the Bensby et al. (2014) sample. It should be noted that this study included more stars reaching longer galactocentric distances. In some of these younger stars (often very active) this could be attributed to the overestimation of Ba by standard methods of LTE abundance analysis (Reddy and Lambert, 2017). The table also includes the regressions obtained for solar twins by Spina et al. (2018) and for the Galactic thin-disc stars with ages younger than 8 Gyr computed by Magrini et al. (2018) for

Y, Zr. Ba, La, and Ce using internal data of GES. It should be noted that Spina et al. (2018) used the orthogonal distance regression (ODR) method to calculate the slopes, while Magrini et al. (2018) used Weighted Least Squares (WLS). The choice of method used to calculate the slopes may slightly vary the results. A quick way to evaluate it is to do a residual test to diagnose heteroscedasticity or homoscedasticity. Due to the apparent absence of heteroscedasticity in our sample, and the high errors in the estimation of ages, we consider the use of the OLS as more reliable.

In the aforementioned Figure 4-1 we also compare our observational results with the models of Prantzos et al. (2018), already described, and Maiorca et al. (2012). The Maiorca et al. (2012) model is an improved version of the Arcetri Galactic chemical evolution model, analogous to the code exposed by Travaglio et al. (1999) and later improved in Travaglio et al. (2004). These improvements include a new prescription for the formation of the ^{13}C pocket for stellar masses below 1.5 $M_{\odot}$, in addition to adopting a fine mass resolution for low mass AGB stars and a relatively small time steps, and consider a detailed dependence on metallicity of the stellar yields. The Maiorca et al. (2012) model closely resembles our observations on elements such as Zr. For Ba, La, Ce, the abundance ratios are similar for the sub-solar ages, although our younger stars do not show so high abundance as are predicted by the model. This could be expected considering that this model takes into account young open clusters, where the abundances of Ba, La, and Ce are more enhanced than field stars of the same metallicity (see, e.g. Baratella et al., 2021). In that model the authors suggested that the observed enhancements could be due to a larger release of neutrons from the ^{13}C(α,n)^{16}O reaction in low mass ($M < 1.5 M_{\odot}$) AGB stars. Marsakov et al. (2016) also discussed the possible reasons for the *s*-process elements overabundances in open clusters, exposing others different from those of nucleosynthesis, such as high and elongated orbits.

The Prantzos et al. (2018) model predicts almost flat trends for the elements of the first *s*-process peak Sr, Y, and Zr from around 9 Gyr to the youngest objects; and for the mixed elements Pr and Nd, as well as for the *r*-dominated elements Sm and Eu, the models show a decrease in abundance ratio with decreasing age, which is also seen in our slopes and in agreement with the GCE. In any case, that continuous decline in [El/Fe I] ratios is steeper than our observations seem to show. For the hs elements, the model reaches its maximum abundance ratio at near 8 Gyr and then slightly decreases beyond that, as age decreases. If we compare this to our results, it appears that the model slightly overestimates and underestimates the

hs abundances in the older and younger stars respectively. This is better seen when comparing with the binned results of Figure 4-2.

The Figure 4-3 shows a compilation of the [El/Fe I] trends for the thin disc as a function of the age estimate. As can be seen, two opposing groups are clearly distinguished: those with an increasing slope, which would correspond to the *r*-process dominated elements Sm and Eu, and the mixed element Pr (magenta colour); and those with negative slopes, which correspond to *s*-process dominated elements Sr, Y, and Ba (blue colour). The other elements show an almost flat slope (gray colour). These trends indicate that the oldest stars were formed in an environment more enriched in elements of the *r*-process, as well as a remarkable production of the elements of the *s*-process throughout the evolution of the Galactic disc, which is consistent with the GCE theory.

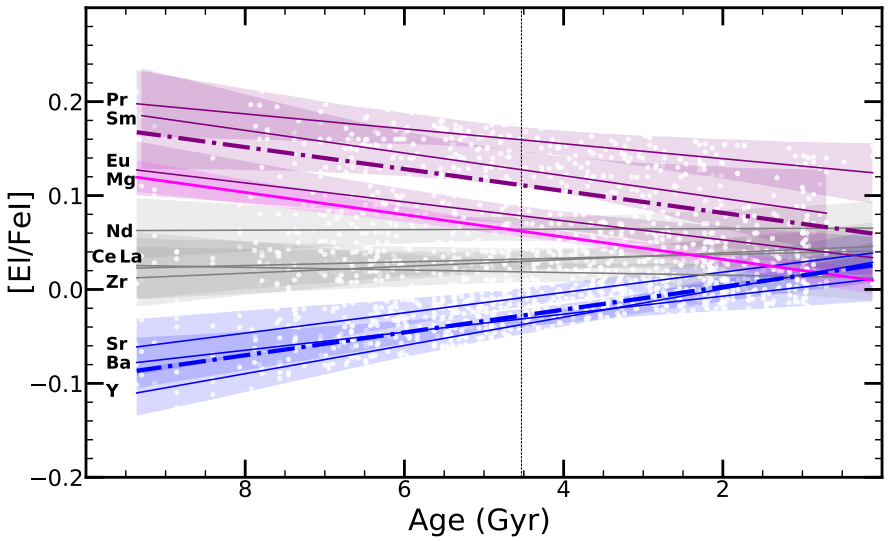

Figure 4-3: Compilation of [El/Fe I] trends as a function of age for the thin-disc stars. The continuous purple lines correspond to the *r*-process dominated elements Eu, Sm and Pr and the thick dash-dotted line is their averaged trend. The continuous blue lines represent the *s*-process dominated elements Y, Sr, and Ba and the thick dash-dotted line is their averaged trend. The gray continuous lines are for elements with negligible [El/Fe I] age trends (Nd, Ce, La, and Zr). The continuous magenta line represents the [Mg/Fe I] age correlation. The shadowed areas show the 95% confidence interval for the regressions and the vertical dashed line marks the solar age.

D'Orazi et al. (2009) found that is an extreme enhancement in the [Ba/Fe] in young open clusters (ages less than a few hundred Myr), which is not followed by

other *s*-process elements such as lanthanum and cerium (*vide* D'Orazi et al., 2022, for a recent review of the problem) . Because the [Ba/Fe] abundances at young ages in our sample of thin disc stars are not far to those of [La/Fe] and [Ce/Fe], and also show close to solar abundances at young ages, we note that our study does not sustains the so-called barium puzzle anomaly (also confronted by Reddy and Lambert (2017)). This implies that an additional intermediate process (*i*-process) would not be necessary, as proposed by (Cowan and Rose, 1977; Mishenina et al., 2015)). In our sample, the youngest stars (with an age estimate below 2 Gyr) are dwarfs and unevolved giants, with a mean uncertainty in their age determination of (+1.17, −0.62) Gyr.

Regarding the thick disc, according to the Figure 4-4 it seems to have a more smoothed behavior than the thin disc. Thus, for the *r*-process dominated elements, only Sm shows a slightly positive slope. Regarding the *s*-process dominated elements, the Y is the one that shows the steepest negative gradient. Magnesium, which we show for comparison, also shows a positive gradient, although smoother than the one in the thin disc. However, as we saw in the Figure 2-10, the age estimates for the thick disc are more confined in the region between 4 and 8 Gyr, which together with the size of the sample makes it difficult to reach definitive conclusions. In the next section we will address in detail the question of age dependence of the elemental abundance rations.

4.1.2. The [El/Fe] versus Age gradients for the open clusters sample

As we have seen, the relation between the abundances of neutron-capture elements and stellar ages has been widely investigated (e.g. D'Orazi et al., 2009; Maiorca et al., 2011, 2012; Mishenina et al., 2013; Jacobson and Friel, 2013; Battistini and Bensby, 2016; Marsakov et al., 2016; Nissen, 2016; Reddy and Lambert, 2017; Delgado Mena et al., 2017; Spina et al., 2018; Casamiquela et al., 2021; Baratella et al., 2021; Zinn et al., 2021; Sales-Silva et al., 2022). However, most of the previous works were limited to the solar neighbourhood region, using both solar twins or star clusters. Exceptions are the works of Magrini et al. (2018) which is based on a sample of open clusters from GES IDR5, about 20 clusters located at various galactocentric distances and the very recent work of Sales-Silva et al. (2022) who used a sample of 42 clusters from the APOGEE survey to investigate the spatial variation of the relation [Ce/α] versus age, finding that is not the same across the Galactic disc, which is possibly due to the dependence of AGB yields

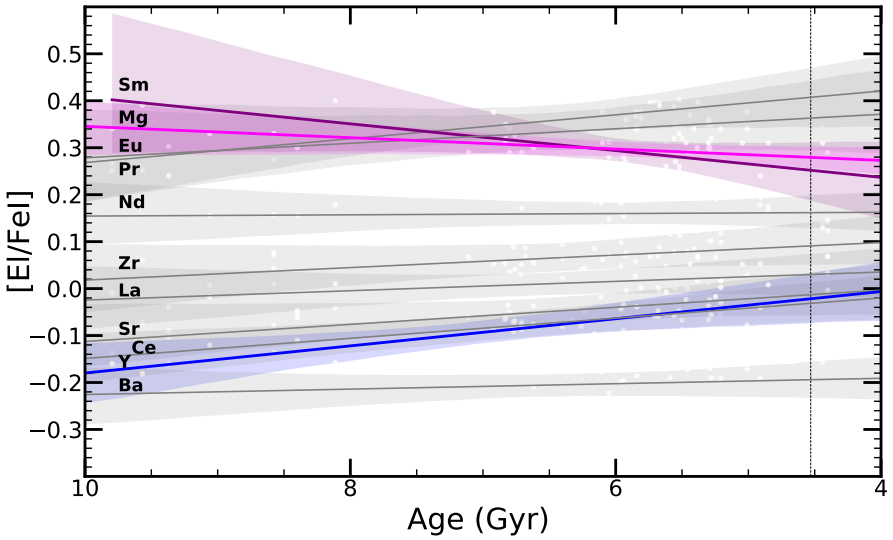

Figure 4-4: Compilation of [El/Fe I] trends as a function of age for the thick-disc stars. The continuous purple line correspond to the *r*-process dominated elements Sm. The continuous blue line represent the *s*-process dominated element Y. The gray continuous lines are for elements with negligible [El/Fe I] age trends. The continuous magenta line represents the [Mg/Fe I] age correlation and the shadowed areas and the vertical dashed line represent the same as in 4-3.

on metallicity.

Unlike previous studies, our sample offers the unique advantage of having a very large sample of OCs, 62 objects, with homogeneously derived abundances of neutron-capture elements, covering a wide range of ages and galactocentric distances (*vide* Figure 2-12). This allows us to study the relationships between ages and abundance ratios in a spatially resolved way, being able to derive them at various galactocentric distances. We divide our sample clusters in three galactocentric regions: an outer region of the Galactic disc, which includes 30 OCs located at a galactocentric distance $R_{gc} > 9$ kpc; a central region, in which our Sun is located, which includes 20 OCs at $7 \leq R_{gc} \leq 9$ kpc; and an inner region, comprising 12 OCs at $R_{gc} < 7$ kpc.

In Figure 4-5, we show the variation of [El/Fe] as a function of [Fe/H] and of age. In the left panels of Figure 4-5, we observe important differences in the clusters belonging to the three regions mentioned above. The clusters in the outer disc are generally metal poorer than the clusters in the inner disc and in the solar neighbourhood, while the differences in [El/Fe] are less pronounced. Typically,

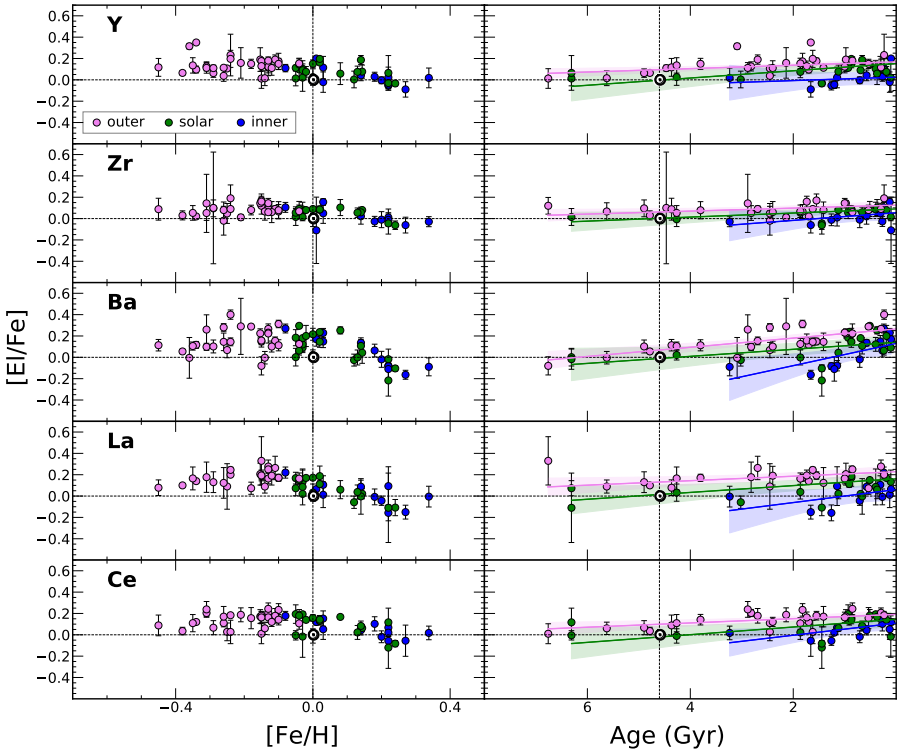

Figure 4-5: The behaviour of [El/Fe] versus metallicity and age. On the left panels, we show [Fe/H] versus [El/Fe], and on the right panels Age versus [El/Fe] for our sample of OCs divided in the three galactocentric regions. In blue, the OCs located in the inner disc, in green those located in the solar neighbourhood, and in pink the ones located in the outer disc. On the right panels, the continuous lines are the univariate linear regressions (one for each radial region, colour-code as the corresponding sample of OCs), while the shaded regions are their confidence intervals.

outer disc clusters have [El/Fe]>0, while the inner disc ones have [El/Fe] solar or sub-solar. The results are more clear looking at the right panels, in which [El/Fe] are shown as a function of the cluster age: for all the elements, [El/Fe] are under-abundant for a given age in the inner disc with respect to those of the outermost regions. For all the three regions, we observe an increasing trend of [El/Fe], confirming previous literature results. [Ba/Fe], as noted in the past (e.g. D'Orazi et al., 2009; Maiorca et al., 2012; Mishenina et al., 2015), has the strongest upward trend.

In Figure 4-6, we show the results of the coefficients of the weighted regressions (WLS) in the three regions in the form [*s*/Fe]=m·Age + c.

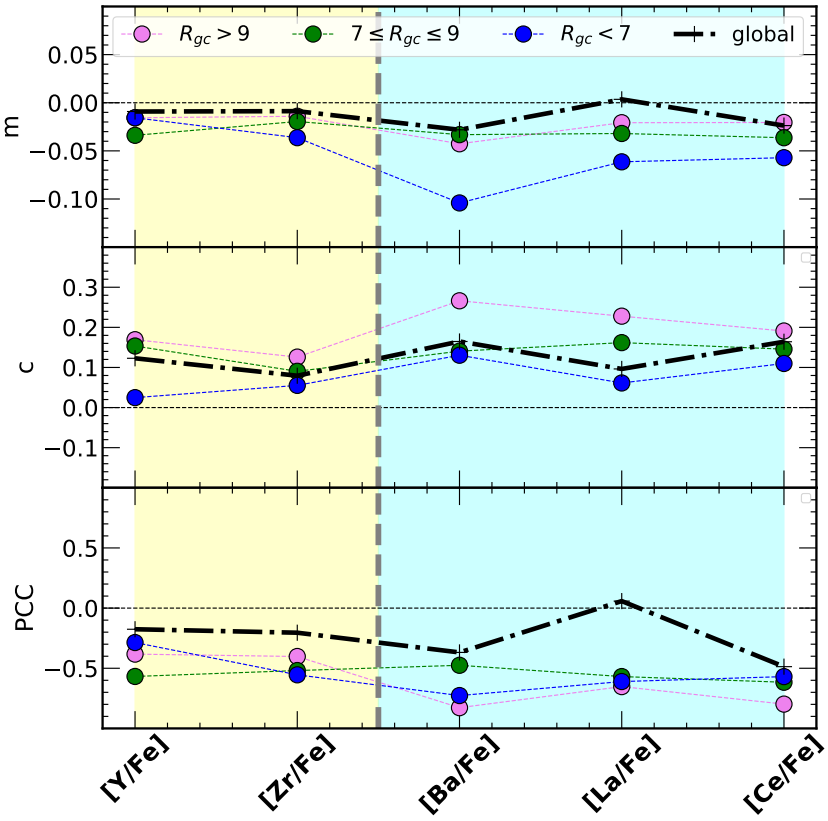

Figure 4-6: Weighted regression coefficients for the Age versus [El/Fe] relation of 62 OCs by R_{gc}. The yellow coloured area corresponds to the elements of the first *s*-process peak (Y and Zr), and the cyan area to those of the second peak (Ba, La and Ce). In the upper panel, we show the slope in dex Gyr^{-1} of the relations. In the middle panel, we present the value of the intercept (dex), while in the bottom panel we have the correlation coefficient. In all panels, we use the following symbols: for the inner region blue circles, for the solar region green circles, for the outer region pink circles, and for the whole sample dashed black lines.

As weight we apply the expression:

$$\frac{1}{(\frac{\sigma}{\sqrt{N}})^2}$$

where σ is the standard deviation of the abundance ratios for the member stars of every cluster, and N is the number of member stars with values of the corresponding abundance ratio. The coefficients are reported in Table A.1 together with Pearson correlation coefficients (PCCs).

We note the different behaviour of the first-peak elements (Y and Zr) with

respect to the second-peak ones (Ba, La, Ce), the former having lower intercept values than the latter. For all *s*-process dominated elements the slope of the regression is steeper in the inner disc than in the other two regions, while the value at the intercept, [El/Fe], is lower in that region (*vide* Figure 4-6).

The different behaviour of Ba with respect to the other two elements of the second peak, La and Ce, is more visible in Figures 4-5 and 4-6, in particular in the inner disc. In the Appendix, in Table A.1 we provide the coefficients of the weighted linear fits for the three radial regions.

In the work of D'Orazi et al. (2009), [Ba/Fe] ratio was found to dramatically increase at decreasing ages, with very high growth in very young stars. As discussed in Baratella et al. (2021), the higher enhancement of [Ba/Fe] with respect to [La/Fe] and [Ce/Fe] in young stars cannot be easily explained, either with non-local thermodynamic equilibrium (NLTE) effects or with stellar nucleosynthesis and chemical evolution models. To look for a plausible explanation, they explored different scenarios related to the formation and behaviour of spectral lines, from the dependence on the different ionisation stages and the sensitivity to the presence of magnetic fields and the effect of stellar activity. However, all these effects cannot fully explain the different behaviour of Ba in young stars. In our sample, we are considering clusters older than 100 Myr, thus we expect a relatively smaller difference between Ba, and the other elements of the second peak. However, as mentioned above, Figures 4-5 and 4-6 show that there are some differences among these elements, as already found in Magrini et al. (2018). Following Mishenina et al. (2015), other possible explanations are related to some extra production of Ba via intermediate neutron-capture process, the so-called i-process, triggered by the mixing or ingestion of H in He-burning stellar layers (Cowan and Rose, 1977; Bertolli et al., 2013). To summarise, though the origin of the [Ba/Fe] increase in young stars does not have a complete theoretical explanation, the large slope of the [Ba/Fe]-age relation makes Ba an excellent age proxy, at least for ages larger than 150 Myr (see, e.g. Spina et al., 2020; Baratella et al., 2021).

4.2. Spatial gradients

The earliest stellar kinematic studies in the Galaxy date back more than a century, with the pioneering works of Eddington, Kapteyn, and Oort, among others, laying the foundation for later studies. While the abundances in the stellar atmospheres in the stellar populations remain mainly unchanged in time (considering low-

and intermediate-mass stars, and elements not affected by mixing, e.g., Li, C, N), their spatial and kinematic distribution undergoes changes throughout their lifetime. Because of that, orbital properties combined with chemical ones provides knowledge of extraordinary value in unraveling the formation and evolution of the Galaxy. The relationship between the kinematic properties with the different stellar populations has also been known for decades (e.g. Eggen et al., 1962). Specifically, they found a clear correlation between [Fe/H], orbital eccentricity and the vertical component of space velocity, with the lowest metallicity orbits corresponding to the more elliptical and withthe highest vertical velocity.

In this section we will study the abundances of neutron-capture elements in relation to the orbital parameters $R_{\rm mean}$ and $|z_{max}|$. The target selection strategy included all stars in the selected magnitude (V < 8 mag) and colour ((B-V) > 0.39), as described in chapter 2. This, together with the division of the sample into thin- and thick discs, makes the sample homogeneous to avoid potential bias in analysing gradients.

4.2.1. Radial gradients

Considering that SFR has been more efficient in the inner disc than in the outer regions, negative [El/H] gradients of metals with galactocentric distance should arise naturally (Matteucci, 2021).

Since the stars do not describe circular orbits, especially the older ones, it is appropriate to determine the stellar $R_{\rm mean}$ (equation 4.1), defined as the average between the two apsides to the Galactic center (the closest and furthest galactocentric distance, so-called peri- and apogalacticon distances respectively).

$$R_{mean} = \frac{R_{ap} + R_{peri}}{2} \tag{4.1}$$

Something that makes the use of $R_{\rm mean}$ instead of $R_{\rm gc}$ interesting is that this orbital parameter is often associated with the stellar birthplace (Grenon, 1987), unveiling the radial migration when compared to present time radius. Thus, an increase in the dispersion of space velocities with age is observed, which results in the so-called diffusion of stellar orbits (Wielen, 1977). Radial mixing effects can lead to biased radial abundance gradients (Sellwood and Binney, 2002), so the use of the birthplace radii could provide more reliable results. The use of R_{mean} indeed can mitigate the effect of "blurring" due to epicyclic oscillations around the guiding radius (Schönrich and Binney, 2009). Although its use is not yet widespread, we

find it in works such as Rocha-Pinto et al. (2004) for a sample composed by 424 late-type dwarfs.

Its use relating it to chemical abundances of neutron-capture elements is even scarcer, however we find it in the works of Edvardsson et al. (1993), who derived abundances of Y, Zr, Ba and Nd among other elements for 189 FG nearby dwarfs; Trevisan and Barbuy (2014) who derived abundances of Y, Ba, La, and Eu for 71 very metal-rich dwarf stars; and Adibekyan et al. (2016), who explored the effect of the $R_{\rm mean}$ on the chemical abundance trend with the condensation temperature for a sample of 39 stars with ages similar to that of the Sun, considering Sr, Y, Zr, Ba, Ce and Nd among other elements.

For the calculation of the regressions for our sample, the individual uncertainties in both independent and dependent variables σ_x and σ_y were taken into account. For this, the Orthogonal Distance Regression (ODR) method was used through the Kapteyn package (Terlouw and Vogelaar, 2016). The results of the radial and vertical abundance gradients for the thin- and thick-disc stars are shown in the Tables 4.2 and 4.3 respectively.

The Figure 4-7 show the radial distribution of the [El/Fe I] ratios, and in the Figure 4-8 the same results as the previous one but binned into equal distributions. That is, as in the Figure 4-2, for each component of the disc, every bin represents the same number of stars. As seen in the Table 4.2 and Figure 4-8, for the thin-disc stars, the radial [El/Fe I] abundance gradients are mainly negligible or slightly negative for the *s*-process dominated elements Sr, Y and Ba, and have a positive tendency for the mixed elements and for the *r*-process dominated. Thus, the largest positive gradients are found in the elements of a mixed nature Nd and Pr, followed by the *r*-dominated process elements Eu and Sm. In contrast to this, the Ba shows a slightly negative gradient. A similar behavior to mixed elements and *r*-process dominated elements were found in Mikolaitis et al. (2019) for $\alpha-$elements (excluding the odd ones).

Figure 7 of the aforementioned Adibekyan et al. (2016) shows the [El/Fe] ratio against $R_{\rm mean}$ for stars with ages from 2.0 to 4.5 Gyr. In that figure we see how the steepest gradient corresponds to the mixed element Nd, while the elements of the first *s*-process peak Sr and Y show an almost flat slope, as well as the hs element Ce. Regardless of sample differences, our results are consistent with this. However, studies on the radial gradient of neutron-capture elements using $R_{\rm mean}$ are scarce, so it is necessary to extend the comparison of results with studies that use the galactocentric distance $R_{\rm gc}$. An example is found in Yong et al. (2005),

who measured radial abundance gradients for a sample of 24 Cepheids in the outer Galactic disc. That work included La and Eu, among other elements, for a range between 12 and 17.2 kpc, finding slopes of -0.013 dex/kpc^{-1} for [La/Fe] and +0.009 dex/kpc^{-1} for [Eu/Fe]. Another example is found in da Silva et al. (2016), who provided Y, La, Ce, Nd and Eu abundance gradients across the Galactic thin disc for 73 classical Cepheids. The authors increased the sample with similar Cepheid abundances reaching a sample of 435 Cepheids and covering a broad range of metallicity. Since classical Cepheids are population I stars, that is, very young stars, their R_{gc} should still be close to that of their birthplaces, and therefore to R_{mean}. In the aforementioned study, the authors found a negligible radial gradient for [Y/Fe], as well as positive gradients for the other elements (hs, mixed and *r*-dominated), both for the initial sample and for the entire Cepheid sample. Our study agrees again with this and expands it to other elements from the same groups. As seen in the Table 4.2 and in the Figure 4-7, we obtained an anticorrelation of [Ba/Fe I] with R_{mean}.

In the work of Luck (2018), the gradients of 8 neutron-capture elements abundances with R_{gc} are analyzed for a sample of 435 Cepheids. In that work the [Ba/Fe] also shows a negative gradient, which is in line with our study. Furthermore, the mixed element Nd and the *r*-process dominated elements Sm and Eu show strong positive gradients, as also does Zr.

Similarly, Adibekyan et al. (2016) also found a more positive gradient for Zr than for the other two ls elements Sr and Y. However, and in agreement with Adibekyan et al. (2016), we did not find such a positively steep gradient for Ce, which is also found in da Silva et al. (2016). In addition, Overbeek et al. (2016) also investigated the gradients of Pr, Nd, Mo, Dy, Gd and Eu to iron ratios as a function of R_{gc} for 23 open clusters, reaching similar results for the aforementioned mixed and *r*-dominated elements, with strong and positive slopes. It should be noted that they found the mixed elements Pr and Nd and also Mo to be enhanced at around 10 kpc and fall to approximately 12 kpc which we cannot check due to the smallness of our sample in that range.

It is also worth mentioning the theoretical present time radial abundance gradients from the Cescutti et al. (2007) models for Ba, La and Eu, calculated for a total range between 4 to 22 kpc, and compared with observational data from Yong et al. (2006) for Cepheids, Yong et al. (2005) for open clusters and Carney et al. (2005) for red giants. For the entire range (4 to 22 kpc) they obtained a radial gradient of [Ba/H], [La/H] and [Eu/H] of -0.021, -0.021 and -0.030 dex/kpc^{-1} respectively.

For a inner range, comprised between 4 to 14 kpc, they got −0.032, −0.032 and −0.036 dex/kpc^{-1}; and for the outer region (16 to 22 kpc), −0.009, −0.008 and −0.013 dex/kpc^{-1}. The above, translated to [El/Fe], indicates positive gradients, with the largest slope for Eu, which agrees with our results, with almost flat slopes in the outermost region.

Regarding the gradients for the thick disc, our results suggest a smoother behavior than those obtained for the thin disc, with negligible gradients for almost all the neutron-capture elements. If we make a detailed comparison of the thick disc with the thin disc as shown in the Figure 4-9, we see how the slopes are lower for the mixed and *r*-dominated elements, while they are slightly higher for the purer *s*-dominated elements Sr, Y and Ba; and the y-intercepts are higher for the thick disc than for the thin disc for the mixed and *r*-dominated elements, and lower for the purer *s*-dominated (Sr, Y and Ba). We recall that Prantzos et al. (2020) gives to Sr and Ba a solar *s*-process percentage of 91% and 89% respectively, and Arlandini et al. (1999) a 92% to Y (*vide* Table 1.1).

A study of the radial gradients for the thin and the thick disc is found in Li et al. (2018), who studied the gradients of the α-elements with $R_{\rm gc}$ for a large sample of stars with abundances derived from the APOGEE catalog. The result was almost negligible slopes also for the thick disc, although the production sites of the α-elements and *s*-process elements are certainly different. The question of the thick disc awaits more abundances of neutron-capture elements for larger samples.

If we compare the results of the thick disc with those of the thin disc, we see once again the contrast between Ba and Eu, which are thought to be pure in nature. The abundances of the Ba for the thick disc are mainly below those of the thin disc throughout the entire $R_{\rm mean}$ range. On the contrary, for the Eu the opposite happens, placing the abundance ratios of the thick disc above those of the thin disc. This same behavior is also seen for the *r*-dominated process element Sm and for the mixed element Pr. For the ls elements the abundances for both components are intermingled. This is clearly seen in the Figure 4-8 with the binned results.

It should be noted that the use of $R_{\rm mean}$ instead of $R_{\rm gc}$ seems to provide slightly lower gradients and distributes the sample wider along the disc regions, while using $R_{\rm gc}$ our sample is more confined to the central region.

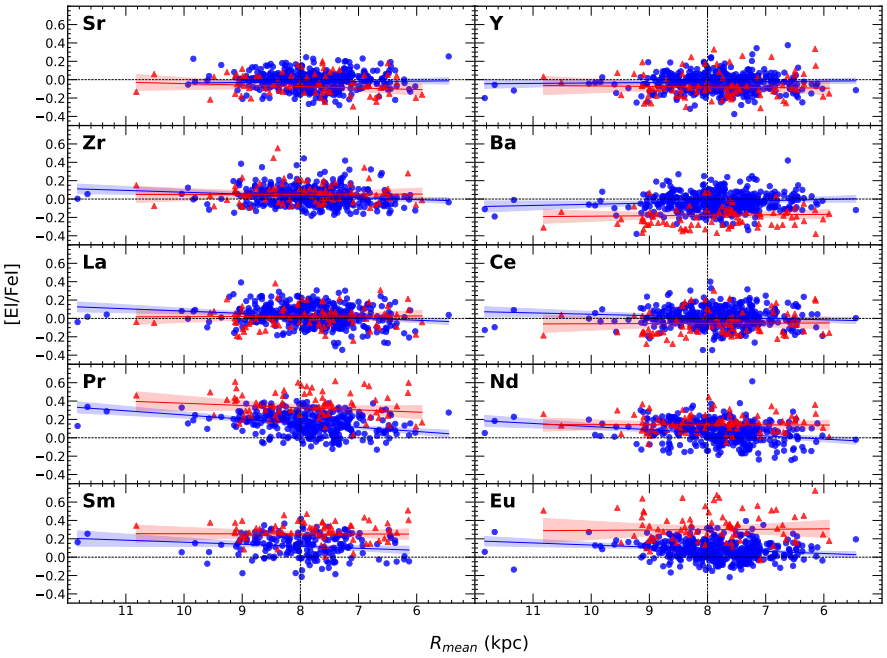

Figure 4-7: [El/Fe I] ratios as a function of the mean galactocentric distances. Symbols as in the previous Figures 3-1 and 4-1. The blue and red lines are the ODR lines for the thin-disc and thick-disc stars respectively. The ODR takes into account the uncertainties in [El/Fe I] and $R_{\rm mean}$. The 95% confidence intervals for the regression lines are shadowed and the dotted lines correspond to the solar values.

4.2.2. Vertical gradients

Since the stars in their orbital displacement describe an oscillatory vertical movement, crossing the Galactic midplane periodically, it is appropriate to define here the maximum vertical height above the Galactic midplane. It is one of the main orbital parameters, together with the e, $R_{\rm ap}$ and $R_{\rm peri}$ which can be obtained from the observed 6D phase-space coordinates. The maximum height $z_{\rm max}$, as well as the apogalacticon, are reached when the u and v components of the space velocities are maximal ($u_{\rm max}$ and $v_{\rm max}$). The following formula (equation 4.2) shows how it is obtained, where Δ is a parameter that specifies the focal point of the coordinate system (Mackereth and Bovy, 2018):

$$z_{max} = \Delta \; cosh \; u_{max} \; cos \; v_{min} \tag{4.2}$$

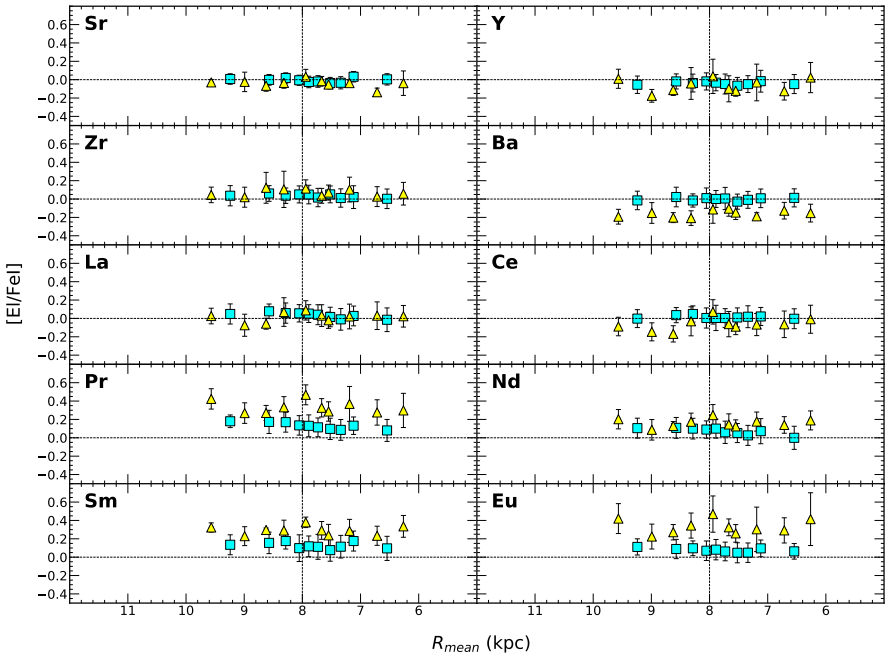

Figure 4-8: [El/Fe I] ratios as a function of the mean galactocentric distances with the results shown in 10 equally distributed bins (q=10). The dashed black lines show the solar values (colours and markers as in Figures 2-9 and 4-2.

Besides being related to the orbital configuration of the Galaxy, its study combined with chemical abundances provides, as with $R_{\rm mean}$, valuable information on the structure and evolution of the Galaxy.

The Figure 4-10 shows the [El/Fe I] abundance ratios of neutron-capture elements with $|z_{\rm max}|$ for the two components of the Galactic disc. On the other hand, the Figure 4-11 shows the same results but in 10 bins for each subcomponent and equally distributed. The bulk of maximum heights is distributed between 0 and 1.3 kpc, except for one star that is at 3.73 kpc. This distribution can be seen in the kernel density estimate (KDE) of the Figure A4 in the Appendix. In the Table 4.2 we show the values of the coefficients of the ODR regressions for the thin disc stars.

As can be seen also in the Figure 4-12, in general the vertical abundance gradients are negative for *s*-process dominated elements and become positive for mixed and *r*-process dominated elements. Specifically, the stronger negative values correspond to the Sr, Y and Ba. If the most negative gradients are to be assigned to the most *s*-process dominated elements, this seems to be in accordance with the

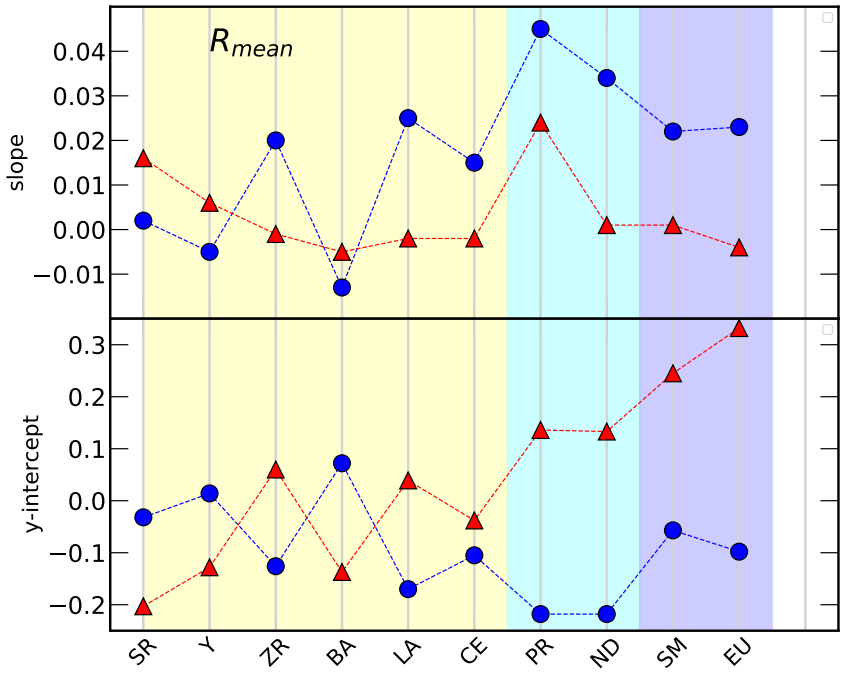

Figure 4-9: Comparison of the values of the ODR coefficients for the thin and the thick disc R_{mean} gradients (markers as usual in this thesis). The coloured areas correspond to the nature of the elements, thus, there is a blue area for the *r*-process dominated elements, a cyan area for the mixed elements and a yellow area for those of the s-process.

solar values assigned by Prantzos et al. (2020) (*vide* Table 1.1), which gives to Sr a 91% followed by 89% to Ba, that is, they have the highest *s*-process purity.

Regarding the slopes in the thick disc, we have negative vertical gradients for most *s*-process dominated elements, which become negligible for *r*-process dominated elements. This behavior is similar to that of R_{mean} gradients, that is, the slopes are smoothed and the intercepts increase. As we saw in the subsection 4.1.1, this also happened with temporal gradients (*vide* Figure 4-4). It can be see a strong negative behavior for almost all the elements, which becomes negligible for the dominated *r*-process elements. When we compare the results of both components as shown in the Figure 4-12, we see how the slopes for the thin disc are always above those of the thick disc except for the Y, an element of high *s*-process purity; and for the other two of also high *s*-process purity Sr and Ba, the values are very close. That is, the lines are further apart for the *r*-process pure and mixed elements, and converge on the elements of maximum *s*-process purity. When we refer to

the y-intercepts, we also see how the *r*-dominated and mixed elements have higher values for the thick disc, while they are lower for the high purity *s*-process elements Sr, Y and Ba. To these three we would also add the Ce, to which Prantzos et al. (2020) and Bisterzo et al. (2014) give a high *s*-process purity in the Sun (*vide* Table 1.1).

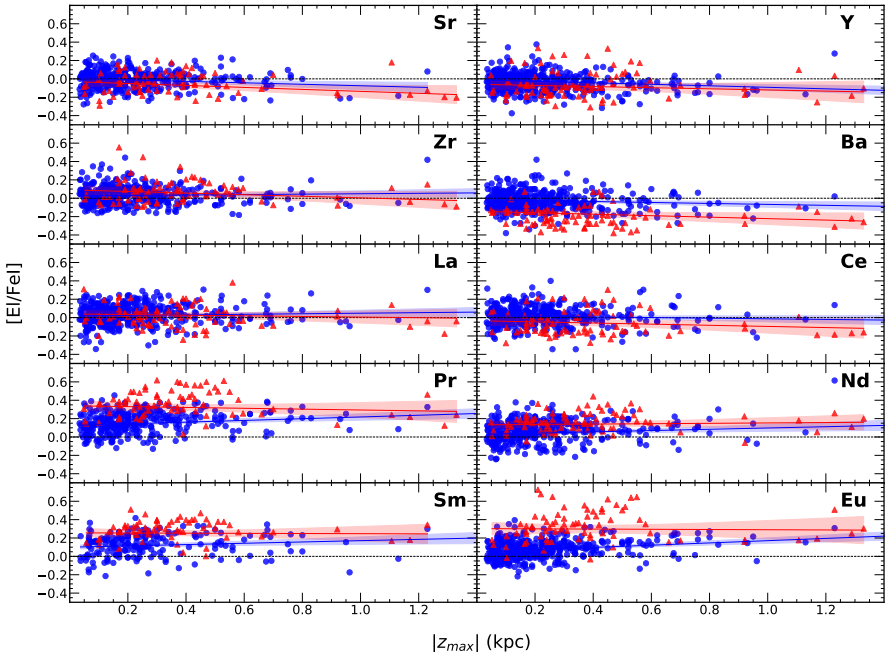

Figure 4-10: [El/Fe I] ratios as a function of $|z_{\rm max}|$. Symbols as in the previous Figures 3-1, 4-1 and 4-7. The blue and red lines are the ODR lines for the thin-disc and thick-disc stars respectively. The ODR takes into account the uncertainties in [El/Fe I] and $|z_{\rm max}|$. The 95% confidence intervals for the regression lines are shadowed and the dotted lines correspond to the solar values.

In general terms, our results show how the gradients for $R_{\rm mean}$ and $|z_{\rm max}|$ are consistent with each other and also with the age gradients (*vide* Figure 4-3). Thus, we find the same behavior for the members of the same group of elements.

As with $R_{\rm mean}$, studies of neutron capture abundance gradients with the maximum vertical height are very scarce. Even so, they are more frequent for other types of elements, such as α-process ones. Because they bear some similarity to those of the *r*-process due to their partly common origin (both processes are associated with sources in short timescales), it is still possible to make some comparison. Some examples for large samples of thin- and thick-disc stars can be found in Mikolaitis

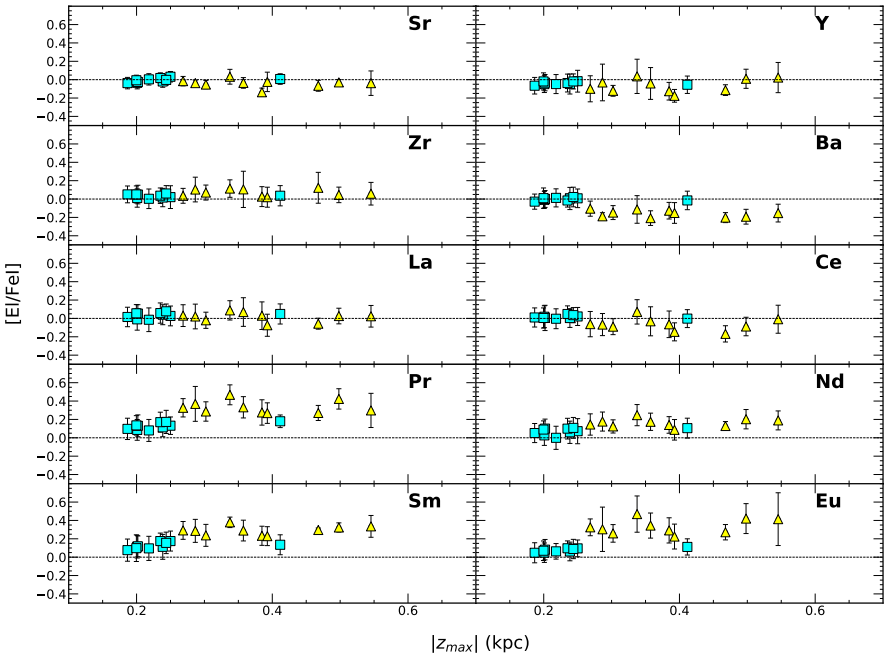

Figure 4-11: [El/Fe I] ratios as a function of the $|z_{\max}|$ with the results shown in 10 equally distributed bins (q=10). The dashed black lines show the solar values (colours and markers as in Figure 2-9, 4-2 and 4-8.

et al. (2014); Duong et al. (2018); Li et al. (2018); Yan et al. (2019). The aforementioned authors coincide in assigning a positive and higher gradient for the thin disc than for the thick disc, the latter being softer or almost negligible. The same positive gradient was also found in Mikolaitis et al. (2019) for the stars of the thin disc. This agrees with the trends of the *r*-process dominated elements exposed in this thesis.

Studies have also been carried out relating the abundance radial gradients in function of $|z_{\max}|$ trying to provide new constraints on the chemical evolution models of the Galaxy. An example is the work of Boeche et al. (2013), in which a large sample of RAVE dwarfs stars is analyzed for several α-process elements. A similar study using neutron-capture elements for a large sample would be necessary for a better understanding of our Galaxy.

The neutron-capture elements are the least well understood ones regarding nucleosynthesis and formation environments. As we have seen in previous chapters, its potential is very high due to its special nature and characteristics. These elements can still provide a lot of knowledge about the formation and enrichment of our

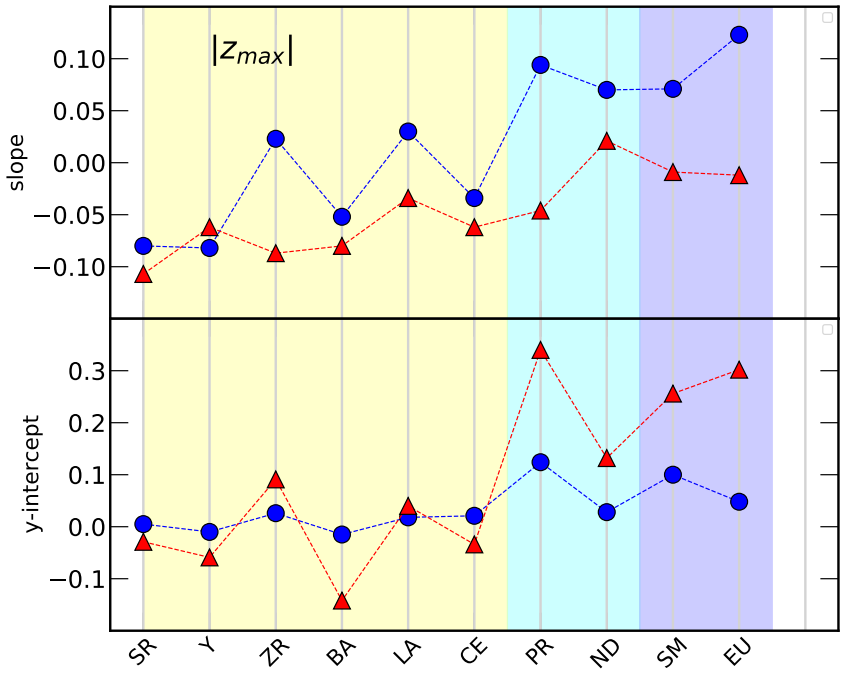

Figure 4-12: Comparison of the values of the ODR coefficients for the thin and the thick disc $|z_{\max}|$ gradients (markers as usual in this thesis). The coloured areas correspond to the nature of the elements, thus, there is a blue area for the *r*-process dominated elements, a cyan area for the mixed elements and a yellow area for those of the *s*-process.

Galaxy. Thus, more observational data is necessary to delve further into them.

Table 4.1: Best linear fits to the [El/Fe I]−age distributions in dex Gyr^{-1} and the Pearson correlation coefficients for the thin disc stars and comparison with other works.

El.	Present work thin disc		Battistini, Bensby thin disc		Spina et al. 2018 solar twins	Magrini et al. 2018 age < 8 Gyr	
	Slope	PCC	Slope*	PCC*	Slope	Slope**	PCC**
Sr	−0.011 ± 0.003	−0.22	−0.023 ± 0.009	−0.40	−0.032 ± 0.002		
Y	−0.015 ± 0.002	−0.30	−0.011 ± 0.002	−0.35	−0.029 ± 0.002	−0.023 ± 0.009	−0.6
Zr	−0.004 ± 0.003	−0.07	−0.003 ± 0.006	+0.11	−0.026 ± 0.002	−0.038 ± 0.013	−0.5
Ba	−0.010 ± 0.003	−0.19	−0.023 ± 0.003	−0.43	−0.032 ± 0.002	−0.027 ± 0.007	−0.8
La	−0.002 ± 0.003	−0.03	+0.004 ± 0.005	+0.09	−0.023 ± 0.002	−0.005 ± 0.015	−0.2
Ce	+0.001 ± 0.003	+0.04	−0.009 ± 0.005	−0.18	−0.024 ± 0.002	−0.016 ± 0.010	−0.5
Pr	+0.008 ± 0.004	+0.13			−0.014 ± 0.003		
Nd	−0.000 ± 0.003	−0.01	+0.006 ± 0.004	+0.14	−0.023 ± 0.002		
Sm	+0.014 ± 0.006	+0.19	+0.010 ± 0.006	+0.22	−0.008 ± 0.002		
Eu	+0.011 ± 0.003	+0.22	+0.011 ± 0.004	+0.24	−0.007 ± 0.002		

* Computed in this work for the potential thin-disc stars with age uncertainties better than 3 Gyr from data by Bensby et al. (2014) and Battistini and Bensby (2016).

** The slope was calculated including open clusters.

Table 4.2: ODR fits to the [El/Fe I]$-R_{\rm mean}$ and $|z_{\rm max}|$ distributions in dex kpc^{-1} for the thin-disc stars.

El.	$R_{\rm mean}$ slope	y-intercept	χ^2	$\lvert z_{\rm max}\rvert$ slope	y-intercept	χ^2
Sr	+0.002 ± 0.007	−0.032 ± 0.052	+0.67	−0.080 ± 0.024	+0.005 ± 0.007	+0.65
Y	−0.005 ± 0.006	+0.014 ± 0.047	+1.00	−0.082 ± 0.024	−0.010 ± 0.006	+0.92
Zr	+0.020 ± 0.007	−0.126 ± 0.052	+0.49	+0.023 ± 0.023	+0.026 ± 0.007	+0.50
Ba	−0.013 ± 0.006	+0.072 ± 0.045	+1.09	−0.052 ± 0.024	−0.015 ± 0.007	+1.09
La	+0.025 ± 0.007	−0.170 ± 0.054	+0.75	+0.030 ± 0.025	+0.018 ± 0.008	+0.77
Ce	+0.015 ± 0.007	−0.105 ± 0.054	+0.69	−0.034 ± 0.027	+0.021 ± 0.008	+0.70
Pr	+0.045 ± 0.009	−0.218 ± 0.063	+1.33	+0.094 ± 0.035	+0.124 ± 0.011	+1.41
Nd	+0.034 ± 0.008	−0.218 ± 0.063	+1.16	+0.070 ± 0.034	+0.028 ± 0.010	+1.20
Sm	+0.022 ± 0.011	−0.057 ± 0.089	+1.10	+0.071 ± 0.039	+0.100 ± 0.014	+1.10
Eu	+0.023 ± 0.006	−0.098 ± 0.049	+0.53	+0.123 ± 0.023	+0.048 ± 0.007	+0.51

Table 4.3: ODR fits to the [El/Fe I]$-R_{\rm mean}$ and $|z_{\rm max}|$ distributions in dex kpc^{-1} for the thick-disc stars.

El.	$R_{\rm mean}$ slope	y-intercept	χ^2	$\lvert z_{\rm max}\rvert$ slope	y-intercept	χ^2
Sr	+0.016 ± 0.011	−0.203 ± 0.086	+1.09	−0.107 ± 0.038	−0.029 ± 0.020	+1.01
Y	+0.006 ± 0.012	−0.128 ± 0.092	+1.53	−0.062 ± 0.040	−0.059 ± 0.020	+1.49
Zr	−0.001 ± 0.014	+0.060 ± 0.114	+0.60	−0.087 ± 0.046	+0.091 ± 0.024	+0.58
Ba	−0.005 ± 0.010	−0.137 ± 0.079	+1.10	−0.080 ± 0.033	−0.142 ± 0.017	+1.03
La	−0.002 ± 0.012	+0.039 ± 0.096	+0.86	−0.034 ± 0.042	+0.040 ± 0.021	+0.85
Ce	−0.002 ± 0.013	−0.038 ± 0.102	+0.90	−0.062 ± 0.045	−0.034 ± 0.021	+0.88
Pr	+0.024 ± 0.013	+0.136 ± 0.099	+1.20	−0.046 ± 0.046	+0.340 ± 0.022	+1.24
Nd	+0.001 ± 0.010	+0.133 ± 0.078	+0.61	+0.021 ± 0.036	+0.132 ± 0.017	+0.61
Sm	+0.001 ± 0.014	+0.245 ± 0.109	+0.67	−0.009 ± 0.050	+0.256 ± 0.023	+0.67
Eu	−0.004 ± 0.018	+0.332 ± 0.144	+1.38	−0.012 ± 0.061	+0.302 ± 0.031	+1.38

5. COSMIC CLOCKS

The stellar age is a key parameter to understand the physical processes of stars and their evolution over time. Simply put, it is the time that elapses from stellar birth to the point of reference. The life of a star is determined mainly by its initial mass, which predicts how long its life will last. Throughout their life, stars go through stellar evolutionary periods that have certain common characteristics. Taken together for different structures and stellar populations, the stellar ages provide us valuable information about the evolution of the Galaxy. However the stars spend most of their life in the Main Sequence (MS), and in whose phase they remain almost unchanged, which makes their calculation by direct techniques difficult. Thus, the ages of stars can only be inferred from observing properties that change with time (Soderblom, 2010), for example in a brief stellar evolutionary phase such as subgiant stars. Although age is one of the most difficult stellar properties to determine, there are several methods for its estimation. These methods can be model dependent or empirical relations, and can be used for specific cases. The attempts are varied, and include techniques and proposals based on nuclear cosmochronology (e.g. Fowler and Hoyle, 1960), asteroseismology (e.g. Ulrich, 1986), gyrochronology (e.g. Barnes, 2003), magnetochronology (Vidotto et al., 2014), kinematics (e.g. Almeida-Fernandes and Rocha-Pinto, 2018), lithium-depletion boundary (LDB) (Basri et al., 1996), or isochrone fitting (e.g. Pont and Eyer, 2004). The use of clusters members is very useful, since it allows assigning and comparing ages to a large number of stars, for which a similar age is expected.

Here we will refer to chemical age calculators, the so-called cosmic clocks, which allow direct estimation of age from abundances. The first and most used chemical clock in recent years is the combination of yttrium and magnesium. In fact, the [Y/Mg] ratio, due to its extraordinary sensitivity to age, the different nature of both elements, as well as their ease of being measured, has been used as a cosmic clock for solar twins (da Silva et al., 2012; Nissen, 2015, 2016; Spina et al., 2016; Tucci Maia et al., 2016). This ratio is metallicity dependent, as shown by Feltzing et al. (2017) by studying a larger sample of solar neighbourhood dwarfs, and concluding that its applicability is unique to solar analogues. However, Slumstrup et al. (2017) widened the range of applicability of this empirical relation presented by Nissen (2016) to the helium-core-burning giants at solar metallicities. The next step was taken by the same authors Nissen et al. (2017), who also confirmed the same relationship for the abundances of the Kepler LEGACY stars, with ages

calculated by asteroseismology. The sub-sample of Kepler LEGACY stars used by the aforementioned authors has a metallicity in a solar range ($-0.15 <$ [Fe/H] $< +0.15$), but the range of effective temperatures is much broader ($5700 < T_{\rm eff} < 6400$ K).

Quantitatively, the aforementioned work of Nissen et al. (2017) obtained for the Kepler stars and solar twins a slope of -0.035 dex Gyr^{-1} and y-intercept of 0.15 dex. This relation was based on ages derived from two techniques, asteroseismology and isochrone fitting, but the slope coefficients are similar to those that they had previously obtained for solar twins in Nissen (2016). On the other hand, Titarenko et al. (2019) studied the age dependence of the [Y/Mg] ratio for turn-off stars in the solar neighbourhood, not finding metallicity dependence with stellar age. They reached a slope of -0.029 dex Gyr^{-1} for the stars on the thin disc and they made an attempt for the thick disc, finding a very high slope for a small sample. The same [Y/Mg] age relation was also calculated by Delgado Mena et al. (2019) for FGK solar-type dwarf stars. In that study, the ages used to evaluate chemical clocks are based on Gaia parallaxes and PARSEC isochrones, obtaining a result for the slope of -0.041 dex Gyr^{-1} for the solar twins. More recently, Casali et al. (2020) analyzed the slope changes with metallicity in solar twins using GES open clusters and field stars. Thus, they conducted a study of this relation in four different metallicity regions, finding a slope of -0.018 dex Gyr^{-1} for [Fe/H] > 0.1, -0.040 for $-0.1 <$ [Fe/H] $< +0.1$, -0.042 for $-0.3 <$ [Fe/H] < -0.1, and -0.038 for $-0.5 <$ [Fe/H] < -0.3. They also did multivariate linear regression using [Fe/H] and age as independent variables, obtaining interesting results. The use of [Y/Mg] and [Ba/Mg] as chemical clocks in dwarf galaxies as Sculptor has also been tested (Skúladóttir et al., 2020).

Casamiquela et al. (2021) recently analyzed abundance-age relations with red clump (RC) stars in 47 OCs, finding that the age-abundance relations show larger scatter for clusters at large distances (d > 1 kpc) than for the Solar neighbourhood, particularly in the outer disc. They also found several combinations with significant slopes, including [Y/Mg] and [Y/Al], with [Ba/α] being the most significant. Finally, the last study that we are aware of is that of Morel et al. (2021), who analyzed the applicability of the abundance-age relations for 13 bright FG dwarfs from the Kepler LEGACY sample with properties beyond solar analogues. Since those stars have precise asteroseismic ages, they compared them to those inferred from empirical abundance-age relations based on PARSEC isochrones and abundances, and concluding that further work is needed for stars that are not solar analogues.

At the same time, new techniques for obtaining ages from chemical abundances have been explored recently, reaching promising results. Hayden et al. (2020) determined reliable ages derived from chemical abundances (including Y and Ba) for a large fraction of the stars in the GALAH survey, using the machine learning algorithm XGBoost. On the other hand, Moya et al. (2022) presented reliable stellar age estimates of FGK stars using chemical abundances and stellar parameters through Bayesian inference techniques.

5.1. The thin and thick disc sample

5.1.1. The Age versus [s/α] relations in the thin disc

To study the [s/α] ratio we take the necessary Mg and Al abundances and the separation of disc populations from Mikolaitis et al. (2019) and Ref. I respectively; and the abundances of the *s*-process elements are from Ref. II. Our sample of Solar neighbourhood thin disc stars for which we have abundances of Y, Mg, and age consist in 368 stars in the following ranges: $T_{\rm eff}$ (K): [4011, 6947]; $\log g$: [1.45, 4.69]; [Fe I/H]: $[-0.6, 0.33]$; Age (Gyr); [0.12, 9.36]. For them we obtained the [Y/Mg] versus age relation shown in the equation 5.1 of the regression line (with a PCC=−0.41), which is represented together with the coloured data in metallicity ranges in the Figure 5-1.

$$[\mathrm{Y/Mg}]_{\rm Thin} = 0.022\,(\pm0.015) - 0.027\,(\pm0.003)\cdot \mathrm{age[Gyr]} \qquad (5.1)$$

When we compare our results with other authors, we see that the equation 5.1 is very similar to that obtained by Titarenko et al. (2019), who investigated for the AMBRE project a sample of 325 turn-off thin-disc stars in the solar neighbourhood. Lin et al. (2020) computed [Y/Mg]–age trends for 2713 solar analogues from the GALAH survey and compared it with that obtained by Nissen (2015), getting a slope also slightly lower (*vide* their Figure 10). Regarding the relation obtained by Nissen et al. (2020), there is a difference in the y-intercept of approximately 0.15 dex, despite having a similar metallicity range. One possible reason is that the young stars in the aforementioned study have a larger $R_{\rm mean}$. Indeed, variations in the mean galactocentric distance seem to lead to changes in the slope and y-intercept. A solid theoretical explanation of this changes has recently been provided, as we will see in the next section 5.2. Thus, we follow Casali et al. (2020) and Magrini et al. (2021) in concluding that this relation is not universal, it has a strong dependence

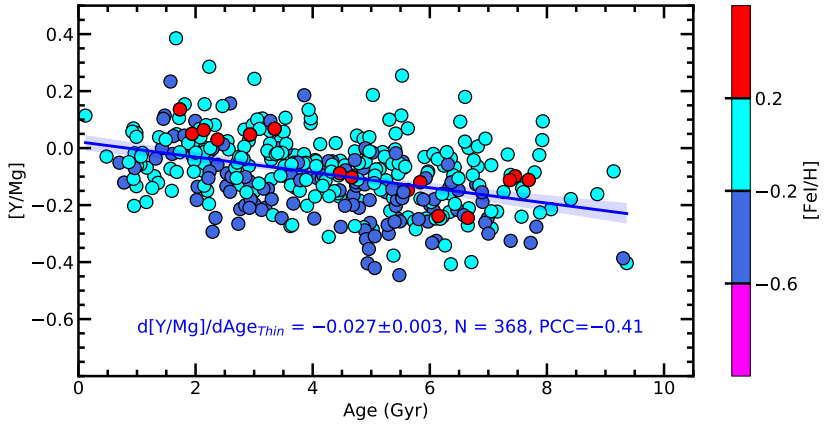

Figure 5-1: [Y/Mg] age relation for Solar neighbourhood thin-disc stars, colour-coded by metallicity intervals as in the Figure 2-2. The continuous line is a linear fit by ordinary least-squares regression to the sample of 368 stars with a shadowed area for the 95% confidence interval.

on metallicity and varies with galactocentric distance, hence it is limited and cannot be extrapolated to the entire Galactic disc.

Sr and Al are also potentially good candidates for cosmic clocks, the former as the *s*-process dominated element and the latter as the α element. Indeed, in the equation 5.2 and Figure 5-2 we show the results for the [Y/Al] age ratio. As we can see, the y-intercept and slope are slightly higher when [Y/Al] is used compared to [Y/Mg], for the same number of stars.

$$[\mathrm{Y/Al}]_{\mathrm{Thin}} = 0.067\ (\pm 0.015) - 0.029\ (\pm 0.003) \cdot \mathrm{age[Gyr]} \tag{5.2}$$

When we use Sr as an *s*-element we get the results shown in the equation 5.3 and Figure 5-3. As we can see, the y-intercept and slope are slightly lower when [Sr/Mg] is used compared to [Y/Mg], for the same number of stars.

$$[\mathrm{Sr/Mg}]_{\mathrm{Thin}} = 0.034\ (\pm 0.015) - 0.023\ (\pm 0.003) \cdot \mathrm{age[Gyr]} \tag{5.3}$$

Finally, when we use Sr as an *s*-element and Al as the α element we get the following results, as shown in the equation 5.4 and Figure 5-4 for the [Sr/Al] age ratio. In the case of [Sr/α] we have abundances for 338 stars, that is, 30 stars less than in the other cases.

The use of Sr has the disadvantage compared to Y that only one spectral line

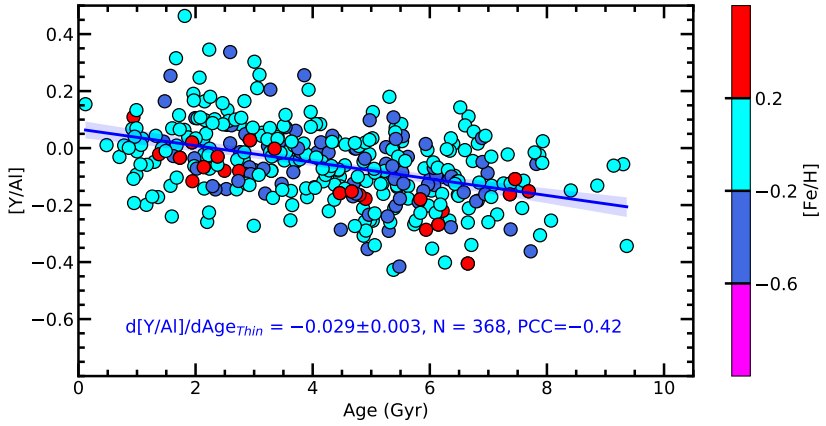

Figure 5-2: [Y/Al] age relation for Solar neighbourhood thin-disc stars, colour-coded by metallicity intervals as in the Figure 2-2 and 5-1.

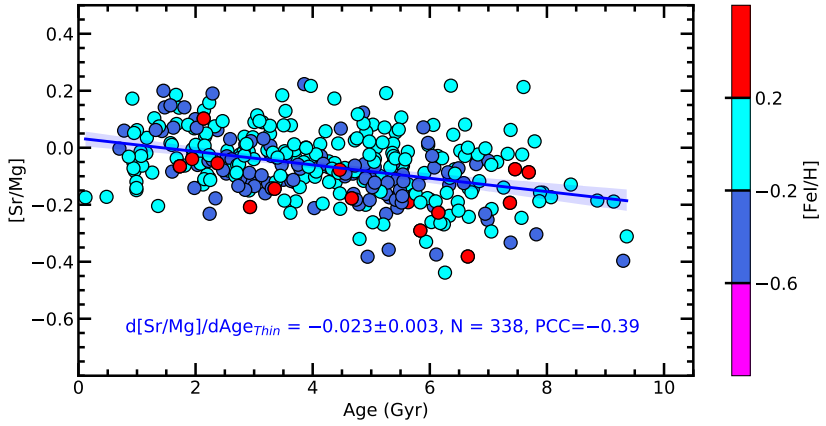

Figure 5-3: [Sr/Mg] age relation for Solar neighbourhood thin-disc stars, colours and symbols as in previous figures above.

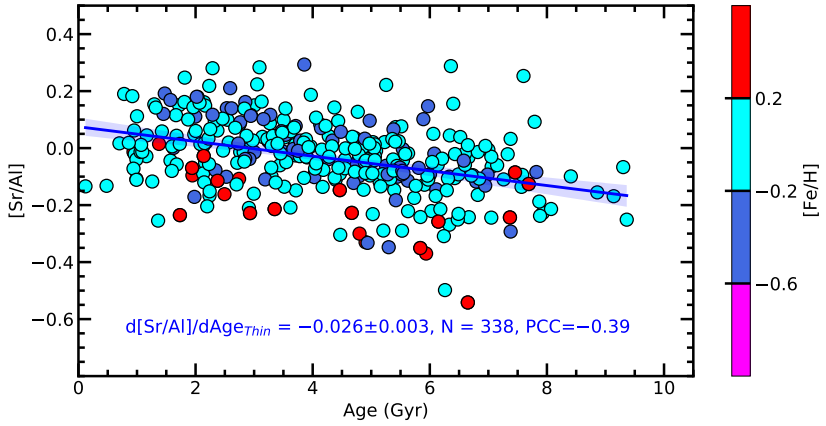

Figure 5-4: [Sr/Al] age relation for Solar neighbourhood thin-disc stars, colours and symbols as in previous figures above.

was used for its calculation. Nissen et al. (2020) also tested the sensitivity of Sr in solar-type stars, obtaining a result slightly lower than that of Y, which is in agreement with our results. In their study they used the same single Sr I 4607.34 Å line as in our work.

As we can see, the y-intercept and slope are slightly higher when [Sr/Al] is used compared to [Sr/Mg], for the same number of stars.

$$[\mathrm{Sr/Al}]_{\mathrm{Thin}} = 0.075\,(\pm 0.016) - 0.026\,(\pm 0.003) \cdot \mathrm{age[Gyr]} \tag{5.4}$$

As we can deduce from the previous results, the use of Al as α element tends to increase the slope, y-intercept and PCC, maximizing the relation, while the use of Sr as s-element tends to decrease it. This can be seen in the Figure 5-5, where the coefficients for the $[s/\alpha]$ regressions considered are compared. This behavior is also found in most of the works by the aforementioned authors in this section. However, this tendency of Al to increase the slope is not seen in Jofré et al. (2020) for a sample of 80 solar twins.

5.1.2. The Age versus $[s/\alpha]$ relations in the thick disc

Regarding the use of the $[s/\alpha]$ ratios as age indicators in the thick disc, the situation is more controversial, and needs to be clarified. Our sample of Solar neighbourhood thick disc stars for which we have abundances of Y, Mg, and their age consist in 76 stars in the following ranges: T_{eff} (K): [3715, 6683]; $\log g$: [0.83, 4.63]; [Fe I/H]:

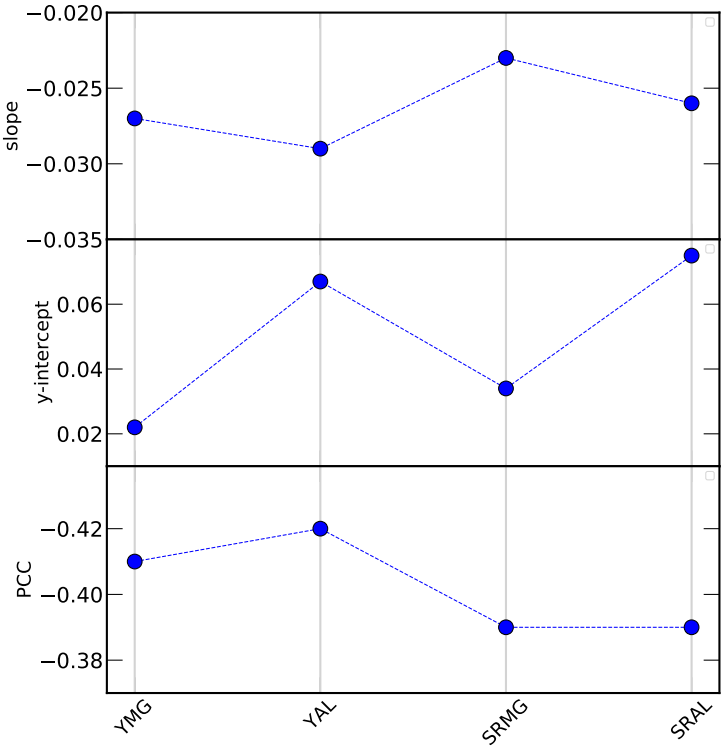

Figure 5-5: [s/α] Age ratios using Y and Sr as s-process elements, combined with Mg and Al as α-elements for the thin disc stars sample.

$[-1.05, 0.03]$; Age (Gyr); [2.71, 10.14]. For this sample we obtained the slope of the equation 5.5, slightly steeper than for the thin disc, and with a PPC = −0.35, slightly lower.

$$[\mathrm{Y/Mg}]_{\mathrm{Thick}} = -0.115\ (\pm 0.079) - 0.041\ (\pm 0.003) \cdot \mathrm{age[Gyr]} \qquad (5.5)$$

Titarenko et al. (2019) also calculated the [Y/Mg]-age ratio for the thick disc, for a sample of 11 turn-off stars with ages from about 11.5 to 14.5 Gyr for the AMBRE project, obtaining a steeper slope. To try to clarify the question, and due to the small size of the sample, we increased it by compiling data from other authors for those we find abundances of Y and Mg, ages and the component separation of the Galactic disc. Thus, our compilation gathers 237 stars of the thick disc coming from Bensby et al. (2014), Adibekyan et al. (2012), Delgado Mena et al. (2017) and Titarenko et al. (2019). In the equation 5.6 and the Figure 5-6 we show the regression results for the collection of 237 stars from the thick disc, finding an almost negligible [Y/Mg] correlation with age (PCC = −0.04).

$$[\mathrm{Y/Mg}]_{\mathrm{Thick,\ comp.}} = -0.303\ (\pm 0.027) - 0.002\ (\pm 0.003) \cdot \mathrm{age[Gyr]} \qquad (5.6)$$

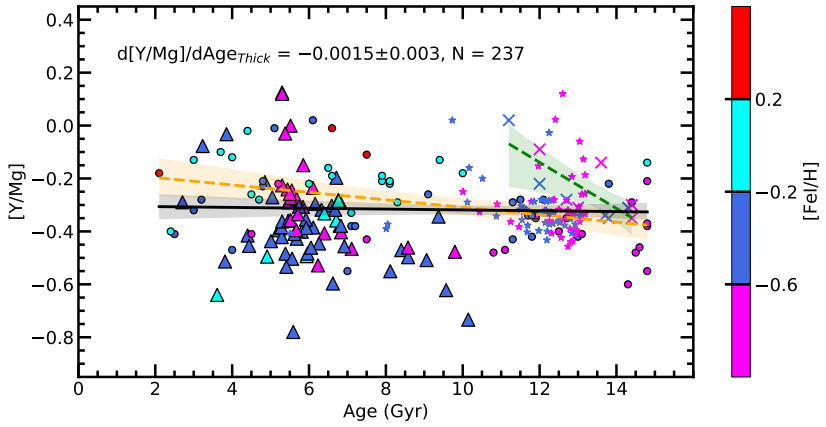

Figure 5-6: [Y/Mg] Age relation for a compilation of 237 stars from the thick-disc stars colour-coded by metallicity as in the previous Figures. The collection of stars consists of those of our sample (triangles), complemented by stars from Bensby et al. (2014) (dots), Adibekyan et al. (2012) and Delgado Mena et al. (2017) (stars), and Titarenko et al. (2019) (crosses). The black continuous line is the regression that fit to the entire sample of 237 stars. The dashed green line is the regression for the AMBRE sample of 11 thick-disc stars from Titarenko et al. (2019); and the dashed yellow line represents the trend that we computed using Bensby et al. (2014) data alone covering the entire investigated age interval. The shadowed areas show the 95% confidence interval for the regression.

Because the Bensby et al. (2014) contains thick-disc stars in a wide range of ages, we computed its regression line for that stellar sample alone. The slope is also quite smooth, and is close to that of the compilation ([Y/Mg] = $-0.168(\pm 0.040) - 0.014(\pm 0.004) \cdot$ age [Gyr]). This seems to agree with the results for the [El/Fe I] age gradients, which appear to be smoother than those of the thin disc (*vide* Figures 4-3 and 4-4). This evidence a different chemical evolution for the thick disc, and suggests that its use as age indicators in this subcomponent of the Galactic disc is not valid. In any case, the question of the thick disc is not yet closed, waiting for an increase in the sample with abundances of neutron-capture elements.

5.2. The open clusters sample from the Gaia-ESO

5.2.1. The Age versus [s/α] relations from open clusters

As we saw at the beginning of the chapter, the idea of combining pairs of elements with different origins, particularly s-process and α-elements (or odd-Z element, as Al, with a similar behaviour to the α-elements), has taken shape in the last decade (see, e.g. Tucci Maia et al., 2016; Nissen, 2016; Feltzing et al., 2017; Fuhrmann et al., 2017; Slumstrup et al., 2017; Titarenko et al., 2019; Casali et al., 2020). The combination of the abundances of an s-process element with other elements with opposite behaviour, such as α-elements, maximise their correlation with stellar age. Several relations have been established and calibrated in the solar neighbourhood (see, e.g. Spina et al., 2016; Delgado Mena et al., 2019; Jofré et al., 2020). In this chapter we aim at extending them in different regions of the Galactic disc, using our sample of open clusters. For each neutron capture peak, we selected the element with the highest percentage from s-process in the Sun (*vide* references in Chapter 1): Y for the first peak and Ba for the second one. We combined them with several α-elements, namely Mg, Si, Ca and Ti, and Al (which can be also considered as an odd-Z element, but has a behaviour very similar to the other α-elements).

To find the best way to describe the relations between the age of the clusters and their chemical characteristics, we used an approach based on multilinear weighted regressions that takes into account age, metallicity and R_{gc}, in the form [s/α] = m_1·Age + m_2· R_{gc} + m_3· [Fe/H] + c. A similar approach was used for example in Delgado Mena et al. (2019) and Casali et al. (2020), who took into account [Fe/H] in their sample of solar-like stars. We computed both a global regression, considering all clusters in the sample, and individual regressions for each radial region. For all regressions, we adopted the same weight system, as described before. In Table A.2 we report the coefficients of the weighted multivariate regressions for the three radial regions, and for the global sample including all clusters at all R_{gc}.

In Figure 5-7, we plot [Y/α] and [Ba/α] versus cluster ages in the three regions of the Galactic disc, as defined above. Here and in the following sections, we will simplify by including Al in the group of α-elements, and thus when referring to [s/α] we also consider Al. In the left panels of Figure 5-7, we find well differentiated behaviours: in the outer and central regions we have decreasing trends of [Y/α] with increasing age, while in the inner region we observe a reverse trend, as already noted, with a smaller sample size, in Magrini et al. (2021). In the right panels of

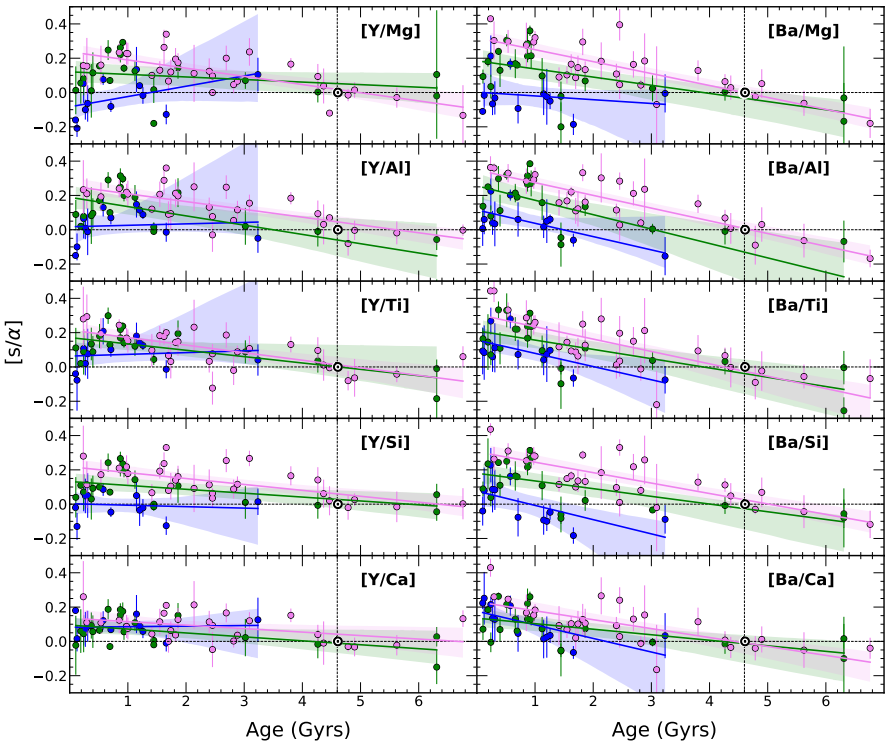

Figure 5-7: Age versus [s/α] for our OC sample divided in the three R_{gc} regions. The regressions curves with their confidence intervals (shaded regions) are shown in each panel. On the left side, we have the abundance ratios [Y/α] versus Age, and on the right side, [Ba/α] versus age. The symbols and colours are the same as in Figure 4-5.

Figure 5-7, the abundance ratios containing Ba and an α element show a decreasing trend with increasing age in all three regions. In addition, the innermost region shows a stronger trend than the others, with a steeper slope.

The coefficients (m_1, m_2, m_3 and c), and the correlation coefficients are also shown in Figure 5-8, in which we separate the abundance ratios with Y and with Ba, for each radial region and for the whole sample. It is interesting to notice that the region that differs the most from the others is the inner region, while the region around the Sun, and the outer region are very similar, and even similar to the global relationship. Therefore, the multivariate regression computed with the whole sample of clusters might still be a good approximation for the solar neighbourhood and the outer region, while it fails to reproduce the inner disc region (cf. Casali et al., 2020).

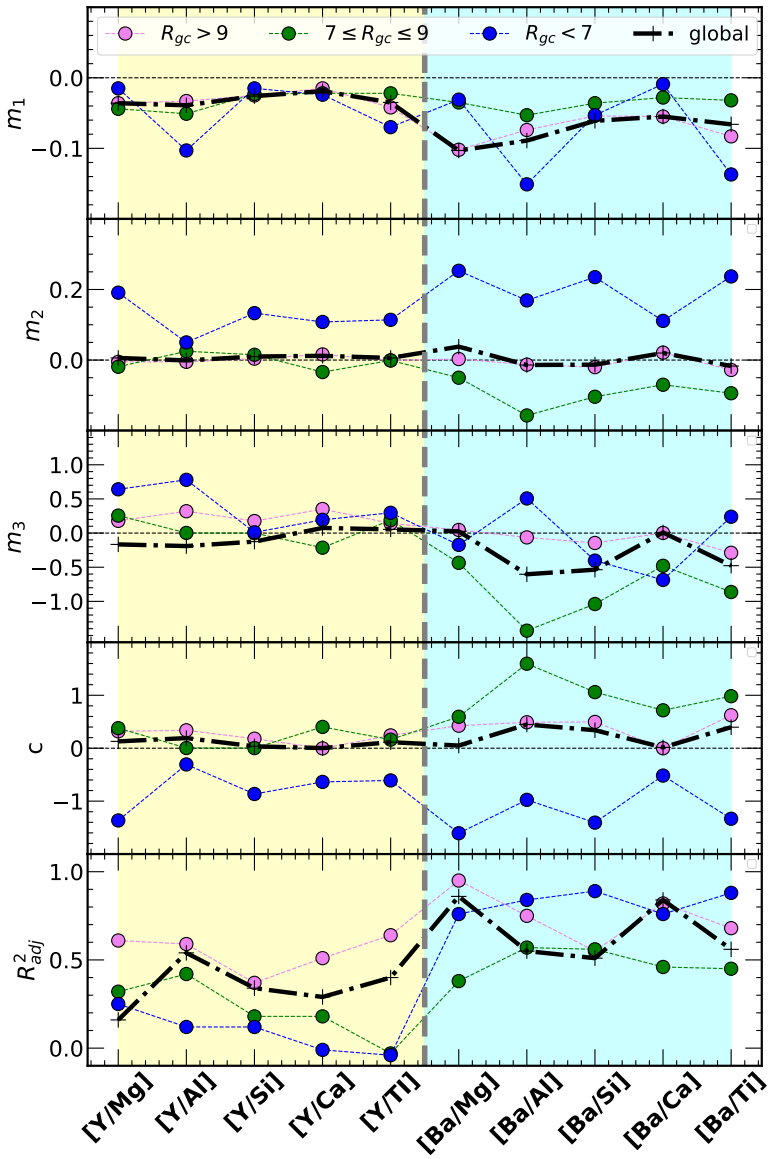

Figure 5-8: Regression coefficients for the [s/α] = m_1·Age + m_2· R_{gc} + m_3· [Fe/H] + c relation. In the upper panel, we show m_1, in the second one m_2, in the third one m_3 and in the fourth one c. In the bottom panel we present the correlation coefficients. In all panels, we use the following symbols: for the inner region blue circles, for the solar region green circles, for the outer region pink circles, and for the whole sample dashed black lines. Yellow region highlights the abundance ratios with Y, and cyan region with Ba.

In the Appendix, we show the three-dimensional views of the relations, for an example abundance ratio [Ba/Al] as a function of both age and [Fe/H] and R_{gc} (Figures A6 and A7).

5.2.2. The role of migration in open clusters

Radial migration plays an important role in the redistribution of stellar populations, particularly the older ones, in our Galaxy. What weight migration has in shaping the spatial distribution of more massive populations, such as clusters, with respect to single stars, is not yet settled (see, e.g. Anders et al., 2017; Chen and Zhao, 2020; Zhang et al., 2021; Netopil et al., 2021). To estimate the possible effect of radial migration in our relationships, we calculated the orbits of our cluster sample using the GALPY code, with the axis-symmetric potential MWPOTENTIAL2014 (Bovy, 2015). We adopted the guiding radius (R_g, defined as the average between the minimum and maximum radius, see, e.g. Halle et al., 2015) instead of their present time R_{gc} to recompute the relations between age and abundance ratios, associating the clusters to the three radial regions on the basis of their R_g. Adopting R_g can, indeed, mitigate the effect of blurring, due to epicyclic oscillations around the guiding radius (Sellwood and Binney, 2002), while it cannot overcome the migrating effect of churning, i.e. the change of R_g due to interactions with a lasting non-axisymmetric pattern such as long-lived spiral arms or long-lived bars (Sellwood and Binney, 2002; Binney and Tremaine, 2008). Using R_g, we found a new redistribution in the three regions: eight clusters might be visitors in their respective regions, initially assigned. The most affected region is the inner disc, which is repopulated with 7 clusters coming mostly from the central region of the disc, with the exception of one cluster coming from the outer region (ESO 92 05). The outer disc is less affected by redistribution. The other seven clusters that move from the solar region to the inner region are: NGC6791, Berkeley 44, NGC6802, NGC4815, Trumpler 20, NGC4337 and Collinder 261. Among them, NGC6791, which is at the same time old and metal rich, is known to have a high probability to be a migrator (cf. Jílková et al., 2012; Netopil et al., 2021). Taking into account the effect of blurring, the regions are redistributed to contain 20 OCs in the inner disc instead of 7; 13 in the solar region instead of 20; and 29 in the outer region instead of 30 (*vide* Figure 5-9).

We recalculate the relations adopting R_g instead of R_{gc}. As expected from the redistribution of the OC between inner, solar-neighbourhood. and outer regions,

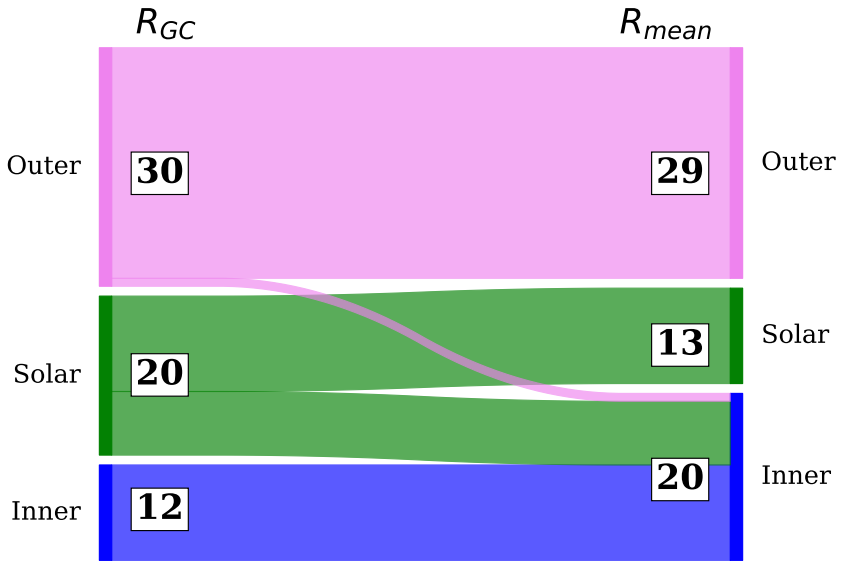

Figure 5-9: Distribution of the 62 OCs in the three considered galactocentric regions (inner, solar and outer). On the left-side of the Figure, we give the number of clusters which are located in each region based on their present R_{gc}, while on the right-side we provide the number of clusters whose mean orbital radius, R_{mean}, falls in each of the three radial region. Radial migration mostly affects and redistributes clusters between the inner disc and the solar region.

only regressions for the inner and solar regions change when replacing R_{gc} by R_g. There is not an improvement in the quality of the fits, with a decreasing in the correlation coefficients in the inner disc and in the solar neighbourhood (about 0.1 lower than those obtained with R_{gc}). In the next sections, we use the relationships obtained with the current galactocentric position.

5.2.3. Comparison with literature results

In this section, we have compared our results with three recent literature works (Casali et al., 2020; Jofré et al., 2020; Casamiquela et al., 2021). In Figure 5-10, we show the coefficient m_1 related to *age*, computed for the samples of open clusters in the outer and solar regions, with the results from Casali et al. (2020) (yellow dots) for a sample of solar-like stars (and later applied to open clusters), Casamiquela et al. (2021) for two samples of open clusters divided in closer than 1 kpc to the Sun and more distant (red dots and triangles respectively), and Jofré et al. (2020) for a sample of 80 solar twins (cyan dots in Figure 5-10).

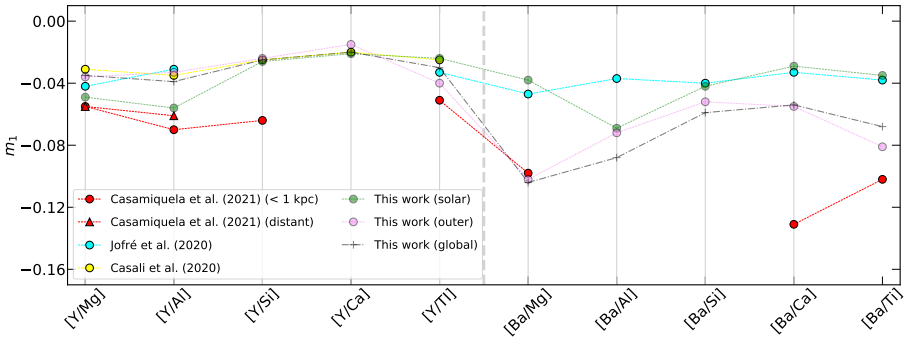

Figure 5-10: Comparison of the first independent variable ($m_1 \cdot$ Age) of our stellar dating relations with those of Casali et al. (2020) (yellow color) for solar-like stars (which were tested in open clusters), Jofré et al. (2020) for a sample of 80 solar twins (cyan color) and those of Casamiquela et al. (2021) for a sample of 47 open clusters (red color).

The samples of solar twins or solar-like stars are to be compared with our sample of clusters in the solar region, while our outer disc sample can be compared with the outermost sample of Casamiquela et al. (2021). The general agreement is very good, and our slopes for the solar region sample agree well with those the solar-like stars from different authors. The largest differences are seen with sample of Casamiquela et al. (2021) for [Ba/Ca] and [Ba/Ti], which might be related to the inclusion of younger clusters in their sample.

5.2.4. Application to open clusters

The first step to verify the validity of our relations and their ability to provide a reliable estimate for the stellar ages, is to reapply the same relations to clusters, by comparing the input ages from isochrone fitting with those obtained from the ten considered chemical clocks. The comparison between the two ages is shown in Figure 5-11.

The cluster ages, for each range of R_{gc}, are computed with the corresponding radial relations or with the global relations (throughout the entire R_{gc} interval). In the panels in each row, we show the results for a given chemical clock. There are three main aspects to note: *i)* the scatter increases for younger ages for almost all relations, *ii)* some relations allow us to recover the input ages with greater accuracy (closer to the 1-to-1 relation) and precision (less scatter) than the others. We have defined our *accuracy* as the mean average difference between input and output ages

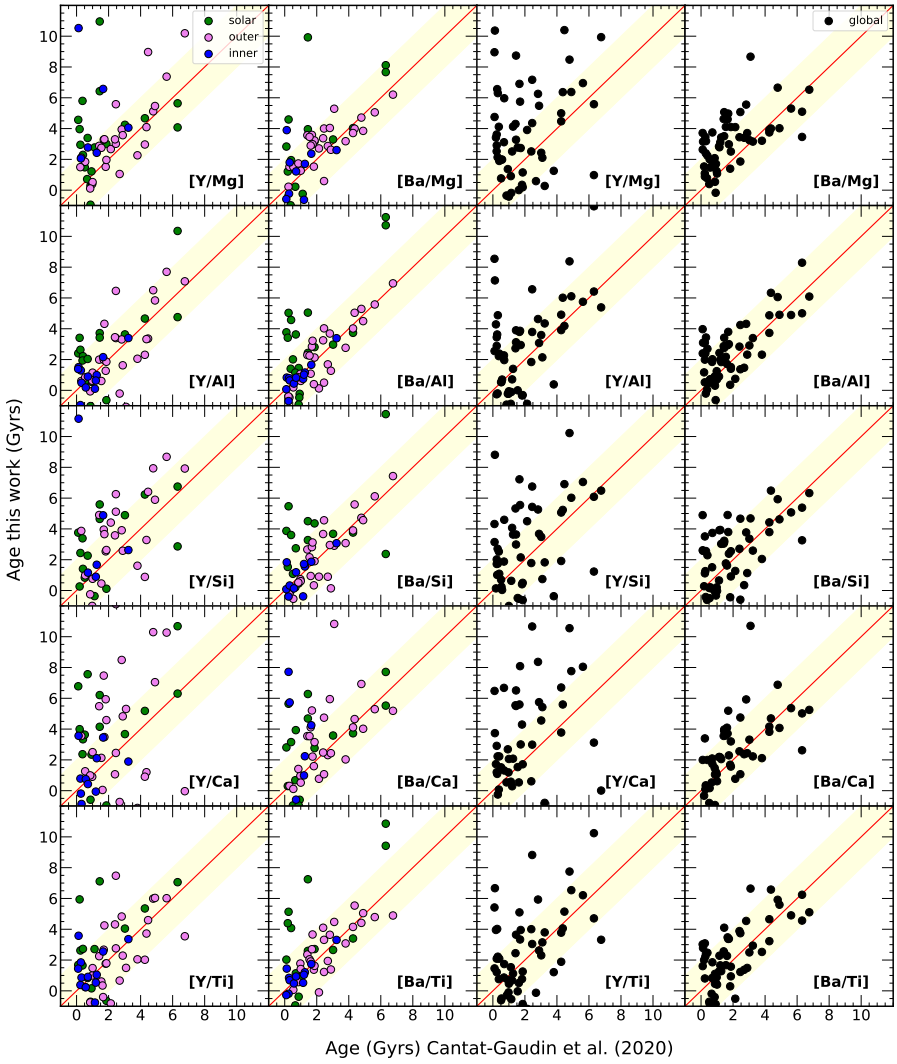

Figure 5-11: Ages computed with our relations versus ages for isochrone fitting (Cantat-Gaudin et al., 2020). In the left two panels, we shown the ages computed with the relations obtained for each radial region. The clusters are colour-coded by R_{gc}. In the right two panels, we show the ages computed with global relations versus the ages from Cantat-Gaudin et al. (2020). The red continuous line is the bisector, and indicates the 1-to-1 relation. The yellow shaded regions indicate the clusters with ages within 2 Gyr from their age from the isochrone fitting.

obtained from our relations (which is indeed a sort of mean bias with respect to the reference values), while the *precision* (which can be considered as the scatter or internal error calibration) as the standard deviation of the mean difference; *iii)* the global relations, in general produce worst results, especially for the younger ages

(which is expected, since younger clusters dominate the inner region, for which the global relations do not work). The *accuracy* and *precision*, as defined above, for all radial bins, including the global one, and for all the considered abundance ratios are shown in Table 5.1.

The best set of relations, in terms of both accuracy, precision, and recovering also of the younger ages, are those involving [Ba/Al], which has indeed among the highest correlation coefficients in the three galactocentric regions. As can be seen in Table A.2, the adjusted coefficients of determination using the [Ba/Al] ratio are 0.75, 0.57 and 0.84 for the outer, solar and inner regions respectively. The global relation has, on the other hand, a lower correlation coefficient, 0.55.

As shown in Table 5.1, the accuracy obtained with the [Ba/Al] relation is 0.1 Gyr in the outer region, −1.4 Gyr in the solar region, and −0.0 Gyr in the inner region, with precision of 0.9, 2.4 and 0.4 Gyr respectively. However, if we exclude in the solar region the three most discrepant clusters, NGC6971, Berkeley 44 and Collinder 261, likely subject to migration (*vide* Section 5.2.2), then the accuracy improve, decreasing to ~ -0.9 Gyr and the precision becomes slightly lower, 2.3 Gyr. These numbers give us a first estimate of the kind of uncertainties to which ages measured with chemical clocks are subject.

5.2.5. Application to individual cluster member stars

Another interesting test is to compare the age of each cluster member with the age obtained from one of our best relation. We select as an example the ages computed with the relations based on the abundance ratio [Ba/Al]. This comparison allows us to make a more realistic estimate of the uncertainties when the relation is applied to the field stars. Within the same cluster, there can be, indeed, considerable variations in abundance ratios, linked to the quality of the measurements, but also to some peculiar enrichment in Ba and in other *s*-process elements. This results in variations between the estimated ages of members of the same clusters, which are expected to be coeval. In Figure 5-12 we show the violin plots of the ages of each stellar member of the clusters calculated using the relations between [Ba/Al] and age, derived independently in the three radial regions. We compare the individual ages with the literature ages from Cantat-Gaudin et al. (2020).

In the outer and inner disc the isochrone fitting ages for almost all clusters falls within the interquartile range of the ages calculated with our relations. However, in the solar region, this does not happen for some clusters, such as NGC6791,

Table 5.1: Accuracy and precision of our relations in recovering the ages of clusters in each of the defined regions and globally.

	R_{gc} > 9	
ratio	accuracy (Gyr)	precision (Gyr)
[Y II/Mg I]	−0.2	2.1
[Y II/Al I]	0.6	2.2
[Y II/Si I]	0.1	2.9
[Y II/Ca I]	−0.1	4.7
[Y II/Ti I]	0.2	1.7
[Ba II/Mg I]	−0.5	1.0
[Ba II/Al I]	0.1	0.9
[Ba II/Si I]	0.3	1.3
[Ba II/Ca I]	−0.5	2.0
[Ba II/Ti I]	0.1	1.1
	7 < R_{gc} < 9 (kpc)*	
[Y II/Mg I]	−1.6 (−1.6)	2.8 (2.1)
[Y II/Al I]	−0.3 (−0.1)	2.1 (1.9)
[Y II/Si I]	0.5 (0.6)	3.4 (3.5)
[Y II/Ca I]	−1.3 (−0.9)	3.3 (3.3)
[Y II/Ti I]	−0.7 (−0.1)	3.8 (3.1)
[Ba II/Mg I]	−0.3 (0.3)	3 (2.4)
[Ba II/Al I]	−1.4 (−0.9)	2.4 (2.3)
[Ba II/Si I]	−0.4 (−0.3)	2.9 (2.6)
[Ba II/Ca I]	−0.3 (−0.1)	2.6 (2.6)
[Ba II/Ti I]	−0.6 (0.1)	2.8 (2.5)
	R_{gc} < 7 (kpc)	
[Y II/Mg I]	2.0	7.0
[Y II/Al I]	−0.1	0.8
[Y II/Si I]	1.2	4.9
[Y II/Ca I]	0.9	2.9
[Y II/Ti I]	−0.4	1.3
[Ba II/Mg I]	0.7	2.3
[Ba II/Al I]	−0.0	0.4
[Ba II/Si I]	0.2	0.9
[Ba II/Ca I]	2.2	5.5
[Ba II/Ti I]	−0.1	0.4
	6 < R_{gc} < 20 (kpc)	
[Y II/Mg I]	−1.3	3.1
[Y II/Al I]	−0.3	2.7
[Y II/Si I]	0.0	3.2
[Y II/Ca I]	−0.3	3.7
[Y II/Ti I]	−0.1	2.4
[Ba II/Mg I]	−1.2	1.5
[Ba II/Al I]	−0.6	1.3
[Ba II/Si I]	−0.3	1.7
[Ba II/Ca I]	−0.2	1.8
[Ba II/Ti I]	−0.2	1.5

* Results after removing discrepant OCs are included in parentheses.

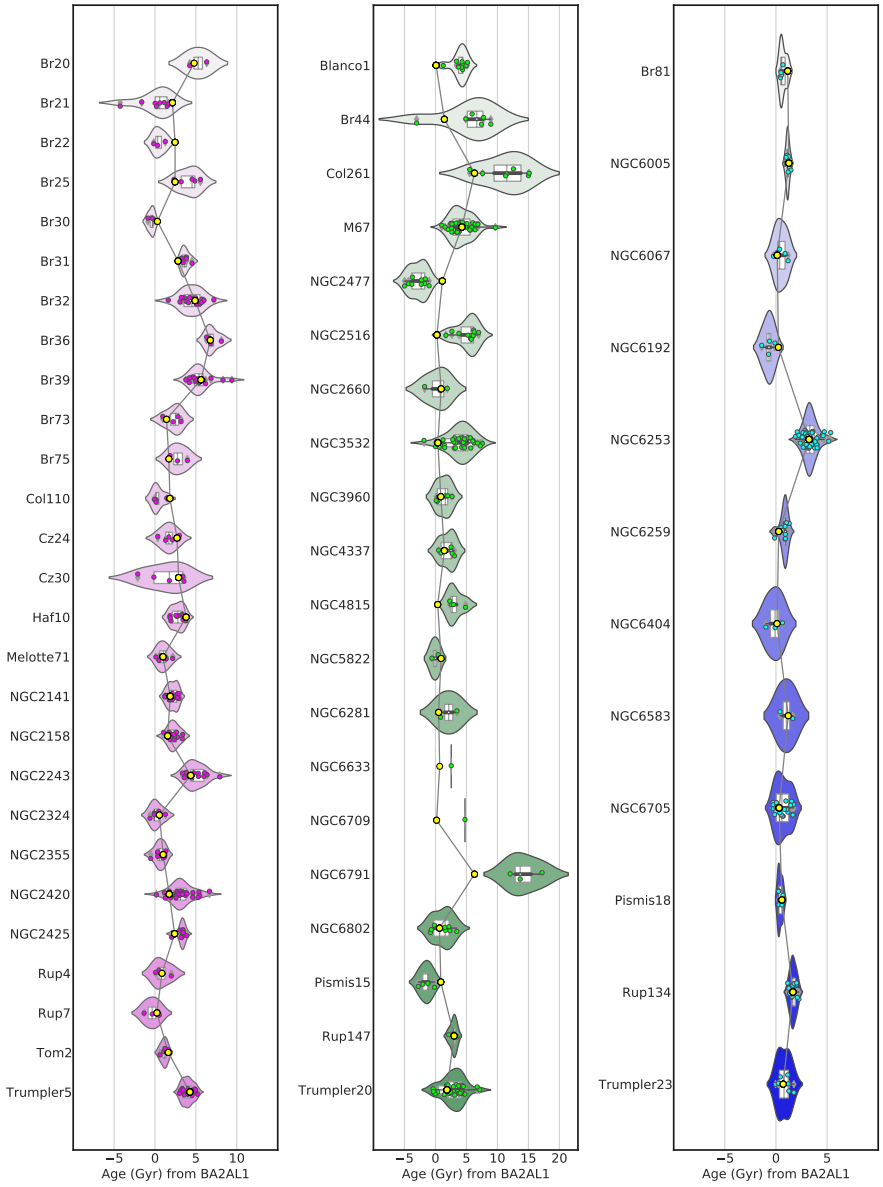

Figure 5-12: Violin plots of the ages of each stellar member of the clusters calculated using the relations inferred from [Ba/Al] for each of the three regions. Each of the coloured dots represents the age of each member star calculated individually, while the yellow dot is the age from Cantat-Gaudin et al. (2020) for each of the clusters. The thick white bar in the center represents the interquartile range and the thin grey line represents the 1.5×IQR, also showing a kernel density estimation with the distribution shape of the data. The left panel shows the clusters in the inner disc, the central panel those in the solar region, and the right one the outer disc clusters.

Collinder 261, NGC4815, or Berkeley 44. As discussed in Section 5.2.2, this supports the high probability of these clusters to be subject to migration. We suppose that they were born in the inner disc as evidenced by their R_g. We then did a further test, calculating their ages with the relation obtained for the inner disc. We have an improvement for NGC6791 and Berkeley 44, while the age of Collinder 261 still remains discrepant. We also have to consider that for NGC6791 the age given by Cantat-Gaudin et al. (2020) is a lower limit, and there are many works that give higher ages for this cluster (e.g. Brogaard et al., 2011, 2012, 2021), thus in the direction of the age obtained with our relations. Furthermore, the above seems to be supported by the fact that other clusters in the solar region that appear to deviate in Figure 5-12 (e.g. NGC6709, Pismis15, NGC5822, NGC6633, NGC2516), have R_{gc} at the edge with the inner region (between 7-7.5 kpc).

Finally, we did a last test by applying the best relations to a sample of GES field stars with similar characteristics to those of the clusters, namely thin-disc stars in approximately the same [Fe/H] and age range as our open cluster sample. The results of the age distribution in [α/Fe]-[Fe/H] plane agree with the expectation for the age distribution in the thin disc (see, e.g. Haywood et al., 2013; Hayden et al., 2015; Buder et al., 2019; Casali et al., 2019, 2020), that is, the oldest stars are those with a higher [α/Fe] ratio, while the youngest have solar or slightly sub-solar ratios. However, taking into account that for field stars the scatter in abundance ratios of age tracers at a given age (calculated with isochrones) is about 0.2 dex, the age determination with chemical clocks is only approximate and of purely statistical value (not real measurements). For more details we refer to section 6 of the Ref. V.

5.2.6. A theoretical explanation

As we have seen, an important limitation of applicability for the [Y/Mg] relation as an age indicator is related to the galactocentric distance. The failure to apply this relationship to the open cluster population in the inner region (R_{gc} < 6.5 kpc) of the Galactic disc by Casali et al. (2020) raised some questions about the efficiency of the *s*-process at high metallicity. Furthermore, Vescovi et al. (2020) proposed a new formulation for mixing induced by magnetic buoyancy in AGB stars. An important effect of magnetic mixing is that it causes a less efficient production of Y at high metallicity. Because a considerable fraction of stars with supersolar metallicity is produced in the inner disc, then their Y abundances are affected by that reduced yields. Using the new AGB yields in which magnetic mixing was

included (MAGN), which is a recent improvement of the FRUITY models (Cristallo et al., 2009, 2011), we were able to reproduce the observed trend in the sample of Gaia-ESO IDR5 clusters from Magrini et al. (2018) at different galactocentric distances. This allowed us to qualitatively explain the coefficient variations in the [Y/Mg]-age relations for a sample of abundances and ages of open clusters located at different regions. The Figure 5-13 shows the [Y/H], [Y/Mg], and [Mg/H] versus age for the Gaia-ESO IDR5 sample of clusters in three radial bins representing the inner disc, the central region of the disc and the outer disc, namely R_{gc} < 6.5 kpc (blue), 6.5 kpc < R_{gc} < 9 kpc (green), and R_{gc} > 9 kpc (violet). The lines exhibit the GCE models for the thin disc at three galactocentric distances (R_{gc} = 6, 8, and 10 kpc) with the MAGN yields (continuous) and with the FRUITY yields (dot-dashed). In the aforementioned Figure 5-13 the ages and R_{gc} of OCs were taken from Cantat-Gaudin et al. (2020), and the star points out the abundance ratio at the solar age and galactocentric distance. For a more detailed explanation, we refer the reader to Ref. III.

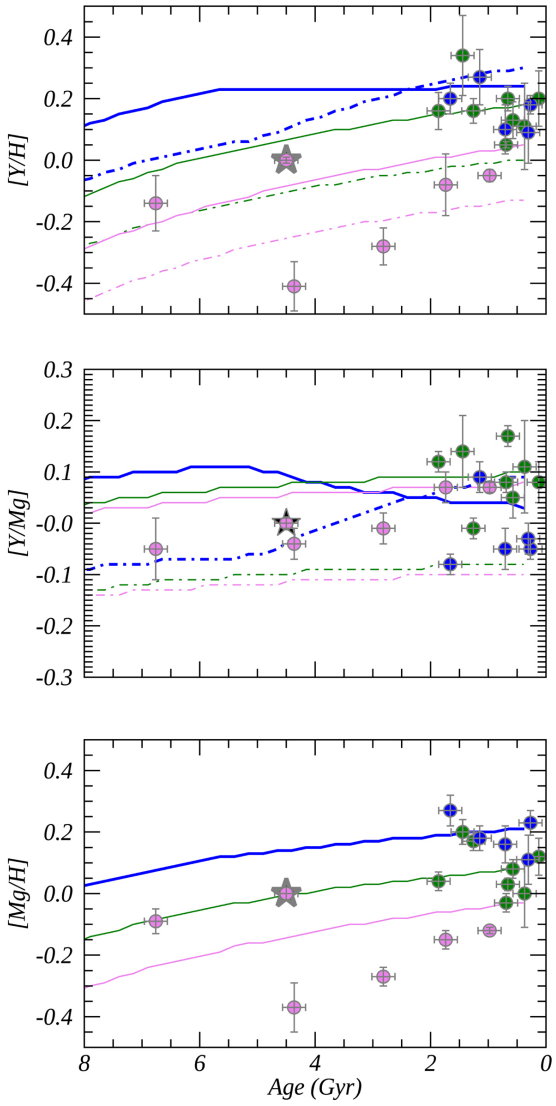

Figure 5-13: [Y/H], [Y/Mg], and [Mg/H] versus age for the Gaia-ESO IDR5 sample of clusters in three radial bins: R_{GC} < 6.5 kpc (blue), 6.5 kpc < R_{GC} < 9 kpc (green), and R_{GC} > 9 kpc (pink). The lines are the GCE models for the thin disc at three R_{GC} = 6, 8, and 10 kpc with the MAGN yields (continuous) and with the FRUITY yields (dot-dashed).

6. CONCLUSIONS AND FUTURE PROSPECTS

6.1. Conspectus

The aim of this thesis is to present, analyse and value the high potential of the neutron-capture elements abundances in the context of the structure and evolution of the Milky Way, trying to bring light to some of its most important open problems. To achieve this objective, and using field stars and open clusters, we rely on the abundance trends of the *s*- and *r*-processes in different ranges of metallicity, age, mean galactocentric distance, and maximum height from the Galactic midplane, as well as their relationship to each other.

In Chapter 1 we introduced the topic, reviewing the definitions, classification, as well as the proposed astrophysical sites for the production of neutron-capture elements. In Chapter 2 we presented the methodology used. In Chapter 3 we addressed the abundance ratios and in Chapter 4 the abundance gradients, both temporal and spatial, and for the two samples (solar neighborhood field stars and open clusters). In Chapter 5 we discuss the use of neutron capture element abundances as cosmic clocks. In this chapter 6 we present the conclusions.

The part of this thesis that uses stars in the solar neighborhood is fundamentally sustained on Ref. II and Ref. I papers, which are the background of the thesis, and complements the studies presented in Mikolaitis et al. (2018), Mikolaitis et al. (2019). Furthermore, these four papers together provide stellar parameters and abundances for a total of 34 elements uniformly derived, using the same method and instrumentation. Concerning the use of abundances of neutron-capture elements from open clusters, the results are sustained by the Ref. III, Ref. IV and Ref. V papers, and expand the studies of Magrini et al. (2018) and Casali et al. (2020), using the observations from the GES iDR5 and GES iDR6 sample, which are also part of this thesis.

Sustained on the above, the following conclusions are stated:

6.2. Conclusions

1. An evaluation of the [El/Fe I] ratios is made as a function of metallicity, comparing the results with the GCE models of Pagel and Tautvaisiene (1997) and Prantzos et al. (2018). The observations show for the elements of the second *s*-process peak a maximum at approximately −0.2 dex, while the

models of Prantzos et al. (2018) exhibit a maximum at about −0.4 dex. A better agreement could be achieved if the LIMS input at higher metallicities (about −0.7 dex) were taken into account in the models.

2. The [hs/ls] ratio is examined to monitor the *s*-process efficiency and the reliability of the GCE models, finding a clearly differentiated behavior for the two components of the Galactic disc: for the stars of the thin disc an almost flat trend, while for the thick disc a downward trend with decreasing metallicity, which proves their different evolutionary histories and reveals the overabundance of light-*s* elements at low metallicities. The observations also indicate that the Prantzos et al. (2018) model should have its maximum at about −0.2 dex, considering the LIMS input at higher metallicities.

3. The comparison between *r*-dominated elements with the *s*-dominated ones suggests that the GCE models have to be further developed in order to account for the higher *r*-process production. In the thick disc the [Eu/Ba] and [Sm/Ba] ratios reach the pure *r*-process values for metal-poor thick-disc stars, meaning that was the only n-capture process active at the beginning of the formation of the thick disc.

4. This study also makes a comparison of the *r*- and α- process elements, taking as the most representative elements of each process the Eu and Mg respectively. Thus, our sample of thick-disc stars shows a more evident decrease in [Eu/Mg] and [r/α] with increasing metallicity compared to the thin-disc stars, which points once again to different chemical evolution of the Galactic disc components.

5. Regarding the variation of [El/Fe] as a function of [Fe/H] in our sample of open clusters, we observe important differences in the clusters belonging to the three defined regions of the Galactic disc. The clusters in the outer disc (R_{gc} > 9 kpc) are generally more metal poor than the clusters in the inner disc (R_{gc} < 7 kpc) and in the solar neighborhood. Typically, outer disc clusters have [El/Fe]>0, while the inner disc ones have [El/Fe] solar or sub-solar.

6. A study of temporal gradients for field stars is carried out, finding abundance correlations consistent with the nature of each group of elements in the GCE context, and with the available literature. Therefore, in the thin disc we find two well differentiated groups with opposite behavior: on the one hand, the elements of the first *s*-process peak Y, Sr and the element of the second

s-process peak Ba showing a clear anti-correlation with age; and on the other hand the mixed element Pr, and the *r*-process dominated elements Sm and Eu showing a positive gradient. The other elements stand in the middle, showing negligible or near negligible gradients.

7. Concerning the age-abundance gradients on the thick disc, these tend to soften or become negligible. Given the size of the sample, this behavior should be confirmed in future research, waiting for an increase in the population and a widening of the age interval for that Galactic component.

8. Some abundance analysis of OCs show the apparent overabundance of [Ba/Fe] in young clusters (ages <100 Myr), which does not happen with other heavy elements and is known as the "barium puzzle". Looking for any trace in the youngest stars of our thin-disc sample (most of them dwarfs and unevolved giants), we found no evidence of the barium abundance anomaly, as it was found also by Reddy and Lambert (2017) and Marsakov et al. (2016).

9. Regarding the age gradients in our open clusters sample, we find that the [El/Fe] are under abundant for a given age in the inner disc (R_{gc} < 7 kpc) with respect to those of the outermost regions. We also found a decreasing gradient with age, being the [Ba/Fe] the one with the strongest trend. For all s-process dominated elements, the slope of the regression is steeper in the inner disc than in the other regions.

10. Regarding our conclusions on cosmic clocks, we sampled the most sensitive and reliable *s*- and α- process elements (Y and Sr on the one hand, and Mg and Al on the other, respectively). We obtained the following relation: $[Y/Mg]_{thin}$ = 0.022(±0.015) −0.027(±0.003)·age[Gyr], based on 371 thin disc stars, in agreement with that obtained by Titarenko et al. (2019) for the sample of 325 turn-off thin-disc stars in the AMBRE project. This is slightly lower than that of other authors for different samples, which mostly comprise solar twins and use thin and thick disc stars together.

11. We analysed the [Y/Mg] and age relation for 76 stars in the thick disc of our sample together with data available from other works in a broad age and metallicity range (reaching a sample of 237 stars), and found that the slope is negligible. This shows a different GCE for the thin and thick Galactic discs and that the [Y/Mg] can not serve as an age indicator in the thick disc.

12. We provide a set of multiple weighted linear regressions in three variables ([Fe/H], R_{gc}, and age) between abundance ratios and stellar ages, calibrated with an appropriate sample of open clusters, whose ages and distances were homogeneously determined using *Gaia* DR2. We estimate the accuracy and precision of each relation in recovering the age of open clusters. Among the considered chemical clocks, [Ba/Al], and in general abundance ratios involving barium, provide the best recovering factor. The relation between [Ba/Al] and age is also able to reproduce the ages of the individual member stars with a precision better than 2 Gyr.

13. An explanation of the non-universality of the [Y/Mg] ratio for its use as a cosmic clock is also provided, based on the magnetic-buoyancy-induced mixing in AGB stars. This phenomenon causes a less efficient production of Y at high metallicity, which affects this ratio on the inner disc. This is verified in the GES IDR5 open cluster sample at different galactocentric distances, and provides a solid explanation to the observations.

14. The spatial gradients of neutron capture elements are discussed. To avoid biased radial abundance gradients, we computed mean galactocentric distances, which are associated with the stellar's birthplace. When we apply the ODR method to the n-capture elements abundance ratios with $R_{\rm mean}$ in the thin disc, we found that the radial abundance-to-iron gradients in the thin disc are negligible for the *s*-process dominated elements and become positive for the *r*-process dominated elements. In the thick disc, the radial abundance-to-iron slopes are negligible.

15. Regarding the maximum height $|z_{\rm max}|$, the vertical gradients are negative for the light *s*-process dominated elements and become positive for the *r*-process dominated elements. In the thick disc, the vertical slopes are predominantly negative.

6.3. Limitations and future prospects

All research has a scope and its limitations, imposed by technology or by the problem itself. At the beginning of this thesis we discussed the statement of the problem and its relevance to justify its study, establishing what can be expected or what we could achieve in the research. Seen in perspective, below we list some of

the frontiers to which this research reaches, how the study could be expanded, as well as some ideas of future studies.

The main limitations of this thesis are those related to the size of the sample, especially for the thick disc population. More abundances of neutron capture elements are necessary in the thick disc, in wider age ranges and location. Also those due to the estimation of stellar ages based on the standard method of the isochrone fitting. The more reliable data we have, we will be in a better position to confirm the findings and make more solid assertions.

The first results from the Gaia-ESO Spectroscopic survey (Magrini et al., 2018), the APOGEE Survey (Cunha et al., 2017), the R-Alliance (Hansen et al., 2018; Sakari et al., 2018), the on-going GALAH (Martell et al., 2017; Griffith et al., 2019) and up-coming WEAVE (Dalton et al., 2016) and 4MOST (de Jong et al., 2019) surveys are current examples of efforts to expand the observational results. Smaller projects like the one in this thesis are also shown to be of high value in bringing useful observational results and acquire solid conclusions.

The abundances of neutron capture elements in halo stars are showing huge potential in determining the role that dwarf galaxies play in the formation of the Milky Way as confirmed by the existence of stellar streams. A concrete example is found in the discovery of a metal-poor star with an extreme *r*-process enhancement and α-element deficiency (Xing et al., 2019), a type of stars that have been found in present-day dwarf galaxies. Hence, a way to broaden the scope of this study would be to address halo stars.

The observational results are also very important for the improvement of the theoretical models, which make a rational reconstruction of the information available to explain the astronomical observations. In this sense, the feedback and synergy between theory and observations must be fluid and up-to-date. For example, by investigating the roles of yields from rotating massive stars and low- and intermediate-mass stars in producing *s*-process dominated elements, as well as the relative roles of neutron star mergers and core-collapse supernova in producing *r*-process dominated elements. In this aspect, we are attentive to new GCE models as those of Grisoni et al. (2020), which appear to fit the thick-disc chemical evolution quite well, as well as the new models from other authors that are to come.

Another aspect that would allow to expand the knowledge about the *r*- and *s*-processes, and therefore, of the GCE, would be the incorporation of new elements. In recent years there have been efforts in that direction, by adding new or little-studied elements such as Mo, Ru, Pr, Gd and Dy (e.g. Mishenina et al., 2019).

Regarding this, the present thesis makes a contribution to the better understanding of Pr, and upcoming Gaia ESO Survey (GES) IDR6 studies will include Mo and Ru. In this context, the possibilities offered by blue / UV spectra (<4000 Å) are also encouraging, and would allow to access to new neutron capture elements. Once again, hopes are placed on new techniques and observing facilities, and the advent of the next generation of spectrographs (e.g. Ernandes et al., 2020). CUBES (Cassegrain U-Band Efficient Spectrograph) and HRMOS (High Resolution Multi-Object Spectrograph) are some examples, the latter is expected to be able to reach Pb measurements, crucial to complete our understanding of the *s*-process.

Regarding the origin of the elements of the *r*-process, it is subject of discussions and still needs to be fully clarified, with the core-collapse supernovae and neutron-star mergers contending for its production. Events of this nature are believed to be responsible for the production of rare elements such as gold and platinum (e.g. Tsujimoto and Shigeyama, 2014), which are found in the earth's crust. A recent study points in the same direction, addressing the issue in dispute from another perspective, through the direct analysis of the ^{244}Pu deposited on Earth (Wallner et al., 2021). Future lines of research on neutron capture elements will surely continue along this path as well.

If we look at our nearest future prospects, more observations for the SPFOT survey are ongoing, so we will soon have more available data to give continuity to this opened research line. Also to complete this study with the Gaia ESO Survey (GES) (Gilmore et al., 2012; Randich et al., 2013), which addresses more than 202,000 spectra (185,800 GIRAFFE, 16,500 UVES) of around 115,600 stars and about a hundred clusters. More specifically, in the context of last data release (GES IDR6), which allows us to expand the sample in a larger range of metallicities, ages and Galactic radius, as well as to explore the population of the Galactic halo, the bulge, the use of open clusters, and including two new neutron capture elements (Ru and Mo), and whose work is already in progress. Searching for *r*-enhanced stars in the Galactic halo as well as in Globular clusters (GCs) using GES IDR6 shows great promise.

The use of Gaia EDR3 (Gaia Collaboration et al., 2021*b*) and with an eye to the DR3 expected for this year will also allow to improve the kinematics and other aspects of this thesis. Thanks also to the ongoing TESS and PLATO missions, among others, the number of stars with accurate asteroseismic ages and masses is increasing, so works like this can be very useful to reveal more about the Galaxy formation and evolution and for characterizing new exoplanets.

This thesis can also be useful for future investigations that address the contributions of neutron capture elements in the Sun, since for some elements there are still some disagreements. The discussion is still open awaiting further consensus, and the observational results are a key piece as well.

The separation between the thin and the thick disc is not always clear, what some authors consider a smooth transition (Bovy et al., 2012, 2016), so it is required to look for new criteria that support the distinction of components. The relative behavior of Ba and Eu for the thin and thick disc offers a high potential. This circumstance should be investigated further, and could serve as a complementary technique for the separation of the components. For example, by using machine learning techniques as Support Vector Classification (SVC) or Linear Discriminant Analysis (LDA) to find the hyperplane that divides, or categorises the thin and the thick disc. This thesis also gave us the opportunity to discover some interesting peculiar stars, for which we reserve a future study. These and many other future lines of research with new ideas can find in neutron capture elements a solid base on which to lean. We are sure that some of them will emerge from this thesis. With the hands on the the sixth internal data release (iDR6) of the Gaia-ESO spectroscopic survey (GES), whose work is already in progress, and the results are promising, we hope to be able to confirm and expand soon the conclusions of this thesis.

Bibliography

Abbott, B. P., Abbott, R., Abbott, T. D. et al. (2017), 'Gravitational Waves and Gamma-Rays from a Binary Neutron Star Merger: GW170817 and GRB 170817A', *Astrophysical Journall* **848**(2), L13.

Adibekyan, V., Delgado-Mena, E., Figueira, P. et al. (2016), 'Abundance trend with condensation temperature for stars with different Galactic birth places', *Astronomy and Astrophysics* **592**, A87.

Adibekyan, V. Z., Sousa, S. G., Santos, N. C. et al. (2012), 'Chemical abundances of 1111 FGK stars from the HARPS GTO planet search program. Galactic stellar populations and planets', *Astronomy and Astrophysics* **545**, A32.

Allende Prieto, C. (2016), 'Solar and stellar photospheric abundances', *Living Reviews in Solar Physics* **13**(1), 1.

Almeida-Fernandes, F. and Rocha-Pinto, H. J. (2018), 'A method to estimate stellar ages from kinematical data', *Monthly Notices of the RAS* **476**(1), 184–197.

Alpher, R. A. (1948), 'A Neutron-Capture Theory of the Formation and Relative Abundance of the Elements', *Physical Review* **74**(11), 1577–1589.

Anders, F., Chiappini, C., Minchev, I. et al. (2017), 'Red giants observed by CoRoT and APOGEE: The evolution of the Milky Way's radial metallicity gradient', *Astronomy and Astrophysics* **600**, A70.

Andrievsky, S. M., Kovtyukh, V. V., Luck, R. E. et al. (2002), 'Using Cepheids to determine the galactic abundance gradient. I. The solar neighbourhood', **381**, 32–50.

Arlandini, C., Käppeler, F., Wisshak, K. et al. (1999), 'Neutron Capture in Low-Mass Asymptotic Giant Branch Stars: Cross Sections and Abundance Signatures', *Astrophysical Journal* **525**(2), 886–900.

Asplund, M., Amarsi, A. M. and Grevesse, N. (2021), 'The chemical make-up of the Sun: A 2020 vision', *arXiv e-prints* p. arXiv:2105.01661.

Asplund, M., Grevesse, N., Sauval, A. J. and Scott, P. (2009), 'The Chemical Composition of the Sun', *Annual Review of Astron and Astrophys* **47**(1), 481–522.

Baratella, M., D'Orazi, V., Carraro, G. et al. (2020), 'The Gaia-ESO Survey: a new approach to chemically characterising young open clusters. I. Stellar parameters, and iron-peak, α-, and proton-capture elements', *Astronomy and Astrophysics* **634**, A34.

Baratella, M., D'Orazi, V., Sheminova, V. et al. (2021), 'The Gaia-ESO Survey: a new approach to chemically characterising young open clusters. II. Abundances of the neutron-capture elements Cu, Sr, Y, Zr, Ba, La, and Ce', *Astronomy and Astrophysics* **653**, A67.

Barklem, P. S., O'Mara, B. J. and Ross, J. E. (1998), 'The broadening of d-f and f-d transitions by collisions with neutral hydrogen atoms', *Monthly Notices of the RAS* **296**(4), 1057–1060.

Barnes, S. A. (2003), 'On the Rotational Evolution of Solar- and Late-Type Stars, Its Magnetic Origins, and the Possibility of Stellar Gyrochronology', *Astrophysical Journal* **586**(1), 464–479.

Basri, G., Marcy, G. W. and Graham, J. R. (1996), 'Lithium in Brown Dwarf Candidates: The Mass and Age of the Faintest Pleiades Stars', *Astrophysical Journal* **458**, 600.

Battistini, C. and Bensby, T. (2016), 'The origin and evolution of r- and s-process elements in the Milky Way stellar disk', *Astronomy and Astrophysics* **586**, A49.

Bensby, T., Feltzing, S. and Lundström, I. (2003), 'Elemental abundance trends in the Galactic thin and thick disks as traced by nearby F and G dwarf stars', *Astronomy and Astrophysics* **410**, 527–551.

Bensby, T., Feltzing, S. and Oey, M. S. (2014), 'Exploring the Milky Way stellar disk. A detailed elemental abundance study of 714 F and G dwarf stars in the solar neighbourhood', *Astronomy and Astrophysics* **562**, A71.

Bertelli Motta, C., Pasquali, A., Richer, J. et al. (2018), 'The Gaia-ESO Survey: evidence of atomic diffusion in M67?', *Monthly Notices of the RAS* **478**(1), 425–438.

Bertelli Motta, C., Salaris, M., Pasquali, A. and Grebel, E. K. (2017), 'Observing the products of stellar evolution in the old open cluster M67 with APOGEE', *Monthly Notices of the RAS* **466**, 2161–2174.

Bertolli, M. G., Herwig, F., Pignatari, M. and Kawano, T. (2013), 'Systematic and correlated nuclear uncertainties in the i-process at the neutron shell closure N = 82', *arXiv e-prints* p. arXiv:1310.4578.

Bethe, H. A. (1939), 'Energy Production in Stars', *Physical Review* **55**(1), 103–103.

Biémont, É., Blagoev, K., Engström, L. et al. (2011), 'Lifetime measurements and calculations in Y^+ and Y^{2+} ions', *Monthly Notices of the RAS* **414**(4), 3350–3359.

Biemont, E., Grevesse, N., Hannaford, P. and Lowe, R. M. (1981), 'Oscillator strengths for Zr I and Zr II and a new determination of the solar abundance of zirconium.', *Astrophysical Journal* **248**, 867–873.

Binney, J. and Tremaine, S. (2008), *Galactic Dynamics: Second Edition*.

Bisterzo, S., Gallino, R., Käppeler, F. et al. (2015), 'The branchings of the main s-process: their sensitivity to α-induced reactions on ^{13}C and ^{22}Ne and to the uncertainties of the nuclear network', *Monthly Notices of the RAS* **449**(1), 506–527.

Bisterzo, S., Travaglio, C., Gallino, R., Wiescher, M. and Käppeler, F. (2014), 'Galactic Chemical Evolution and Solar s-process Abundances: Dependence on the ^{13}C-pocket Structure', *Astrophysical Journal* **787**(1), 10.

Blanchard, P. K., Berger, E., Fong, W. et al. (2017), 'The Electromagnetic Counterpart of the Binary Neutron Star Merger LIGO/Virgo GW170817. VII. Properties of the Host Galaxy and Constraints on the Merger Timescale', *Astrophysical Journal, Letters* **848**(2), L22.

Bloecker, T. (1995), 'Stellar evolution of low and intermediate-mass stars. I. Mass loss on the AGB and its consequences for stellar evolution.', *Astronomy and Astrophysics* **297**, 727.

Bodenheimer, P. (1966), 'Depletion of Deuterium and Beryllium during Pre-Main Evolution', *Astrophysical Journal* **144**, 103.

Boeche, C., Siebert, A., Piffl, T. et al. (2013), 'Chemical gradients in the Milky Way from the RAVE data. I. Dwarf stars', *Astronomy and Astrophysics* **559**, A59.

Boissier, S. and Prantzos, N. (1999), 'Chemo-spectrophotometric evolution of spiral galaxies - I. The model and the Milky Way', *Monthly Notices of the RAS* **307**(4), 857–876.

Bovy, J. (2015), 'galpy: A python Library for Galactic Dynamics', *Astrophysical Journal, Supplement* **216**(2), 29.

Bovy, J., Rix, H.-W. and Hogg, D. W. (2012), 'The Milky Way Has No Distinct Thick Disk', *Astrophysical Journal* **751**(2), 131.

Bovy, J., Rix, H.-W., Schlafly, E. F. et al. (2016), 'The Stellar Population Structure of the Galactic Disk', *Astrophysical Journal* **823**(1), 30.

Bramante, J. and Linden, T. (2016), 'On the r-process Enrichment of Dwarf Spheroidal Galaxies', *The Astrophysical Journal* **826**(1), 57.

Bregman, J. N. (1980), 'The galactic fountain of high-velocity clouds.', *Astrophysical Journal* **236**, 577–591.

Bressan, A., Marigo, P., Girardi, L. et al. (2012), 'PARSEC: stellar tracks and isochrones with the PAdova and TRieste Stellar Evolution Code', *Monthly Notices of the RAS* **427**(1), 127–145.

Brogaard, K., Bruntt, H., Grundahl, F. et al. (2011), 'Age and helium content of the open cluster NGC 6791 from multiple eclipsing binary members. I. Measurements, methods, and first results', *Astronomy and Astrophysics* **525**, A2.

Brogaard, K., Grundahl, F., Sandquist, E. L. et al. (2021), 'Age and helium content of the open cluster NGC 6791 from multiple eclipsing binary members. III. Constraints from a subgiant', *Astronomy and Astrophysics* **649**, A178.

Brogaard, K., VandenBerg, D. A., Bruntt, H. et al. (2012), 'Age and helium content of the open cluster NGC 6791 from multiple eclipsing binary members. II. Age dependencies and new insights', *Astronomy and Astrophysics* **543**, A106.

Bucher, B., Tang, X. D., Fang, X. et al. (2015), 'First Direct Measurement of ^{12}C (^{12}C,n)^{23}Mg at Stellar Energies', **114**(25), 251102.

Buder, S., Lind, K., Ness, M. K. et al. (2019), 'The GALAH survey: An abundance, age, and kinematic inventory of the solar neighbourhood made with TGAS', *Astronomy and Astrophysics* **624**, A19.

Burbidge, E. M., Burbidge, G. R., Fowler, W. A. and Hoyle, F. (1957), 'Synthesis of the Elements in Stars', *Reviews of Modern Physics* **29**(4), 547–650.

Burstein, D. (1979), 'Structure and origin of S0 galaxies. III. The luminosity distribution perpendicular to the plane of the disks in S0's.', *Astrophysical Journal* **234**, 829–836.

Busso, M. and Gallino, R. (1997), 's-Process Abundances in AGB Stars At Various Metallicities and Their Theoretical Interpretation', *Nuclear Physics A* **621**, 431–434.

Busso, M., Gallino, R., Lambert, D. L., Travaglio, C. and Smith, V. V. (2001), 'Nucleosynthesis and Mixing on the Asymptotic Giant Branch. III. Predicted and Observed s-Process Abundances', *The Astrophysical Journal* **557**(2), 802–821.

Busso, M., Gallino, R. and Wasserburg, G. J. (1999), 'Nucleosynthesis in Asymptotic Giant Branch Stars: Relevance for Galactic Enrichment and Solar System Formation', *Annual Review of Astron and Astrophys* **37**, 239–309.

Busso, M., Vescovi, D., Palmerini, S., Cristallo, S. and Antonuccio-Delogu, V. (2021), 's-processing in AGB Stars Revisited. III. Neutron Captures from MHD Mixing at Different Metallicities and Observational Constraints', *The Astrophysical Journal* **908**(1), 55.

Cameron, A. G. W. (1960), 'New Neutron Sources of Possible Astrophysical Importance.', *Astronomical Journal* **65**, 485.

Cantat-Gaudin, T., Anders, F., Castro-Ginard, A. et al. (2020), 'Painting a portrait of the Galactic disc with its stellar clusters', *Astronomy and Astrophysics* **640**, A1.

Carney, B. W., Yong, D., Teixera de Almeida, M. L. and Seitzer, P. (2005), 'Elemental Abundance Ratios in Stars of the Outer Galactic Disk. II. Field Red Giants', *Astronomical Journal* **130**(3), 1111–1126.

Casali, G., Magrini, L., Tognelli, E. et al. (2019), 'The Gaia-ESO survey: Calibrating a relationship between age and the [C/N] abundance ratio with open clusters', *Astronomy and Astrophysics* **629**, A62.

Casali, G., Spina, L., Magrini, L. et al. (2020), 'The Gaia-ESO survey: the non-universality of the age-chemical-clocks-metallicity relations in the Galactic disc', *Astronomy and Astrophysics* **639**, A127.

Casamiquela, L., Soubiran, C., Jofré, P. et al. (2021), 'Abundance-age relations with red clump stars in open clusters', *Astronomy and Astrophysics* **652**, A25.

Cescutti, G. and Chiappini, C. (2014), 'Explaining the Ba, Y, Sr, and Eu abundance scatter in metal-poor halo stars: constraints to the r-process', *Astronomy and Astrophysics* **565**, A51.

Cescutti, G., Matteucci, F., François, P. and Chiappini, C. (2007), 'Abundance gradients in the Milky Way for α elements, iron peak elements, barium, lanthanum, and europium', *Astronomy and Astrophysics* **462**(3), 943–951.

Chabrier, G. (2003), 'Galactic Stellar and Substellar Initial Mass Function', *Publications of the ASP* **115**(809), 763–795.

Chen, H.-Y., Vitale, S. and Foucart, F. (2021), 'The relative contribution to heavy metals production from binary neutron star mergers and neutron star-black hole mergers', *arXiv e-prints* p. arXiv:2107.02714.

Chen, Y. Q. and Zhao, G. (2020), 'Open clusters as tracers on radial migration of the galactic disc', *Monthly Notices of the RAS* **495**(3), 2673–2681.

Chiappini, C. (2001), 'The Formation and Evolution of the Milky Way', *American Scientist* **89**(6), 506.

Chiappini, C., Matteucci, F. and Gratton, R. (1997), 'The Chemical Evolution of the Galaxy: The Two-Infall Model', *Astrophysical Journal* **477**(2), 765–780.

Chiappini, C., Matteucci, F. and Romano, D. (2001), 'Abundance Gradients and the Formation of the Milky Way', *Astrophysical Journal* **554**(2), 1044–1058.

Chiosi, C. (1980), 'Chemical evolution of the galactic disk: the inflow problem.', *Astronomy and Astrophysics* **83**, 206–216.

Clayton, D. D., Fowler, W. A., Hull, T. E. and Zimmerman, B. A. (1961), 'Neutron capture chains in heavy element synthesis', *Annals of Physics* **12**(3), 331–408.

Clayton, D. D. and Rassbach, M. E. (1967), 'Termination of the s-PROCESS', *Astrophysical Journal* **148**, 69.

Coleman, G. D. and Worden, S. P. (1976), 'Mass Loss from Dwarf M Stars Through Stellar Flaring', *Astrophysical Journal* **205**, 475–481.

Corliss, C. H. and Bozman, W. R. (1962), *Experimental transition probabilities for spectral lines of seventy elements; derived from the NBS Tables of spectral-line intensities*.

Costantin, L., Pérez-González, P. G., Méndez-Abreu, J. et al. (2021), 'A Duality in the Origin of Bulges and Spheroidal Galaxies', *Astrophysical Journal* **913**(2), 125.

Côté, B., Eichler, M., Arcones, A. et al. (2019), 'Neutron Star Mergers Might Not Be the Only Source of r-process Elements in the Milky Way', *Astrophysical Journal* **875**(2), 106.

Côté, B., Fryer, C. L., Belczynski, K. et al. (2018), 'The Origin of r-process Elements in the Milky Way', *Astrophysical Journal* **855**(2), 99.

Cowan, J. J., Roederer, I. U., Sneden, C. and Lawler, J. E. (2011), r-Process Abundance Signatures in Metal-Poor Halo Stars, *in* A. McWilliam, ed., 'RR Lyrae Stars, Metal-Poor Stars, and the Galaxy', Vol. 5, p. 223.

Cowan, J. J. and Rose, W. K. (1977), 'Production of ^{14}C and neutrons in red giants.', *Astrophysical Journal* **212**, 149–158.

Cowley, C. R. and Corliss, C. H. (1983), 'Moderately accurate oscillator strengths from NBS intensities - II.', *Monthly Notices of the RAS* **203**, 651–659.

Cristallo, S., Abia, C., Straniero, O. and Piersanti, L. (2015), 'On the Need for the Light Elements Primary Process (LEPP)', *Astrophysical Journal* **801**(1), 53.

Cristallo, S., La Cognata, M., Massimi, C. et al. (2018), 'The Importance of the ^{13}C(α,n)^{16}O Reaction in Asymptotic Giant Branch Stars', *Astrophysical Journal* **859**(2), 105.

Cristallo, S., Piersanti, L., Straniero, O. et al. (2011), 'Evolution, Nucleosynthesis, and Yields of Low-mass Asymptotic Giant Branch Stars at Different Metallicities. II. The FRUITY Database', *Astrophysical Journal, Supplement* **197**(2), 17.

Cristallo, S., Straniero, O., Gallino, R. et al. (2009), 'Evolution, Nucleosynthesis, and Yields of Low-Mass Asymptotic Giant Branch Stars at Different Metallicities', *Astrophysical Journal* **696**(1), 797–820.

Cunha, K., Frinchaboy, P. M., Souto, D. et al. (2016), 'Chemical abundance gradients from open clusters in the Milky Way disk: Results from the APOGEE survey', *Astronomische Nachrichten* **337**(8-9), 922.

Cunha, K., Smith, V. V., Hasselquist, S. et al. (2017), 'Adding the s-Process Element Cerium to the APOGEE Survey: Identification and Characterization of Ce II Lines in the H-band Spectral Window', *Astrophysical Journal* **844**(2), 145.

Cutri, R. M., Wright, E. L., Conrow, T. et al. (2021), 'VizieR Online Data Catalog: AllWISE Data Release (Cutri+ 2013)', *VizieR Online Data Catalog* p. II/328.

da Silva, R., Lemasle, B., Bono, G. et al. (2016), 'Neutron-capture elements across the Galactic thin disk using Cepheids', *Astronomy and Astrophysics* **586**, A125.

da Silva, R., Porto de Mello, G. F., Milone, A. C. et al. (2012), 'Accurate and homogeneous abundance patterns in solar-type stars of the solar neighbourhood: a chemo-chronological analysis', *Astronomy and Astrophysics* **542**, A84.

Dalton, G., Trager, S., Abrams, D. C. et al. (2016), Final design and progress of WEAVE: the next generation wide-field spectroscopy facility for the William Herschel Telescope, *in* C. J. Evans, L. Simard and H. Takami, eds, 'Ground-based and Airborne Instrumentation for Astronomy VI', Vol. 9908 of *Society of Photo-Optical Instrumentation Engineers (SPIE) Conference Series*, p. 99081G.

Davidson, M. D., Snoek, L. C., Volten, H. and Doenszelmann, A. (1992), 'Oscillator strengths and branching ratios of transitions between low-lying levels in the barium II spectrum.', *Astronomy and Astrophysics* **255**, 457–458.

De Cia, A., Jenkins, E. B., Fox, A. J. et al. (2021), 'Large metallicity variations in the Galactic interstellar medium', *Nature* **597**(7875), 206–208.

de Jager, C., Nieuwenhuijzen, H. and van der Hucht, K. A. (1988), 'Mass loss rates in the Hertzsprung-Russell diagram.', *Astronomy and Astrophysicss* **72**, 259–289.

de Jong, R. S., Agertz, O., Berbel, A. A. et al. (2019), '4MOST: Project overview and information for the First Call for Proposals', *The Messenger* **175**, 3–11.

Delgado Mena, E., Moya, A., Adibekyan, V. et al. (2019), 'Abundance to age ratios in the HARPS-GTO sample with Gaia DR2. Chemical clocks for a range of [Fe/H]', *Astronomy and Astrophysics* **624**, A78.

Delgado Mena, E., Tsantaki, M., Adibekyan, V. Z. et al. (2017), 'Chemical abundances of 1111 FGK stars from the HARPS GTO planet search program. II. Cu, Zn, Sr, Y, Zr, Ba, Ce, Nd, and Eu', *Astronomy and Astrophysics* **606**, A94.

Den Hartog, E. A., Lawler, J. E., Sneden, C. and Cowan, J. J. (2003), 'Improved Laboratory Transition Probabilities for Nd II and Application to the Neodymium Abundances of the Sun and Three Metal-poor Stars', *Astrophysical Journal, Supplement* **148**(2), 543–566.

Deutsch, A. J. (1959), Mass loss in red giants, *in* J. L. Greenstein, ed., 'The Hertzsprung-Russell Diagram', Vol. 10, p. 109.

D'Odorico, S., Peimbert, M. and Sabbadin, F. (1976), 'Pregalactic helium abundance and abundance gradients across our Galaxy from planetary nebulae.', *Astronomy and Astrophysics* **47**, 341.

Donati, G. B. (1863), 'On the Striæ of Stellar Spectra, from the Memorie Astronomiche', *Monthly Notices of the RAS* **23**, 100.

Dong, D., Hallinan, G., Nakar, E. et al. (2021), 'A transient radio source consistent with a merger-triggered core collapse supernova', *Science* **373**, 1125–1129.

Dopita, M. A. and Ryder, S. D. (1994), 'On the Law of Star Formation in Disk Galaxies', *Astrophysical Journal* **430**, 163.

D'Orazi, V., Baratella, M., Lugaro, M., Magrini, L. and Pignatari, M. (2022), 'The Complex Behaviour of s-Process Element Abundances at Young Ages', *Universe* **8**(2), 110.

D'Orazi, V., Magrini, L., Randich, S. et al. (2009), 'Enhanced Production of Barium in Low-Mass Stars: Evidence from Open Clusters', *Astrophysical Journal, Letters* **693**(1), L31–L34.

Duong, L., Freeman, K. C., Asplund, M. et al. (2018), 'The GALAH survey: properties of the Galactic disc(s) in the solar neighbourhood', *Monthly Notices of the RAS* **476**(4), 5216–5232.

Eddington, A. S. (1919), 'The sources of stellar energy', *The Observatory* **42**, 371–376.

Edvardsson, B., Andersen, J., Gustafsson, B. et al. (1993), 'The chemical evolution of the galactic disk. I. Analysis and results.', *Astronomy and Astrophysics* **500**, 391–442.

Eggen, O. J., Lynden-Bell, D. and Sandage, A. R. (1962), 'Evidence from the motions of old stars that the Galaxy collapsed.', *Astrophysical Journal* **136**, 748.

Epstein, R. I., Lattimer, J. M. and Schramm, D. N. (1976), 'The origin of deuterium', *Nature* **263**, 198–202.

Ernandes, H., Evans, C. J., Barbuy, B. et al. (2020), Stellar astrophysics in the near-UV with VLT-CUBES, *in* 'Society of Photo-Optical Instrumentation Engineers (SPIE) Conference Series', Vol. 11447 of *Society of Photo-Optical Instrumentation Engineers (SPIE) Conference Series*, p. 1144760.

Esteban, C., Peimbert, M., Torres-Peimbert, S. and Rodríguez, M. (2002), 'Optical Recombination Lines of Heavy Elements in Giant Extragalactic H II Regions', *The Astrophysical Journal* **581**(1), 241–257.

Famiano, M. A., Boyd, R. N., Kajino, T. et al. (2008), 'Effects of β-decays of excited-state nuclei on the astrophysical r-process', *Journal of Physics G Nuclear Physics* **35**(2), 025203.

Feltzing, S., Bensby, T. and Lundström, I. (2003), 'Signatures of SN Ia in the galactic thick disk. Observational evidence from alpha -elements in 67 dwarf stars in the solar neighbourhood', *Astronomy and Astrophysics* **397**, L1–L4.

Feltzing, S., Howes, L. M., McMillan, P. J. and Stonkutė, E. (2017), 'On the metallicity dependence of the [Y/Mg]-age relation for solar-type stars', *Monthly Notices of the RAS* **465**(1), L109–L113.

Fermi, E. (1934), 'Radioactivity Induced by Neutron Bombardment', *Nature* **133**(3368), 757.

Forsberg, R., Jönsson, H., Ryde, N. and Matteucci, F. (2019), 'Abundances of disk and bulge giants from high-resolution optical spectra. IV. Zr, La, Ce, Eu', *Astronomy and Astrophysics* **631**, A113.

Fowler, W. A. and Hoyle, F. (1960), 'Nuclear cosmochronology', *Annals of Physics* **10**(2), 280–302.

François, P., Depagne, E., Hill, V. et al. (2007), 'First stars. VIII. Enrichment of the neutron-capture elements in the early Galaxy', *Astronomy and Astrophysics* **476**(2), 935–950.

Frebel, A. (2018), 'From Nuclei to the Cosmos: Tracing Heavy-Element Production with the Oldest Stars', *Annual Review of Nuclear and Particle Science* **68**(1), 237–269.

Freiburghaus, C., Rosswog, S. and Thielemann, F. K. (1999), 'R-Process in Neutron Star Mergers', *Astrophysical Journall* **525**(2), L121–L124.

Friel, E. D. (1999), 'Open Clusters as a Record of the Past', *Astrophysics and Space Science* **265**, 271–278.

Fuhrmann, K. (1998), 'Nearby stars of the Galactic disk and halo', *Astronomy and Astrophysics* **338**, 161–183.

Fuhrmann, K., Chini, R., Kaderhandt, L., Chen, Z. and Lachaume, R. (2017), 'The barium-to-iron enrichment versus age relation of ancient disc stars', *Monthly Notices of the RAS* **471**(3), 3768–3774.

Fujimoto, S.-i., Kotake, K., Yamada, S., Hashimoto, M.-a. and Sato, K. (2006), 'Magnetohydrodynamic Simulations of a Rotating Massive Star Collapsing to a Black Hole', *The Astrophysical Journal* **644**(2), 1040–1055.

Fukui, Y., Habe, A., Inoue, T., Enokiya, R. and Tachihara, K. (2021), 'Cloud-cloud collisions and triggered star formation', *Publications of the Astronomical Society of Japan* **73**, S1–S34.

Gaia Collaboration, Brown, A. G. A., Vallenari, A. et al. (2018), 'Gaia Data Release 2. Summary of the contents and survey properties', *Astronomy and Astrophysics* **616**, A1.

Gaia Collaboration, Brown, A. G. A., Vallenari, A. et al. (2021*a*), 'Gaia Early Data Release 3. Summary of the contents and survey properties', *Astronomy and Astrophysics* **649**, A1.

Gaia Collaboration, Brown, A. G. A., Vallenari, A. et al. (2021*b*), 'Gaia Early Data Release 3. Summary of the contents and survey properties', *Astronomy and Astrophysics* **649**, A1.

Gaia Collaboration, Prusti, T., de Bruijne, J. H. J. et al. (2016), 'The Gaia mission', *Astronomy and Astrophysics* **595**, A1.

Gallino, R., Arlandini, C., Busso, M. et al. (1998), 'Evolution and Nucleosynthesis in Low-Mass Asymptotic Giant Branch Stars. II. Neutron Capture and the S-Process', *Astrophysical Journal* **497**(1), 388–403.

Gallino, R., Bisterzo, S., Straniero, O., Ivans, I. I. and Käppeler, F. (2006), 'Metallicity dependence of light and heavy s-process elements in AGB stars.', *Memorie della Società Astronomica Italiana* **77**, 786.

Gehren, T., Nissen, P. E., Kudritzki, R. P. and Butler, K. (1985), Abundance gradients in the galactic disk from young B-type stars in clusters: first results., *in* 'European Southern Observatory Conference and Workshop Proceedings', Vol. 21 of *European Southern Observatory Conference and Workshop Proceedings*, pp. 171–185.

Genovali, K., Lemasle, B., da Silva, R. et al. (2015), 'On the α-element gradients of the Galactic thin disk using Cepheids', *Astronomy Astrophysics* **580**, A17.

Gilmore, G., Randich, S., Asplund, M. et al. (2012), 'The Gaia-ESO Public Spectroscopic Survey', *The Messenger* **147**, 25–31.

Gilmore, G. and Reid, N. (1983), 'New light on faint stars - III. Galactic structure towards the South Pole and the Galactic thick disc.', *Monthly Notices of the RAS* **202**, 1025–1047.

Goldberg, L., Muller, E. A. and Aller, L. H. (1960), 'The Abundances of the Elements in the Solar Atmosphere.', *Astrophysical Journal, Supplement* **5**, 1.

Goriely, S. (1999), 'Uncertainties in the solar system r-abundance distribution', *Astronomy and Astrophysics* **342**, 881–891.

Gratton, R. G., Carretta, E., Matteucci, F. and Sneden, C. (2000), 'Abundances of light elements in metal-poor stars. IV. [Fe/O] and [Fe/Mg] ratios and the history of star formation in the solar neighborhood', *Astronomy and Astrophysics* **358**, 671–681.

Grenon, M. (1987), 'Past and present metal abundance gradient in the galactic disc.', *Journal of Astrophysics and Astronomy* **8**, 123–139.

Grevesse, N., Asplund, M. and Sauval, A. J. (2007), 'The Solar Chemical Composition', *Space Science Reviews* **130**(1-4), 105–114.

Griffith, E., Johnson, J. A. and Weinberg, D. H. (2019), 'Abundance Ratios in GALAH DR2 and Their Implications for Nucleosynthesis', *Astrophysical Journal* **886**(2), 84.

Grisoni, V., Cescutti, G., Matteucci, F. et al. (2020), 'Modelling the chemical evolution of Zr, La, Ce, and Eu in the Galactic discs and bulge', *Monthly Notices of the RAS* **492**(2), 2828–2834.

Guiglion, G., de Laverny, P., Recio-Blanco, A. and Prantzos, N. (2018), 'The AMBRE Project: r-process elements in the Milky Way thin and thick discs', *Astronomy and Astrophysics* **619**, A143.

Gull, M., Frebel, A., Hinojosa, K. et al. (2021), 'R-process-rich Stellar Streams in the Milky Way', *Astrophysical Journal* **912**(1), 52.

Gummersbach, C. A., Kaufer, A., Schaefer, D. R., Szeifert, T. and Wolf, B. (1998), 'B stars and the chemical evolution of the Galactic disk', *Astronomy and Astrophysics* **338**, 881–896.

Gustafsson, B., Edvardsson, B., Eriksson, K. et al. (2008), 'A grid of MARCS model atmospheres for late-type stars. I. Methods and general properties', *Astronomy and Astrophysics* **486**(3), 951–970.

Halle, A., Di Matteo, P., Haywood, M. and Combes, F. (2015), 'Quantifying stellar radial migration in an N-body simulation: blurring, churning, and the outer regions of galaxy discs', *Astronomy and Astrophysics* **578**, A58.

Hansen, T. T., Holmbeck, E. M., Beers, T. C. et al. (2018), 'The R-process Alliance: First Release from the Southern Search for R-process-enhanced Stars in the Galactic Halo', *Astrophysical Journal* **858**(2), 92.

Harris, H. C. (1981), 'Photometric abundances of classical Cepheids and the gradient in the galactic disk.', *Astronomical Journal* **86**, 707–718.

Hayden, M. R., Bovy, J., Holtzman, J. A. et al. (2015), 'Chemical Cartography with APOGEE: Metallicity Distribution Functions and the Chemical Structure of the Milky Way Disk', *Astrophysical Journal* **808**, 132.

Hayden, M. R., Recio-Blanco, A., de Laverny, P., Mikolaitis, S. and Worley, C. C. (2017), 'The AMBRE project: The thick thin disk and thin thick disk of the Milky Way', *Astronomy and Astrophysics* **608**, L1.

Hayden, M. R., Sharma, S., Bland-Hawthorn, J. et al. (2020), 'The GALAH Survey: Chemical Clocks', *arXiv e-prints* p. arXiv:2011.13745.

Haywood, M., Di Matteo, P., Lehnert, M. D., Katz, D. and Gómez, A. (2013), 'The age structure of stellar populations in the solar vicinity. Clues of a two-phase formation history of the Milky Way disk', *Astronomy and Astrophysics* **560**, A109.

Heil, M., Käppeler, F., Uberseder, E., Gallino, R. and Pignatari, M. (2007), 'The s process in massive stars', *Progress in Particle and Nuclear Physics* **59**(1), 174–182.

Heiter, U., Lind, K., Bergemann, M. et al. (2021), 'Atomic data for the Gaia-ESO Survey', *Astronomy and Astrophysics* **645**, A106.

Helmi, A., Babusiaux, C., Koppelman, H. H. et al. (2018), 'The merger that led to the formation of the Milky Way's inner stellar halo and thick disk', *Nature* **563**(7729), 85–88.

Helmi, A., White, S. D. M., de Zeeuw, P. T. and Zhao, H. (1999), 'Debris streams in the solar neighbourhood as relicts from the formation of the Milky Way', *Nature* **402**(6757), 53–55.

Hillebrandt, W., Nomoto, K. and Wolff, R. G. (1984), 'Supernova explosions of massive stars - The mass range 8 to 10 solar masses', *Astronomy and Astrophysics* **133**(1), 175–184.

Horowitz, C. J., Arcones, A., Côté, B. et al. (2019), 'r-process nucleosynthesis: connecting rare-isotope beam facilities with the cosmos', *Journal of Physics G Nuclear Physics* **46**(8), 083001.

Horta, D., Ness, M. K., Rybizki, J., Schiavon, R. P. and Buder, S. (2021), 'Neutron-capture elements record the ordered chemical evolution of the disc over time', *arXiv e-prints* p. arXiv:2111.01809.

Hou, J.-L., Chang, R.-X. and Chen, L. (2002), 'Abundance Gradient from Open Clusters and Implications for the Galactic Disk Evolution', *Chinese Journal of Astronomy Astrophysics* **2**, 17–32.

Howes, L. M., Lindegren, L., Feltzing, S., Church, R. P. and Bensby, T. (2019), 'Estimating stellar ages and metallicities from parallaxes and broadband photometry: successes and shortcomings', *Astronomy and Astrophysics* **622**, A27.

Huang, S. S. (1956), 'A dynamical problem in binary systems and its bearing on stellar evolution.', *Astronomical Journal* **61**, 49–61.

Huggins, W. and Miller, W. A. (1864), 'On the Spectra of Some of the Fixed Stars', *Philosophical Transactions of the Royal Society of London Series I* **154**, 413–435.

Ibata, R. A., Gilmore, G. and Irwin, M. J. (1994), 'A dwarf satellite galaxy in Sagittarius', *Nature* **370**(6486), 194–196.

Ivarsson, S., Litzén, U. and Wahlgren, G. M. (2001), 'Accurate Wavelengths, Oscillator Strengths and Hyperfine Structure in Selected Praseodymium Lines of Astrophysical Interest', *Physica Scripta* **64**(5), 455–461.

Jackson, R. J., Jeffries, R. D., Wright, N. J. et al. (2022), 'The Gaia-ESO Survey: Membership probabilities for stars in 63 open and 7 globular clusters from 3D kinematics', *Monthly Notices of the RAS* **509**(2), 1664–1680.

Jacobson, H. R. and Friel, E. D. (2013), 'Zirconium, Barium, Lanthanum, and Europium Abundances in Open Clusters', *Astronomical Journal* **145**(4), 107.

Janes, K. A. (1979), 'Evidence for an abundance gradient in the galactic disk.', *Astrophysical Journal, Supplement* **39**, 135–156.

Jayatissa, H., Rogachev, G. V., Goldberg, V. Z. et al. (2020), 'Constraining the ^{22}Ne(α,γ)^{26}Mg and ^{22}Ne(α,n)^{25}Mg reaction rates using sub-Coulomb α-transfer reactions', *Physics Letters B* **802**, 135267.

Jílková, L., Carraro, G., Jungwiert, B. and Minchev, I. (2012), 'The origin and orbit of the old, metal-rich, open cluster NGC 6791. Insights from kinematics', *Astronomy and Astrophysics* **541**, A64.

Jofré, P., Heiter, U. and Soubiran, C. (2019), 'Accuracy and Precision of Industrial Stellar Abundances', *Annual Review of Astron and Astrophys* **57**, 571–616.

Jofré, P., Jackson, H. and Tucci Maia, M. (2020), 'Traits for chemical evolution in solar twins. Trends of neutron-capture elements with stellar age', *Astronomy and Astrophysics* **633**, L9.

Jönsson, H., Ryde, N., Nordlander, T. et al. (2017), 'Abundances of disk and bulge giants from high-resolution optical spectra. I. O, Mg, Ca, and Ti in the solar neighborhood and Kepler field samples', *Astronomy and Astrophysics* **598**, A100.

Jurgenson, C. A., Fischer, D. A., McCracken, T. M. et al. (2014), Design of a radial velocity spectrograph for the Moletai Astronomical Observatory, *in* S. K. Ramsay, I. S. McLean and H. Takami, eds, 'Ground-based and Airborne Instrumentation for Astronomy V', Vol. 9147 of *Society of Photo-Optical Instrumentation Engineers (SPIE) Conference Series*, p. 91477F.

Jurgenson, C., Fischer, D., McCracken, T. et al. (2016), 'Design and Construction of VUES: The Vilnius University Echelle Spectrograph', *Journal of Astronomical Instrumentation* **5**(2), 1650003–239.

Jurić, M., Ivezić, Ž. et al. (2008), 'The Milky Way Tomography with SDSS. I. Stellar Number Density Distribution', *Astrophysical Journal* **673**(2), 864–914.

Kajino, T., Aoki, W., Balantekin, A. B. et al. (2019), 'Current status of r-process nucleosynthesis', *Progress in Particle and Nuclear Physics* **107**, 109–166.

Käppeler, F. (2012), Stellar neutron capture rates and the s process, *in* 'European Physical Journal Web of Conferences', Vol. 21 of *European Physical Journal Web of Conferences*, p. 03006.

Kappeler, F., Beer, H. and Wisshak, K. (1989), 's-process nucleosynthesis-nuclear physics and the classical model', *Reports on Progress in Physics* **52**(8), 945–1013.

Käppeler, F., Gallino, R., Bisterzo, S. and Aoki, W. (2011), 'The s process: Nuclear physics, stellar models, and observations', *Reviews of Modern Physics* **83**(1), 157–194.

Karakas, A. I. and Lattanzio, J. C. (2014), 'The Dawes Review 2: Nucleosynthesis and Stellar Yields of Low- and Intermediate-Mass Single Stars', *Publications of the ASA* **31**, e030.

Karakas, A. I. and Lugaro, M. (2016), 'Stellar Yields from Metal-rich Asymptotic Giant Branch Models', *The Astrophysical Journal* **825**(1), 26.

Kasparova, A. V., Katkov, I. Y., Chilingarian, I. V. et al. (2016), 'The diversity of thick galactic discs', *Monthly Notices of the RAS* **460**(1), L89–L93.

Katz, D., Sartoretti, P., Cropper, M. et al. (2019), 'Gaia Data Release 2. Properties and validation of the radial velocities', *Astronomy and Astrophysics* **622**, A205.

Kobayashi, C., Karakas, A. I. and Lugaro, M. (2020), 'The Origin of Elements from Carbon to Uranium', *Astrophysical Journal* **900**(2), 179.

Kordopatis, G., Recio-Blanco, A., de Laverny, P. et al. (2011), 'A spectroscopic survey of thick disc stars outside the solar neighbourhood', *Astronomy and Astrophysics* **535**, A107.

Korotin, S. A., Andrievsky, S. M., Hansen, C. J. et al. (2015), 'Grid of theoretical NLTE equivalent widths of four Ba ii lines and barium abundance in cool stars', *Astronomy and Astrophysics* **581**, A70.

Kroupa, P. (2001), 'On the variation of the initial mass function', *Monthly Notices of the RAS* **322**(2), 231–246.

Kroupa, P., Tout, C. A. and Gilmore, G. (1993), 'The Distribution of Low-Mass Stars in the Galactic Disc', *Monthly Notices of the RAS* **262**, 545–587.

Kruijssen, J. M. D., Pfeffer, J. L., Chevance, M. et al. (2020), 'Kraken reveals itself - the merger history of the Milky Way reconstructed with the E-MOSAICS simulations', *Monthly Notices of the RAS* **498**(2), 2472–2491.

Lamb, S. A., Howard, W. M., Truran, J. W. and Iben, I., J. (1977), 'Neutron-capture nucleosynthesis in the helium-burning cores of massive stars.', *Astrophysical Journal* **217**, 213–221.

Larson, R. B. (1976), 'Models for the formation of disc galaxies.', *Monthly Notices of the RAS* **176**, 31–52.

Lattimer, J. M. and Schramm, D. N. (1974), 'Black-Hole-Neutron-Star Collisions', *Astrophysical Journal* **192**, L145.

Lawler, J. E., Bonvallet, G. and Sneden, C. (2001), 'Experimental Radiative Lifetimes, Branching Fractions, and Oscillator Strengths for La II and a New Determination of the Solar Lanthanum Abundance', *Astrophysical Journal* **556**(1), 452–460.

Lawler, J. E., Den Hartog, E. A., Sneden, C. and Cowan, J. J. (2006), 'Improved Laboratory Transition Probabilities for Sm II and Application to the Samarium

Abundances of the Sun and Three r-Process-rich, Metal-poor Stars', *Astrophysical Journal, Supplement* **162**(1), 227–260.

Lawler, J. E., Sneden, C., Cowan, J. J., Ivans, I. I. and Den Hartog, E. A. (2009), 'Improved Laboratory Transition Probabilities for Ce II, Application to the Cerium Abundances of the Sun and Five r-Process-Rich, Metal-Poor Stars, and Rare Earth Lab Data Summary', *Astrophysical Journal, Supplement* **182**(1), 51–79.

Lawler, J. E., Wickliffe, M. E., den Hartog, E. A. and Sneden, C. (2001), 'Improved Laboratory Transition Parameters forEu II and Application to the Solar Europium Elemental and Isotopic Composition', *Astrophysical Journal* **563**(2), 1075–1088.

Lebzelter, T. and Hron, J. (2003), 'Technetium and the third dredge up in AGB stars. I. Field stars', *Astronomy and Astrophysics* **411**, 533–542.

Lemasle, B., François, P., Genovali, K. et al. (2013), 'Galactic abundance gradients from Cepheids. α and heavy elements in the outer disk', *Astronomy and Astrophysics* **558**, A31.

Li, C., Zhao, G., Zhai, M. and Jia, Y. (2018), 'The Formation and Evolution of Galactic Disks with APOGEE and the Gaia Survey', *Astrophysical Journal* **860**(1), 53.

Limongi, M. and Chieffi, A. (2018), 'Presupernova Evolution and Explosive Nucleosynthesis of Rotating Massive Stars in the Metallicity Range -3 $\leq$ [Fe/H] $\leq$ 0', *Astrophysical Journal, Supplement* **237**(1), 13.

Lin, J., Asplund, M., Ting, Y.-S. et al. (2020), 'The GALAH survey: temporal chemical enrichment of the galactic disc', *Monthly Notices of the RAS* **491**(2), 2043–2056.

Liu, F., Asplund, M., Yong, D. et al. (2016), 'The chemical compositions of solar twins in the open cluster M67', *Monthly Notices of the RAS* **463**(1), 696–704.

Lodders, K. (2019), 'Solar Elemental Abundances', *arXiv e-prints* p. arXiv:1912.00844.

Longland, R., Iliadis, C. and Karakas, A. I. (2012), 'Reaction rates for the s-process neutron source ^{22}Ne + α', *Physical Review C* **85**(6), 065809.

Luck, R. E. (2018), 'Cepheid Abundances: Multiphase Results and Spatial Gradients', *Astronomical Journal* **156**(4), 171.

Luck, R. E., Andrievsky, S. M., Kovtyukh, V. V., Gieren, W. and Graczyk, D. (2011), 'The Distribution of the Elements in the Galactic Disk. II. Azimuthal and Radial Variation in Abundances from Cepheids', *Astronomical Journal* **142**(2), 51.

Luri, X., Brown, A. G. A., Sarro, L. M. et al. (2018), 'Gaia Data Release 2. Using Gaia parallaxes', *Astronomy and Astrophysics* **616**, A9.

Lynden-Bell, D. and Lynden-Bell, R. M. (1995), 'Ghostly streams from the formation of the Galaxy's halo', *Monthly Notices of the RAS* **275**(2), 429–442.

Maciel, W. J. and Koppen, J. (1994), 'Abundance gradients from disk planetary nebulae: O, Ne, S, and AR', *Astronomy and Astrophysics* **282**, 436.

Maciel, W. J., Lago, L. G. and Costa, R. D. D. (2006), 'An estimate of the time variation of the abundance gradient from planetary nebulae. III. O, S, Ar, and Ne: a comparison of PN samples', *Astronomy and Astrophysics* **453**(2), 587–593.

Mackereth, J. T. and Bovy, J. (2018), 'Fast Estimation of Orbital Parameters in Milky Way-like Potentials', *Publications of the ASP* **130**(993), 114501.

Magrini, L., Sestito, P., Randich, S. and Galli, D. (2009), 'The evolution of the Galactic metallicity gradient from high-resolution spectroscopy of open clusters', *Astronomy and Astrophysics* **494**(1), 95–108.

Magrini, L., Spina, L., Randich, S. et al. (2018), 'The Gaia-ESO Survey: the origin and evolution of s-process elements', *Astronomy and Astrophysics* **617**, A106.

Magrini, L., Vescovi, D., Casali, G. et al. (2021), 'Magnetic-buoyancy-induced mixing in AGB stars: a theoretical explanation of the non-universal relation of [Y/Mg] to age', *Astronomy and Astrophysics* **646**, L2.

Magrini, L., Viscasillas Vázquez, C., Casali, G. et al. (2022), 'The Abundance of S-Process Elements: Temporal and Spatial Trends from Open Cluster Observations', *Universe* **8**(2), 64.

Maiorca, E., Magrini, L., Busso, M. et al. (2012), 'News on the s Process from Young Open Clusters', *Astrophysical Journal* **747**(1), 53.

Maiorca, E., Randich, S., Busso, M., Magrini, L. and Palmerini, S. (2011), 's-processing in the Galactic Disk. I. Super-solar Abundances of Y, Zr, La, and Ce in Young Open Clusters', *Astrophysical Journal* **736**(2), 120.

Mao, J., Zhou, P., Simionescu, A. et al. (2021), 'Elemental Abundances of the Hot Atmosphere of Luminous Infrared Galaxy Arp 299', *The Astrophysical Journal Letters* **918**(1), L17.

Marsakov, V. A., Gozha, M. L., Koval', V. V. and Shpigel', L. V. (2016), 'Peculiarities of the abundances of neutron-capture elements in Galactic open clusters', *Astronomy Reports* **60**(1), 61–72.

Martell, S. L., Sharma, S., Buder, S. et al. (2017), 'The GALAH survey: observational overview and Gaia DR1 companion', *Monthly Notices of the RAS* **465**(3), 3203–3219.

Mashonkina, L. and Gehren, T. (2001), 'Heavy element abundances in cool dwarf stars: An implication for the evolution of the Galaxy', *Astronomy and Astrophysics* **376**, 232–247.

Mashonkina, L., Gehren, T., Travaglio, C. and Borkova, T. (2003), 'Mg, Ba and Eu abundances in thick disk and halo stars', *Astronomy and Astrophysics* **397**, 275–284.

Matsuno, T., Hirai, Y., Tarumi, Y. et al. (2021), '*R*-process enhancements of Gaia-Enceladus in GALAH DR3', *arXiv e-prints* p. arXiv:2101.07791.

Matteucci, F. (2003), *The Chemical Evolution of the Galaxy*, Kluwer Academic Publishers, Dordrecht.

Matteucci, F. (2014), 'Chemical Evolution of the Milky Way and Its Satellites', *Saas-Fee Advanced Course* **37**, 145.

Matteucci, F. (2021), 'Modelling the chemical evolution of the Milky Way', *Astronomy and Astrophysics Reviews* **29**(1), 5.

Matteucci, F. and Francois, P. (1989), 'Galactic chemical evolution : abundance gradients of individual elements.', *Monthly Notices of the RAS* **239**, 885–904.

Matteucci, F. and Francois, P. (1992), 'Oxygen abundances in halo stars as tests of galaxy formation', *Astronomy and Astrophysics* **262**(1), L1–L4.

Matteucci, F., Romano, D., Arcones, A., Korobkin, O. and Rosswog, S. (2014), 'Europium production: neutron star mergers versus core-collapse supernovae', *Monthly Notices of the RAS* **438**(3), 2177–2185.

Mauron, N. and Josselin, E. (2011), 'The mass-loss rates of red supergiants and the de Jager prescription', *Astronomy and Astrophysics* **526**, A156.

Meggers, W. F., Corliss, C. H. and Scribner, B. F. (1975), *Tables of spectral-line intensities. Part I, II_- arranged by elements.*

Mentel, (2014–), 'mendeleev – a python resource for properties of chemical elements, ions and isotopes'.
URL: *https://github.com/lmmentel/mendeleev*

Merrill, P. W. (1952), 'Spectroscopic Observations of Stars of Class', *Astrophysical Journal* **116**, 21.

Messa, M., Adamo, A., Calzetti, D. et al. (2018), 'The young star cluster population of M51 with LEGUS - II. Testing environmental dependences', *Monthly Notices of the RAS* **477**(2), 1683–1707.

Meszaros, P. and Rees, M. J. (1992), 'Tidal Heating and Mass Loss in Neutron Star Binaries: Implications for Gamma-Ray Burst Models', *Astrophysical Journal* **397**, 570.

Miglio, A., Chiappini, C., Mosser, B., Davies, G. R., Freeman, K., Girardi, L., Jofré, P., Kawata, D., Rendle, B. M., Valentini, M. et al. (2017), 'PLATO as it is : A legacy mission for Galactic archaeology', *Astronomische Nachrichten* **338**(6), 644–661.

Mikolaitis, Š., Drazdauskas, A., Minkevičiūtė, R. et al. (2019), 'High-resolution spectroscopic study of dwarf stars in the northern sky. Na to Zn abundances in two fields with radii of 20 degrees', *Astronomy and Astrophysics* **628**, A49.

Mikolaitis, Š., Hill, V., Recio-Blanco, A. et al. (2014), 'The Gaia-ESO Survey: the chemical structure of the Galactic discs from the first internal data release', *Astronomy and Astrophysics* **572**, A33.

Mikolaitis, Š., Tautvaišienė, G., Drazdauskas, A. et al. (2018), 'Spectroscopy of Dwarf Stars Around the North Celestial Pole', *Publications of the ASP* **130**(989), 074202.

Miles, B. M. and Wiese, W. L. (1969), 'Critical Evaluation of Transition Probabilities for Ba I and Ba II', *Atomic Data* **1**, 1.

Miller, G. E. and Scalo, J. M. (1979), 'The Initial Mass Function and Stellar Birthrate in the Solar Neighborhood', *Astrophysical Journal, Supplement* **41**, 513.

Mints, A. and Hekker, S. (2017), 'A Unified tool to estimate Distances, Ages, and Masses (UniDAM) from spectrophotometric data', *Astronomy and Astrophysics* **604**, A108.

Mishenina, T., Pignatari, M., Carraro, G. et al. (2015), 'New insights on Ba overabundance in open clusters. Evidence for the intermediate neutron-capture process at play?', *Monthly Notices of the RAS* **446**(4), 3651–3668.

Mishenina, T., Pignatari, M., Gorbaneva, T. et al. (2019), 'Enrichment of the Galactic disc with neutron-capture elements: Mo and Ru', *Monthly Notices of the RAS* **489**(2), 1697–1708.

Mishenina, T. V., Pignatari, M., Korotin, S. A. et al. (2013), 'Abundances of neutron-capture elements in stars of the Galactic disk substructures', *Astronomy and Astrophysics* **552**, A128.

Morel, T., Creevey, O. L., Montalbán, J., Miglio, A. and Willett, E. (2021), 'Testing abundance-age relations beyond solar analogues with Kepler LEGACY stars', *Astronomy and Astrophysics* **646**, A78.

Moya, A., Sarro, L. M., Delgado-Mena, E. et al. (2022), 'Stellar dating using chemical clocks and Bayesian inference', *arXiv e-prints* p. arXiv:2201.05228.

Myeong, G. C., Vasiliev, E., Iorio, G., Evans, N. W. and Belokurov, V. (2019), 'Evidence for two early accretion events that built the Milky Way stellar halo', *Monthly Notices of the RAS* **488**(1), 1235–1247.

Necib, L., Ostdiek, B., Lisanti, M. et al. (2020), 'Evidence for a vast prograde stellar stream in the solar vicinity', *Nature Astronomy* **4**, 1078–1083.

Netopil, M., Oralhan, İ. A., Çakmak, H., Michel, R. and Karataş, Y. (2021), 'The Galactic metallicity gradient shown by open clusters in the light of radial migration', *Monthly Notices of the RAS* .

Nishimura, S., Kotake, K., Hashimoto, M. et al. (2006), 'r-Process Nucleosynthesis in Magnetohydrodynamic Jet Explosions of Core-Collapse Supernovae', *Astrophysical Journal* **642**(1), 410–419.

Nissen, P. E. (2015), 'High-precision abundances of elements in solar twin stars. Trends with stellar age and elemental condensation temperature', *Astronomy and Astrophysics* **579**, A52.

Nissen, P. E. (2016), 'High-precision abundances of Sc, Mn, Cu, and Ba in solar twins. Trends of element ratios with stellar age', *Astronomy and Astrophysics* **593**, A65.

Nissen, P. E., Christensen-Dalsgaard, J., Mosumgaard, J. R. et al. (2020), 'High-precision abundances of elements in solar-type stars. Evidence of two distinct sequences in abundance-age relations', *Astronomy and Astrophysics* **640**, A81.

Nissen, P. E., Silva Aguirre, V., Christensen-Dalsgaard, J. et al. (2017), 'High-precision abundances of elements in Kepler LEGACY stars. Verification of trends with stellar age', *Astronomy and Astrophysics* **608**, A112.

Nomoto, K., Iwamoto, K., Nakasato, N., Thielemann, F. K., Brachwitz, F., Tsujimoto, T., Kubo, Y. and Kishimoto, N. (1997), 'Nucleosynthesis in type Ia supernovae', *Nuclear Physics A* **621**, 467–476.

Nugis, T. and Lamers, H. J. G. L. M. (2000), 'Mass-loss rates of Wolf-Rayet stars as a function of stellar parameters', *Astronomy and Astrophysics* **360**, 227–244.

Ojima, T., Ishimaru, Y., Wanajo, S., Prantzos, N. and François, P. (2018), 'Stochastic Chemical Evolution of Galactic Subhalos and the Origin of r-process Elements', *The Astrophysical Journal* **865**(2), 87.

Önehag, A., Korn, A., Gustafsson, B., Stempels, E. and Vandenberg, D. A. (2011), 'M67-1194, an unusually Sun-like solar twin in M67', *Astronomy and Astrophysics* **528**, A85.

Overbeek, J. C., Friel, E. D. and Jacobson, H. R. (2016), 'New Neutron-capture Measurements in 23 Open Clusters. I. The r-Process', *Astrophysical Journal* **824**(2), 75.

Pagel, B. E. J. (1989), 'An analytical model for the evolution of primary elements in the Galaxy.', *Revista Mexicana de Astronomia y Astrofisica* **18**, 161–172.

Pagel, B. E. J. and Patchett, B. E. (1975), 'Metal abundances in nearby stars and the chemical history of the solar neighbourhood.', *Monthly Notices of the RAS* **172**, 13–40.

Pagel, B. E. J. and Tautvaisiene, G. (1995), 'Chemical evolution of primary elements in the Galactic disc: an analytical model', *Monthly Notices of the RAS* **276**(2), 505–514.

Pagel, B. E. J. and Tautvaisiene, G. (1997), 'Galactic chemical evolution of primary elements in the solar neighbourhood - II. Elements affected by the s-process', *Monthly Notices of the RAS* **288**(1), 108–116.

Pancino, E., Lardo, C., Altavilla, G. et al. (2017), 'The Gaia-ESO Survey: Calibration strategy', *Astronomy and Astrophysics* **598**, A5.

Pardi, M. C., Ferrini, F. and Matteucci, F. (1995), 'Evolution of Spiral Galaxies. IV. The Thick Disk in the Solar Region as an Intermediate Collapse Phase', *Astrophysical Journal* **444**, 207.

Parkinson, W. H., Reeves, E. M. and Tomkins, F. S. (1976), 'Neutral calcium, strontium and barium: determination of f values of the principal series by the hook method', *Journal of Physics B Atomic Molecular Physics* **9**(2), 157–165.

Payne, C. H. (1925), Stellar Atmospheres; a Contribution to the Observational Study of High Temperature in the Reversing Layers of Stars., PhD thesis, RADCLIFFE COLLEGE.

Peimbert, M., Torres-Peimbert, S. and Rayo, J. F. (1978), 'Abundance gradients in the Galaxy derived from H II regions.', *Astrophysical Journal* **220**, 516–524.

Perego, A., Vescovi, D., Fiore, A. et al. (2022), 'Production of Very Light Elements and Strontium in the Early Ejecta of Neutron Star Mergers', *The Astrophysical Journal* **925**(1), 22.

Peters, J. G. (1968), 'Nucleosynthesis by the s-PROCESS in Stars of 9 and 15 Solar Masses', *Astrophysical Journal* **154**, 225.

Pian, E., D'Avanzo, P., Benetti, S. et al. (2017), 'Spectroscopic identification of r-process nucleosynthesis in a double neutron-star merger', *Nature* **551**(7678), 67–70.

Pignatari, M., Gallino, R., Heil, M. et al. (2010), 'The Weak s-Process in Massive Stars and its Dependence on the Neutron Capture Cross Sections', *Astrophysical Journal* **710**(2), 1557–1577.

Piskunov, N. E., Kupka, F., Ryabchikova, T. A., Weiss, W. W. and Jeffery, C. S. (1995), 'VALD: The Vienna Atomic Line Data Base.', *Astronomy and Astrophysicss* **112**, 525.

Plez, B. (2012), 'Turbospectrum: Code for spectral synthesis'.

Pont, F. and Eyer, L. (2004), 'Isochrone ages for field dwarfs: method and application to the age-metallicity relation', *Monthly Notices of the RAS* **351**(2), 487–504.

Portinari, L. and Chiosi, C. (2000), 'On radial gas flows, the Galactic Bar and chemical evolution in the Galactic Disc', *Astronomy and Astrophysics* **355**, 929–948.

Prantzos, N., Abia, C., Cristallo, S., Limongi, M. and Chieffi, A. (2020), 'Chemical evolution with rotating massive star yields II. A new assessment of the solar s- and r-process components', *Monthly Notices of the RAS* **491**(2), 1832–1850.

Prantzos, N., Abia, C., Limongi, M., Chieffi, A. and Cristallo, S. (2018), 'Chemical evolution with rotating massive star yields - I. The solar neighbourhood and the s-process elements', *Monthly Notices of the RAS* **476**(3), 3432–3459.

Prochaska, J. X., Naumov, S. O., Carney, B. W., McWilliam, A. and Wolfe, A. M. (2000), 'The Galactic Thick Disk Stellar Abundances', *Astronomical Journal* **120**(5), 2513–2549.

Quillen, A. C., Minchev, I., Bland-Hawthorn, J. and Haywood, M. (2009), 'Radial mixing in the outer Milky Way disc caused by an orbiting satellite', *Monthly Notices of the RAS* **397**(3), 1599–1606.

Raiteri, C. M., Gallino, R., Busso, M., Neuberger, D. and Kaeppeler, F. (1993), 'The Weak s-Component and Nucleosynthesis in Massive Stars', *Astrophysical Journal* **419**, 207.

Rana, N. C. (1991), 'Chemical evolution of the Galaxy.', *Annual Review of Astron and Astrophys* **29**, 129–162.

Randich, S., Gilmore, G. G., Magrini, L. et al. (2022), 'The Gaia-ESO Survey: Survey implementation, data products, open cluster survey, and legacy', *Astronomy and Astrophysics* **(accepted)**.

Randich, S., Gilmore, G. and Gaia-ESO Consortium (2013), 'The Gaia-ESO Large Public Spectroscopic Survey', *The Messenger* **154**, 47–49.

Randich, S. and Magrini, L. (2021), 'Light elements in the Universe', *Frontiers in Astronomy and Space Sciences* **8**, 6.

Rauer, H., Catala, C., Aerts, C. et al. (2014), 'The PLATO 2.0 mission', *Experimental Astronomy* **38**(1-2), 249–330.

Recchi, S., Spitoni, E., Matteucci, F. and Lanfranchi, G. A. (2008), 'The effect of differential galactic winds on the chemical evolution of galaxies', *Astronomy and Astrophysics* **489**(2), 555–565.

Recio-Blanco, A., de Laverny, P., Kordopatis, G. et al. (2014), 'The Gaia-ESO Survey: the Galactic thick to thin disc transition', *Astronomy and Astrophysics* **567**, A5.

Reddy, A. B. S. and Lambert, D. L. (2017), 'Solar Twins and the Barium Puzzle', *Astrophysical Journal* **845**(2), 151.

Ricker, G. R., Winn, J. N., Vanderspek, R. et al. (2015), 'Transiting Exoplanet Survey Satellite (TESS)', *Journal of Astronomical Telescopes, Instruments, and Systems* **1**, 014003.

Rocha-Pinto, H. J., Flynn, C., Scalo, J., Hänninen, J., Maciel, W. J. and Hensler, G. (2004), 'Chemical enrichment and star formation in the Milky Way disk. III. Chemodynamical constraints', *Astronomy and Astrophysics* **423**, 517–535.

Roederer, I. U., Hattori, K. and Valluri, M. (2018), 'Kinematics of Highly r-process-enhanced Field Stars: Evidence for an Accretion Origin and Detection of Several Groups from Disrupted Satellites', *Astronomical Journal* **156**(4), 179.

Rojas-Arriagada, A., Recio-Blanco, A., de Laverny, P. et al. (2016), 'The Gaia-ESO Survey: Separating disk chemical substructures with cluster models. Evidence of a separate evolution in the metal-poor thin disk', *Astronomy and Astrophysics* **586**, A39.

Russell, H. N. (1929), 'On the Composition of the Sun's Atmosphere', *Astrophysical Journal* **70**, 11.

Rutherfurd, L. M. (1863), 'Astronomical observations with spectroscope', *American Journal of Science* **35**(103), 71–77.

Sacco, G. G., Morbidelli, L., Franciosini, E., Maiorca, E. et al. (2014), 'The Gaia-ESO Survey: processing FLAMES-UVES spectra', *Astronomy and Astrophysics* **565**, A113.

Sakari, C. M., Placco, V. M., Farrell, E. M. et al. (2018), 'The R-Process Alliance: First Release from the Northern Search for r-process-enhanced Metal-poor Stars in the Galactic Halo', *Astrophysical Journal* **868**(2), 110.

Sales-Silva, J. V., Daflon, S., Cunha, K. et al. (2022), 'Exploring the S-process History in the Galactic Disk: Cerium Abundances and Gradients in Open Clusters from the OCCAM/APOGEE Sample', *The Astrophysical Journal* **926**(2), 154.

Salpeter, E. E. (1955), 'The Luminosity Function and Stellar Evolution.', *Astrophysical Journal* **121**, 161.

Scalo, J. M. (1986), 'The Stellar Initial Mass Function', *Fundamental Cosmic Physics* **11**, 1–278.

Schmidt, M. (1959), 'The Rate of Star Formation.', *Astrophysical Journal* **129**, 243.

Schönrich, R. A. and Weinberg, D. H. (2019), 'The chemical evolution of r-process elements from neutron star mergers: the role of a 2-phase interstellar medium', *Monthly Notices of the RAS* **487**(1), 580–594.

Schönrich, R. and Binney, J. (2009), 'Chemical evolution with radial mixing', *Monthly Notices of the RAS* **396**(1), 203–222.

Scott, N., van de Sande, J., Sharma, S. et al. (2021), 'Identification of an [α/Fe]—Enhanced Thick Disk Component in an Edge-on Milky Way Analog', *The Astrophysical Journal Letters* **913**(1), L11.

Searle, L. (1971), 'Evidence for Composition Gradients across the Disks of Spiral Galaxies', *Astrophysical Journal* **168**, 327.

Searle, L. and Zinn, R. (1978), 'Composition of halo clusters and the formation of the galactic halo.', *Astrophysical Journal* **225**, 357–379.

Seeger, P. A., Fowler, W. A. and Clayton, D. D. (1965), 'Nucleosynthesis of Heavy Elements by Neutron Capture.', *Astrophysical Journal, Supplement* **11**, 121.

Sellwood, J. A. and Binney, J. J. (2002), 'Radial mixing in galactic discs', *Monthly Notices of the RAS* **336**(3), 785–796.

Shapiro, P. R. and Field, G. B. (1976), 'Consequences of a New Hot Component of the Interstellar Medium', *Astrophysical Journal* **205**, 762–765.

Shaver, P. A., McGee, R. X., Newton, L. M., Danks, A. C. and Pottasch, S. R. (1983), 'The galactic abundance gradient.', *Monthly Notices of the RAS* **204**, 53–112.

Siegel, D. M., Barnes, J. and Metzger, B. D. (2019), 'Collapsars as a major source of r-process elements', *Nature* **569**(7755), 241–244.

Simmerer, J., Sneden, C., Cowan, J. J. et al. (2004), 'The Rise of the s-Process in the Galaxy', *Astrophysical Journal* **617**(2), 1091–1114.

Simonetti, P., Matteucci, F., Greggio, L. and Cescutti, G. (2019), 'A new delay time distribution for merging neutron stars tested against Galactic and cosmic data', *Monthly Notices of the RAS* **486**(2), 2896–2909.

Skrutskie, M. F., Cutri, R. M., Stiening, R. et al. (2006), 'The Two Micron All Sky Survey (2MASS)', *Astronomical Journal* **131**(2), 1163–1183.

Skúladóttir, Á., Hansen, C. J., Choplin, A. et al. (2020), 'Neutron-capture elements in dwarf galaxies. II. Challenges for the s- and i-processes at low metallicity', *Astronomy and Astrophysics* **634**, A84.

Skúladóttir, Á. and Salvadori, S. (2020), 'Evidence for $\gtrsim$4 Gyr timescales of neutron star mergers from Galactic archaeology', *Astronomy and Astrophysics* **634**, L2.

Slumstrup, D., Grundahl, F., Brogaard, K. et al. (2017), 'The [Y/Mg] clock works for evolved solar metallicity stars', *Astronomy and Astrophysics* **604**, L8.

Smartt, S. J., Chen, T. W., Jerkstrand, A. et al. (2017), 'A kilonova as the electromagnetic counterpart to a gravitational-wave source', *Nature* **551**(7678), 75–79.

Smiljanic, R., Korn, A. J., Bergemann, M. et al. (2014), 'The Gaia-ESO Survey: The analysis of high-resolution UVES spectra of FGK-type stars', *Astronomy and Astrophysics* **570**, A122.

Sneden, C. A. (1973), Carbon and Nitrogen Abundances in Metal-Poor Stars., PhD thesis, THE UNIVERSITY OF TEXAS AT AUSTIN.

Sneden, C., Cowan, J. J. and Gallino, R. (2008), 'Neutron-capture elements in the early galaxy.', *Annual Review of Astron and Astrophys* **46**, 241–288.

Sneden, C., Preston, G. W., McWilliam, A. and Searle, L. (1994), 'Ultra–Metal-poor Halo Stars: The Remarkable Spectrum of CS 22892-052', *Astrophysical Journall* **431**, L27.

Soderblom, D. R. (2010), 'The Ages of Stars', *Annual Review of Astron and Astrophys* **48**, 581–629.

Souto, D., Allende Prieto, C., Cunha, K. et al. (2019), 'Chemical Abundances of Main-sequence, Turnoff, Subgiant, and Red Giant Stars from APOGEE Spectra. II. Atomic Diffusion in M67 Stars', *Astrophysical Journal* **874**(1), 97.

Spina, L., Meléndez, J., Karakas, A. I. et al. (2016), 'Nucleosynthetic history of elements in the Galactic disk. [X/Fe]-age relations from high-precision spectroscopy', *Astronomy and Astrophysics* **593**, A125.

Spina, L., Meléndez, J., Karakas, A. I. et al. (2018), 'The temporal evolution of neutron-capture elements in the Galactic discs', *Monthly Notices of the RAS* **474**(2), 2580–2593.

Spina, L., Nordlander, T., Casey, A. R. et al. (2020), 'How Magnetic Activity Alters What We Learn from Stellar Spectra', *Astrophysical Journal* **895**(1), 52.

Spite, F., Spite, M., Barbuy, B. et al. (2018), 'Abundance patterns of the light neutron-capture elements in very and extremely metal-poor stars', *Astronomy and Astrophysics* **611**, A30.

St. John, C. E. and Moore, C. E. (1928), 'On the Presence of the Rare-Earth Elements in the Sun', *Astrophysical Journal* **68**, 93.

Stanghellini, L., Magrini, L., Villaver, E. and Galli, D. (2010), 'The population of planetary nebulae and H II regions in M 81. A study of radial metallicity gradients and chemical evolution', *Astronomy and Astrophysics* **521**, A3.

Stothers, R. (1969), 'Mass Loss from Pulsating Neutron Stars', *Nature* **223**(5203), 279–280.

Strömgren, B. (1940), *On the Chemical Composition of the Solar Atmosphere*, p. 218.

Suess, H. E. and Urey, H. C. (1956), 'Abundances of the Elements', *Reviews of Modern Physics* **28**(1), 53–74.

Surman, R., McLaughlin, G. C., Ruffert, M., Janka, H. T. and Hix, W. R. (2008), 'r-Process Nucleosynthesis in Hot Accretion Disk Flows from Black Hole-Neutron Star Mergers', *Astrophysical Journall* **679**(2), L117.

Talbot, R. J., J. and Arnett, W. D. (1975), 'The evolution of galaxies. IV. Highly flattened disks.', *Astrophysical Journal* **197**, 551–570.

Tammann, G. A., Loeffler, W. and Schroeder, A. (1994), 'The Galactic Supernova Rate', *Astrophysical Journal, Supplement* **92**, 487.

Tautvaišienė, G., Mikolaitis, Š., Drazdauskas, A. et al. (2020), 'Chemical Composition of Bright Stars in the Continuous Viewing Zone of the TESS Space Mission', *Astrophysical Journal, Supplement* **248**(1), 19.

Tautvaišienė, G., Viscasillas Vázquez, C., Mikolaitis, Š. et al. (2021), 'Abundances of neutron-capture elements in thin- and thick-disc stars in the solar neighbourhood', *Astronomy and Astrophysics* **649**, A126.

Terlouw, J. P. and Vogelaar, M. G. R. (2016), 'Kapteyn Package: Tools for developing astronomical applications'.

The, L. S., El Eid, M. F. and Meyer, B. S. (2000), 'A New Study of s-Process Nucleosynthesis in Massive Stars', *Astrophysical Journal* **533**(2), 998–1015.

Thompson, T. A. and ud-Doula, A. (2018), 'High-entropy ejections from magnetized proto-neutron star winds: implications for heavy element nucleosynthesis', *Monthly Notices of the RAS* **476**(4), 5502–5515.

Ting, Y.-S. and Rix, H.-W. (2019), 'The Vertical Motion History of Disk Stars throughout the Galaxy', *Astrophysical Journal* **878**(1), 21.

Tinsley, B. M. (1980), 'Evolution of the Stars and Gas in Galaxies', *Fundamental Cosmic Physics* **5**, 287–388.

Titarenko, A., Recio-Blanco, A., de Laverny, P., Hayden, M. and Guiglion, G. (2019), 'The AMBRE Project: [Y/Mg] stellar dating calibration with Gaia', *Astronomy and Astrophysics* **622**, A59.

Travaglio, C., Galli, D., Gallino, R. et al. (1999), 'Galactic Chemical Evolution of Heavy Elements: From Barium to Europium', *Astrophysical Journal* **521**(2), 691–702.

Travaglio, C., Gallino, R., Arnone, E. et al. (2004), 'Galactic Evolution of Sr, Y, And Zr: A Multiplicity of Nucleosynthetic Processes', *Astrophysical Journal* **601**(2), 864–884.

Travaglio, C., Gallino, R., Busso, M. and Gratton, R. (2001), 'Lead: Asymptotic Giant Branch Production and Galactic Chemical Evolution', *Astrophysical Journal* **549**(1), 346–352.

Trevisan, M. and Barbuy, B. (2014), 'Heavy elements in old very metal-rich stars', *Astronomy and Astrophysics* **570**, A22.

Trippella, O., Busso, M., Palmerini, S., Maiorca, E. and Nucci, M. C. (2016), 's-Processing in AGB Stars Revisited. II. Enhanced 13C Production through MHD-induced Mixing', *Astrophysical Journal* **818**(2), 125.

Truran, J. W., Cowan, J. J., Pilachowski, C. A. and Sneden, C. (2002), 'Probing the Neutron-Capture Nucleosynthesis History of Galactic Matter', *Publications of the ASP* **114**(802), 1293–1308.

Tsikoudi, V. (1979), 'Photometry and structure of lenticular galaxies. I - NGC 3115', *Astrophysical Journal* **234**, 842–853.

Tsujimoto, T. and Shigeyama, T. (2014), 'Enrichment history of r-process elements shaped by a merger of neutron star pairs', *Astronomy and Astrophysics* **565**, L5.

Tucci Maia, M., Ramírez, I., Meléndez, J. et al. (2016), 'The Solar Twin Planet Search. III. The [Y/Mg] clock: estimating stellar ages of solar-type stars', *Astronomy and Astrophysics* **590**, A32.

Ulrich, R. K. (1986), 'Determination of Stellar Ages from Asteroseismology', *Astrophysical Journall* **306**, L37.

Unsöld, A. (1948), 'Quantitative Spektralanalyse der Sonnenatmosphäre. Mit 2 Textabbildungen.', *Zeitschrift fuer Astrophysik* **24**, 306.

Vangioni, E., Goriely, S., Daigne, F., François, P. and Belczynski, K. (2016), 'Cosmic neutron-star merger rate and gravitational waves constrained by the r-process nucleosynthesis', *Monthly Notices of the RAS* **455**(1), 17–34.

Vangioni, E. and Olive, K. A. (2019), 'The cosmic evolution of magnesium isotopes', *Monthly Notices of the RAS* **484**(3), 3561–3572.

Vescovi, D., Cristallo, S., Busso, M. and Liu, N. (2020), 'Magnetic-buoyancy-induced Mixing in AGB Stars: Presolar SiC Grains', *Astrophysical Journall* **897**(2), L25.

Vidotto, A. A., Gregory, S. G., Jardine, M. et al. (2014), 'Stellar magnetism: empirical trends with age and rotation', *Monthly Notices of the RAS* **441**(3), 2361–2374.

Viscasillas Vázquez, C., Magrini, L., Casali, G. et al. (2022), 'The Gaia-ESO Survey: Age-chemical-clock relations spatially resolved in the Galactic disc', *arXiv e-prints* p. arXiv:2202.04863.

Wallner, A., Froehlich, M. B., Hotchkis, M. A. C. et al. (2021), '60fe and 244pu deposited on earth constrain the r-process yields of recent nearby supernovae', *Science* **372**(6543), 742–745.

Watson, D., Hansen, C. J., Selsing, J. et al. (2019), 'Identification of strontium in the merger of two neutron stars', *Nature* **574**(7779), 497–500.

Weidner, C. and Kroupa, P. (2005), 'The Variation of Integrated Star Initial Mass Functions among Galaxies', *Astrophysical Journal* **625**(2), 754–762.

White, S. D. M. and Rees, M. J. (1978), 'Core condensation in heavy halos: a two-stage theory for galaxy formation and clustering.', *Monthly Notices of the RAS* **183**, 341–358.

Wielen, R. (1977), 'The Diffusion of Stellar Orbits Derived from the Observed Age-Dependence of the Velocity Dispersion', *Astronomy and Astrophysics* **60**(2), 263–275.

Woolf, V. M. and West, A. A. (2012), 'The M dwarf problem in the Galaxy', *Monthly Notices of the RAS* **422**(2), 1489–1494.

Woosley, S. E. and Weaver, T. A. (1995), 'The Evolution and Explosion of Massive Stars. II. Explosive Hydrodynamics and Nucleosynthesis', *Astrophysical Journal Supplement* **101**, 181.

Woosley, S. E., Wilson, J. R., Mathews, G. J., Hoffman, R. D. and Meyer, B. S. (1994), 'The r-Process and Neutrino-heated Supernova Ejecta', *Astrophysical Journal* **433**, 229.

Worthey, G., Dorman, B. and Jones, L. A. (1996), 'The G Dwarf Problem Exists in Other Galaxies', *Astronomical Journal* **112**, 948.

Xing, Q.-F., Zhao, G., Aoki, W. et al. (2019), 'Evidence for the accretion origin of halo stars with an extreme r-process enhancement', *Nature Astronomy* **3**, 631–635.

Yan, Y., Du, C., Liu, S. et al. (2019), 'Chemical and Kinematic Properties of the Galactic Disk from the LAMOST and Gaia Sample Stars', *Astrophysical Journal* **880**(1), 36.

Yoachim, P. and Dalcanton, J. J. (2006), 'Structural Parameters of Thin and Thick Disks in Edge-on Disk Galaxies', *Astronomical Journal* **131**(1), 226–249.

Yong, D., Carney, B. W. and Teixera de Almeida, M. L. (2005), 'Elemental Abundance Ratios in Stars of the Outer Galactic Disk. I. Open Clusters', *Astronomical Journal* **130**(2), 597–625.

Yong, D., Carney, B. W., Teixera de Almeida, M. L. and Pohl, B. L. (2006), 'Elemental Abundance Ratios in Stars of the Outer Galactic Disk. III. Cepheids', *Astronomical Journal* **131**(4), 2256–2273.

Yoshii, Y. (1982), 'Density distribution of faint stars in the direction of the north galactic pole.', *Publications of the ASJ* **34**, 365–379.

Zhang, H., Chen, Y. and Zhao, G. (2021), 'Radial Migration from the Metallicity Gradient of Open Clusters and Outliers', *Astrophysical Journal* **919**(1), 52.

Zinn, J. C., Stello, D., Elsworth, Y. et al. (2021), 'The K2 Galactic Archaeology Program Data Release 3: Age-abundance patterns in C1-C8, C10-C18', *arXiv e-prints* p. arXiv:2108.05455.

A. Appendices

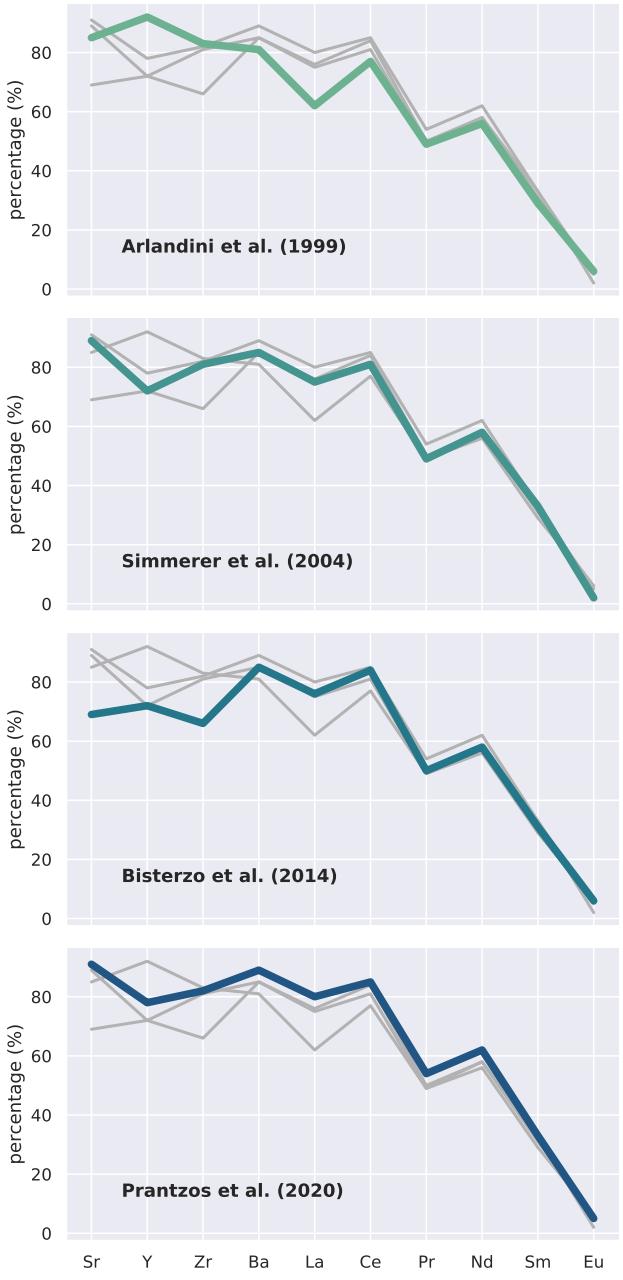

Figure A1: Comparison of the solar *s*-process contribution percentages as given by several authors.

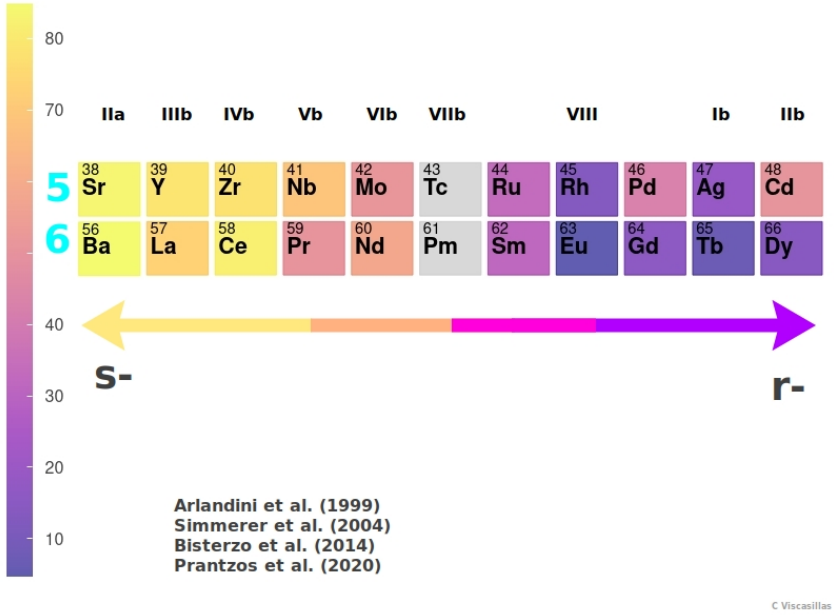

Figure A2: Elements of periods 5 and 6 colored by their *s*-process contribution percentage in the Sun (averaged percentage of Arlandini et al. (1999); Simmerer et al. (2004); Bisterzo et al. (2014); Prantzos et al. (2020)

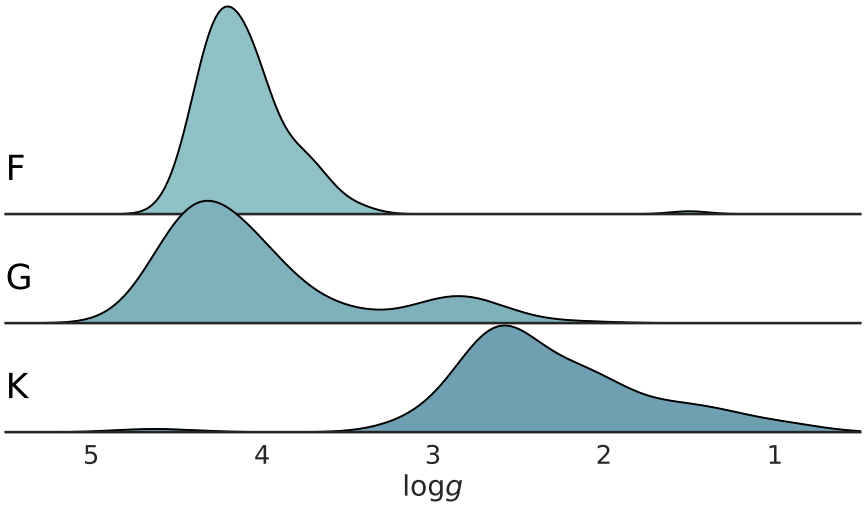

Figure A3: Distribution of stars in our sample by spectral type and log*g* using probability density curves.

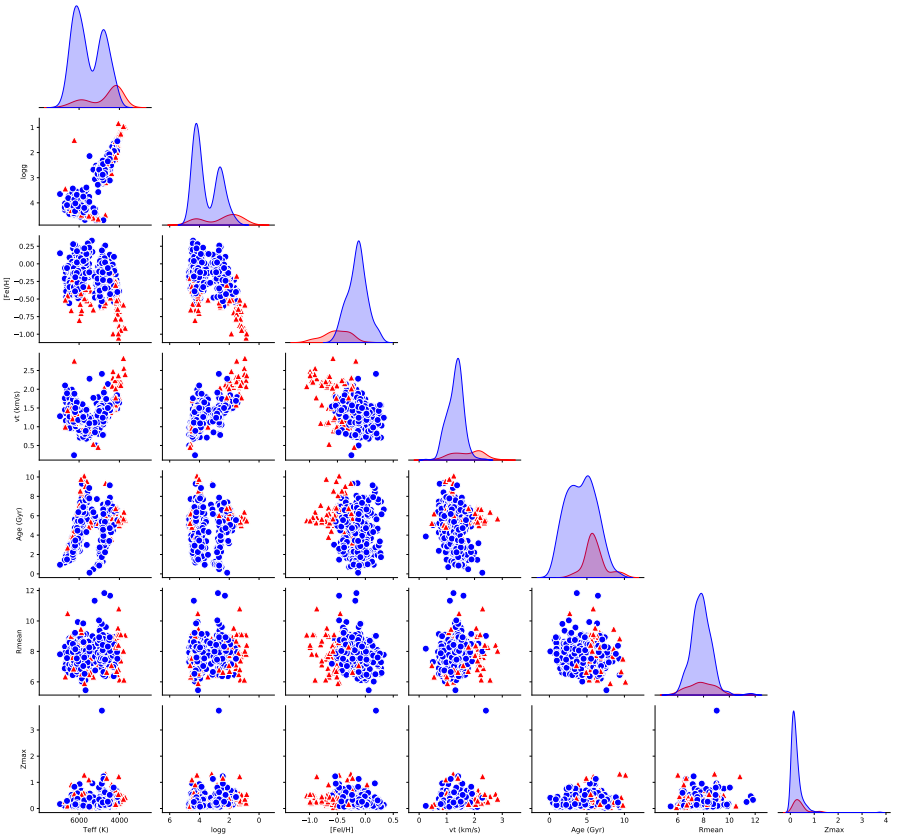

Figure A4: Pairwise relationship of stellar parameters for the sample divided into 424 thin disk stars (blue dots) and 82 thick disk stars (orange triangles). The diagonal plots are kernel density estimate (KDE).

Table A.1: WLS fitting coefficients of the relation [s-/Fe] = m_1·Age + c for the Open Clusters in the three regions.

	$R_{gc} > 9$			$7 \leq R_{gc} \leq 9$			$R_{gc} < 7$		
	m_1	c	PCC	m_1	c	PCC	m_1	c	PCC
[Y II/Fe]	−0.016±0.007	0.169±0.021	−0.38	−0.034±0.012	0.153±0.019	−0.57	−0.016±0.017	0.025±0.027	−0.29
[Zr I/Fe]	−0.014±0.007	0.126±0.019	−0.40	−0.019±0.009	0.090±0.015	−0.52	−0.036±0.018	0.055±0.027	−0.55
[Ba II/Fe]	−0.043±0.006	0.266±0.019	−0.83	−0.033±0.014	0.141±0.033	−0.48	−0.104±0.031	0.130±0.048	−0.73
[La II/Fe]	−0.021±0.006	0.228±0.017	−0.65	−0.032±0.013	0.162±0.026	−0.57	−0.061±0.027	0.061±0.024	−0.61
[Ce II/Fe]	−0.020±0.003	0.191±0.007	−0.80	−0.036±0.012	0.145±0.024	−0.62	−0.057±0.027	0.110±0.032	−0.57

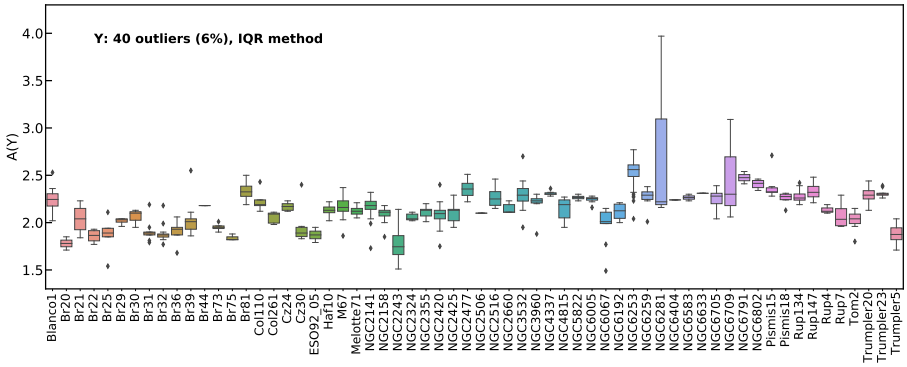

(a)

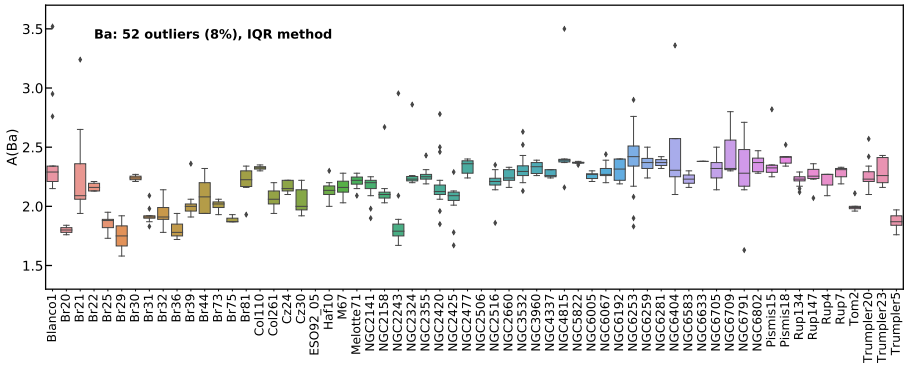

(b)

Figure A5: Boxplots with the interquartile range of the abundance for each of the clusters with the outliers (observations that fall below Q1 - 1.5 IQR or above Q3 + 1.5 IQR). Figure A5a for Y2 and A5b for Ba2.

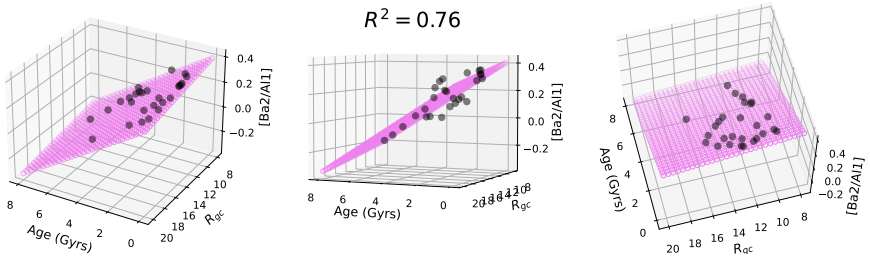

(a) [Ba/Al] as a function of Age and R_{gc} in the outer region

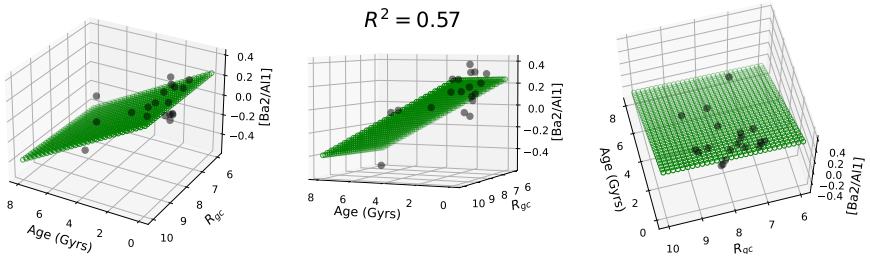

(b) [Ba/Al] as a function of Age and R_{gc} in the solar region

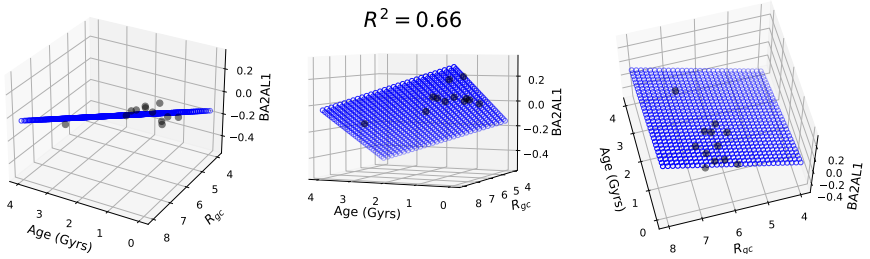

(c) [Ba/Al] as a function of Age and R_{gc} in the inner region

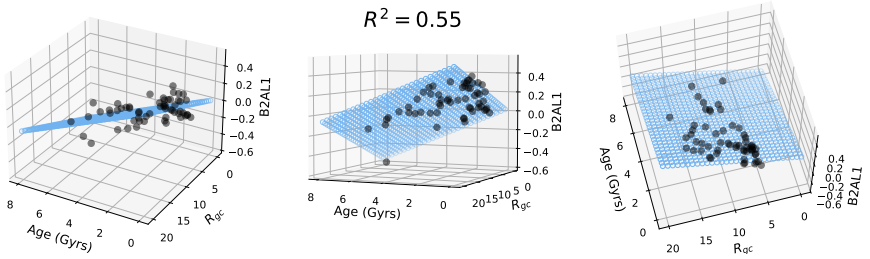

(d) [Ba/Al] as a function of Age and R_{gc} in the global interval

Figure A6: [Ba/Al] = m_1·Age + m_2· R_{gc} + c relation 3D representations in the three regions defined in this work and the whole sample as seen from 3 different perspectives.

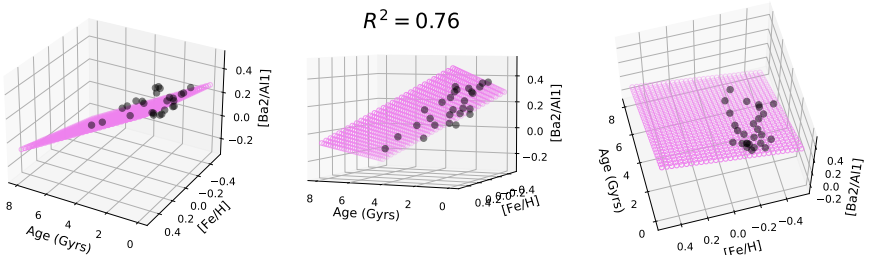

(a) [Ba/Al] as a function of Age and [Fe/H] in the outer region

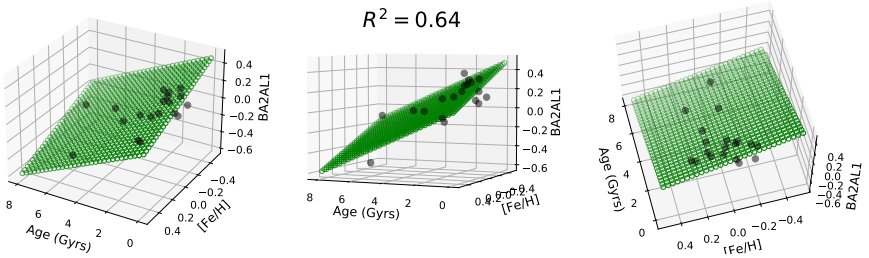

(b) [Ba/Al] as a function of Age and [Fe/H] in the solar region

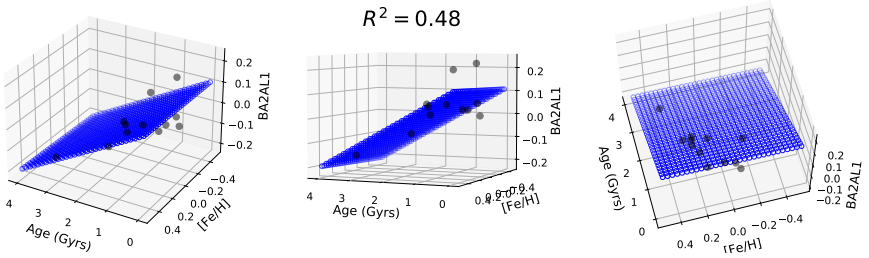

(c) [Ba/Al] as a function of Age and [Fe/H] in the inner region

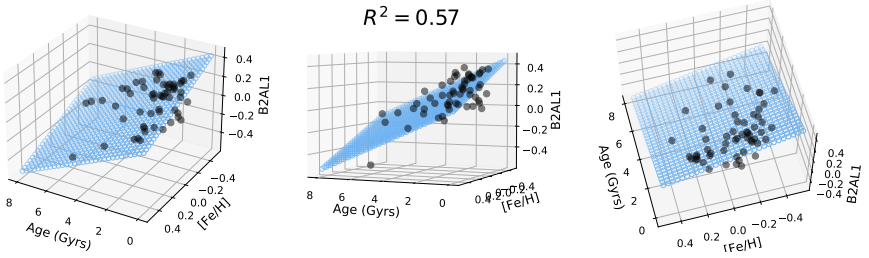

(d) [Ba/Al] as a function of Age and [Fe/H] in the global interval

Figure A7: [Ba/Al] = m_1·Age + m_2· [Fe/H] + c relation 3D representations in the three regions defined in this work and the whole sample as seen from 3 different perspectives.

Table A.2: Weighted multilinear regressions of 3 variables fitting coefficients of the relation $[s/\alpha] = m_1 \cdot \text{Age} + m_2 \cdot R_{gc} + m_3 \cdot [\text{Fe/H}] + \text{c}$ for the Open Clusters in every region and the coefficients of the inverted stellar dating relation $\text{Age} = m'_1 \cdot [\text{s-}/\alpha] + m'_2 \cdot R_{gc} + m'_3 \cdot [\text{Fe/H}] + \text{c'}$

				R_{gc} > 9 kpc					
[s-/α]	$m_1 \pm \Delta m_1$	$m_2 \pm \Delta m_2$	$m_3 \pm \Delta m_3$	c $\pm \Delta c$	R^2_{adj}	c'	m_1'	m_2'	m_3'
[Y/Mg]	−0.036± 0.007	−0.005±0.006	0.179±0.103	0.319±0.076	0.61	8.861	−27.778	−0.139	4.972
[Y/Al]	−0.033±0.007	−0.005±0.006	0.320±0.115	0.338±0.076	0.59	10.242	−30.303	−0.152	9.697
[Y/Si]	−0.025±0.009	0.004±0.006	0.176±0.121	0.180±0.081	0.37	7.2	−40.0	0.16	7.04
[Y/Ca]	−0.015±0.008	0.016±0.005	0.352±0.129	−0.003±0.068	0.51	−0.2	−66.667	1.067	23.467
[Y/Ti]	−0.042±0.007	−0.001±0.007	0.142±0.119	0.242±0.084	0.64	5.762	−23.81	−0.024	3.381
[Ba/Mg]	−0.102±0.005	0.003±0.007	0.046±0.010	0.425±0.092	0.95	4.167	−9.804	0.029	0.451
[Ba/Al]	−0.074±0.009	−0.013±0.007	−0.063±0.121	0.490±0.094	0.75	6.622	−13.514	−0.176	−0.851
[Ba/Si]	−0.054±0.010	−0.020±0.007	−0.145±0.134	0.496±0.091	0.55	9.185	−18.519	−0.37	−2.685
[Ba/Ca]	−0.055±0.006	0.021±0.000	0.002±0.000	−0.001±0.000	0.82	−0.018	−18.182	0.382	0.036
[Ba/Ti]	−0.083±0.011	−0.028±0.008	−0.289±0.186	0.623±0.108	0.68	7.506	−12.048	−0.337	−3.482
				7 < R_{gc} < 9 kpc					
[Y/Mg]	−0.044±0.015	−0.019±0.034	0.256±0.314	0.379±0.272	0.32	8.614	−22.727	−0.432	5.818
[Y/Al]	−0.051±0.014	0.025±0.001	0.002±0.000	0.004±0.000	0.42	0.078	−19.608	0.49	0.039
[Y/Si]	−0.023±0.010	0.015±0.003	−0.001±0.000	0.002±0.000	0.18	0.087	−43.478	0.652	−0.043
[Y/Ca]	−0.022±0.011	−0.034±0.026	−0.214±0.163	0.402±0.213	0.18	18.273	−45.455	−1.545	−9.727
[Y/TI]	−0.022±0.016	−0.001±0.038	0.191±0.295	0.162±0.304	−0.03	7.364	−45.455	−0.045	8.682
[Ba/Mg]	−0.035±0.015	−0.050±0.043	−0.436±0.414	0.594±0.343	0.38	16.971	−28.571	−1.429	−12.457
[Ba/Al]	−0.053±0.028	−0.157±0.074	−1.429±0.530	1.596±0.573	0.57	30.113	−18.868	−2.962	−26.962
[Ba/Si]	−0.036±0.020	−0.104±0.053	−1.039±0.419	1.060±0.410	0.56	29.444	−27.778	−2.889	−28.861
[Ba/Ca]	−0.028±0.013	−0.070±0.032	−0.479±0.273	0.716±0.258	0.46	25.571	−35.714	−2.5	−17.107
[Ba/Ti]	−0.032±0.017	−0.094±0.045	−0.863±0.329	0.983± 0.353	0.45	30.719	−31.25	−2.938	−26.969
				R_{gc} < 7 kpc					
[Y/Mg]	−0.015±0.074	0.191±0.115	0.641±0.786	−1.365±0.789	0.25	−91.0	−66.667	12.733	42.733
[Y/Al]	−0.103±0.066	0.050±0.100	0.780±0.726	−0.307±0.683	0.12	−2.981	−9.709	0.485	7.573
[Y/Si]	−0.015±0.056	0.133±0.082	0.011±0.620	−0.865±0.567	0.12	−57.667	−66.667	8.867	0.733
[Y/Ca]	−0.024±0.037	0.108±0.067	0.194±0.355	−0.637±0.450	−0.01	−26.542	−41.667	4.5	8.083
[Y/Ti]	−0.070±0.064	0.114±0.107	0.297±0.654	−0.609±0.711	−0.04	−8.7	−14.286	1.629	4.243
[Ba/Mg]	−0.031±0.033	0.254±0.041	−0.173±0.279	−1.606±0.253	0.76	−51.806	−32.258	8.161	−5.581
[Ba/Al]	−0.151±0.035	0.169±0.043	0.507±0.367	−0.976±0.299	0.84	−6.464	−6.623	1.119	3.358
[Ba/Si]	−0.053±0.029	0.235±0.042	−0.403±0.287	−1.406±0.277	0.89	−26.528	−18.868	4.434	−7.604
[Ba/Ca]	−0.009±0.043	0.111±0.056	−0.686±0.307	−0.517±0.354	0.76	−57.444	−111.111	12.333	−76.222
[Ba/Ti]	−0.137±0.029	0.237±0.049	0.239±0.307	−1.333±0.330	0.88	−9.73	−7.299	1.73	1.745
				global					
[Y/Mg]	−0.036±0.011	0.006±0.010	−0.166±0.122	0.129±0.079	0.16	3.583	−27.778	0.167	−4.611
[Y/Al]	−0.039±0.007	−0.001±0.005	−0.190±0.060	0.191±0.032	0.54	4.897	−25.641	−0.026	−4.872
[Y/Si]	−0.026±0.006	0.010±0.005	−0.125±0.062	0.035±0.032	0.34	1.346	−38.462	0.385	−4.808
[Y/Ca]	−0.019±0.006	0.012±0.004	0.075±0.068	0.003±0.038	0.29	0.158	−52.632	0.632	3.947
[Y/Ti]	−0.035±0.007	0.006±0.007	0.054±0.086	0.114±0.060	0.40	3.257	−28.571	0.171	1.543
[Ba/Mg]	−0.103±0.006	0.038±0.003	0.025±0.021	0.050±0.046	0.86	0.485	−9.709	0.369	0.243
[Ba/Al]	−0.089±0.012	−0.014±0.009	−0.603±0.134	0.448±0.083	0.55	5.034	−11.236	−0.157	−6.775
[Ba/Si]	−0.061±0.009	−0.013±0.007	−0.536±0.112	0.340±0.068	0.51	5.574	−16.393	−0.213	−8.787
[Ba/Ca]	−0.055±0.005	0.020±0.002	0.009±0.014	0.015±0.030	0.84	0.273	−18.182	0.364	0.164
[Ba/Ti]	−0.066±0.008	−0.017±0.008	−0.477±0.102	0.397±0.076	0.56	6.015	−15.152	−0.258	−7.227

Acknowledgements

When a goal is reached and the end of a project comes, it is time to look back and see the period that has elapsed with perspective. The first thoughts are for the people who have made it possible. For those who are gone, my parents, who gave me life, for their example and virtues. My gratitude to my supervisor Gražina for giving me this great opportunity and for getting me involved in such a fascinating subject of my thesis, for your support and hours of sleeplessness to come to fruition and achieve successful completion. Also special thanks to Laura Magrini, my "MW Gaia" COST mentor at INAF-Arcetri AO (Italy) for your praiseworthy support and valuable teachings, source of motivation and fruitful collaboration, also in the context of the Gaia ESO Survey (GES). To the "Astro-spectroscopy and Exoplanet Group" team members: Yuriy, excellent office mate, colleague and friend, for your wonderful welcome and making my daily routine easier and more joyful; Šarūnas, Arnas, Vilius, Renata, Edita, Erika, Rimvydas and Markus, for your daily support and friendship. To the professors and consultants of my three doctoral exams: "Data and image analysis" (9 ECTS), "Astrospectroscopy" (9 ECTS), and "Galactic Astronomy" (12 ECTS), for your valuable teachings and advice. To the Doctoral Committee of Physical Sciences (02P) and its secretary Justė Kudzytė and to the Administration of the Faculty of Physics, headed by the dean Juozas Šulskus, and those of TFAI; to Lina Janionienė, Simona Akamauskaitė, Vida Dubonienė and the members of the Doctoral Department, for your help and kindness during the four years. To Kristina Aponienė, Doctoral Administrator at the Faculty of Physics. To Diana Leleikiene, Administrator at the Vilnius University Press. To my previous teachers, mentors and supervisors, whose example and motivation encouraged and inspired me to follow in the footsteps of astronomy. In particular I want to thank to Josefina Faen Ling (OARMA, USC), Rimvydas Janulis (MAO, VU), Leonardo Vanzi (AIUC), Frank Tramper and Danny Lennon (ESA), and Ehsan Moravveji (KU Leuven). Finally, to all the teachers, scientists and colleagues whose example and encouragement inspired me throughout my life to pursue a career in science.

Santrauka

Problemos išdėstymas ir tyrimo temos aktualumas

Galaktikos formavimosi, struktūros ir evoliucijos supratimas yra vienas iš pagrindinių atvirų astronomijos klausimų. Norint visapusiškai suprasti, būtina tiksliai žinoti skirtingų žvaigždžių populiacijų chemines ir kinematines savybes, palyginti jas su galaktikos modeliais. Šiuo atveju neutronų pagavimo elementai yra pagrindiniai elementai dėl jų ypatingos nukleosintezės, kuri apima du gerai diferencijuotus skirtingos kilmės ir pobūdžio procesus (vadinamus *s*- ir *r*-procesais). Taigi, neutronų pagavimo elementai dažnai naudojami kaip ryšys tarp astronominių stebėjimų, cheminės evoliucijos modelių ir branduolinės astrofizikos. *S*-procesas yra įdomus mažos masės asimptotinės milžinių sekos žvaigždžių fizikoje, o *r*-procesas yra vertingas tiriant neutronines žvaigždes ir gravitacines bangas. Vienas iš labiausiai vertinamų neutronų pagavimo elementų pritaikymo būdų yra jų tiesioginis naudojimas kaip kosminių laikrodžių. Dėl visų šių ypatingų savybių neutronų pagavimo elementai yra labai informatyvūs ir sulaukia ypatingo susidomėjimo.

Problemos, kurios vis dar išlieka neutronų pagavimo elementų kontekste, yra įvairios ir skirtingo lygio. Kai kurios iš jų yra susiję su santykiniu neutronų pagavimo procesų indėliu į cheminių elementų gamybą, su didele elementų gausų sklaida neturtingose metalais žvaigždėse. Lyginant nukleosintezės teorijas ir stebėjimus vis dar trūksta sutarimo dėl *r*-proceso astrofizikinių vietų ir elementų išeigos. Tradicinių *r*-proceso elementų gamybos vietų peržiūros būtinumą palaiko ir spektroskopinis neutronų pagavimo elementų identifikavimas dviejų neutroninių žvaigždžių susijungime, užfiksuotame gravitacinių bangų šaltinyje GW170817 (Pian ir kt. 2017).

Kitas svarbus veiksnys yra gausos gradientai, kurių egzistavimas Galaktikoje yra akivaizdžiai aptiktas remiantis įvairiais galaktikos objektais (pvz., HII regionais, planetiniais ūkais, B spektrinio tipo žvaigždėmis, padrikaisiais žvaigždžių spiečiais) ir teoriniais modeliavimais. Lengvesnių už geležį elementų gausos gradientai yra gerai žinomi jau keletą dešimtmečių, tačiau dėl neutronų pagavimo elementų, vis dar reikia platesnio sutarimo. Rezultatų nesutapimams įtakos gali turėti ir žvaigždžių migracija.

"Gaia" kosminio teleskopo ir didelių spektroskopinių tyrimų eroje, kai sujungiama daugybės žvaigždžių astrometrija ir cheminė sudėtis, trūkstamas kintamasis yra laikas. Tada žvaigždžių amžius yra vienas geidžiamiausių astronomijos parametrų. Jo žinios apima žvaigždžių ir astronominių įvykių išsidėstymą tam tikru laiku. Amžiaus nustatymui naudojamų metodų skaičius per pastaruosius dešimtmečius išaugo (pvz., Howes ir kt., 2019). Tačiau dauguma šių metodų turi daug apribojimų. Pastaraisiais metais neutronų pagavimo elementai buvo atskleisti

kaip puikūs žvaigždžių spiečių ir Saulės dvynių amžiaus indikatoriai. Jų kaip kosminių laikrodžių naudojimas šiuo metu yra aktuali tema astronomijoje (pvz., Morel ir kt., 2021), ši disertacija taip pat prisideda prie šio klausimo gvildenimo.

Tikslai ir užduotys

Neutronų pagavimo elementai dėl savo nukleosintezės procesų specifiškumo, taip pat dėl jų astrofizinių kilmės vietų suteikia išskirtinę informaciją apie Galaktikos formavimąsi ir evoliuciją. Pagrindinis šio disertacinio darbo tikslas yra apžvelgti naujausius šios srities pasiekimus, parodyti didelį neutronų pagavimo cheminių elementų potencialą ir prisidėti prie jų vaidmens nustatymo Saulės aplinkoje, taigi ir Galaktikos diske.

Pagrindinis šio disertacinio darbo tikslas – apžvelgti naujausius pasiekimus neutronų pagavimo elementų tyrimuose, parodyti aukštą jų potencialą ir prisidėti prie geresnio jų pažinimo, nustatant jų vaidmenį Galaktikos diske. Norint pasiekti šį tikslą, išsamiai analizuojamos dešimties *s*- ir *r*-procesų elementų gausos įvairiuose metalingumo, amžiaus, vidutinio galaktocentrinio atstumo ir maksimalaus aukščio nuo Galaktikos plokštumos diapazonuose. Tam buvo išanalizuoti daugiau nei pusės tūkstančio ryškių ($V < 8$ mag) FGK spektrinių klasių žvaigždžių, esančių Saulės kaimynystėje, spektrai. Analizuojamame rinkinyje turėjo būti identifikuotos plonojo ir storojo Galaktikos diskų žvaigždės, kad būtų galima nustatyti jų evoliucijos istorijas.

Kadangi neutronų pagavimo elementai priklauso skirtingoms grupėms pagal jų dominavimą kiekviename procese, kurių kiekvienas turi savo ypatybes, tarp mūsų uždavinių taip pat buvo nustatyti jų diferencijuotą elgesį, tiksliai nustatyti jų gradientus erdveje ir laike, taip pat įvertinti jų kaip kosminių laikrodžių naudojimą ir taikymo aprėptį. Atlikdami šią paskutinę užduotį, mes taip pat panaudojome padrikųjų žvaigždžių spiečių stebėjimus, atliktus "Gaia ESO apžvalgoje" (GES; Gilmore ir kt. 2012 ir Randich ir kt. 2013).

Mokslinis naujumas ir ginami teiginiai

Disertaciniame darbe panaudojant aukštos skiriamosios gebos spektrus ir sintetinių spektrų metodiką ištirtos ryškios Saulės aplinkoje esančios žvaigždės garantuoja tikslius ir kokybiškus rezultatus. Daugumai šiame darbe tirtų žvaigždžių neutronų pagavimo elementų gausa nustatyta pirmą kartą. Rezultatų svarbą didina tai, kad šios žvaigždės yra TESS ir būsimos PLATO kosminių misijų egzoplanetų paieškos objektai. Ištirtų žvaigždžių skaičius, taip pat didelis analizuotų neutronų pagavimo elementų skaičius apima mažiau ištirtus elementus, tokius kaip Sr, Pr ir Sm, taip pat reprezentatyviausius kiekvieno proceso elementus. Žvaigždžių atskyrimas

į Galaktikos disko komponentus leidžia diferencijuoti neutronų pagavimo procesus šiuose galaktikos komponentuose. Disertaciniame darbe taip pat naudojama didelė Gaia ESO apžvalgos padrikųjų žvaigždžių spiečių imtis, siekiant kalibruoti žvaigždžių amžių ir *s*-proceso bei α-elementų gausos santykį [s/α]. Dėl bendrų žvaigždžių narių ypatybių padrikieji spiečiai yra vieni patikimiausių Galaktikos cheminės evoliucijos indikatorių. Plataus radialinio atstumo nuo Galaktikos centro diapazonas leido išsamiai ištirti ir radialinius gausos gradientus.

Atlikus [El/Fe I] gausos santykių kaip metalingumo funkcijos palyginimą su Galaktikos cheminės evoliucijos (GCE) modeliais, stebėjimai rodo, kad antrojo *s*-proceso smailės elementams reikėtų pakeisti naudojamų modelių įvestis. Prantzos ir kt. (2018) modeliuose sutapimas su stebėjimų duomenimis būtų geresnis jei mažų ir vidutinių masių žvaigždžių įnašas prasidėtų prie didesnio metalingumo (apie –0.7), kas pastūmėtų modelio maksimumą link [Fe/H]= –0.2. Kalbant apie plonojo ir storojo disko populiacijų elgseną, kai kuriems elementams pastebimas aiškus skirtumas tarp abiejų Galaktikos disko komponenčių, ypač Ba ir Eu, atitinkamai reprezentuojantiems grynąją *s*- ir *r*-procesų gamybą. Išanalizavę lengvųjų ir sunkiųjų *s*-proceso elementų gausų [hs/ls] santykį, patvirtinome aiškų skirtumą tarp Galaktikos plonojo ir storojo diskų evoliucijos. Palygindami *r*-proceso elemento Eu ir α-elemento Mg gausas, nustatėme, kad storojo disko žvaigždėms [Eu/Mg] didėjant metalingumui mažėja sparčiau lyginant su plonojo disko žvaigždėmis, o tai irgi rodo skirtingą galaktikos plonojo ir storojo diskų cheminę evoliuciją.

Tyrinėdami elementų gausos ir amžiaus gradientus, nustatėme gausos koreliacijas, atitinkančias kiekvienos elementų grupės pobūdį GCE kontekste ir esamą literatūrą. Plonajame diske randame pirmosios *s*-proceso smailės Y ir Sr elementų ir antrosios *s*-proceso smailės elemento Ba aiškią antikoreliaciją su amžiumi; tuo tarpu, mišrus elementas Pr ir labiau *r*-proceso gaminami elementai Sm ir Eu rodo teigiamą gradientą. Kalbant apie storojo disko amžiaus gradientus, jie elgiasi panašiai, tačiau gradientai yra silpnesni arba jų praktiškai nėra. Jauniausioms mūsų plonojo disko rinkinio žvaigždėms neradome bario gausos anomalijos („bario galvosūkio“) įrodymų.

Tyrinėdami amžiaus gradientus padrikųjų žvaigždžių spiečių rinkinyje nustatėme, kad [El/Fe] tam tikram amžiui vidiniame diske (R_{gc} < 7 kpc) yra mažesni nei atokesniuose regionuose. Taip pat nustatėme, kad su amžiumi gradientai mažėja, o [Ba/Fe] rodo stipriausią tendenciją. Visų elementų, kuriuose dominuoja *s*-procesas, regresijos nuolydis vidiniame diske yra statesnis nei kituose regionuose.

Taip pat pateikiami ir aptariami neutronų pagavimo elementų erdviniai gradientai, kuriuos galėjome ištirti panaudojant naujausius Gaia kosminio palydovo astrometrinius duomenis, leidžiančius tiksliau apskaičiuoti žvaigždžių vidutinius galaktocentrinius atstumus ir didžiausią vertikalų atstumą nuo Galaktikos plokštu-

mos. Radialiniai elementų ir geležies gausų santykio gradientai plonajame diske yra nereikšmingi elementams, kuriuose dominuoja *s*-procesas, ir tampa teigiami elementams, kuriuose dominuoja *r*-procesas. Vertikalūs gradientai yra neigiami elementams, kuriuose dominuoja lengvasis *s*-procesas, ir tampa teigiami elementams, kuriuose dominuoja *r*-procesas. Storajame diske radialiniai elementų gausos geležies atžvilgiu gradientai yra nereikšmingi, o vertikalūs gradientai daugiausia yra neigiami.

Tirdami cheminių laikrodžių klausimą, mes atrinkome jautriausius ir patikimiausius *s*-proceso ir α-elementus. Plonojo disko Saulės aplinkos žvaigždėms mes apskaičiavome [Y/Mg] ir amžiaus priklausomybę $[\mathrm{Y/Mg}]_{thin}$ = 0.022(±0.015) −0.027(±0.003)·age[Gyr], taip pat nustatėme, kad galima panaudoti ir Al bei Sr. Taip pat nustatėme, kad skirtingų žvaigždžių imtys iš skirtingų galaktocentrinių atstumų gali lemti priklausomybių skirtumus. Storojo disko atveju, išplėtę žvaigždžių rinkinį duomenimis iš kitų darbų ir platesniame amžiaus ir metalingumo diapazone, nustatėme, kad gausų santykių ir amžiaus priklausomybė yra nereikšminga. Tai rodo skirtingą diskų evoliucijos istoriją ir elementų gausų santykių netinkamumą žvaigždžių amžiaus nustatymui.

Tirdami padrikuosius spiečius patvirtinome, kad nėra vieno visam diskui galiojančio amžiaus ir cheminės sudėties ryšio, nes yra priklausomybė nuo galaktocentrinės padėties, susijusios žvaigždžių formavimosi istorija Galaktikoje ir su mažos ir vidutinės masės žvaigždžių *s*-proceso elementų išeigos priklausomybe. Taip pat nustatėme, kad jaunų disko žvaigždžių [Ba/α] gausos santykis yra jautresnis amžiui nei [Y/α], o jo gradientas mažiau priklauso nuo galaktocentrinio atstumo. Taip pat pateikiame stebėjimo įrodymų, kad [Y/Mg] santykis yra neuniversalus kaip kosminis laikrodis dėl skirtingo *s*-proceso efektyvumo esant dideliam metalingumui.

Asmeninis indėlis

Pagrindinė šio disertacinio darbo dalis, pagrįsta Lietuvoje Molėtų astronomijos observatorijoje gautais duomenimis, bendradarbiaujant su Astrospektroskopijos ir egzoplanetų komanda bei turint nuosavą Vilniaus universiteto infrastruktūrą. Duomenis rinko ir apdorojo anksčiau minėta komanda. Asmeninis autoriaus indėlis apima atominių duomenų paruošimą, išankstinį spektro linijų parinkimą, hipersmulkiosios struktūros (HFS) analizę; ir iš dalies parametrų, tokių kaip amžius, orbitos ir kinematika, gausos nustatymas ir apskaičiavimas; taip pat baigiamasis duomenų apdorojimas, statistinis apdorojimas, tyrimas, konceptualizavimas ir kritinė analizė, vadovaujant disertacinio darbo vadovei.

Disertacinio darbo dalis, kurioje naudojami UVES, Paranalyje (Čilė) esančio labai didelio teleskopo (VLT) didelės raiškos optinio spektrografo duomenys, atlikta Gaia-ESO apžvalgos (GES) konsorciumo rėmuose, dalyvaujant tarptautinei

astronomų komandai. Asmeninis autoriaus indėlis apima duomenų analizės užduotis, tokias kaip gausų normalizavimas, žvaigždžių narystė padrikuosiuose spiečiuose, amžiaus ir orbitų nustatymas, statistinis apdorojimas, taip pat konceptualizavimas ir galutinė mokslinė analizė. Dalį šio darbo autorius atliko INAF-Arcetri astronomijos observatorijoje Italijoje COST mokslinės stažuotės metu.

Disertacijos struktūra

Šį darbą sudaro 6 skyriai, prieš kuriuos pateikiami pradiniai aiškinamieji puslapiai ir baigiasi bibliografija ir priedais.

- *Pirmasis skyrius* yra įvadinis ir skirtas neutronų pagavimo elementų Galaktikoje apibrėžimui ir klasifikavimui bei problemos kontekstualizavimui.
- *Antrame skyriuje* detaliai aprašomi metodai, naudojami baigiamojo darbo tikslams pasiekti, įskaitant gausos nustatymo ir paklaidų aprašymą, amžių ir orbitų skaičiavimą.
- *Trečiame skyriuje* kalbama apie elementų gausos santykius įvairaus metalingumo žvaigždėse, suskirstant elementus į grupes ir lyginant juos tarpusavyje bei dviejose Galaktikos disko komponentėse.
- *Ketvirtajame skyriuje* analizuojami gausos gradientai tiek pagal amžių, tiek radialine ir vertikalia kryptimis; taip pat skiriant išsamų dėmesį gausų kaip kosminių laikrodžių naudojimui.
- *Penktasis skyrius* skirtas neutronų pagavimo elementų gausos naudojimui ir taikymui nustatant amžių tiek Saulės aplinkoje esančioms žvaigždėms, tiek padrikiesiems spiečiams.
- *Šeštame skyriuje* pateikiamos išvados ir apžvelgiamos ateities perspektyvos.

ĮVADAS

Pirmajame skyriuje pristatoma neutronų pagavimo elementų reikšmė astrofizikiniame kontekste.

1.1 skirsnyje apžvelgiama žvaigždžių spektruose randamų cheminių elementų įvairovė, sąlygota daugelio termobranduolinių procesų. Cheminių elementų gausos ir jų pasiskirstymas Galaktikos komponentuose leidžia suprasti jos cheminio sodrinimo scenarijus ir atsekti kosminius įvykius, suformavusius dabartinę Galaktiką.

1.2 skirsnyje neutronų pagavimo elementai klasifikuojami pagal skirtingus veiksnius, taip pat pateikiama juos gaminančios lėto ir greito neutronų pagavimo nukleosintezės apžvalga.

1.3 skirsnyje aptariama Saulės sistemos ir Saulės, kaip mūsų etaloninės žvaigždės, gausa ir įvairių procesų indėlis.

1.4 skirsnyje apžvelgiamos astrofizikinės vietos ir mechanizmai, turtinantys Galaktiką neutronų pagavimo elementais, tokie kaip supernovų sprogimai, asimptotinės milžinių sekos žvaigždžių bei neurtoninių žvaigždžių susiliejimų įtaka.

MOKSLINIŲ TYRIMŲ METODOLOGIJA

2 skyriuje aptariama tyrimų metodika, taikyta Saulės aplinkos žvaigždžių tyrimams (2.1 skirsnis) ir padrikųjų žvaigždžių spiečių tyrimams (2.2 skirsnis).

2.1 skirsnis prasideda stebėjimams naudotų prietaisų apžvalga, taip pat žvaigždžių imties, kurią sudaro 506 ryškios FGK spektrinio tipo žvaigždės, aprašymu. Taigi, Molėtų astronomijos observatorijoje žvaigždės buvo stebimos trijuose šiaurinio dangaus laukuose, žr. 1 pav.) naudojant 1,65 m Ritchey-Chretien teleskopą ir didelės skiriamosios gebos šviesolaidinį Vilniaus universiteto ešelinį spektrografą (VUES, Jurgenson ir kt 2014).

Toliau pateikiamas duomenų gavimo ir apdorojimo aprašymas (2.1.2 poskyris), o po to seka poskyris, skirtas atmosferos parametrams (2.1.3 poskyris). Žvaigždžių rinkinys apibendrintas 2 pav. ir apima įvairaus metalingumo žvaigždes nykštukines, submilžines ir milžines.

2.1.4 poskyryje atskleista gausos nustatymo metodika, įskaitant spektro linijų sąrašą (kurį sudaro 35 spektrinės linijos 10-čiai neutronų pagavimo elementų), priimta Saulės gausos skalė, taip pat gausos analizė ir jos paklaidos. Elementų gausa buvo nustatyta diferencine spektrinių linijų sinteze, naudojant MARCS vienmačius žvaigždžių atmosferos modelius (Gustafsson ir kt., 2008) ir atsižvelgiant į hipersmulkios struktūros efektus. Vidutinės žvaigždžių atmosferos parametrų nustatymo paklaidos yra tokios: a) nykštukėms ($\log g > 3.5$): $\sigma T_{\rm eff} = 48$ K, $\sigma \log g = 0.30$, σ[Fe/H] $= 0.11$, and $\sigma v_{\rm t} = 0.28$ km s^{-1}; b) milžinėms ($\log g \leq 3.5$): $\sigma T_{\rm eff} = 57$ K, $\sigma \log g = 0.21$, σ[Fe/H] $= 0.11$, and $\sigma v_{\rm t} = 0.22$ km s^{-1}.

2.1.5 poskyryje pateiktas žvaigždžių amžių ir orbitinių parametrų nustatymas. Tirtų žvaigždžių radialinėms padėtims Galaktikos diske įvertinti buvo naudojamas vidutinis galaktocentrinis atstumas R_{mean} leidžiantis atlikti išsamesnį tyrimą, nei daugelyje kitų darbų naudoti matomieji galaktocentriniai atstumai. Žvaigždžių amžiaus ir kinematinių parametrų nustatymas leido atsižvelgti į žvaigždžių migracijos įtaką. Galiausiai, žvaigždžių kinematika ir cheminė sudėtis leido jas atskirti į Galaktikos disko komponentus, t.y. plonąjį ir storąjį diskus (2.1.6 poskyris), o tai leidžia tyrinėti jų evoliuciją.

Padrikųjų žvaigždžių spečių analizė aprašyta 2.2 skyriuje. Naudojome IDR6 Gaia-ESO tyrimo duomenis (Gilmore et al. 2012; Randich et al. 2013), gautus atlikus UVES spektrų spektrinę analizę (skiriamoji galia R = 47,000 ir spektrinis

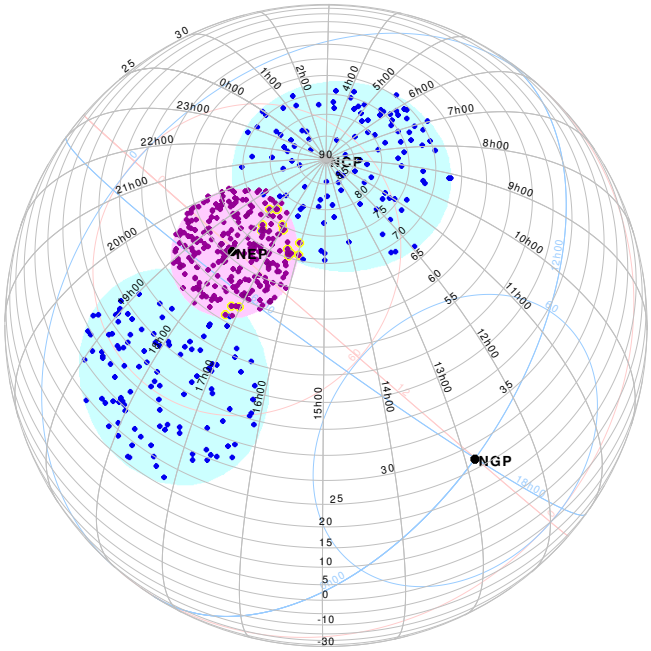

1 pav. Mūsų 506 žvaigždžių imties padėtis, pavaizduota dangaus sferoje. Mėlyna spalva preliminarūs PLATO laukai ir purpurinė TESS laukas. Šiaurinis dangaus polius (NCP), šiaurinis ekliptikos polius (NEP) ir šiaurinis Galaktikos polius (NGP) bei apskritimai, apibrėžiantys jų pagrindines plokštumas, taip pat rodomi palyginimui.

diapazonas 480–680 nm). Išsami informacija apie duomenų apdorojimą ir analizę pateikta 2.2.1 poskyryje. 2.2.2 poskyryje taip pat pateikiamas imties aprašymas, narystės atrankos metodika ir pritaikyta Saulės gausos skalė. Buvo tirtos 788 žvaigždės, priklausančios 62 padrikiesiems spiečiams, kurių amžius $\geq$ 100 mln. metų. Rinkinys apima platų R_{gc} diapazoną, nuo maždaug 5 iki 20 kpc, amžiai nuo 0,1 iki 7 mlrd. metų ir metališkumai [Fe/H] nuo −0,45 iki 0,35.

GAUSŲ SANTYKIAI

3 skyrius yra skirtas gausos santykiams, 3.1 skirsnyje analizuojant [El/Fe I] santykius kaip metališkumo funkciją 10-čiai neutronų pagavimo elementų plonajame ir storajame Galaktikos diskuose. Elementai aptariami suskirsčius į grupes: pirmojo *s*-proceso piko elementai Sr, Y ir Zr (3.1.1 poskyris), antrojo *s*-proceso piko Ba, La ir Ce elementai ir mišrūs elementai Pr ir Nd (3.1.2 ir 3.1.3 poskyriai), galiausiai *r*-proceso dominuojami elementai Sm ir Eu (3.1.4 poskyris).

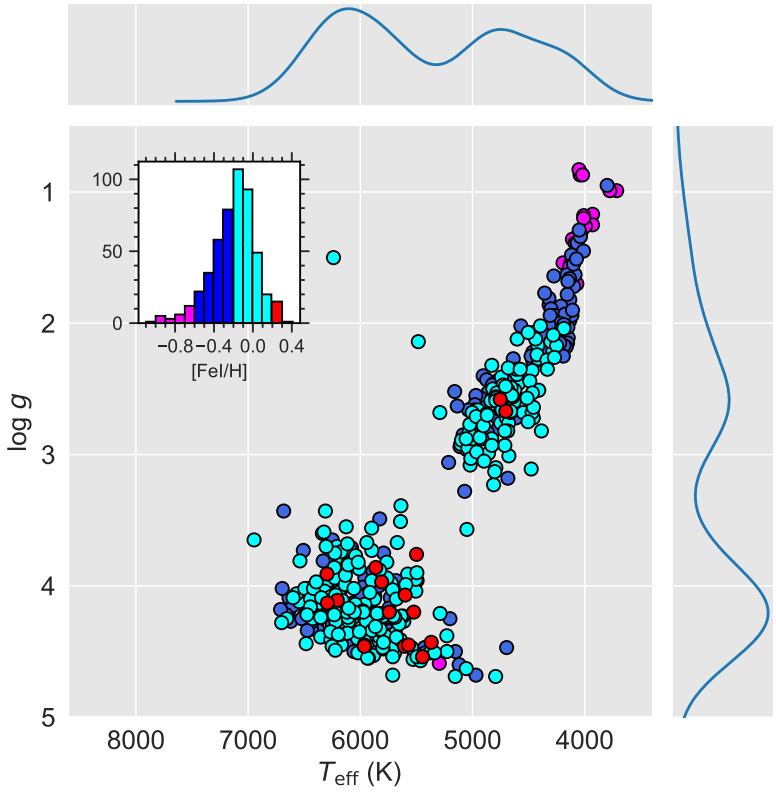

2 pav. Kylio diagrama, užkoduota pagal metališkumą ir kurioje parodytas dvimatis tankio pasiskirstymas ir metališkumo histograma tirtam 506 žvaigždžių rinkiniui.

Rezultatai buvo lyginami su Prantzos et al. (2018) ir pusiau empiriniais Pagel ir Tautvaišienė (1997) modeliais, kurie buvo pirmasis bandymas modeliuoti neutronų pagavimo elementų evoliuciją Galaktikoje (žr. 3 pav.). Apskritai, modeliai atitinka stebėjimo duomenų tendencijas, tačiau Prantzos ir kt. (2018) modeliuose sutapimas su stebėjimų duomenimis būtų geresnis jei mažų ir vidutinių masių žvaigždžių įnašas prasidėtų prie didesnio metalingumo (apie −0.7), kas pastumtų modelio maksimumą link [Fe/H]= −0.2.

3.2 skyriuje, nagrinėjant sunkiųjų ir lengvųjų *s*-proceso elementų [hs/ls] santykius (žr. 4 pav.), išvada dėl galimo Prantzos ir kt. (2018) modelių patobulinimo matosi dar aiškiau.

3.3 skirsnyje pateikiama [r/s] santykio ir [Fe I/H] analizė, leidžianti mums pažvelgti į žvaigždžių formavimosi istoriją galaktikos diske. Tiksliau, palyginame [Eu/Ba] ir [Sm/Ba] gausos santykius su [Fe I/H] su modelių prognozėmis plonajam diskui, kurį pateikė Prantzos ir kt. (2018) ir aukščiau minėti Pagel ir Tautvaišienė (1997). Rezultatai taip pat lyginami su gryno *r*-proceso santykiu, gautu naudojant

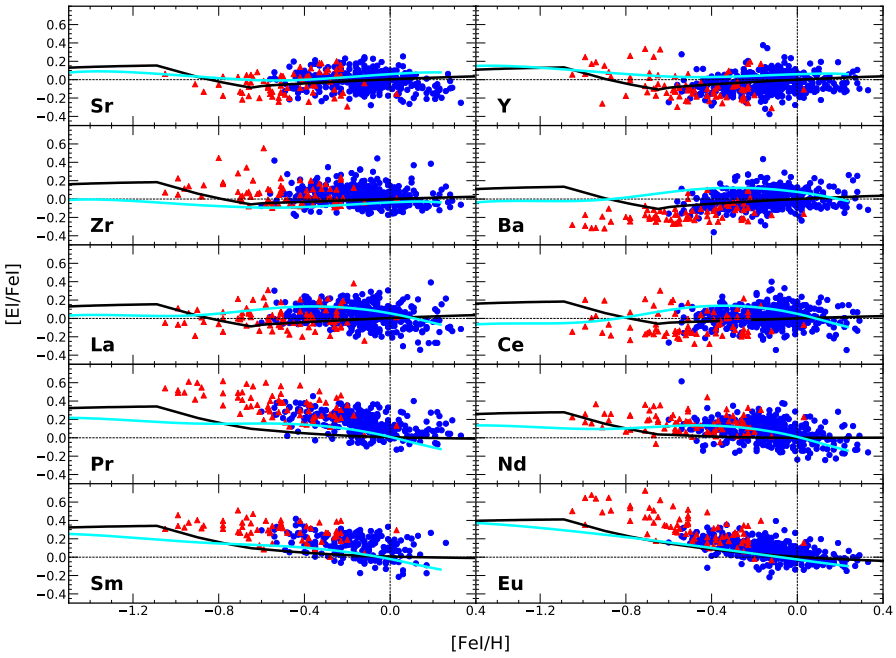

3 pav. Elementų gausos kitimo tendencijos [Fe I/H] atžvilgiu. Mėlyni taškai žymi plono disko žvaigždes, o raudoni trikampiai – storojo disko žvaigždes. Ištisinės mėlynos spalvos linijos rodo Prantzos ir kt. (2018) modelius, o juodos linijos Pagel ir Tautvaišienė (1997) modelius.

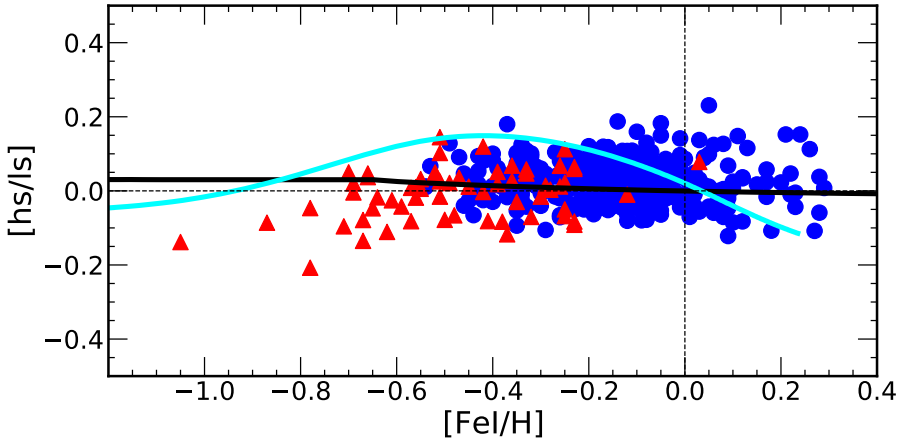

4 pav. Hs (Ba, La, Ce, Nd) ir ls (Sr, Y, Zr) gausos santykis [Fe I/H] atžvilgiu lyginant su Galaktikos cheminės evoliucijos modeliais (spalvos ir žymėjimai kaip 3 pav.).

Bisterzo et al. (2014) ir Saulės gausą iš Grevesse ir kt. (2007). Aiškiai matome [Eu/Ba] santykio mažėjimą kaip metališkumo funkciją, ir šis santykis yra artimas grynojo *r*-proceso vertėms neturtingoms storojo disko žvaigždėms, o tai reiškia, kad *r*-procesas buvo vienintelis neutronų pagavimo procesas aktyvus storojo disko formavimosi pradžioje.

Galiausiai skyrius baigiasi 3.4 skirsniu, kuriame pateikiamas abiejų Galaktikos disko komponentų [r/α] ir [Fe I/H] priklausomybių palyginimas. Skirtingai nuo kitų autorių, kurie anksčiau nustatė vienodas tendencijas (pvz., Delgado-Mena ir kt., 2017), mes storajam Galaktikos diskui nustatėme didėjančią tendenciją mažėjant metališkumui, sutinkant su Guiglion ir kt. (2018).

GAUSŲ GRADIENTAI

4 skyrius skirtas neutronų pagavimo elementų gausos gradientams pagal žvaigždžių amžių ir padėtį Galaktikoje. Palyginę gausos gradientus plonajame ir storajame Galaktikos diskuose, galime atskleisti jų evoliucijos istorijas. Skyrius padalintas į dvi dalis: viena skirta gradientams pagal amžių (4.1 skirsnis), o kita – erdviniams gradientams (4.2 skirsnis).

Skyrius prasideda [El/Fe I]-amžiaus gradientais dviejuose disko komponentuose (4.1.1 poskyris). Kiekvienam gausos santykiui pateikiami tiesinės regresijos koeficientai. Iš 5 pav. matosi, kad *s*-proceso elementai Sr, Y ir Ba plonajame diske turi stiprią neigiamą gausos koreliaciją su amžiumi, o elementų, kuriuose dominuoja *r*-procesas, gausos su amžiumi didėja. Rezultatai buvo palyginti su Prantzos ir kt. (2018) bei Maiorca ir kt. (2012) modeliais bei kitų autorių rezultatais. Jauniausiose mūsų imties plonojo disko žvaigždėse neradome bario gausos anomalijos požymių.

4.1.2 poskyryje pateikiame ryšius tarp amžiaus ir elementų gausų santykio padrikųjų spiečių imtyje, suskirsčius juos į galaktocentrinio atstumo intervalus. Mes padalijome spiečių rinkinį į tris galaktocentrinius regionus (vidinį, Saulės ir išorinį) ir pastebėjome skirtumus tarp skirtingiems Galaktikos disko regionams priklausančių grupių.

4.2 skirsnis prasideda radialiniais gausos gradientais (4.2.1 poskyris). Vietoje kitų autorių dažnai naudojamo R_{gc} disertaciniame darbe naudojome R_{mean}, nes šis orbitos parametras daug labiau siejasi su žvaigždžių gimimo vieta. Žvaigždžių migracija gali sąlygoti pakitusius radialinius gausos gradientus, todėl gimimo vietą labiau atspindinčio R_{mean} naudojimas suteikia patikimesnius rezultatus. Disertaciniame darbe pateikti apskaičiuoti gradientai plonojo ir storojo Galaktikos diskų Saulės aplinkos žvaigždėms. 4.2.2 paskyryje pateikti apskaičiuoti vertikalieji gausų gradientai tolstant nuo Galaktikos plokštumos.

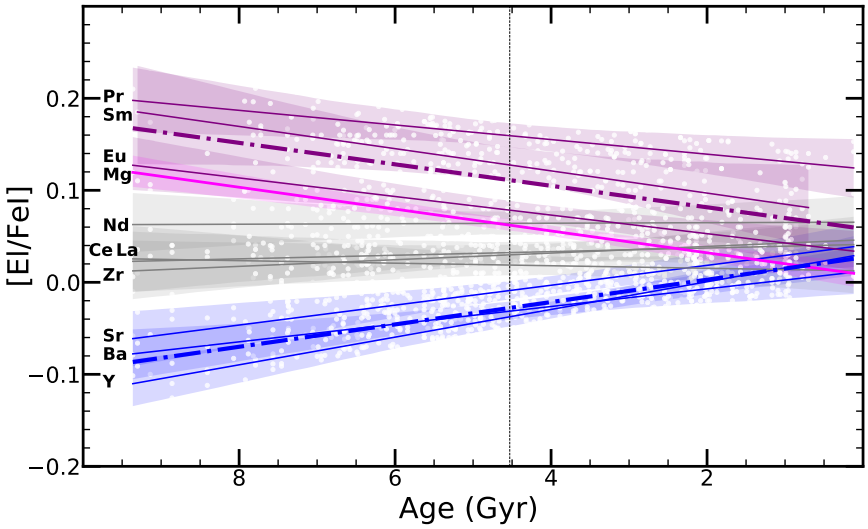

5 pav. [El/Fe I] ir amžiaus sąryšiai plonojo Galaktikos disko žvaigždėms.

CHEMINIAI LAIKRODŽIAI

Vienas iš vertingiausių neutronų gaudymo elementų pritaikymo būdų yra jų naudojimas kaip kosminiai laikrodžiai. 5 skyriuje išbandome jų naudojimą kaip abiejų Galaktikos disko komponentų amžiaus rodiklius. Pastaraisiais metais [Y/Mg] santykis pasirodė esąs perspektyvus kosminis laikrodis Saulės dvyniams (pvz., Delgado-Mena ir kt., 2019 m. ir jame pateiktos nuorodos). Nuo tada buvo stengiamasi išplėsti jo naudojimą kitose žvaigždžių populiacijose. Naujausi tyrimai parodė, kad šis [Y/Mg] amžiaus santykis kaip kosminis laikrodis nėra universalus, stipriai priklauso nuo metališkumo ir kinta priklausomai nuo galaktocentrinio atstumo (pvz., Casali ir kt., 2020, Casamiquela ir kt., 2021). Disertaciniame darbe tyrėme ir pateikėme [s/α] gausų santykių ir amžiaus sąryšius, atskirai plonajam ir storajam diskams (5.1 poskyris) ir padrikiesiems plonojo disko spiečiams (5.2 poskyris).

Plonojo disko imčiai Saulės aplinkoje (5.1.1 poskyris) gavome rezultatą, gerai atitinkantį su panašios imties Titarenko ir kt. (2019) darbu. Mes taip pat išbandėme [Y/Al], [Sr/Mg] ir [Sr/Al] taikymo galimybes. Analizuojant storąjį diską (5.1.2 poskyris), gausų ir amžiaus sąryšio įvertinimui mūsų duomenis papildėme kitų autorių darbais ir nustatėme (žr. 6 pav.), kad [Y/Mg] yra neveiksmingas amžiaus indikatorius.

5.2 skirsnis skirtas padrikųjų žvaigždžių spiečių panaudojimui elementų gausos ir amžiaus sąryšiams nustatyti plonajame Galaktikos diske. Norėdami rasti geriausią būdą apibūdinti sąryšius naudojome daugiatiesinę svertinę regresiją, ku-

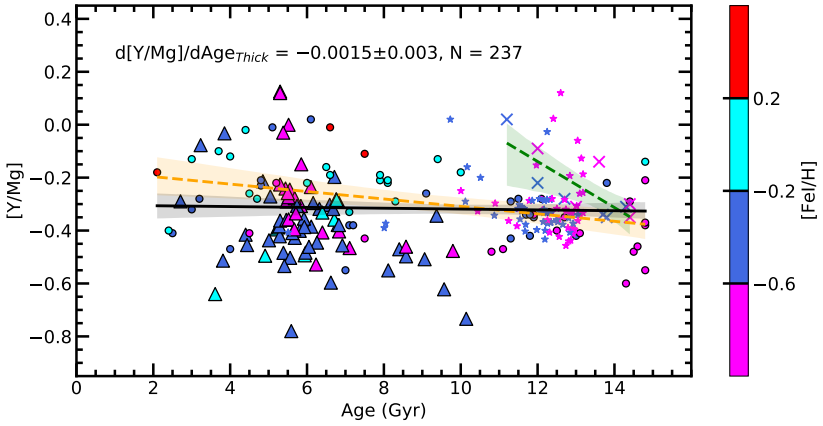

6 pav. [Y/Mg] ir amžiaus sąryšis 237 storojo Galaktikos disko žvaigždžių kompiliacijai. Žalia punktyrine linija pavaizduotas Titarenko ir kt. (2019) gradientas, geltona punktyrine linija pavaizduotas disertaciniame darbe apskaičiuotas gradientas pagal Bensby ir kt. (2014) duomenis.

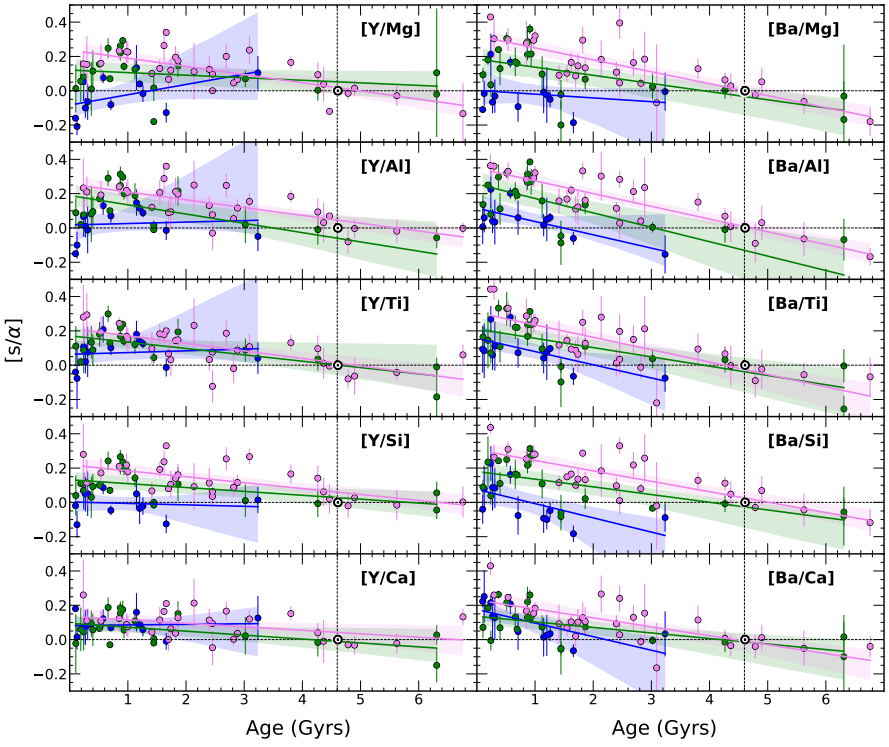

7 pav. Amžiaus ir [s/α] sąryšiai padrikiesiems žvaigždžių spiečiams, esantiems vidiniame, Saulės aplinkos ir išoriniame Galaktikos plonojo disko regionuose.

rioje atsižvelgiama į amžių, metališkumą ir R_{gc} ([s/α] = m_1·Age + m_2· R_{gc} + m_3· [Fe/H] + c). Pirmiausia kalibravome sąryšius tarp žvaigždžių amžiaus ir gausos santykio [s/α] (5.2.1 poskyris) (žr. 7 pav.). Dėl plačios galaktocentrinio išsidėstymo aprėpties mes ištyrėme šių sąryšių pokyčius vidiniame, Saulės aplinkos ir išoriniame disko regionuose.

Taip pat ištyrėme migracijos vaidmenį mūsų imtyje (5.2.2 poskyris) ir palyginome savo rezultatus su turima literatūra (5.2.3 poskyris). Mes palyginome spiečių amžių amžių įvertinimo tikslumą (5.2.4 poskyris) ir atskirų spiečiaus narių bei lauko žvaigždžių amžių nustatymo tikslumą (5.2.5). Nustatėme, kad nėra vieno amžiaus ir cheminio laikrodžio santykio, galiojančio visam diskui. 5.2.6 poskyryje mes teoriškai interpretavome pastebėtus [Y/H] ir [Y/Mg] gausos santykius žvaigždžių spiečiuose, esančiuose Galaktikos vidiniame diske, naudodami naują receptą, pagrįstą magnetiniu maišymu asimptotinės milžinių sekos žvaigždėse, lemiantį mažiau efektyvią itrio gamybą esant dideliam metališkumui.

IŠVADOS

6 skyriaus 6.1 skirsnyje pateikiamas disertacijos konspektas, 6.2 skirsnyje pateikiamos išvados, o 6.3 skirsnyje apžvelgiami apribojimai ir ateities perspektyvos. Žemiau pateikiame išvadas:

1. Palyginus [El/Fe I] santykius kaip metališkumo funkciją su Pagel ir Tautvaišienė (1997) bei Prantzos ir kt. (2018) Galaktikos cheminės evoliucijos modeliais nustatyta, kad antrojo *s*-proceso piko elementų maksimumas Prantzos ir kt. (2018) modeliuose turėtų būti ties maždaug −0,2 metalingumu. Geresnis sutapimas būtų pasiektas, jei modeliai pradėtų įskaityti mažų ir vidutinės masės žvaigždžių įtaką ties didesniu metališkumu (apie −0,7).

2. Atlikus [hs/ls] ir metalingumo sąryšio palyginimą su evoliucijos modeliais nustatyta, kad plonojo disko žvaigždės, kaip ir numatyta, priklausomybės beveik neturi, o storojo disko rodo mažėjimo tendenciją mažėjant metalingumui, kas įrodo skirtingas diskų evoliucijos istorijas ir atskleidžia storajame diske intensyvesnę lengvųjų *s*-proceso elementų gamybą lyginant su sunkiaisiais esant mažam metalingumui. Pastebėjimai taip pat rodo, kad Prantzos ir kt. (2018) modelio maksimumas turėtų būti ties maždaug −0,2 metalingumu, įskaitant mažų ir vidutinės masės žvaigždžių įtaką ties didesniu metalingumu.

3. Elementų, kuriuose dominuoja *r*-procesas, palyginimas su *s*-proceso dominuojamais elementais rodo, kad modeliai turi būti toliau tobulinami, kad

būtų atsižvelgta į didesnę r-proceso gamybą. Storajame diske [Eu/Ba] ir [Sm/Ba] santykis pasiekia grynojo r-proceso vertes nemetalingose storojo disko žvaigždėse, tai reiškia, kad tai buvo vienintelis aktyvus neutronų pagavimo procesas storojo disko formavimosi pradžioje.

4. Palyginus r-proceso elemento Eu ir α-elemento Mg, kaip reprezentatyviausių kiekvieno proceso elementų gausų santykius, storojo disko žvaigždžių imtyje akivaizdžiai matomas [Eu/Mg] mažėjimas didėjant metališkumui, palyginti su plonojo disko žvaigždėmis, o tai rodo skirtingą abiejų Galaktikos komponentų cheminę evoliuciją.

5. Analizuojant [El/Fe] kaip [Fe/H] funkciją padrikųjų spiečių imtyje, buvo pastebėti skirtumai tarp trijuose Galaktikos disko regionuose esančių spiečių. Išorinio disko (R_{gc} > 9 kpc) spiečiai paprastai yra mažiau metalingi nei vidiniame diske (R_{gc} < 7 kpc) ir Saulės aplinkoje esantys spiečiai, o [El/Fe] skirtumai yra mažiau ryškūs. Paprastai išorinio disko spiečiai turi [El/Fe]>0, o vidinio disko turi [El/Fe] panašius ar mažesnius nei Saulėje.

6. Atlikus elementų gausų ir žvaigždžių amžiau gradientų tyrimą, plonajame diske nustatyta, kad s-proceso dominuojami elementai Y, Sr ir Ba rodo aiškią antikoreliaciją su amžiumi; tuo tarpu mišrusis elementas Pr ir r-proceso duminuojami elementai Sm ir Eu rodo teigiamus gradientus. Kiti elementai rodo nereikšmingus gradientus.

7. Storajame diske gausos ir amžiaus gradientai yra gana nežymūs. Tyrimai šiuo klausimu turi būti pratęsti išplečiant tiriamų žvaigždžių amžiaus intervalą.

8. Kadangi kai kurių padrikųjų žvaigždžių spiečių gausų analizė rodo [Ba/Fe] perteklių (paprastai jaunesniuose nei 100 mln. metų spiečiuose), o tai nestebima kitų sunkiųjų elementų atveju, vadinamąją bario anomaliją ištyrėme turimame Saulės aplinkos žvaigždžių (daugiausiai nykštukių ir nepraevoliucionavusių milžinių) rinkinyje ir jos neradome kaip ir Reddy ir Lambert (2017) bei Marsakovas ir kt. (2016).

9. Tirdami gausos gradientus pagal amžių padrikųjų spiečių rinkinyje nustatėme, kad [El/Fe] vienodo amžiaus spiečiuose, esančiuose vidiniame diske (R_{gc} < 7 kpc) yra mažesnė nei spiečiuose, esančiuose atokesniuose regionuose. Mes taip pat nustatėme, kad su amžiumi gradientas mažėja, o [Ba/Fe] rodo stipriausią tendenciją. Visiems elementams, kuriuose dominuoja s-procesas, regresijos nuolydis vidiniame diske yra statesnis nei kituose regionuose.

10. Tiriant kosminius laikrodžius, mes analizavome atitinkamai jautriausius ir patikimiausius s-proceso (Y ir Sr) ir α elementus (Mg ir Al). Pagal 371 plonojo Galaktikos disko žvaigždžių rinkinį nustatėme [Y/Mg] ir amžiaus sąryšio gradientą $[\mathrm{Y/Mg}]_{thin} = 0.022(\pm0.015) - 0.027(\pm0.003)\cdot\mathrm{age[Gyr]}$, sutampantį su Titarenko ir kt. (2019) nustatytu pagal 325 plono disko žvaigždžių rinkinį AMBRE projekte. Gradientas yra šiek tiek mažesnis nei kiti autoriai gauna Saulės analogų rinkiniams arba rinkinyje neatskyrus plonojo ir storojo diskų žvaigždes.

11. Storojo disko atveju, kai išplėtėme turimų 76 žvaigždžių rinkinį duomenimis iš kitų darbų taip praplėsdami amžiaus ir metalingumo diapazonus, pagal gautą 237 žvaigždžių rinkinį nustatėme, kad [Y/Mg] ir amžiaus gradientas yra nereikšmingas. Tai rodo skirtingą abiejų disko komponentų cheminę evoliuciją ir kad [Y/Mg] negali tarnauti kaip amžiaus indikatorius storajame diske.

12. Pateikiame svertines tiesines regresijas pagal tris kintamuosius ([Fe/H], R_{gc} ir amžių) tarp gausos santykio ir žvaigždžių amžiaus, kalibruotas pagal padrikųjų spiečių imtį, kurių amžius ir atstumai buvo homogeniškai nustatyti naudojant Gaia DR2. Mes įvertiname kiekvieno santykio tikslumą ir paklaidas atkuriant padrikųjų spiečių amžių. Tarp nagrinėjamų cheminių laikrodžių [Ba/Al] ir kiti gausos santykiai bario atžvilgiu, yra tinkamiausi amžiaus atkūrimui. Ryšys tarp [Ba/Al] ir amžiaus taip pat gali atkurti atskirų spiečiaus žvaigždžių narių amžių didesniu nei 2 mlrd. metų tikslumu.

13. Taip pat pateikiamas [Y/Mg] santykio neuniversalumo paaiškinimas, kai jis naudojamas kaip kosminis laikrodis, remiantis magnetinio plūdrumo sukeltu maišymu asimptotinėse milžinių sekos žvaigždėse. Šis reiškinys sukelia ne tokią efektyvią itrio gamybą esant dideliam metališkumui, o tai turi įtakos šio santykio vertėms vidiniame diske. Tai buvo patikrinta GES iDR5 padrikųjų spečių, esančių skirtinguose galaktocentriniuose atstumuose, duomenimis ir pateikia tvirtą stebėjimų paaiškinimą.

14. Analizuojant neutronų pagavimo elementų erdvinius gradientus buvo naudojami vidutiniai galaktocentriniai atstumai, kurie labiau atspindi žvaigždžių susidarymo vietas. Nustatyta, kad radialiniai gausos gradientai plonajame diske yra nereikšmingi elementams, kuriuose dominuoja s-procesas, ir tampa teigiami elementams, kuriuose dominuoja r-procesas. Storajame diske radialiniai gausų gradientai yra nereikšmingi.

15. Vertikalieji gausos gradientai yra neigiami elementams, kuriuose dominuoja *s*-procesas, ir tampa teigiami elementams, kuriuose dominuoja *r*-procesas. Storojo disko vertikalieji gausų gradientai dažniausiai yra neigiami.

BIBLIOGRAFIJA

Battistini, C. and Bensby, T. (2016), A&A 586, A49.

Bensby, T., Feltzing, S. and Oey, M. S. (2014)', AA 562, A71.

Bisterzo, S., Travaglio, C., Gallino, R., Wiescher, M. and Käppeler, F. (2014), Astrophysical Journal 787(1), 10.

Casali, G., Spina, L., Magrini, L. et al. (2020), A&A 639, A127.

Casamiquela, L., Soubiran, C., Jofré, P. et al. (2021), A&A 652, A25.

Delgado Mena, E., Tsantaki, M., Adibekyan, V. Z. et al. (2017), A&A 606, A94.

Delgado Mena, E., Moya, A., Adibekyan, V. et al. (2019), A&A 624, A78.

Gilmore, G., Randich, S., Asplund, M. et al. (2012), The Messenger 147, 25–31.

Guiglion, G., de Laverny, P., Recio-Blanco, A. and Prantzos, N. (2018), A&A 619, A143. Grevesse, N., Asplund, M. and Sauval, A. J. (2007), Space Science Reviews 130(1-4), 105–114.

Gustafsson, B., Edvardsson, B., Eriksson, K. et al. (2008), A&A 486(3), 951–970.

Howes, L. M., Lindegren, L., Feltzing, S., Church, R. P. and Bensby, T. (2019), A&A 622, A27. Jurgenson, C. A., Fischer, D. A., McCracken, T. M. et al. (2014), 'Ground-based and Airborne Instrumentation for Astronomy V', Vol. 9147 of SPIE.

Maiorca, E., Magrini, L., Busso, M. et al. (2012), ApJ 747(1), 53.

Marsakov, V. A., Gozha, M. L., Koval', V. V. and Shpigel', L. V. (2016), Astronomy Reports 60(1), 61–72.

Morel, T., Creevey, O. L., Montalbán, J., Miglio, A. and Willett, E. (2021), A&A 646, A78. Pagel, B. E. J. and Tautvaišienė, G. (1997), Monthly Notices of the RAS 288(1), 108–116.

Pian, E., D'Avanzo, P., Benetti, S. et al. (2017), Nature 551(7678), 67–70.

Prantzos, N., Abia, C., Limongi, M., Chieffi, A. and Cristallo, S. (2018)', Monthly Notices of the RAS 476(3), 3432–3459.

Randich, S., Gilmore, G. and GES Consortium (2013), The Messenger 154, 47–49.

Reddy, A. B. S. and Lambert, D. L. (2017), ApJ 845(2), 151.

Titarenko, A., Recio-Blanco, A., de Laverny, P., Hayden, M. and Guiglion, G. (2019), A&A 622, A59.

TRUMPOS ŽINIOS APIE DISERTANTĄ

Gimęs Galicijoje, šiaurės vakarų Ispanijos regione, Autorius yra įgijęs mechanikos inžinierius bei astronomijos ir astrofizikos magistro laipsnius, šiuo metu yra Vilniaus universiteto Teorinės fizikos ir astronomijos instituto jaunesnysis mokslo darbuotojas Astrospektroskopijos ir egzoplanetų grupėje. Jis yra vienas iš „Gaia ESO Survey“ (GES), „MW-Gaia COST Action“ tyrėjų, buvo projekto „Žvaigždės ir egzoplanetos TESS ir JWST kosminių misijų kontekste“ projekto specialistas. Stažavosi Molėtų astronomijos observatorijoje Lietuvoje (vadovas Rimvydas Janulis); AIUC Astroinžinerijos centre Čilėje (vadovas Leonardo Vanzi) ir Salonikų seisminėje stotyje Graikijoje (vadovas Eleftheria Papadimitriou). Jis stažavosi Europos kosmoso agentūros (ESA) Misijos operacijų skyriuje (SCI-OO), vykdydamas projektą apie masės praradimą ir žvaigždžių vėją Wolf Rayet tipo žvaigždėse (vadovai: Frank Tramper ir Danny Lennon), kur parengė magistro darbą “OB žvaigždžių astroseismologija” (vadovas: Ehsan Moravveji). Autoriui buvo suteikta MW-Gaia COST Action mokslinių tyrimų stažuotė INAF Arcetri astronomijos observatorijoje Italijoje (vadove Laura Magrini) ir mokslinis apsilankymas KU Leuven Astronomijos institute Belgijoje. Jam buvo skirtos stipendijos studijuoti keliuose pasaulio universitetuose: Ruso universitete (Bulgarija); Verakruso universitete (Meksika); Popiežiškajame Čilės universitete; Salonikų Aristotelio universitete (Graikija). Jis buvo Pramonės inžinierių aukštosios technikos mokyklos Mechanikos katedros ir UNED Europos mokymo planavimo biuro Ispanijoje bendradarbis. Jam buvo paskirtos Europos sąjungos Erasmus SMS, Erasmus SMP, Erasmus+, Erasmus EILC, Comenius ir Grundtvig stipendijos; taip pat Santander Ibero-America ir Ispanijos universitetų rektorių konferencijos (CRUE) stipendijos. Jis dirbo mokytojo asistentu Druskininkų „Atgimimo” mokykloje ir Žemaitijos kolegijoje bei Klaipėdos universitete. Skaitė paskaitą Vilniaus universiteto Vaikų universitete. Kelerius metus dirbo elektronikos apsaugos įmonėje UAB „Trikdis“. Yra kelių mokslinių asociacijų narys, tarp jų Europos astronomų draugija (EAS) ir Europlanet draugija, taip pat yra Europos astronomijos švietimo asociacijos (EAAE) nacionalinis atstovas. Autorius domisi mokslo istorija yra apie pusšimčio biografijų autorius Karališkosios istorijos akademijos žodyne, taip pat keliose knygose ir daugiau nei šimte straipsnių įvairiomis tematikomis, dalyvavo daugiau nei pusšimtyje kursų, mokyklų ir pažintinių vizitų keliose tarptautinėse mokslo institucijose, inžinerinėse įmonėse ir elektrinėse, gavo įvairių apdovanojimų ir pripažinimų, turi oficialius sertifikatus graikų, bulgarų, lietuvių, vokiečių, anglų kalbomis iš įvairių užsienio universitetų, taip pat CLIL kvalifikaciją mokytojams. Jis vedęs ir turi sūnų.

Published content and contributions related to the thesis

Web of Science Researcher ID: AAA-6482-2020
Scopus Author ID: 57212684836
SAO/NASA Astrophysics Data System; ORCID; Publons; SciProfiles: 2023172

WoS-Scopus peer-reviewed papers:

- "Chemical Composition of Bright Stars in the Continuous Viewing Zone of the TESS Space Mission". G. Tautvaišienė; Š. Mikolaitis; A. Drazdauskas; E. Stonkutė; R. Minkevičiūtė; H. Kjeldsen; K. Brogaard; C. von Essen; F. Grundahl; E. Pakštienė; V. Bagdonas; **C. Viscasillas Vázquez** (2020). The Astrophysical Journal Supplement Series, Volume 248 , Issue 1, id.19. DOI: 10.3847/1538-4365/ab8b67

- "Magnetic-buoyancy-induced mixing in AGB stars: a theoretical explanation of the non-universal relation of [Y/Mg] to age". L. Magrini; D. Vescovi; G. Casali; S. Cristallo; **C. Viscasillas Vázquez**; G. Cescutti; L. Spina; M. Van Der Swaelmen, and S. Randich (2021). Astronomy & Astrophysics, Volume 646, id.L2. DOI: 10.1051/0004-6361/202040115

- "Abundances of neutron-capture elements in thin- and thick-disc stars in the solar neighbourhood". G. Tautvaišienė; **C. Viscasillas Vázquez**; Š. Mikolaitis; E. Stonkutė; R. Minkevičiūtė; A. Drazdauskas; V. Bagdonas (2021). Astronomy & Astrophysics, Volume 649, id.A126. DOI: 10.1051/0004-6361/202039979

- "The abundance of s-process elements: temporal and spatial trends from open cluster observations". L. Magrini; **C. Viscasillas Vázquez**; G. Casali; M. Baratella; V. D'Orazi; L. Spina; S. Randich; S. Cristallo; D. Vescovi (2022). Universe 8(2), 64. DOI:10.3390/universe8020064

- "The Gaia-ESO Survey: Age-chemical clock relations spatially resolved in the Galactic disc". **C. Viscasillas Vázquez**, L. Magrini, G. Casali, G. Tautvaišienė, L. Spina, M. Van der Swaelmen, S. Randich, T. Bensby, A. Bragaglia, E. Friel, S. Feltzing, G.G. Sacco, A. Turchi, F. Jiménez-Esteban, V. D'Orazi, E. Delgado-Mena, Š. Mikolaitis, A. Drazdauskas, R. Minkevičiūtė, E. Stonkutė, V. Bagdonas, D. Montes, G. Guiglion, M. Baratella, H. M. Tabernero, G. Gilmore, E. Alfaro, P. Francois, A. Korn, R. Smiljanic, M. Bergemann, E. Franciosini, A. Gonneau, A. Hourihane, C. C. Worley, S. Zaggia (2022). Astronomy & Astrophysics, Volume 660, id.A135. DOI:https://doi.org/10.1051/0004-6361/202142937

WoS-Scopus conference papers (proceedings)

- "The role of asymptotic giant branch stars in the chemical evolution of the Galaxy". G. Tautvaišienė, **C. Viscasillas Vázquez**, V. Bagdonas, R. Smiljanic, A. Drazdauskas, Š. Mikolaitis, R. Minkevičiūtė, E. Stonkutė. Proceedings of the International Astronomical Union (IAU), Volume 14 , Symposium S343: Why Galaxies Care About AGB Stars: A Continuing Challenge through Cosmic Time. Cambridge University Press, Volume 343, pp. 510-511 (2018). DOI: 10.1017/S1743921318005665

VizieR On-line Data Catalogs

- "High-resolution spectroscopy of TESS stars". G. Tautvaišienė; Š. Mikolaitis; A. Drazdauskas; E. Stonkutė; R. Minkevičiūtė; H. Kjeldsen; K. Brogaard; C. von Essen; F. Grundahl; E. Pakštienė; V. Bagdonas; **C. Viscasillas Vázquez**. J/ApJS/248/19.

- "Abundances of neutron-capture elements". G. Tautvaišienė; **C. Viscasillas Vázquez**; Š. Mikolaitis; E. Stonkutė; R. Minkevičiūtė; A. Drazdauskas; V. Bagdonas.
  J/A+A/649/A126.

Scientific talks

- "Exploiting the abundances of neutron-capture elements from the latest Gaia-ESO Survey (GES) data release". **C. Viscasillas Vázquez**; L. Magrini; M. van der Swaelmen; G. Casali; G. Cescutti; G. Tautvaisiene; S. Randich. MW-Gaia workshop. Breaking Barriers: Inspiring the Next Generation. Santiago de Compostela, May 23, 2022

- "Abundances of neutron capture elements in revealing the evolution of the Galactic disc". **C. Viscasillas Vázquez**. 44th Lithuanian National Physics Conference, Center for Physical Sciences and Technology. Vilnius, October 7, 2021.

- "The neutron capture elements: abundance gradients and age indicators in the thin and thick disc". **C. Viscasillas Vázquez**. SPOK. Arcetri Astrophysical Observatory - INAF. June 25, 2021 (virtual).

- "Chemical abundances of neutron capture elements in the Milky Way". **C. Viscasillas Vázquez**. University of Queens. Three Minute Thesis (3MT). Vilnius, March, 24, 2021.

- "Chemical abundances of s- and r-process elements in the Solar Vicinity". **C. Viscasillas Vázquez** on behalf of G. Tautvaišienė, Š. Mikolaitis, V. Bagdonas, R. Minkevičiutė, E. Stonkutė, A. Drazdauskas, E. Pakštienė and R. Janulis. XIV.0 Scientific SEA Meeting (virtual). Spanish Astronomical Society (SEA). RC3: The Milky Way and its components. July 14, 2020.

- "Elementos de captura neutrónica y evolución química de la Galaxia". **C. Viscasillas Vázquez**. Ramon Maria Aller Astronomical Observatory. University of Santiago de Compostela (USC). Spain. July 18, 2019.

Scientific posters

- "Distribution patterns of chemical abundances of neutron capture elements in sub-components of the Galactic disc". **C. Viscasillas Vázquez**, G. Tautvaišienė; Š. Mikolaitis; E. Stonkutė; R. Minkevičiūtė; A. Drazdauskas; V. Bagdonas. EAS. S15: Gaia: The (TWO) Billion Star Galaxy Census: The Science of EDR3 and the promise of DR3. June 28 - July 2, 2021.

- "Stellar ages based on neutron capture and alpha elements: the thin and thick disc cases". G. Tautvaišienė, **C. Viscasillas Vázquez**, Š. Mikolaitis, E. Stonkutė, R. Minkevičiūtė, A. Drazdauskas, V. Bagdonas, Y. Chorniy. European Astronomical Society Annual Meeting (EAS). S1: A holistic view of the Milky Way: linking ages, chemistry and kinematics. June 28 - July 2, 2021.

- "Abundances of neutron capture elements in dwarf stars of the Solar neighborhood located towards the north celestial pole". **C. Viscasillas Vázquez**, G. Tautvaišienė; Š. Mikolaitis, V. Bagdonas; R. Minkevičiūtė; A. Drazdauskas; E. Stonkutė; L. Klebonas; E. Pakštienė; R. Janulis. Europlanet Summer School 2019 "Space missions: ground-based observations and science communication", Molėtai, 2019.

- "Abundances of neutron capture elements in dwarf stars of the Solar neighborhood located towards the north celestial pole". **C. Viscasillas Vázquez**, G. Tautvaišienė; Š. Mikolaitis, V. Bagdonas; R. Minkevičiūtė; A. Drazdauskas; E. Stonkutė; L. Klebonas; E. Pakštienė; R. Janulis. 53rd ESLAB symposium. Noordwijk, 2019. DOI: 10.5281/zenodo.2634527

- "The role of asymptotic giant branch stars in the chemical evolution of the Galaxy". G. Tautvaišienė, **C. Viscasillas Vázquez**, V. Bagdonas, R. Smiljanic, A. Drazdauskas, Š. Mikolaitis, R.Minkevičiūtė, E. Stonkutė. IAU Symposium 343. Vienna, 2018.

Vilnius University Press
9 Saulėtekio Ave., Building III, LT-10222 Vilnius
Email: info@leidykla.vu.lt, www.leidykla.vu.lt
bookshop.vu.lt, journals.vu.lt
Print run copies 15